Stationary intraoral tomosynthesis imaging for vertical root fracture detection

A THESIS
SUBMITTED TO THE FACULTY OF
UNIVERSITY OF MINNESOTA
BY

Michael Warren Regan Anderson, DDS

IN PARTIAL FULFILLMENT OF THE REQUIREMENTS
FOR THE DEGREE OF
MASTER OF SCIENCE

Dr. Laurence Gaalaas, Dr. Brian Barsness, Dr. Mansur Ahmad, Dr. Scott McClanahan

August 2017

ACKNOWLEDGEMENTS

Dr. Carolina Rodriguez-Figueroa, Dr. Samantha Roach, and Dr. Brian Barsness

Thank you for your mentorship for the last four years. Your faith in me provided the confidence to apply to this wonderful program. Your continued support since then has shaped me into the endodontists I am privileged to become. There is such dignity in your craft as educators. I look forward our friendship for many years.

Dr. Scott McClanahan

Thank you for taking a chance on me. I will never forget meeting with you as a third-year dental student, when you informed me that the program is typically uninterested in new graduates. And yet, somehow, I was accepted into our program later that year. I hope to have exceeded your expectations during residency. I want to make you proud in my career to prove it a risk worth taking. This residency and your influence therein have so profoundly shaped the course of my professional life.

Dr. Laurence Gaalaas

It has been such a pleasure collaborating with you on this project. I am so grateful that we could work together, and I appreciate all your insight along the way. In addition to pursuing interesting research matters, I feel lucky to have cultivated a working relationship and friendship with you for the last two years. I imagine we will have much to talk about in clinical and potentially research collaborations in the future.

Dr. Mansur Ahmad

I cannot express how appreciative I am for your mentorship, support, and friendship for the last five years. You have had an uncanny way of so positively impacting my life at such pivotal moments. I will always be grateful to you.

Dr. Deborah Knaup

Thank you for serving as an evaluator on this project. I appreciate you making time in an especially busy period to support me. I am so optimistic and happy to start working with you in Rochester.

Christy Inscoe

Thank you for your dedication by completing the imaging at the University of North Carolina, and for being such a pleasure to work with.

Dr. Jay Fuillerant

I sincerely value your hard work on this project. I truly needed your assistance and appreciate you going above and beyond to help complete the project, especially when we had to start completely over.

DEDICATION

This thesis is dedicated to my wife, Dr. Tarah Regan Anderson. Your sacrifices and endurance have made completing residency possible. Your generosity and selflessness are shadowed only by your brilliance.

This thesis is dedicated to my parents who, in addition to their unconditional love, have always instilled in me the value of education.

Table of Contents

List of Tables

List of Figures

INTRODUCTION

There are few entities in dentistry that frustrate endodontists more than vertical root fractures. They doom otherwise seemingly perfectly treated teeth both endodontically and restoratively, and can be tremendously problematic to diagnose definitively. Such a confluence of challenges can be exasperating and embarrassing for dentists and endodontists. Cracked teeth in general present less with certain classic signs, but rather are typified by "classic confusion" for the patient and dentist alike (1).

Knowing that the symptoms of vertical root fracture can be inconsistent and variable, it becomes even more desirable to diagnose them radiographically. There has been considerable research attempting to quantify the accuracy in clinical diagnosis of vertical root fractures (VRF) with radiographic technologies such as periapical imaging and cone-beam computed tomography (CBCT). While those research efforts will be discussed in greater detail, one of the most recent systematic reviews and meta-analyses indicates sensitivity in diagnosis based on periapical imaging among obturated teeth to be merely 24% (2).

Cone-beam CT has aided in the diagnosis of vertical root fractures, especially by allowing for axial slice reconstruction and evaluation for a characteristic alveoloar bone loss pattern typical of fractured roots. Sensitivity of VRF detection with CBCT may be as high as 75% in obturated teeth (2), although there is a high degree of bias is most of the reports of VRF detection (3). While this is certainly an improvement compared to two-dimensional radiography, cone-beam CT technology is no catholicon in detection of these fractures, and CT imaging bears the further disadvantages of cost, access, and increased radiation compared to two-dimensional radiography. This is frustrating to

patients and practitioners alike because failure in recognition of vertical root fractures can lead to futile treatment efforts, while their speculative diagnosis results in unecessary extractions of teeth.

Stationary intraoral tomosynthesis (s-IOT), or henceforth simply tomosynthesis, imaging is a radiographic technology that may have appications in dentistry. Tomosynthesis imaging uses a multi-source X-ray array that allows for a acquisition of multiple basis images and subsequent reconstruction of a 3D volume. This technology has been applied to chest (4–6), abdominal (7), musculosckeletal (8,9), and breast imaging applications (4,5,10). A group of researchers in the Department of Physics at the University of North Carolina at Chapel Hill have developed a miniature, carbon nanotube based x-ray sources compatible with a digital intraoral radiographic sensor and therefore possibly appliciable in dentistry. It is the small size of these carbon nanotubes that allow them to be distrubted in a compact array small enough to be manipulated on a conventional intraoral dental x-ray source arm.

Tomosynthesis imaging presents certain advantages, including high resolution, low radiation, and that the planar volume can be scrolled through on the z-axis, or, “in and out” of the image plane. They recently piloted its utility in caries detection (11). As a clinician in endodontics, there seem to be many possible applications for such a technology, detection of root fractures among them. Applications of this novel technology into uninvestigated clinical challenges nurtered a collaboration between a clinical team at the Univesity of Minnesota and a group of engineers at the University of North Carolina in the undertaking of this project.

The purpose of this study was to compare the radiographic detection of induced

vertical root fractures among periapical, limited-FOV CBCT, and stationary intraoral tomosythesis imaging, as well as the relationship between these variables and their impact on evaluator confidence in diagnosis of vertical root fractures.

REVIEW OF LITERATURE & BACKGROUND

VERTICAL ROOT FRACTURES: THE ENTITY, DIAGNOSIS, & TREATMENT

Vertical root fractures are among the five types of longitudinal cracks in teeth: craze lines, fractured cusp, cracked tooth, split tooth, and vertical root fracture (1,12). A vertical root fractures is defined as "a complete or incomplete fracture initiated from the root at any level, usually directed buccolingually [that] may involve one…or both proximal surfaces, and may extend coronally toward the cervical periodontal attachment" (1). While classically it was imagined that root fractures initiated at the apex and extended coronally (13), it is now thought that they can initiate as smaller cracks at any level of the root surface (1,14). These fractures become pathologic because they harbor bacteria (15) and act as pathways for further spread of pulpal or periapical disease (12). Histologically, Walton demonstrated these fractures to contain "bacteria, necrotic tissue, food debris, and unidentifiable amorphous substances" (16). As such VRF's are not simply a structural defect but an infectious etiology.

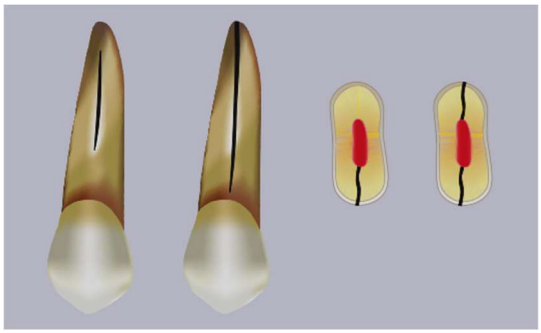

Figure #1: Facial view and horizontal cross section of vertical root fractures. VRF's can be complete or incomplete, typically extend in a bucco-lingual direction, and they can initiate at any point on the root surface. From Rivera (1)

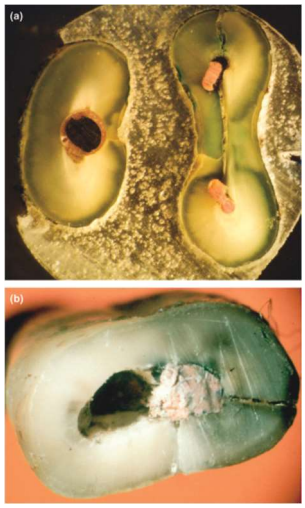

Figure #2: Cross-sectional photographs of two incomplete vertical root fractures. From Tamse (17)

The exact prevalence of vertical root fractures is not precisely known. The overall prevalence has been reported as 5% in a retrospective radiological study (18). Two studies evaluating extracted teeth identified that vertical root fractures being present in 11% and 20% of extracted endodontically treated teeth (19,20). Definitive quantification of their incidence is so difficult because so too is their diagnosis challenging.

Signs and symptoms of vertical root fractures are variable, and are far from pathognomonic which makes their definitive diagnosis difficult.

Author	Number of teeth	Osseous defect	Mild-to-moderate pain	Sinus tract	Perio-type abscess
Meister et al. (8)*	32	93	66	13	28
Tamse (7)†	25	64	41	14	24
Testori et al. (17)†	36	78	58	42	53
Tamse et al. (5)*	92	67	55	35	34

*Retrospective survey of original cases.
†Retrospective survey of original and published cases.
VRF, vertical root fracture.

Table #1: Signs and symptoms of VRF observed in retrospective studies in percent of teeth examined. From Tamse (17)

The most consistent combination of symptoms is a narrow, isolated probing depths and sinus tract in a tooth with a history of root canal therapy (1,13). This osseous defect is typically present on the buccal surface of a root, and is most common on maxillary molars and premolars as well as mesial roots of mandibular molars (13). The shape of the characteristic bone defect has been described as "V-shaped dehiscence" of buccal cortical plate found in 91% of fractures, while a less common "U-shaped dehiscence" present on the lingual surface (21).

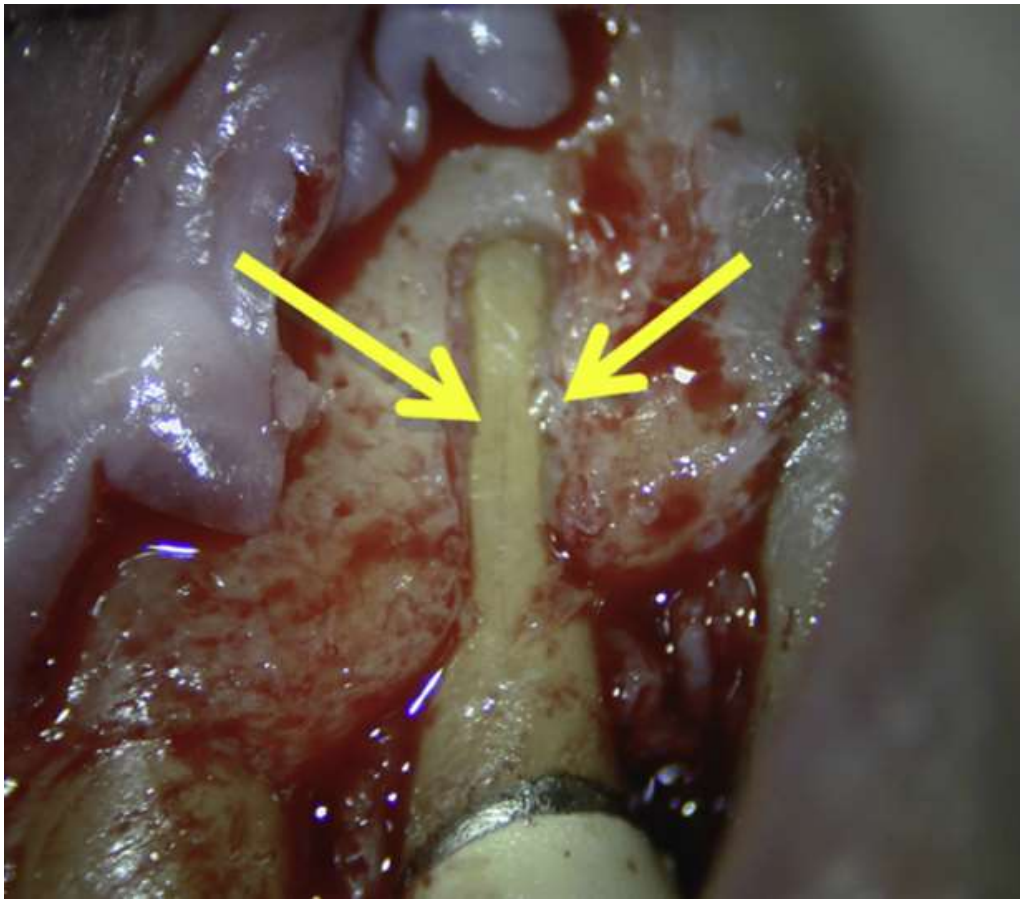

Figure #3: Photograph of surgical exposure of buccal bony dehiscence associated with vertical root fracture #13. From Todd (22)

A sinus tract is found between 35% (23) and 42% (24) of the time, and it is typically found nearer to the gingival margin than sinus tracts typical of endodontic

disease with chronic apical abscesses (13,25), as depicted in Figure #4. Some authors have correlated the presence of double or multiple sinus tracts with vertical root fractures (25,26), but this finding may be misleading since multiple sinus tracts have also been correlated with actinomyces predominated endodontic infections (27).

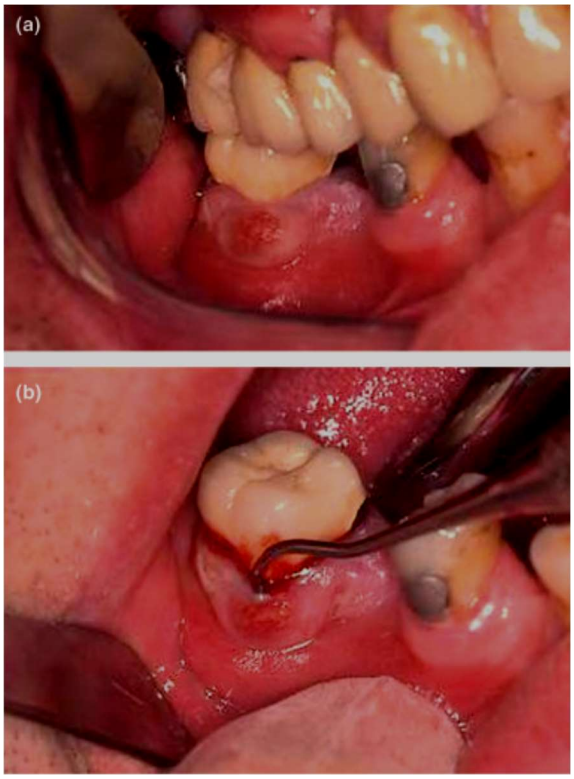

Figure #4: Photographs of sinus tract commonly found on fractured teeth. As depicted, these sinus tracts may be more cervically located and associated with deep, narrow probing depth. From Tamse (17)

The age of the tooth itself is a risk factor cracks and fractures. Certainly, it is true that older teeth will have been exposed to years of additional function and wear that could lead to fracture initiation. But furthermore, there are physical changes to the properties of dentin as teeth age that predispose them to fracture. It has been demonstrated that dentin from older teeth and dentin that has been dehydrated will both lead to decreased endurance strength that will increase the risk of fracture initiation as well as rate of propagation (28,29).

The most consistent risk factor for the development of vertical root fractures is

previous endodontic therapy (30), especially with a cold lateral obturation technique (31,32). It is possible that several aspects of endodontic treatment contribute to fracture risk, including loss of tooth structure, induced stress from instrumentation and obturation, post-space preparation and placement, and both type and adequacy of definite restoration may be contributors (33). Root shape and curvature contribute to their susceptibility to root fracture, as does remaining dentin wall thickness after instrumentation (14,34,35). As such, conservative preparations may reduce likelihood of fracture (14).

The forces and strain induced during obturation has been correlated with the development of root fractures, contributing to the fact that endodontic therapy is such a risk factor for vertical root fractures. Specifically with cold lateral obturation, the use of finger spreaders, especially with excessive force can induce root fracture. Holcomb, Pitts & Nichols identified that a spreader force of 1.5 kg could be enough to induce root fracture (34); meanwhile, Saw & Messer identified an average load of 16.1 kg induced fracture, which is higher than typical forced used with this obturation technique (36). Hand spreaders induce significantly more root strain than do finger spreaders (37). Finger spreader use is associated with vertical root fracture, but the use of nickel-titanium spreaders penetrate deeper and generate less root strain than stainless steel spreaders (38,39).

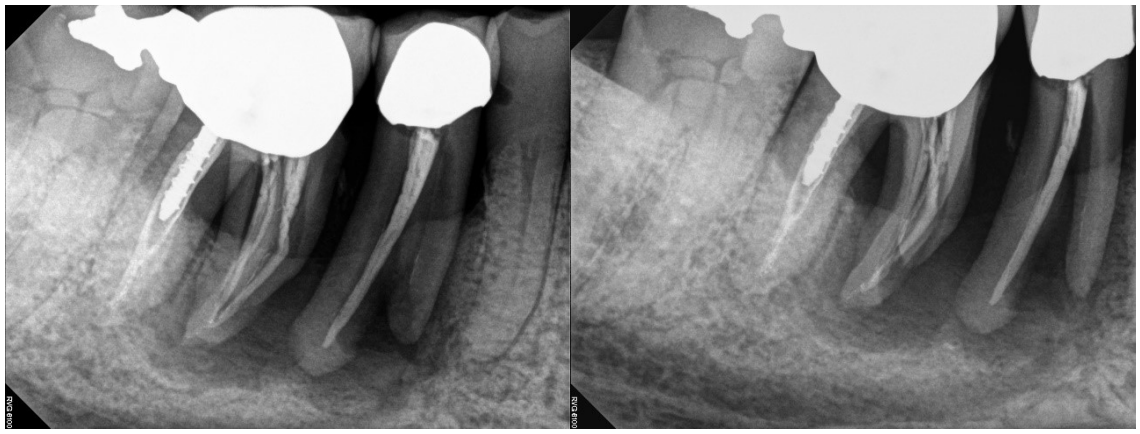

Figure #5: Periapical radiographs clinically obtained by primary investigator of #29-30 demonstrating vertical root fractures with separation of root fragments, presumably associated with excessive obturation forces

Obturation techniques that use thermoplasticized gutta-percha also induce root strain, and may therefore contribute to risk of vertical root fracture. Obtura and cold lateral techniques both induce similar overall root strains (36). When evaluating the location and distribution of this force, lateral compaction requires less force than vertical compaction to induce the same stress near the apex, and that stress localization in cold lateral obturation is more concentrated and therefore more likely to induce root fracture (40).

In addition to obturation, there is evidence that the chemicals used in non-surgical root canal therapy may weaken dentin, although there is some controversy in the literature therein. For example, five weeks of exposure to sodium hypochlorite decreased dentin strength by 59% (41). Sodium hypochlorite in higher concentrations can adversely impact the flexural strength, elastic modulus, and microhardness of dentin (42–44). The clinical significance of those impact may be marginal however based on the limited time of exposure of root dentin to sodium hypochlorite in routine endodontic treatment.

While sodium hypochlorite reacts with the organic components of the root canal

system and root dentin, ethylenediaminetretraacetic acid (EDTA) interacts with the inorganic component by acting as a chelating agent. When sodium hypochlorite and EDTA are used in combination and both inorganic and organic phases are removed, there is a concurrent deleterious effect on dentin strength and hardness (44,45).

In the long term, it appears that exposure of dentin to calcium hydroxide for longer than 30 days is correlated with a decrease in dentin strength (41,46). However, it has been reported up to 30 days this effect is not significant (47), and this timeframe is in most cases representative of the duration of exposure in multiple visit endodontics. In some contrast to this finding, it has also been reported that $Ca(OH)_2$ caused a 35% drop in flexural strength after 10 days without subsequent change between 10 days and 30 days; in this case authors concluded that calcium hydroxide's effect on dentin to be self-limiting and restricted to superficial layers of dentin (48). These differences in experimental conclusions may likely be accounted for by differences in study design. Nonetheless, it is at least possible that the disinfecting chemicals employed in endodontics have an impact on the physical properties of dentin that might leave teeth more susceptible to fracture.

Post and dowel placement have also been correlated with fracture induction (17). This relates firstly to the post reparation itself insofar as the process removes dentin. Remaining dentin thickness is a significant risk factor in the prevention of vertical root fractures (14,49). So too can the post itself induce fractures. A post under function will to varying extents concentrate forces within the tooth near the fulcrum of leverage and at the apical extent of the post; this is why posts with inadequate length, particularly when they do not extend past the crest of bone, are more likely to induce fractures (50).

Fracture risk can also be mitigated to some extent by using post materials whose moduli of elasticity and coefficients of thermal expansion are similar to those of dentin (51,52). It has been demonstrated that parallel, passive, prefabricated fiber posts are least likely to induce fracture (53).

Therefore, for a variety of reasons endodontically treated teeth are at risk for development of fracture. Kishen's review on mechanisms and risks for fractures in endodontically treated teeth summarizes the factors that impact the stresses on these teeth as being impacted by "(1) the material properties of the crown, post, and core material, (2) the shape of the post, (3) the adhesive strength at the crown–tooth, core–tooth, and core– post, post–tooth interfaces, (4) the magnitude and direction of occlusal loads, (5) the amount of available tooth structure, and (6) the anatomy of the tooth" (50) .

Although they typically present in previously treated teeth, vertical root fractures can quite rarely occur in unobturated teeth. Vertical root fractures in unobturated teeth have been reported most commonly in an Asian population, with advanced age, and on first molars (54–56). There is a correlation with such fractures in vital teeth with bruxism or clenching (57). While these fractures may be easier to identify radiographically, their scarcity make these clinical correlations of diminished value.

Ultimately, the only definitive means of identification of a vertical root fracture is its surgical exposure for staining and direct visualization (25,26,58,59). This is particularly true for early or incomplete root fractures that may not be evident on any radiographic modality and their symptoms may resemble other pathological entities, such as cemental tear (60,61), periodontal disease, or persistent endodontic disease (1)(17). As such, correct diagnosis of a vertical root fracture is imperative to avoid misguided or

futile treatment efforts. Unfortunately, at this time, the predicable treatment options of a vertical root fracture are only to remove it, whether by root resection, root amputation, or tooth extraction (1,17,25).

Some more eccentric treatment modalities have been investigated. An *in vitro* attempt to fuse fractured root segments using either CO_2 or Nd:YAG lasers was unsuccessful in all 81 samples (62). However, one clinical case report of root fracture fusion demonstrated adequate though incomplete healing (63). It has been suggested that bonding, specifically with 4-methacryloxyethyl trimellitate anhyride/methacrylate-tri-n-butyl borane (4-META/MMA-TBB) resin cement, to internally bond root fractured root segments may prolong tooth survival (64). Case reports also exist of extraction replantation of vertically root fractured teeth with this resin cement (65–68). So too has it been suggested that the use of enamel matrix derivative during intentional replantation of bonded teeth with root fractures may induce cementum deposition and decrease the incidence of root resorption (69). While dentists and endodontics continue to struggle with treatments aimed at preserving those teeth with vertical root fractures somehow, the abundance of clinical evidence demonstrates that these teeth, particularly single rooted fractured teeth, have a questionable or unfavorable prognosis.

Our struggles to predictably and conservatively treat vertical root fractures amplify the importance of preventing them, such as preservation of tooth structure, post placement, and minimization of root strain(1,12,32,34–39,59,70). Given that vertical root fractures can be difficult to identify clinically or to treat, it would be so helpful to somehow consistently identify them radiographically.

RADIOGRAPHIC TECHNOLOGIES: PERIAPICAL RADIOGRAPHY & CONE-

BEAM COMPUTED TOMOGRAPHY

Periapical two-dimensional radiography is still the workhorse of modern imaging in endodontic diagnosis, treatment, and follow-up. Indeed, periapical imaging the standard of care and the imaging modality of choice in the diagnosis of the endodontic patient and for immediate post-operative imaging (71). The first application of intraoral radiography in endodontics by Dr. Edmund Kells in 1899 set the stage for the central use of periapical imaging today in endodontics. Since that time, periapical imaging technology has improved with greater contrast and resolution as well as the development of digital imaging instead of film. Simultaneously, new imaging modalities such as cone-beam computed tomography have become indispensable to many modern endodontists in diagnosis and delivery of care to patients. As has been and will be discussed, despite the wealth of additional information afforded by these new technologies, they are still imperfect. This motivates engineers, radiologists and endodontists to collaborate to develop and apply new radiographic technologies, potentially such as stationary intraoral tomosynthesis.

Periapical images are generated when an incident beam of x-ray photons pass through tissue where some of those photons will be deflected or absorbed and the others strike the sensor to generate an image. Historically, film was used and developed, but most endodontists today use digital sensors, whether they are charge-coupled devices (CCD) or complementary metal oxide semiconductor (CMOS), and less commonly photostimulable phosphor plates. Digital intraoral radiography advantages include lower radiation, instant image, no processing equipment, convenience of storage and access, facilitation of teleradiography, image manipulation, and comparable image quality

(72,73).

With periapical imaging, there are certain techniques and cues in interpretation that must be employed to circumvent the fact that they are a flattened two-dimensional representation of three-dimensional tissues. Potential problems in interpretation derive from, for example, distortion and overlap. First, based on the angle between the surface of the sensor, plane of the tooth, and direction of the central ray, the resulting image may be foreshortened or elongated. The paralleling and bisecting angle techniques are two methods for minimizing the degree of such distortion, which can be facilitated by the use of Rinn XCP's or hemostat with bite tab, in order to have a more reproducible image, accurate estimated working length, and identification of periapical radiolucencies (74–76).

Loss of periapical bone is not always visualized on periapical radiographs despite their histologic presence. Multiple radiographs may be necessary to identify such a lesion using periapical imaging (77). There are anatomical factors that can complicate their identification, such as the zygomatic arch that can obscure them by overlap (78), maxillary sinus (79), or the mental foramen which can resemble a periapical radiolucency (80,81). Histologic periapical inflammation may be present at least 30% of the time without any periapical radiographic changes (82). The relative location of the lesion with respect to the root itself may obscure the lesion through overlap (79). These radiolucencies may not appear on a periapical radiograph until erosion of the buccal or lingual cortical plate occur (82–84). All of these factors contribute to a sensitivity of PARL on mandibular posterior teeth of just 65% and specificity of 78% on two-dimensional radiography (85).

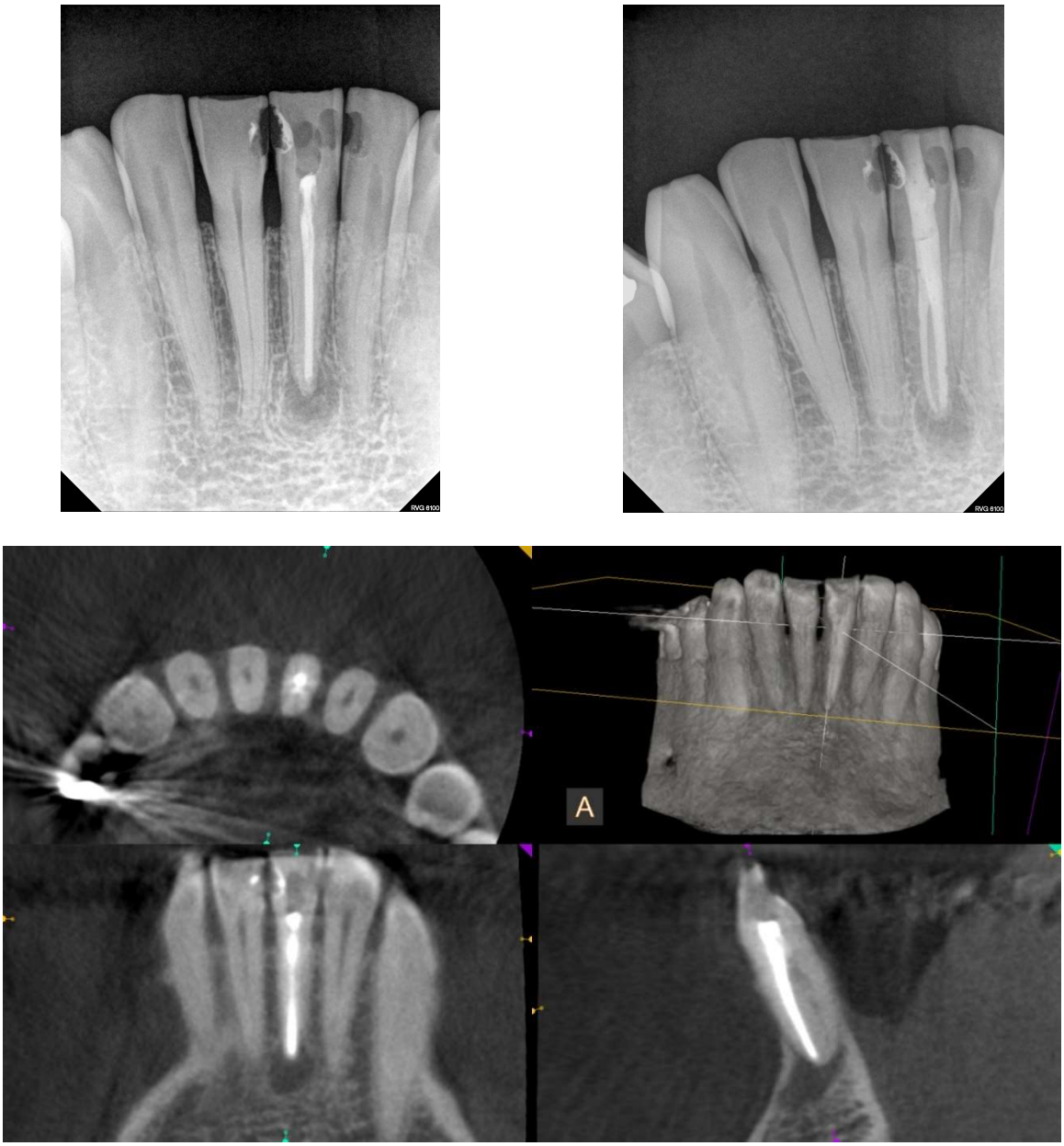

Figure #6: A clinical case where CBCT imaging (bottom) confirmed a missed lingual canal as presumptive etiology for persistent apical periodontitis with preoperative (upper left) and immediate postoperative (upper right) periapical radiographs.

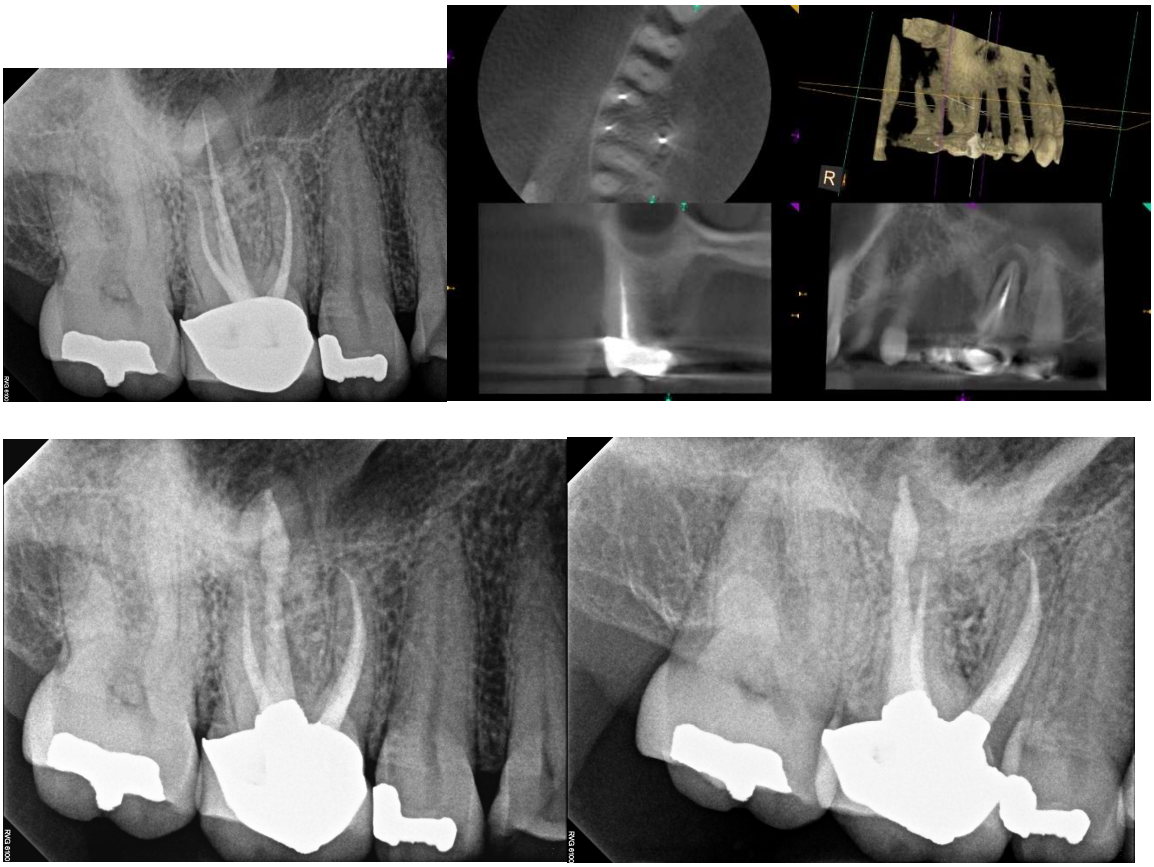

Figure #7: A preoperative radiograph and CBCT imaging (above) revealed evidence of missed MB2 canal and palatal internal resorption in the apical third. At six month post-treatment evaluation (lower), the patient was asymptomatic & functional and periapical radiolucencies decreased in size.

The buccal object rule is one of the oldest and best-known methods of applying multiple images exposed from different angles to make geometric inferences with respect to location of objects in the third dimension relative to one another (86–88). Characteristic features on periapical radiographs can be helpful in evaluating for multiple canals and canal morphology, such as fast-breaks, bullseyes or asymmetrical working images (89,90). So too do asymmetrical obturations suggest the presence of a missed canal, which was identified in one clinical study to be the case 89% of the time (91) with no difference between the use of conventional film or digital radiography (92).

These limitations of periapical imaging, including structure imposition,

elongation, foreshortening, overlap, anatomical confounders, and delayed appearance of periapical radiolucencies, are largely resolved by using cone-beam computed tomography in endodontics. Nonetheless, there are still limitations and disadvantages to that technology as well.

CBCT volumes are obtained by using a rotating x-ray source that emits a divergent pyramid-shaped beam of radiation through the patient onto a detector that rotates opposite the source; as the source and detector rotate around the target, a series of planar two-dimensional basis images are acquired and then compiled into a three-dimensional volume (93). Since the volume is reconstructed largely distortion-free, the resulting three-dimensional images are not subject to elongation or foreshortening, unlike periapical imaging. This allows CBCT imaging to establish accurate estimated working lengths (94).

CBCT overcomes most of the limitations of periapical imaging (95). CBCT aids the endodontist in assessing for root form and canal detection (22,96–98). CBCT has been demonstrated to provide improved location of critical structures to be aware of non-surgical and surgical endodontic treatment (99,100), such as the inferior alveolar canal (101,102), mental foramen (81,103), maxillary sinus (104). The use of limited field of view or narrow field of view CBCT technology has improved resolution, reduced noise, and decreased radiation that is highly applicable to endodontics (22).

As previously discussed, two-dimensional images alone are inadequate in detection all periapical radiolucencies. In one study, periapical images detected 54% and panoramic radiographs 28% of the periapical radiolucencies detected on CBCT (105). This finding has been confirmed in several well-designed studies that consistently

demonstrate that CBCT is superior in the detection of periapical lesions compared to the use of periapical radiographs (106,107).

For these reasons among others, the AAE & AAOMR in a joint position statement recommend the use of CBCT as the imaging modality of choice in many endodontic clinical situations (71). Such situations include complex anatomy, suspicion of fracture, endodontic retreatment and surgery planning, implant placement, trauma, and resorption. So, the use of CBCT as an adjunct to periapical imaging is becoming increasingly essential to the endodontist in clinical diagnosis, planning, treatment, and follow-up.

Cone-beam computed tomography imaging is not without certain limitations and disadvantages. Some have discussed the medicolegal liability associated with full interpretation of scans (108). CBCT is susceptible to artifacts, including beam hardening, metal artifact, ring artifact, cone beam effect artifact, motion artifact, aliasing artifact and noise artifact (109). Beam hardening is created by radiopaque objects in the field that creates a false area of decreased attenuation resulting in a dark band adjacent to radiopaque objects, such as gutta-percha. Metal objects create white streaks across the volume due to their high attenuation. Metal artifact and beam hardening can occur around the same radiopaque object. Ring artifacts are visualized in axial slices if there is defective or malfunctioning detector element in the source. Cone beam effect artifacts result from the pyramidal shape of the x-ray beam that causes the periphery of the volume, especially the most superior and inferior extents, to appear darker and with greater noise than more central areas of the field. Streaks and double images, known as motion artifact, can appear if the patient moves during scanning. Noise artifact is an unstructured graininess resulting from random variation in photons that produce a

Figure #8: An 8-year old female developed pulpal necrosis following a bike accident. The tooth was treated with NSRCT and access restoration by another provider. When evaluated by the primary investigator two years after initial treatment, the patient reported persistent pain and demonstrated a deep, purulent palatal periodontal defect. CBCT imaging was essential in identifying a coronal oblique cervical fracture that was unapparent on periapical imaging.

mottled appearance on the volume. Although of these artifacts can be prevented or managed, so too can others complicate interpretation of CBCT volumes, especially in endodontically treated and heavily restored teeth with extensive radiopaque materials on and within.

TOMOSYNTHESIS IMAGING

Tomosynthesis imaging is a radiographic technology that has been applied outside of dentistry and, if used in dentistry, may present benefits to clinicians in screening, diagnosis, and treatment. A team at the University of North Carolina has developed a series of technological innovations and clinical prototypes to allow for stationary intraoral tomosynthesis (s-IOT) experimentation.

They developed a carbon nanotube X-ray source that allow for novel applications and source geometries difficult or impossible with conventional X-ray sources. The carbon nanotubes allow for electron emission through field emission or Fowler-Nordheim tunneling (110). Use of these "cold cathodes" for X-ray production allow for electron emission without thermal side effects. These compact carbon nanotubes can be geometrically distributed to emit spatially-distributed field emission X-ray source arrays, as seen in Figure #9 and Figure #20 (111). The spatially-distributed carbon nanotube array with unique geometries creates a series of projection images from different angles without the need for any mechanical movement of the radiographic source or sensor. The projection images are then reconstructed into stacked planar images that can be scrolled through on the "z-axis," the third dimension "in and out" of the planar images (with the "x-axis" and "y-axis" representing the plane of a conventional 2D image).

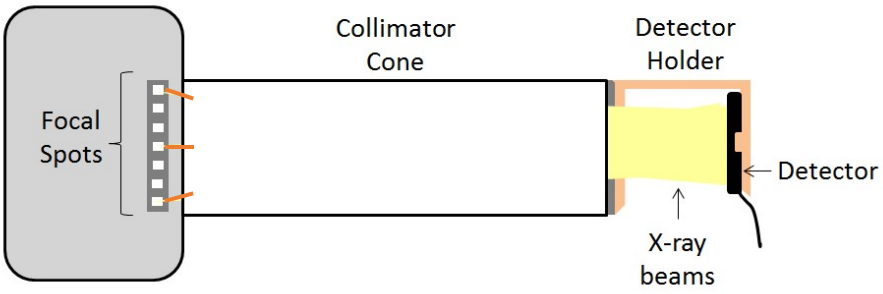

Figure #9: s-IOT system schematic illustrating source-detector geometry and collimator configuration; three representative x-ray beams are shown (117)

Whereas physically larger iterations of this technology have been applied to other tissues such as breast tissue (112), compacting this technology allows s-IOT to image much smaller structures like teeth. This clinical system, empowered by the new carbon nanotube array, is an application of stationary tomosynthesis to intraoral structures (11). The s-IOT imaging system developed for the present study provided improved imaging speed, quality, and system simplicity from previous prototypes and prior attempts at using tomosynthesis for dental imaging.

This group first applied stationary intraoral tomosynthesis to caries detection. In a reader study they found in a pilot study a 36% increase in sensitivity for caries detection (113). The present study investigates fracture detection. They also have an upcoming IRB-approved patient trial for investigation of a clinical prototype at the UNC School of Dentistry (ClinicalTrials.gov: NCT02873585).

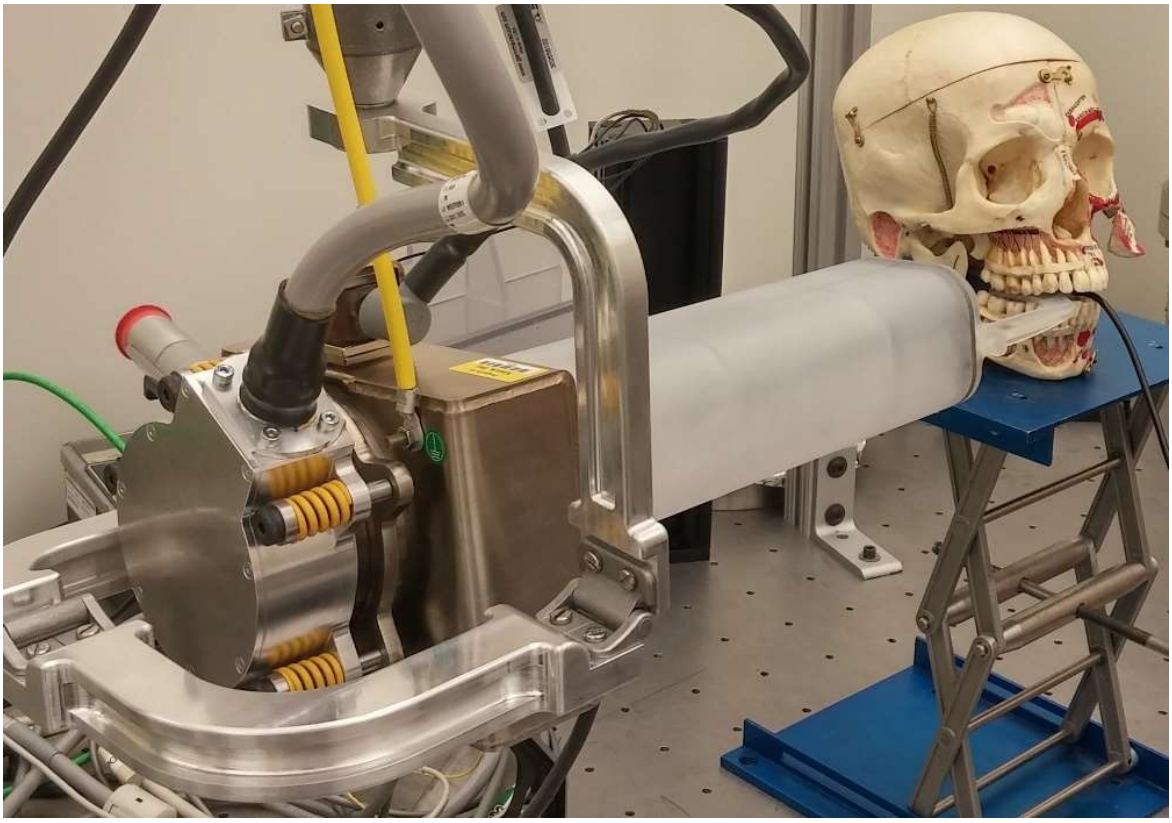

Figure #10: Stationary intraoral tomosynthesis prototype source used in tomosynthesis imaging

RADIATION DOSE

Radiation dose and the associated risks of ionizing radiation are a concern for patients and providers alike. Certainly, this is a relevant question as we consider the possible implementation of a new radiographic technology in patient care. Exposure for routine dental radiographs have decreased with the implementation of digital imaging. Digital radiographs have led to 50-80% decrease in radiation exposure compared to conventional films (79). Meanwhile, the increased information afforded by CBCT is accompanied by an increased radiation exposure to patients. Practitioners should use radiography in accordance with the principle of ALARA. Understanding that there is no

truly safe dose of ionizing radiation, the question becomes under what circumstances the value of the exposure exceeds the risk associated with the radiation exposure.

Ionizing Radiation Dosages *(approximate)*

Activity	Effective Dose in µSv	Dose as Days of Equivalent Background Radiation
1 day background radiation, sea level	7-8	1
1 digital PA radiograph	6	1
4 dental bite-wing radiographs, F-speed film	38	5
FMX; PSP or F-speed film	171	21
Kodak® CBCT focused field, anterior	4.7	0.71
Kodak® CBCT focused field, maxillary posterior	9.8	1.4
Kodak® CBCT focused field, mandibular posterior	38.3	5.47
3D Accuitomo, J. Morita	20	3
NewTom 3G, ImageWorks	68	8
Chest x-ray	170	25
Mammogram	700	106
Medical CT, head	2,000	243
Medical Cat Scan (Spiral CT abdomen)	10,000	1,515
Federal Occupation Safety Limit per Year	50,000	7,575

Table #2: Radiation dose associated with different radiographic technologies. Calculated radiographic exposure is also informed by the tissues included in the target, which is why CBCT imaging has differing doses depending on target area. From the AAE (114)

The resulting impact, as in morbidity and mortality, associated with ionizing radiation is a controversial question. Some have identified the risk of dental radiology as "vanishingly small [and] virtually impossible to determine" (115). By narrowing the field of view in CBCT, the radiation dose is decreased in addition to improving noise and resolution. There is reasonable consensus that the diagnostic information made available by CBCT imaging in select cases justifies the inherent increase in exposure (71,114,116). Nonetheless, an imaging modality that provides equal or additional diagnostic information with less radiation exposure to the patient is desirable.

The exposure of tomosynthesis imaging is comparable to a single periapical

radiograph. In this study, the maximum exposure for stationary intraoral tomosynthesis was set to not exceed the dose for a single photostimulable phosphor plate image (117). It is remarkable that tomosynthesis imaging provides three-dimensional information with such a low exposure to the patient. This is one of several reasons that make tomosynthesis an attractive technology to apply to dentistry and endodontics.

RADIOGRAPHIC DETECTION OF VERTICAL ROOT FRACTURES

Radiographically, vertical root fractures are inconsistently visualized on traditional periapical radiographs, particularly incomplete vertical root fractures (13,57,118–128). Although periapical radiographs have excellent resolution, in order for the fracture to appear on the radiograph, there must separation of the root fragments or the fracture direction must be approximately parallel the x-ray beam—specifically, within 4 degrees (129).

Beyond direct visualization of the fracture itself, the radiographic appearance of root fractures on periapical imaging is characterized by the "halo" and "periodontal" pattern of periradicular radiolucencies (13,24,121,130), and mandibular molars are more likely to present with a furcation radiolucency (13). However, radiographic detection of this characteristic bone loss is only evident in 50% of cases in periapical imaging (57). Since fracture orientation is typically bucco-lingual among vertical root fractures, the initial boney defect that develops will at least in the early stages be superimposed with the root itself, thereby obscuring visualization of the defect on periapical imaging until it is large enough that involves the proximal surfaces of the root (17). This will delay the radiographic presentation of bone loss that might indicate the presence of a root fracture.

Since the clear majority of vertical root fractures are previously endodontically

treated, the radiopaque obturation material can obscure visualization of a fracture on periapical radiographs by superimposition. Although superimposition is not a concern in CBCT imaging, induction of beam hardening and metal artifacts can interfere with the identification of root fractures (109). Despite these artifacts, CBCT has improved detection of vertical root fractures compared to periapical radiographs alone, and at this time CBCT may be the best, although imperfect, modality for clinical radiographic identification of vertical root fracture (22,71).

Among the first to characterize the identification of vertical root fractures between computed tomography and periapical radiographs was Youssadeh et al. in 1999. Their study is commonly referenced in many imaging studies on the topic, and their definitions are used in the present study as well. For dental radiographs, fracture diagnoses were "based on direct visualization of a radiolucent line that traversed the root only, without propagation into the surround alveolus. CT findings of a root fracture were characterized by a separation of the adjacent root segments visualized on at least two contiguous sections without continuation of the hypoattenuated line into the adjacent tissue" (131). These definitions are included in the directions to evaluators in the present study. This study identified an average sensitivity of fracture detection as 23% for dental radiographs and 100% for CT. However, this study is in some senses misapplied in dental and endodontic literature. First, the training of the evaluators is different from dentists, endodontists, and radiologists because all the authors of this study are medical doctors, not dentists. Secondly, the CT modality that was utilized was medical CT. Medical CT has a very high resolution, but comes with a high cost and high radiation dose; this radiation is much higher than cone-beam CT used in endodontics. Since medical grade

CT is not commonly used in dentistry, their quantitative results are less applicable than has sometimes been suggested in dental and endodontic literature.

There are several ex vivo and clinical studies that have quantified the accuracy of detection of vertical root fracture with the use of periapical and CBCT imaging with a broad range of reported sensitivities.

Hassan et al. evaluated fractures induced with a chisel and identified sensitivity for VRF detection of CBCT were 79% and for periapical images 37%. The specificity of CBCT was reduced by the presence of obturation material, but its overall accuracy was not influenced. Both the and overall accuracy of periapical radiographs were reduced by the presence of obturation material. The results showed an overall higher accuracy for CBCT (0.86) scans than periapical imaging (0.66) for detecting VRF (125). Ozer et al. induced fractures with hammer and chisel and identified an accuracy for detecting vertical root fractures for CBCT scans as 0.2mm-wide VRF's (70%) and 0.4mm-wide VRF's (90%) compared with periapical imaging (43.3% and 60%, respectively) (132). These studies demonstrate that there is good but imperfect detection of vertical root fractures, although it must be pointed out that the size of the fractures they generated were quite large—possibly large enough to be clinically unrepresentative.

That criticism is echoed by Brady et al., who endeavored to measure the width of induced fractures and to correlate that fracture size with detection rates (127). Unlike the 200-400 micrometer fractures in Hassan and Ozer, Brady used an Instron machine to induce incomplete root fractures and distinguished between greater and less than 50 micrometer cracks, with a range of 30-110 micrometers. The sensitivity of CBCT was 27-28% while periapical radiography was just 3%. This demonstrates how significantly

our detection of vertical root fractures can be impacted by the study design and more specifically the width of the fracture.

Patel et al. similarly used cadaver mandibles with induced fractures using an Instron machine to induce incomplete and complete vertical root fractures. They identified a sensitivity of dental imaging to be just 5% and CBCT 57% (122). This has the advantage of some of the attenuation of mandibular alveolus, but full cadaver samples would be most representative, as they discuss. They used phosphor plates for their dental radiographs, which can be of lower resolution compared to CCD and CMOS sensors. They found that the presence of obturation material in canals had an impact on detection of fractures.

Part of what makes vertical root fractures so difficult to visualize radiographically on CBCT is that these fractures are often quite small and the voxel size may be too large to see the crack itself. The Nyquest Theorem identifies the limitation of an image's ability to identify a crack or fracture defect to equal twice the voxel size used to scan the object (22). The Carestream 9000 has a voxel size of 76 micrometers, so by this theorem none of the fractures described by Brady as 30-110 micrometers would be visible on CBCT. This is why when evaluating for a crack on CBCT one must look for the characteristic periodontal bone loss if there is inadequate resolution and excessive noise to visualize the fracture of the root wall. Fayad et al. summarized the five radiographic characteristics of vertical root fracture on CBCT imaging as: "1. Loss of bone in the mid-root area with intact bone coronal and apical to the defect 2. Absence of the entire buccal plate of bone in axial, coronal, and/or 3D reconstructed view 3. Radiolucency around a root where a post terminates 4. Space

between the buccal and/or lingual plate of bone and root surface 5. Visualization of the VRF on the CBVT views" (133). None of these features actually involve visualizing the fracture itself, nor are they going to result in a pathognomonic appearance in all cases.

Furthermore, scan time is a confounding variable that might skew result among in vitro and ex vivo studies imaging root fractures. With a scan time of at least thirty seconds, there will inevitably be some amount of patient movement in a clinical image that will be absent with extracted teeth. Even simple blood flow and breathing will create small movements in a living patient that are impossible to completely eliminated in an imaging process that takes time. Benchtop studies with extracted teeth will artificially improve the image quality of extracted teeth in CBCT volumes because the samples do not move. Therefore, the same root fracture that might be visible on an ex vivo sample could be obscured in a scan of a live patient.

There have also been clinical studies attempting to evaluate root fracture detection. Wang et al. evaluated 135 teeth that were already suspected of being fractured. The sensitivity and specificity of root fractures diagnosed were 26% and 100%, respectively, for periapical radiography and 89.5% and 97.5%, respectively, for CBCT. The sensitivity of CBCT was reduced in the presence of root canal fillings but its specificity remained unaffected (134). Clearly there is a difference in radiographic detection demonstrated here, but that these teeth were already suspected of fractures will inflate the sensitivity of radiographic detection based on this nonrandom sample population.

Edlund et al. in a clinical study evaluated 32 teeth suspected of vertical root

fracture. These teeth were radiographed on iCAT CBCT and then these teeth were surgically evaluated for root fracture. Two oral radiologists interpreted these blinded CBCT volumes for root fractures. They found no correlation between signs and symptoms and presence of fracture. They identified a sensitivity of 87% and 75% for the use of CBCT, and there was no comparison to two-dimensional dental radiography (135).

Figure #11: Surgical confirmation of fracture based on suggestive CBCT findings (135)

Chavda & Mannocci scanned with CBCT and periapical imaging 21 unrestorable teeth, then evaluated for fractures after atraumatic extraction. They identified a sensitivity of 16% for periapical and 27% for CBCT imaging (119). This model, although underpowered, presents a more randomized sample compared to Wang's model because these were not teeth already suspected of fracture, and this may account for their dramatically lower detection rate for both periapical and CBCT imaging. However, it is difficult to refute the possibility that fractures were induced in the process of extraction. Whereas in Wang et al. and Edlund et al. the clinical samples were nonrandom because

they were already suspected of vertical root fracture, these teeth were differently nonrandom because they were all deemed unrestorable and planned for extraction.

Most of these benchtop, ex vivo, and clinical studies have demonstrated that the presence of obturation material has a negative impact on vertical root fracture identification (22,108,119,125,134,136). It is by this logic that Vizzotto demonstrated that detection a mesiolingual canal in maxillary molar retreatments could be improved by first removing radiopaque obturation material prior to scanning with CBCT (118).

Looking to the highest level of evidence available, a recent systematic review and meta-analysis by Chang et al. on the utility of CBCT imaging in the diagnosis of vertical root fractures among endodontically treated teeth. They reported among the four studies included (among which Edlund et al. was included) a range of sensitivity of fracture detection between 84-100% and specificity of 64-100% (3). Despite these seemingly favorable values, they critique the included and many excluded studies for having high bias and limited sample size. They indicate that interpretation of fracture presence on CBCT is a highly subjective and observer dependent process. Ultimately, their systematic review indicates that without further data CBCT is only of limited utility in the diagnosis of clinical root fractures, particularly when considering positive predictive value.

These publications addressing the accuracy in detection of vertical root fractures exemplify the imperfection of existing modalities, and why a new radiographic technology may be superior for teeth suspected of fracture. Such a problem provides the motivation for this study.

SPECIFIC AIMS

The specific aims of the present study are as follows:

- To assess and compare the accuracy of radiographic detection of simulated vertical root fractures between periapical, limited-FOV CBCT, and tomosynthesis imaging.
- To determine how the presence of obturation material in the root canal space impacts radiographic detection of simulated vertical root fractures between periapical, limited-FOV CBCT, and tomosynthesis imaging.
- To compare the level of evaluator certainty in diagnosis of simulated vertical root fractures among periapical, limited-FOV CBCT, and tomosynthesis imaging.
- To correlate increased level of evaluator confidence with accuracy of diagnosis among periapical, limited-FOV CBCT, and tomosynthesis imaging in the diagnosis of root fractures.
- To determine if using two periapical radiographs offers a diagnostic advantage in the detection of simulated root fractures over a single periapical radiograph.

HYPOTHESES

The null hypotheses are as follows:

- There is no difference in accuracy of radiographic detection of simulated vertical root fractures between periapical, limited-FOV CBCT, and tomosynthesis imaging.
- The presence of obturation material in the root canal space has no impact on radiographic detection of simulated vertical root fractures between periapical, limited-FOV CBCT, and tomosynthesis imaging.
- Imaging modality, among periapical, limited FOV CBCT, and tomosynthesis imaging, will have no impact on evaluator confidence in diagnosis of simulated VRFs.
- There is no correlation between increased level of evaluator confidence and accuracy of diagnosis among periapical, limited-FOV CBCT, and tomosynthesis imaging in the diagnosis of root fractures.
- Using two periapical radiographs provides no diagnostic advantage in the diagnosis of VRFs compare to a single periapical radiograph.

MATERIALS AND METHODS

The methods and use of extract human teeth were granted Federal Category 4 exemption for records and tissue specimens by the University of Minnesota Institutional Review Board (**IRB HSC:** 1601E82161) because human tissues utilized were deidentified and previously collected. In this IRB Exception application, Dr. Michael Regan Anderson was identified as primary investigator, Dr. Brian Barsness as faculty

academic advisor, and Dr. Laurence Gaalaas as research collaborator. With the application approved the study was exempted from the full IRB review and further oversight.

TOOTH FRACTURE PILOT

There was an initial pilot project experimenting with methods of fracture induction. Extracted samples of human mandibular molars were instrumented first by establishment of glide path with #10 and #15 Flex-O K-type hand files. Visual patency was established and working length determined at canal exit, resulting in a flush preparation. Tooth samples with overtly oval canal configuration or with multiple canals were treated as multiple canals. Instrumentation followed with ProTaper Gold (Densply Sirona) rotary nickel-titanium files at 300 rpm in sequence from S1 to F4 at 0 to 1mm from canal exit.

The primary investigator experimented with a series of instruments and methods of fracture induction during this pilot. Overall, it became clear that induced fractures of mandibular molars, particularly their mesial roots, often lead to segmental shear fracture of entire pieces of root dentin. It was also observed that desiccation of root dentin led to future propagation of fractures and fragment diatheses. It was thus concluded that tooth samples should be kept moist, particularly after fracture induction for sample stability and control.

Figure #12: Induced fracture typical of fracture pilot. These fractures were too extensive to be clinically relevant. This pilot informed the method of fracture induction for future experiments

Consistent root fractures were inconsistently

induced when wedge was applied from the coronal. When wedging was applied to the apex, these fractures were often too dramatic to be clinically representative.

IMAGING PILOT

A second pilot was endeavored whose intent was to mount maxillary molars in simulated alveolar bone. If acceptable, these samples would be used to compare canal identification and working length assessment between periapical, cone-beam CT, and tomosynthesis imaging. Thirty maxillary molar fully developed human extracted tooth samples were coated with a thin layer of rubber cement to simulate a periodontal ligament, and they were mounted in simulated alveolar bone mixture made of ground walnuts and plaster. The details of this mounting process are described in greater detail in the subsequent section. These teeth were imaged on limited-FOV CBCT and periapical imaging. These tooth samples were then transported to the University of North Carolina, but were unfortunately lost in the mail. For this reason, the details of this pilot are largely omitted from this section.

This pilot was of value to study design despite the unlucky conclusion. The periapical and cone-beam imaging demonstrated that that the simulated alveolus technique achieves an acceptable radiographic appearance, simulating marrow spaces and PDL space. The technique was subsequently modified so that two layers of rubber cement were used instead of one two create a wider and more physiologic PDL. Among adults 32-50 years old, the average PDL width is 0.18mm (137), and a double layer of cement created a simulated PDL closer to these measurements.

TOOTH SAMPLE PREPARATION

For the project at hand, initially one-hundred mandibular premolar extracted tooth

samples were collected with the assistance of a dental student research assistant under supervision of the primary investigator. These teeth were human tooth samples collected by dental students and stored in the UMN SOD Endodontic Research Room for investigations like this.

Tooth samples were stored in 10% formalin. Formalin was utilized for several reasons. The first is practical: these existing samples were already stored in 10% formalin when obtained by the primary investigator. Formalin has been demonstrated to be an acceptable storage medium for many in vitro experiments (138). Formalin has been demonstrated to be effective as a high-level disinfectant (139,140). It is often utilized for in vitro testing because it has low impact on dentin bonding strength (138,141,142), although that is irrelevant to the purposes of this study. The disadvantage of formalin is that it is a hazardous and carcinogenic material (140).

The investigator discarded samples that were incompletely developed, had existing fracture(s) as visualized under microscopic evaluation, featured large restorations apical to the CEJ, alveolar bone was attached, or radicular anatomy so unique that their memorable anatomy might jeopardize blinding of the samples on imaging interpretation.

As each tooth sample was selected from the jar, it was first decoronated at the cemento-enamel junction using a high-speed handpiece with an #878 diamond bur and water irrigation. Decoronation served to facilitate fracture induction as well as to create a more uniform radiographic appearance among tooth samples to eliminate distinctive features (e.g. restorations) that might be memorable to evaluators in the course of their interpretation. Instrumentation of the decoronated root sample was completed first by establishment of glide path with #8 (if necessary), #10, and #15 Flex -O K-type hand

files. Visual patency was established and working length determined at canal exit, resulting in a flush preparation. Tooth samples with overtly oval canal configuration or when multiple canals were present were treated as multiple canals. Instrumentation followed with ProTaper Gold (Dentsply Sirona, York, PA) rotary nickel-titanium files at 300 rpm in sequence from S1 to F4 at 0 to 1mm from canal exit. Canals were irrigated with tap water using ProRinse® side-vented 30-g irrigation syringe (Dentsply Sirona, York, PA) between files. As each sample was decoronated and instrumented as described, it was randomly assigned using a coin-flip into either fracture present or absent groups. The thirty root samples assigned as fracture absent were set aside and stored in formalin to prevent desiccation of the dentin; each sample assigned to fracture present were fractured as follows.

Figure #13: Coin used for randomization

Fractures were induced and artificial. The fracture process was adapted from the protocol described by Mora et al. (143), and the method was refined during the fracture pilot study. As each tooth sample was assigned by coinflip into the fracture group, a small steel wedge was lodged into the canal space of the premolar root sample. 2x2" cotton gauze was placed on the surface of the table as well as on the apex of the root sample. Tapping of a 150 gram flat surgical mallet on the apex of the root with the wedge stabilized on the benchtop induced root fractures. Roots that were broken rather than fractured were discarded and replaced with a new tooth sample selected randomly from among the remaining 100 premolar samples, prepared as above, and incorporated into the fracture group. For fractures where a radicular segment was loose, they were cemented

with Loctite® Super Glue cyanoacrylate to stabilize the segment. Efforts were made to minimize any residual fragment displacement created by excess thickness of glue. This process of assignment to fracture absent and fracture present groups with corresponding induction of fracture was repeated until there were thirty in each group, totaling sixty root samples.

The process of fracture induction occasionally slightly crushed the apex of the root sample as depicted in Figure #14, subtly altering their radiographic appearance. So, an Endo-Z carbide bur on highspeed handpiece with water irrigation was used to resect approximately 1mm of the root end surface in order to eliminate any characteristic impact induced by mallet in the fracture process. Accordingly, the same 1mm resection was performed on the fracture absent teeth.

Figure #14: Flattening damage to apex resulting from fracture induction, sometimes creating a unique radiographic appearance that might indicate to the evaluator the presence of a fracture. For this reason, a 1mm resection was performed on the apex of all samples, regardless of fracture status.

Within these two groups of thirty root samples, they were subsequently subdivided using coin-flip into two more groups, obturated and empty. Thus, the four experimental groups were:

- Unobturated and fracture absent (X)
- Unobturated and fracture present (XC)

- Obturated and fracture absent (F)
- Obturated and fracture present (CF)

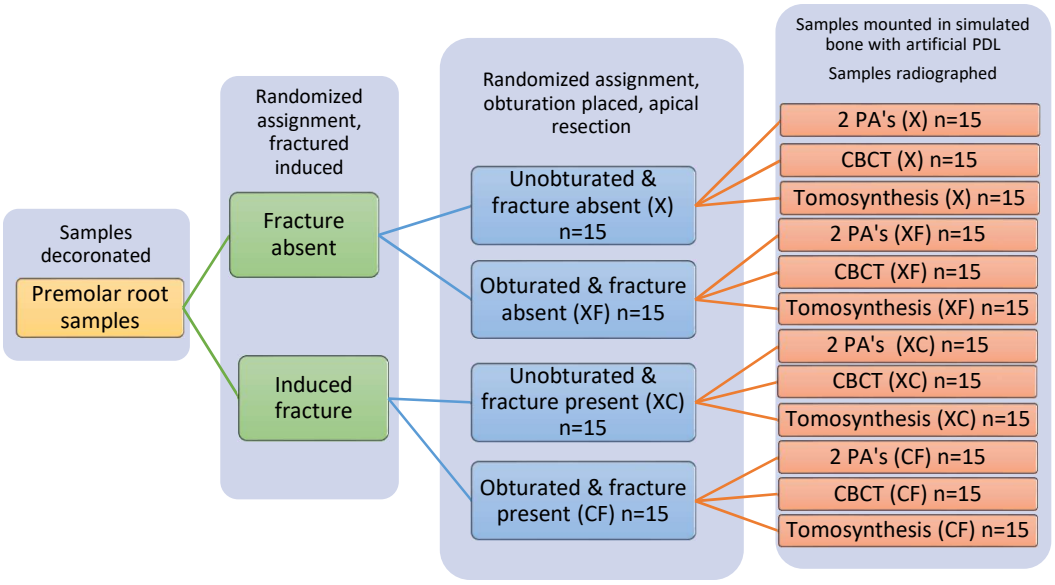

Figure #15: Randomized assignment and sample preparation flowchart

Obturation was completed using ProTaper Gold® gutta-percha molded cones (Densply Sirona, York, PA) coated in Loctite® Super Glue (Henkel, Dusseldorf, Germany) cyanoacrylate cement. The cones were seated completely, even if overextended. Multiple master cones were used for teeth prepared as multiple canals. A scalpel was used to cut any protruding gutta-percha at the coronal and apical extents of the sample so that gutta-percha was flush coronally and apically.

Neither sealer nor alpha-phase warm gutta-percha was used in the obturation process. It was determined that these flowable obturation materials in warm vertical obturation techniques forces radiopaque obturation material into the crack itself, making it much more apparent radiographically. Clinically, vertical root fractures occur most

frequently subsequent to root canal therapy (13). Furthermore, compaction techniques (whether cold lateral, warm vertical, or otherwise) induce sufficient force to break off fractured segments previously induced. For this reason, cyanoacrylate was used to stabilize the fractures and cement gutta-percha obturating material into canals using a single cone technique.

All samples were then mounted into simulated alveolar bone with the assistance of a senior dental student. Each root sample was coated in two layers of Elmer's rubber cement, which provided the radiolucent simulation of a periodontal ligament space. Once dried, roots were individually mounted into simulated alveolar bone using a 2:1 ratio of Type 2 gypsum quick-set plaster (Kerr® Snow White™ Plaster #1, Romulus, MI) mixed with walnuts. The radiopaque plaster and radiolucent walnuts simulate bone marrow spaces. Samples were formed using plastic ice-cube trays as molds. Once set for at least one hour, these samples were individually trimmed to approximately 1.5cm width and depth and 2.0cm in height such that the root sample flush with the surface of the plaster coronally and otherwise completely contained within the plaster. Each sample was marked by and experienced dental clinician to indicate approximate central and shift image horizontal angulations to be used in periapical and tomosynthesis imaging.

Figure #16: Photographs of mounted sample X2 (unobturated and fracture absent) and F3 (obturated and fracture absent). Ink lines provided a rough indication of shifted angles for periapical and tomosynthesis imaging.

IMAGING

These sixty prepared and mounted samples were all imaged using three modalities: periapical imaging, cone-beam CT, and tomosynthesis.

Figure #17: Two-dimensional radiographic settings

Periapical imaging was performed using Carestream RVG 6100 size 2 intraoral sensor (Kodak, Rochester, NY). This sensor is a CMOS Scintillator with a 19 micron pixel dimension, 4096 grey levels, and 24 lp/mm resolution (144). The Preva DC intraoral X-ray source was set at 70 kVp, 6 mA and 0.160 seconds exposure time. Samples were placed directly on the sensor and covered in approximately 1cm thick layer of boxing wax. Radiographs were exposed at both a straight angle and shifted angle of approximately 20 degrees.

Figure #18: Imaging setup for periapical imaging

Cone-beam images were obtained on a Carestream 9000 limited-field of view cone-beam CT (Kodak, Rochester, NY). They were placed on an experimental manifold fabricated by the primary investigator. Each sample was imaged individually under pediatric settings at 68 kVp, 2.0 mA, total scan time 10.80 seconds, and a voxel size of 76 micrometers. Mounted tooth samples were surrounded circumferentially in an approximately 1 cm thick layer of boxing wax to simulate soft tissues attenuation.

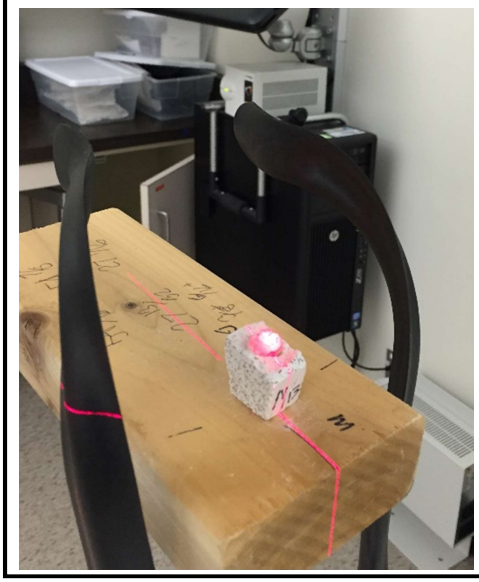

Figure #19: Imaging manifold for CBCT imaging.
Note: all samples in this study were also surrounded by an approximately 1 cm layer of wax, which is not featured in this photo

After periapical and CBCT imaging was complete at the University of Minnesota Division of Endodontics, all samples were shipped to University of North Carolina where they were exposed to tomosynthesis imaging by collaborators in the Zhang lab. Technical details for imaging techniques have been previously described (113,117). Mounted tooth samples were placed atop the tomosynthesis intraoral sensor prototype beneath a 1cm slab of boxing wax to simulate soft tissue attenuation. They were imaged with stationary intraoral tomosynthesis with anode voltage of 70 kVp and each source producing 7mA of tube current. Tomosynthesis images were recorded on a CMOS sensor at one frame per second. A computer system was used using a simultaneous algebraic reconstruction (117)

to produce forty-five slices of variable thickness, typically 500 micrometers. Computation time for reconstruction took about ten seconds.

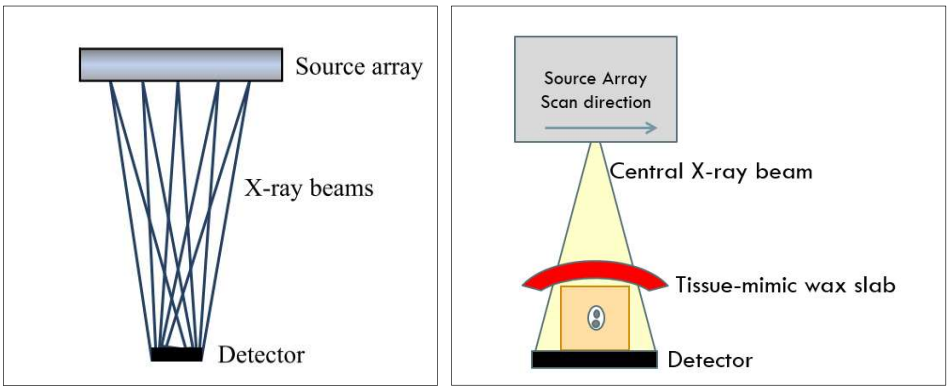

Figure #20: System diagram and imaging for tomosynthesis

Tomosynthesis stacks were exposed from a series of angles—centered, right, left, and vertical. For the purposes of this study, only the centered images were included for interpretation by evaluators. These images were then mailed on drive to the primary investigator.

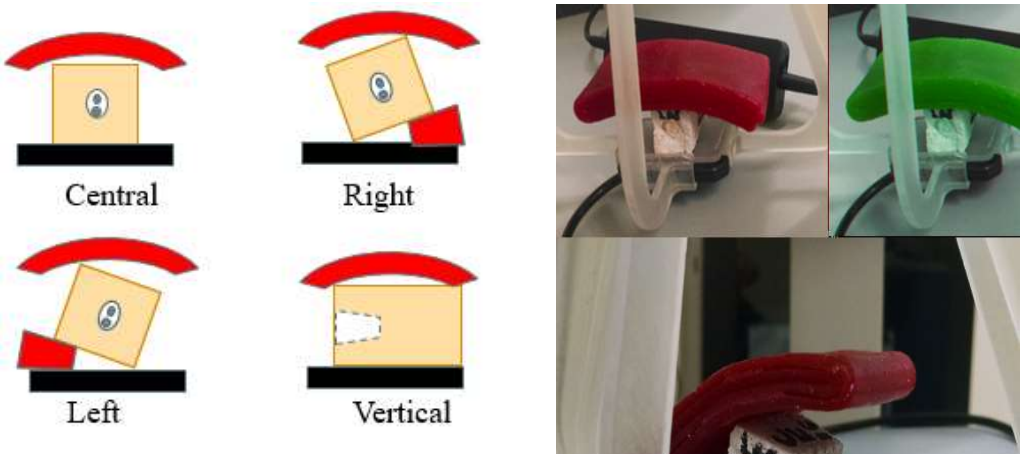

Figure #21: Representation of the four tomosynthesis imaging angles. For the present study, only the central angle was included for evaluation

INTERPRETATION

All imaging data were interpreted by five blinded, calibrated evaluators. The evaluators included four endodontists and one oral radiologist. The written instructions for interpretation are attached in “Appendix II: Evaluator instructions”. All evaluators were provided these written instructions and an in person instructional session and calibration, except for one examiner who was calibrated by telephone. They were introduced to the protocol and associated technologies with opportunities for questions.

Verification that monitors were of diagnostic resolution and contrast using a TG18-QC test pattern, as is pictured at the end of Appendix II: Evaluator Instructions. This test pattern, used with permission of the American Association of Physicists in Medicine, is a synthetic pattern based on a the description provided in the TG18 Report and is scaled down in this publication, although it would be viewed at one-to-one relationship between image pixels and display pixels in its use (145).

The monitor information for viewing images are as follows:

Evaluator 1: Dell P1913S 19” LED monitor at 1280x1024 pixel resolution at 60 Hz.

Evaluator 2: Dell 2713 27” LED monitor at 2560x1440 pixel resolution at 60 Hz

Evaluator 3: Dell P2213 22” LED monitor at 1680x1050 pixel resolution at 60 Hz.

Evaluator 4: Samsung U28E510D 28" Ultra HD 4K LED Monitor at 3840x2160 pixel resolution at 60 Hz.

Evaluator 5: Dell P2213 22” LED monitor at 1680x1050 pixel resolution at

60 Hz.

The original imaging samples were compiled, deidentified, and randomized using a random number generator (146), identified as blinded Samples #1 through #180. That random number generator (146) was subsequently used to create 20% repeats from among these original samples; Samples #181 through #216 constituted these repeats for the purpose of evaluating intra-examiner reliability.

Evaluators were provided a drive containing a Microsoft Excel spreadsheet for data recording and a list folders titled by sample number—#1 through #216. They were instructed to open CBCT and tomosynthesis volumes in RadiAnt DICOM Viewer (Version 3.4.2, Medixant, Poznan, Poland). Evaluators were provided instructions on the use of this software and manipulation of imaging, including adjustment of contrast and brightness. CBCT volumes would present by default the axial slice perspective. It has been consistently demonstrated that axial slices are significantly more accurate than sagittal and coronal slices in detecting vertical root fractures (126,146–148), and the axial perspective is routinely the primary view in studies evaluating the presence of vertical root fractures (117,118,142,149,150) because this perspective is perpendicular to the direction of VRF propagation (131). Nonetheless, evaluators were trained how to view the coronal and sagittal perspective for evaluation at their discretion; it was only requisite to evaluate the entire volume from the axial perspective. Periapical radiograph samples were exported as TIFF files to be opened directly into default image viewing software.

Evaluators, as described in Appendix II, accessed each sample in numerical order without going back after viewing a sample. For each sample, an evaluator recorded two pieces of information: presence/absence of fracture and their level of confidence in that

assessment. Fracture presence was a binary 0/absent or 1/present. Level of confidence was recorded on a scale of 1 to 5: 5 signifying 100% confidence, 3 signifying 50% confidence, and 1 signifying 0% confidence. There were one of each of these recording per sample among CBCT and tomosynthesis images. For periapical images, there were two images contained in each folder. Evaluators viewed image #1 independently and recorded fracture presence and confidence under sample "a" (e.g. #4a). Then, image #2 was viewed and a new assessment would be made considering both samples in diagnosis (e.g. #4b), without then making a change to the first assessment. The evaluator could use the pair of images rather than just the second image alone. This dual assessment construct among periapical images addresses the utility of single versus multiple angles in the identification of fractures in periapical radiographs.

STATISTICS

Evaluator data were compiled and analyzed using SAS V9.3 (Cary, NC). A generalized estimating equations (GEE) model was utilized. GEE models are a sort generalized linear model that allows for evaluation of regression parameters (151). Such parameters include imaging modality, observer, obturation status, fracture presence, and confidence. What makes GEE appropriate in this case is that it considers the potential correlation of the repeated assessments on the same samples.

The evaluator interpretation data for cracks were evaluated based on imaging modality for sensitivity, specificity, and overall accuracy, both based on evaluators as individuals as well as in aggregate. These variables were also correlated with the impact of obturation on sensitivity, specificity, and accuracy. These factors were correlated with

relationship between evaluator confidence and accuracy to determine if subjective reported confidence is associated with increased accuracy.

RESULTS

SENSITIVITY, SPECIFICITY & ACCURACY

Analysis of data is listed below in a series of tables describing sensitivity, specificity and accuracy of fracture diagnosis by evaluator as well as in aggregate. Each modality is listed.

As described in the methods section, each sample with periapical imaging included a pair of radiographs. Evaluators would make an assessment for the first image (sample PAa) and then make a second assessment based on having the pair of images (PAb). In other words, CBCT and tomosynthesis images were compared with both an individual as well as a pair of periapical radiographs taken from differing angles.

The following table includes a generalized estimating equations modeling of sensitivity of fracture detection based on modality. These sensitivities are listed in Table #3 based on each evaluator, obturation status, and overall. The difference between imaging modality and sensitivity was statistically significant ($p=0.0067$). The effect of obturation overall was statistically significant ($p=0.0231$). Sensitivity was greatest with the use of CBCT imaging (92.5% overall) and least with a single periapical image imaging (65.3% overall). Tomosynthesis (75.0%) was superior to a single periapical image (PAa) in fracture detection, but less than the pair of periapical images combined (PAb, 80.5%).

In a similar format within Table #4, the calculated specificities based on each evaluator, obturation status, and overall are compared. Unlike sensitivity, there was not a significant difference between imaging modality (p=0.4211). The calculated sensitivities ranged between 81.8% for tomosynthesis 90.7% for a single periapical radiograph. Neither was there a significant interaction between modality and obturation status (p=0.3138). Tomosynthesis, while demonstrating an improvement in sensitivity, had the lowest specificity among the imaging modalities. The impact of obturation did not have a significant impact on sensitivity, both overall (p=0.6774) as well as by modality.

With respect to overall accuracy, Table #5 describes accuracy in the same format as sensitivity and specificity. Although there was a strong trend towards significance, the overall effect of modality was not statistically significant (p=0.0594). As will be soon discussed, it seems likely that this value would likely be statistically significant with further training and familiarity with tomosynthesis technology, due to fewer false positives. The estimated accuracies from the model are 86.1%, 78.0%, 81.5%, and 76.1% for CBCT, PAb, and tomosynthesis, respectively. The impact of obturation status on accuracy was also not statistically significant, (p=0.1084).

Table #3: Effect of Imaging Modality and Obturation Status on Sensitivity (%)

Evaluator/Modality	Filled	Not Filled	Overall
Evaluator 1			
CBCT	86.7	93.3	90.0
PAa	33.3	73.3	53.3
PAb	53.3	86.7	70.0
Tomo	46.7	80.0	63.3
Evaluator 2			
CBCT	86.7	100	93.3
PAa	66.7	86.7	76.7
PAb	73.3	100	86.7
Tomo	66.7	86.7	76.7
Evaluator 3			
CBCT	86.7	93.3	90.0
PAa	40.0	93.3	66.7
PAb	53.3	100	76.7
Tomo	46.7	80.0	63.3
Evaluator 4			
CBCT	80.0	93.3	86.7
PAa	46.7	80.0	63.3
PAb	60.0	93.3	76.7
Tomo	66.7	80.0	73.3
Evaluator 5			
CBCT	86.7	93.3	90.0
PAa	46.7	86.7	66.7
PAb	53.3	93.3	73.3
Tomo	73.3	86.7	80.0
Overall			
CBCT	*85.3*	*94.7*	**92.5**
PAa	*46.7*	*84.0*	**65.3**
PAb	*58.7*	*94.7*	**80.5**
Tomo	*60.0*	*82.7*	**75.0**

SAS V9.3 was used for the analysis.

Table #4: Effect of Imaging Modality and Obturation Status on Specificity (%)

Evaluator/Modality	Filled	Not Filled	Overall
Evaluator 1			
CBCT	80.0	93.3	86.7
PAa	100	93.3	96.7
PAb	93.3	93.3	93.3
Tomo	93.3	93.3	93.3
Evaluator 2			
CBCT	66.7	60.0	63.3
PAa	80.0	86.7	83.3
PAb	73.3	66.7	70.0
Tomo	86.7	80.0	83.3
Evaluator 3			
CBCT	66.7	93.3	80.0
PAa	100	80.0	90.0
PAb	80.0	80.0	80.0
Tomo	80.0	66.7	73.3
Evaluator 4			
CBCT	93.3	100	96.7
PAa	100	86.7	93.3
PAb	93.3	93.3	93.3
Tomo	93.3	80.0	86.7
Evaluator 5			
CBCT	80.0	80.0	80.0
PAa	93.3	86.7	90.0
PAb	100.0	80.0	90.0
Tomo	66.7	60.0	63.3
Overall			
CBCT	*77.3*	*85.3*	**83.1**
PAa	*94.7*	*86.7*	**90.7**
PAb	*88.0*	*82.7*	**86.9**
Tomo	*84.0*	*76.0*	**81.8**

SAS V9.3 was used for the analysis.

Table #5: Effect of Imaging Modality and Obturation Status on Accuracy (%)

Evaluator/Modality	Filled	Not Filled	Overall
Evaluator 1			
CBCT	83.3	93.3	88.3
PAa	66.7	83.3	75.0
PAb	73.3	90.0	81.7
Tomo	70.0	86.7	78.3
Evaluator 2			
CBCT	76.7	80.0	78.3
PAa	73.3	86.7	80.0
PAb	73.3	83.3	78.3
Tomo	76.7	83.3	80.0
Evaluator 3			
CBCT	76.7	93.3	85.0
PAa	70.0	86.7	78.3
PAb	66.7	90.0	78.3
Tomo	63.3	73.3	68.3
Evaluator 4			
CBCT	86.7	96.7	91.7
PAa	73.3	83.3	78.3
PAb	76.7	93.3	85.0
Tomo	80.0	80.0	80.0
Evaluator 5			
CBCT	83.3	86.7	85.0
PAa	70.0	86.7	78.3
PAb	76.7	86.7	81.7
Tomo	70.0	73.3	71.7
Overall			
CBCT	*81.3*	*90.0*	**86.1**
PAa	*70.7*	*85.3*	**78.0**
PAb	*73.3*	*88.7*	**81.5**
Tomo	*72.0*	*79.3*	**76.1**

SAS V9.3 was used for the analysis.

IMPACT OF OBTURATION

Generalized estimated equations modeling was used to correlate the relationship between the presence of obturation material on the sensitivity, specificity, and accuracy of fracture detection. Obturation significantly decreased the sensitivity (p=.0023) and accuracy (p=0.0260) with periapical radiographs. Obturation also significantly reduced sensitivity of fracture detection overall, whereas it did not have an impact on specificity and accuracy otherwise.

Table #6: Significance of obturation status on fracture identification

	Sensitivity	Specificity	Accuracy
CBCT	p=0.4369	p=0.3237	p=0.1813
PAb	p=0.0023	p=0.4127	*p=0.0260*
Tomo	p=0.1294	p=0.2689	p=0.3673
Overall	*p=0.0231*	p=0.6774	p=0.6774

SAS V9.3 was used for the analysis. P-values less than 0.05 were considered statistically significant.

EVALUATOR CERTAINTY

By adding the certainty variable to the regression, evaluator confidence could be correlated with their accuracy. Generalized estimated equations indicated a statistically significant relationship (p=0.0022) between increased confidence and accuracy, wherein the calculated odds ratio (95% CI) was 1.52 (1.11-2.08). So, the odds of being accurate are 1.52 higher for a 1 increased integer in evaluator certainty. In other words, evaluators were over three times more likely to be corrected with a reported confidence of 5 than 3.

RELIABILITY

Intra-examiner reliability was assessed based on the 20% repeat interpretations included in the evaluated image set. Each evaluator's reliability, or consistency, is reported below. The intra-examiner reliability ranged from 64% to 81%, which is a

substantial but imperfect level of agreement. This will be discussed in reference to similar observer studies.

Table #7: Intra-examiner reliability

Evaluator 1	Kappa = 0.742
Evaluator 2	Kappa = 0.659
Evaluator 3	Kappa = 0.636
Evaluator 4	Kappa = 0.793
Evaluator 5	Kappa = 0.810
Average intra-examiner reliability	Kappa = 0.729

Similarly, a reliability assessment was calculated based on modality in the form of inter-examiner reliability. This compared the five raters pooled for the non-repeated data, meaning the first 180 samples. The calculated kappa values, as well as a pooled inter-examiner score are included below. The greatest inter-rater consistency was among CBCT at 68%. The lowest was for tomosynthesis imaging at 54%. The average inter-examiner reliability across the imaging modalities was 64%.

Table #8: Inter-examiner reliability

CBCT	Kappa = 0.684
PAa	Kappa = 0.651
PAb	Kappa = 0.664
Tomosynthesis	Kappa = 0.537
Overall inter-examiner reliability	Kappa = 0.639

NUMBER OF PERIAPICAL RADIOGRAPHS

Table #9 below describes how the use of a single periapical radiograph compares to the use of a pair of radiographs taken from different angles. For both sensitivity and accuracy, the rate improved both among obturated, unobturated, and overall. It is also interesting to note that specificity slightly decreased with the use of a second image. This trend makes sense. Specificity reflects false-positives in fracture detection. If a fracture was falsely identified in the first radiograph, the evaluators tended to still identify that a

fracture was present. However, if a fracture was not falsely identified on the first image, the second image provided a second opportunity to indicate a false-positive, thereby decreasing sensitivity between first image and a pair of images. However, this may be more a factor of study design than clinical reality.

Table #9: Number of periapical radiographs

	Obturated	Unobturated	Overall
Sensitivity			
PAa	*46.7*	*84.0*	**65.3**
PAb	*58.7*	*94.7*	**80.5**
Specificity			
PAa	*94.7*	*86.7*	**90.7**
PAb	*88.0*	*82.7*	**86.9**
Accuracy			
PAa	*70.7*	*85.3*	**78.0**
PAb	*73.3*	*88.7*	**81.5**

DISCUSSION

To summarize the ability of evaluators to diagnose induced vertical root fractures in extracted root samples, the following table summarizes the sensitivity, specificity, and overall accuracy based on the pooled evaluator data.

Table #10: Interpretation summary

	Obturated	Unobturated	Overall
Sensitivity			
CBCT	*85.3**	*94.7**	**92.5***
PAa	*46.7**	*84.0**	**65.3***
PAb	*58.7**	*94.7**	**80.5***
Tomo	*60.0**	*82.7**	**75.0***
Specificity			
CBCT	*77.3*	*85.3*	**83.1**
PAa	*94.7*	*86.7*	**90.7**
PAb	*88.0*	*82.7*	**86.9**
Tomo	*84.0*	*76.0*	**81.8**
Accuracy			
CBCT	*81.3*	*90.0*	**86.1**
PAa	*70.7**	*85.3**	**78.0**
PAb	*73.3**	*88.7**	**81.5**
Tomo	*72.0*	*79.3*	**76.1**

SAS V9.3 was used for the analysis. P-values less than 0.05 were considered statistically significant, and significant differences indicated with *.

Figure #22: Interpretation summary graph

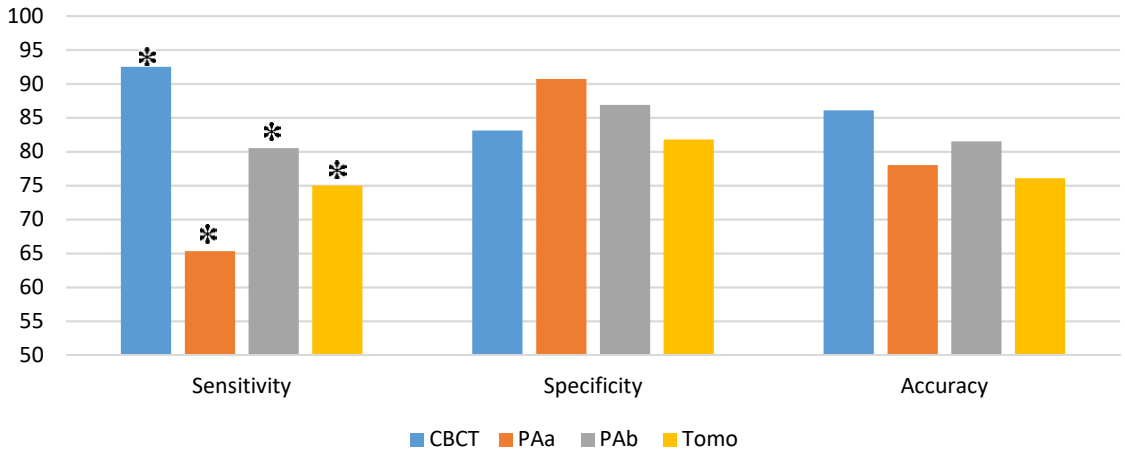

Within the limitations of this study, it appears that intraoral tomosynthesis may provide an advantage in the diagnosis of vertical root fractures. CBCT remains the most accurate and sensitive means of detecting root fractures directly. Furthermore, as was discussed in literature review, CBCT imaging also allows for evaluation of characteristic bone loss patterns that surround the fracture and aid in their diagnosis. Of course, since these fractures were induced among extracted teeth, in this study there was no periradicular bone loss or characteristic boney defects to identify.

While sensitivity of tomosynthesis was superior to a single periapical image, there was not a significant difference in terms of specificity. It is much easier to determine when a fracture is present than to say assuredly that a fracture is absent. However, upon reflection, there are a series of reasons why the specificity of tomosynthesis may be depressed, which would also result in a depressed accuracy values, due to increased evaluator false positives.

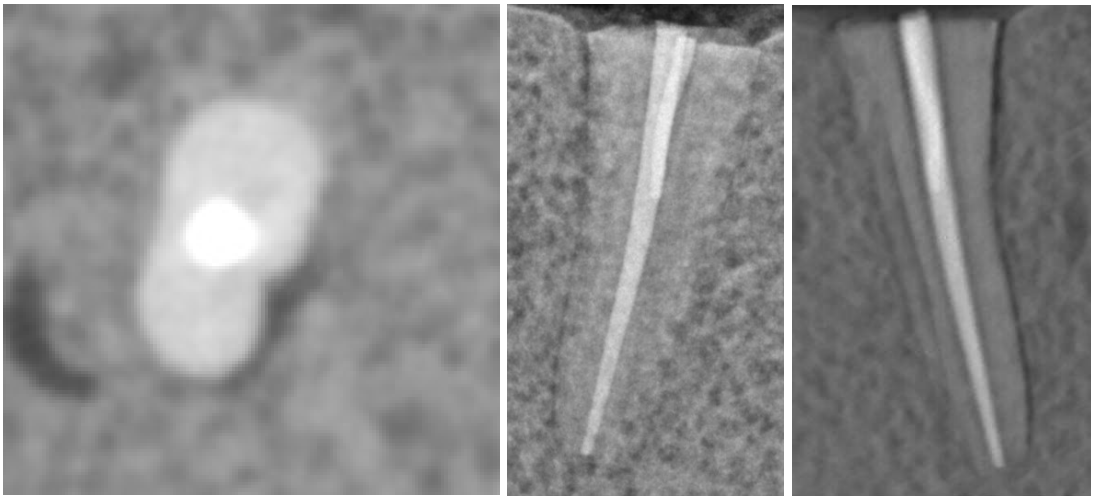

Figure #23: Obturated and fracture present sample (F5) CBCT axial slice, periapical, and tomosynthesis slice demonstrate how the proximal root concavity evident on CBCT creates a radiolucent band on tomosynthesis imaging that was often interpreted as a fracture by examiners.

There are several sources of false positives that can partially account for this observation. External root concavities often created artifacts that seemed to resemble vertical root fractures.

One morphological variant that is quite common among mandibular premolars (which all the experimental samples were) that will feature a root concavity are those with Type IV canal anatomy and C-shaped canals. The prevalence of Type IV anatomy is 24% among mandibular first premolars, with 14% having C-shaped canal systems (152). These findings are higher in individuals of African (153) and Asian (154) descent . Such samples in this study were often confused as fractured. These Type IV featured well-defined vertical radiolucent bands due to their external root concavities resulting in an artifact.

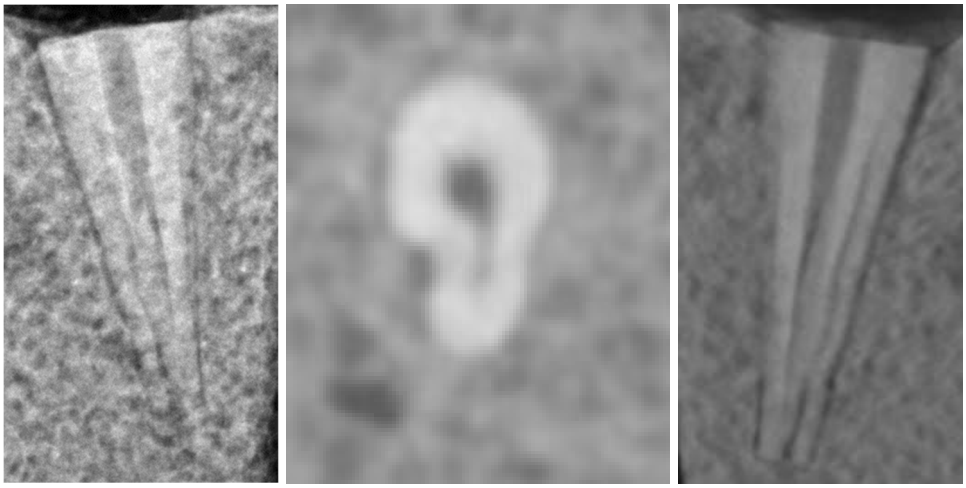

Figure #24: Unobturated & fracture absent sample (X7) with Type IV & C-shape anatomy in the apical third. The CBCT axial slice (middle) reveals no fracture and a radicular concavity that results in a radiolucent defect confused as a fracture in the tomosynthesis image (right)

It stands to reason that these types of artifacts could be more readily identified with further experience, access, training, and familiarity to tomosynthesis technology. All

of the evaluators in this study were familiar and comfortable in the interpretation of periapical images and CBCT volumes. With additional training and calibration, the rate of false positives might be decreased, thereby resulting in a more competitive sensitivity, specificity and accuracy.

FRACTURE INDUCTION

Review of related literature elucidates questions of study design and how they might impact conclusions drawn from the data. The first point has to do with the nature of the root fractures, whether clinical or induced. Clinical samples of root fractures are in many ways preferable with the disadvantage of limited availability, especially because their confirmed detection can be so difficult. When these teeth are still in the mouth, as in Edlund et al, it cannot be guaranteed that the teeth were fractured without surgical visual exposure. Ex vivo samples as in Wang et al. might have fractures induced, propagated or affected in the extraction process.

Induced fractures are commonly evaluated, but there is such variability and unpredictability in the size and location of the induced fractures without assurance that the fractures are clinically representative. This point is iterated by Brady et al. and is a worthy critique. Their protocol allowed for fractures between 30-110 microns for incomplete fractures, and under 300 microns for complete fractures. Hassan and Ozer induce fractures with a chisel and hammer, which resulted in fractures larger than 200 microns.

Another concern with ex vivo and induced samples is that the extent of cracks can change over the course of the experiment. It may be possible that over time induced fractures can continue to propagate. This is certainly true of desiccated teeth that small

cracks and incomplete cracks when desiccated will propagate and turn into complete cracks—this was observed during the initial pilot study. This concern is particularly true in the present study where teeth had to be prepared and imaged at one institution and transported 1,100 miles for tomosynthesis imaging. In this case, it was not possible to image the teeth at the same time. The use of cyanoacrylate and mounting of the teeth in rubber cement and plaster may have aided in stabilizing the fractures. It does not appear that there were any noticeable changes as a result of this delay between modalities, but that may be possible.

Induced fractures were utilized in the present study because it was the only practical option based on availability and the need to transport them. The advantages were that the tooth samples could be prepared in a controlled fashion and allowed for a large sample of teeth.

The most glaring disadvantage of induced fractures is that they are not necessarily clinically representative and there is such unpredictability in the resultant fracture. It seems clear that these fractures were relatively large and likely overstated. The size and extent of fractures were certainly variable. That being said, root fractures are inherently clinically variable over the course of their progression.

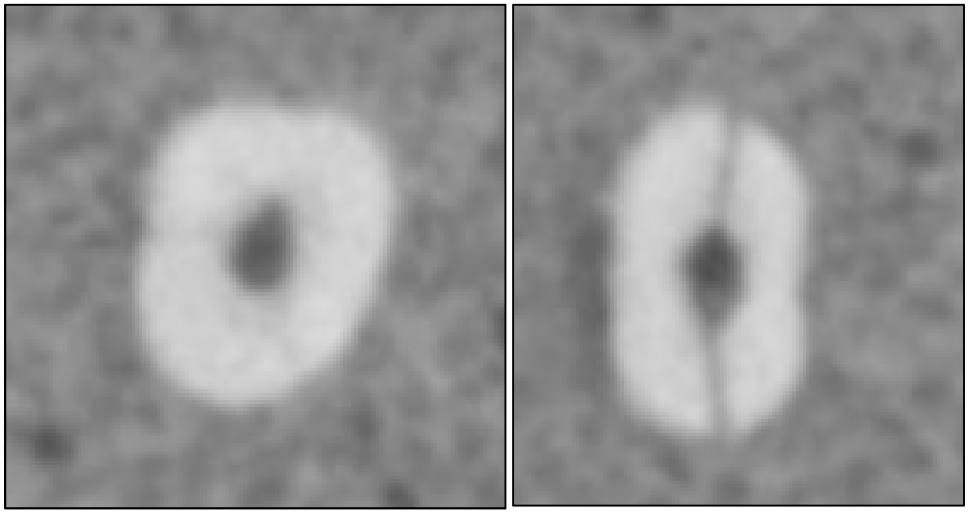

Figure #25: A comparison of axial slices from two fractured samples (CF12 & CF14), demonstrating the variation of fracture size and resulting ease of detection

It may be preferable to induce fractures with the use of an Instron machine. Brady et al. and Patel et al. used Instron machines to induce both complete and incomplete fractures. For Brady et al, increased force was applied until a 20% decrease in resistance was detected (127). The induced fractures in that case are more likely to be incomplete fractures and understated compared the majority of induced fractures in this study. In any case, the purpose of this study was to compare the technologies. Even if the fractures were induced and potentially large, the comparison established is still a fair comparison. The next step would be to apply the technology clinically, which is already an IRB approved project to be undertaken at UNC (ClinicalTrials.gov: NCT02873585).

IMPACT OF OBTURATION

It is worth pointing out the method of obturation in this study is to some extent problematic. A single cone technique was used, and glue was used instead of sealer. As previously discussed, the justification for this design was out of concern that thermoplasticization, warm gutta-percha, and sealer would push into existing fractures

with radiopaque material. This concern is especially real when the size of these fractures were relatively large.

However, not only was the obturation technique used in this study not clinically representative, it also created its own slightly misleading artifact. The radiolucent band adjacent to the obturation material could deceptively resemble root segment diastasis, as seen in Figure #26.

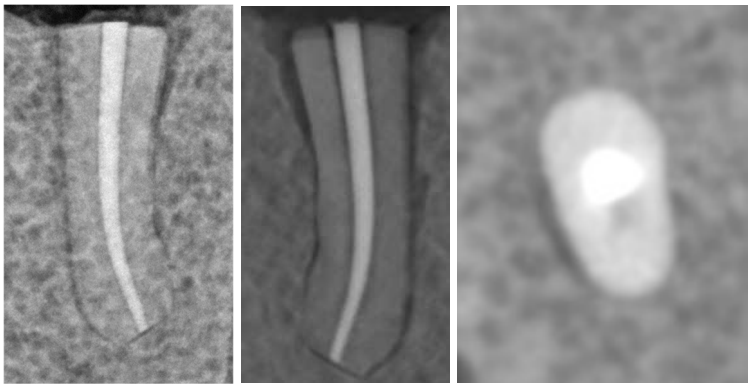

Figure #26: Obturated and fracture absent sample (F11) demonstrating radiolucent bands adjacent to gutta-percha due to experimental obturation technique that could suggest root separation

Analyzing the impact of obturation material in fracture detection provides clinically applicable information. Obturation significantly reduced sensitivity of fracture detection overall ($p=0.0231$). Obturation material did also significantly decrease accuracy with periapical radiographs. Furthermore, although not statistically significant in extent, the accuracy was higher in each modality in unobturated teeth than in obturated teeth.

These data suggest that removing obturation material from canal will improve sensitivity of detection of root fractures in periapical, CBCT, and tomosynthesis imaging. Vizzotto demonstrated that removal of obturation material from canals in endodontic retreatment can improve detection and location of a missed MB2 canal in maxillary molars (155). A similar suggestion can be drawn from these data—removal of obturation

material may improve sensitivity of fracture detection, although this practice is not compulsory.

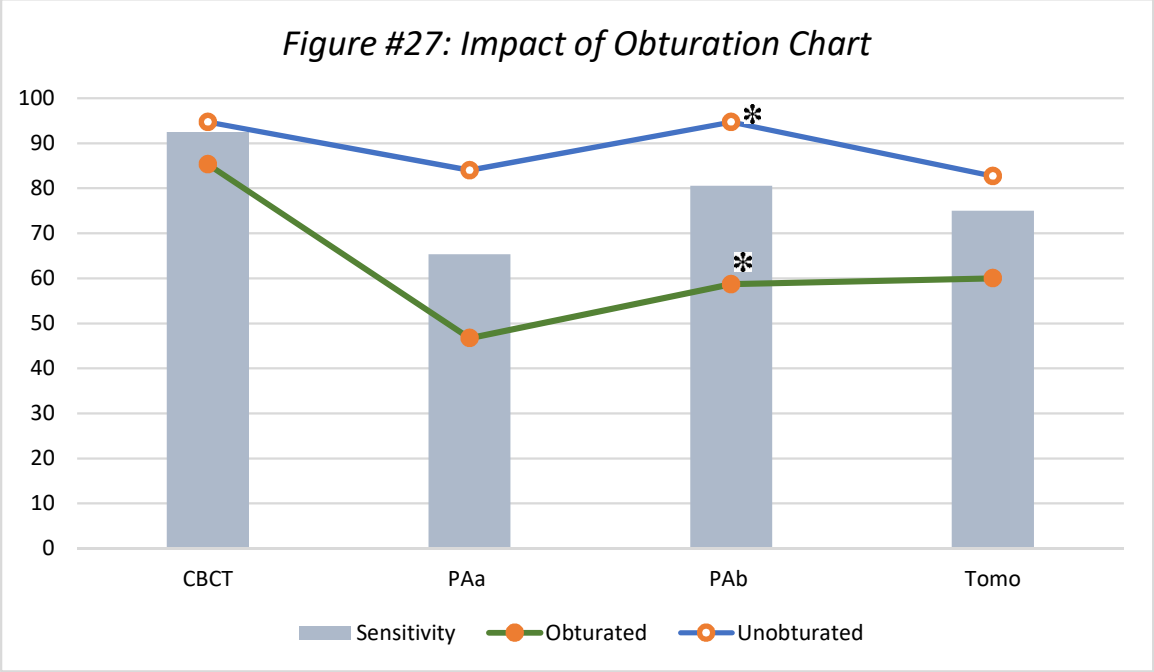

If we apply these data to clinical practice, this presents another advantage of tomosynthesis imaging. The presence of obturation material significantly decreased sensitivity and accuracy of fracture detection in periapical imaging ($p=0.0023$ and $p=0.0260$, respectively), while there was not a significant difference for CBCT and tomosynthesis imaging. Therefore, tomosynthesis images demonstrate a diminished impact of obturation status in root fracture detection compared to periapical imaging. Since the vast majority of root fractures occur in endodontically treated teeth, this trend is an advantage afforded by tomosynthesis imaging technology.

REFLECTIONS ON TOMOSYNTHESIS IMAGING

This pilot study demonstrated several unique characteristics of tomosynthesis imaging that inform improvements in this study and how the technology may be useful

clinically, whether with respect to fracture identification or otherwise.

It is quite clear that although tomosynthesis provides a degree of three-dimensional information based on z-axis scrolling, tomosynthesis is still an angle dependent image. Evaluators in this study were only provided a single tomosynthesis to evaluate, although in the imaging process four different angles were captured (centered, left, right, vertical), as described in Methods. However, further review of these differing angled images resulted in quite different resolution of root fractures in tomosynthesis, as poignantly demonstrated in Figure #28. It has been well established that with periapical radiographs, multiple angles provide a diagnostic advantage in identification of periapical radiolucencies (77). So too is it recommended to multiple angulations for the identification of horizontal root fracture when suspected in trauma (156). These same recommendations may be applied to tomosynthesis imaging, especially in the identification of fractures.

This methodological deficiency is probably the most unfortunate consequence of the lost samples resulting in incomplete pilot. The degree to which tomosynthesis imaging is angle dependent may have been revealed though completion of that pilot. There could be great value in repeating this study including multiple tomosynthesis angles rather than simply the central angle.

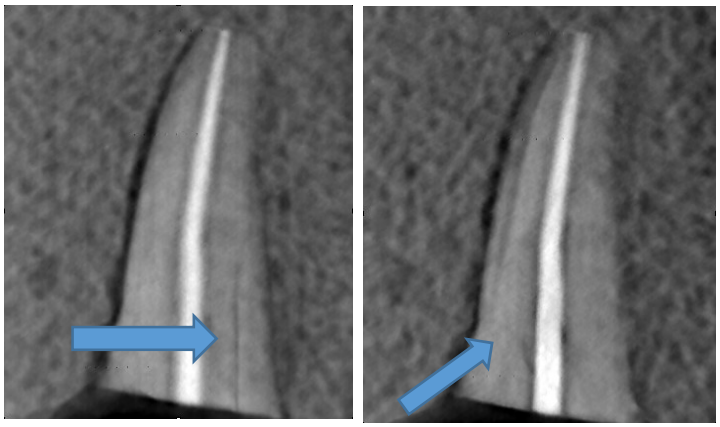

CENTRAL

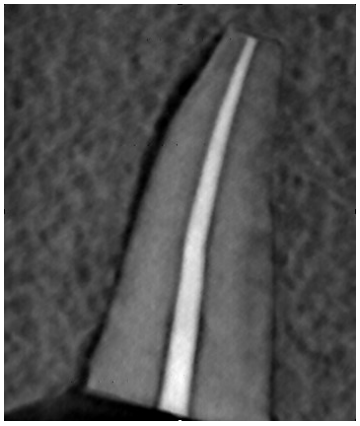

LEFT

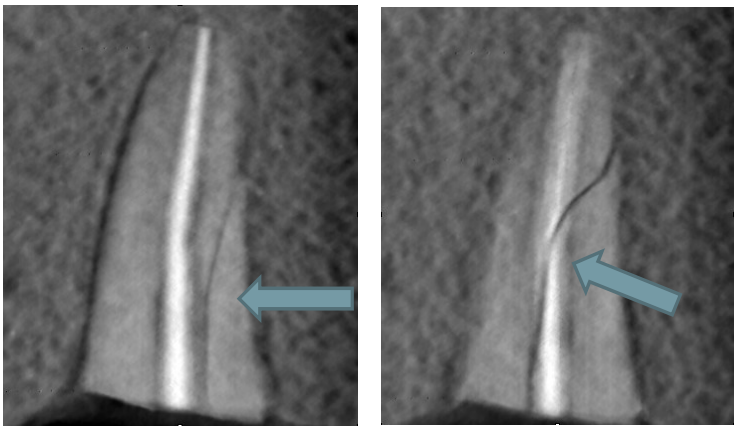

RIGHT

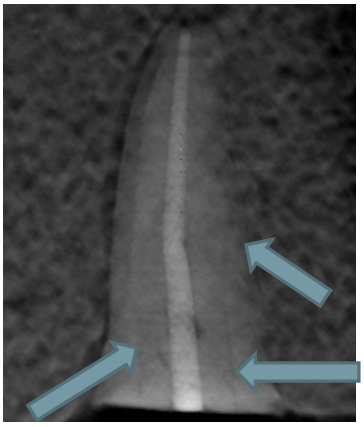

VERTICAL

Figure #28: Fracturing of an obturated sample (CF6) resulted in multiple fractures. Imaging with tomosynthesis at four different angles. The varying angles resulted in quite dissimilar presentation and resolution of those fractures. This exemplifies the great degree to which tomosynthesis is angle dependent in fracture identification.

To ensure accurate reconstruction of the tomosynthesis stack, the source to image and source to target distance is fixed. The geometry of the array and reconstruction, however; dictate that z-axis resolution is greatest at the center of the stack and decreases with increasing distance from center. Navigating tomosynthesis stacks confirms that, quite often, there would be excellent resolution of the tooth sample in the center of the stack. But when scrolling in the z-axis away from the center towards the buccal and lingual extent of the stack, resolution would decrease dramatically. Figure #29 demonstrates this special artifact in resolution. The central slice demonstrates excellent resolution; however, the furthest buccal and lingual slices demonstrate poor resolution. This may have impacted fracture detection in the present study, and would be a major consideration in its clinical utility.

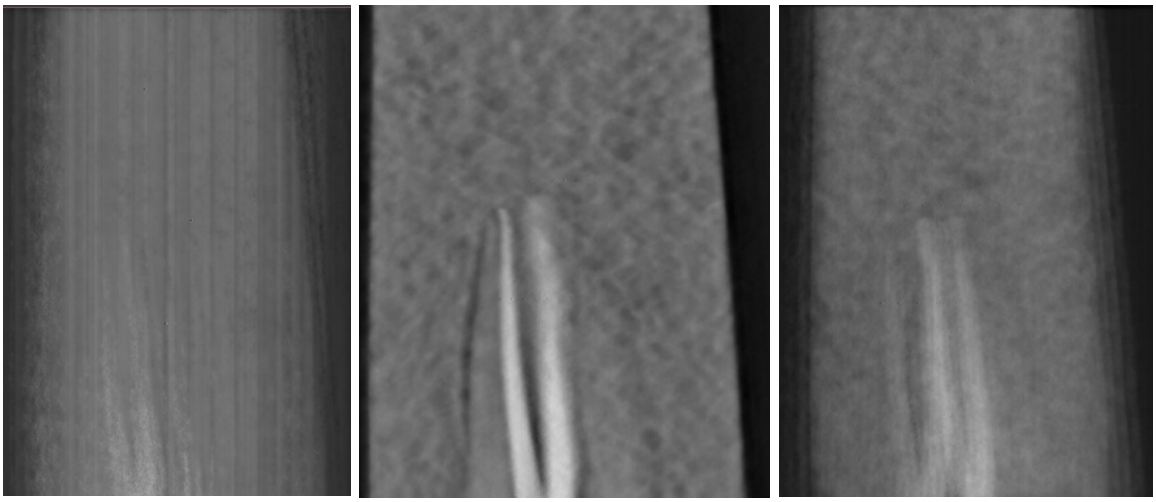

Figure #29: Three slices from a stack of samples CF10. The furthest buccal slice (left), central slice (middle) and furthest lingual slice (right) demonstrate that resolution in tomosynthesis stacks is variable. The greatest resolution is found centrally in the stack with poor resolution on the periphery

RADIOGRAPHS ARE INTERPRETTED, NOT READ

In a pair of landmark publications, Goldman & Pearson demonstrated that radiographic interpretation is exactly that: interpretive and subjective. Among 253 randomized cases evaluated by six different evaluators, there was only 43% agreement on whether or not periapical radiolucencies were present (157). This same group agreed on categorization of endodontic treatment success versus failure 73% of the time (157). These measures are inter-examiner agreement.

Three evaluators from this same group were asked to evaluate the same cases they had evaluated in the 1972 study, and each evaluator only agreed with him or herself 75-83% of the time only six to eight months later (158). So in other words, Goldman's publications demonstrated with periapical imaging an intra-examiner reliability of 75-83% and inter-examiner reliability of 43-73% in periapical radiolucency detection.

Brady similarly presented kappa values for inter-examiner and intra-examiner agreement with repeated measures in evaluation of vertical root fracture presence. Inter-examiner agreement among complete fracture samples imaged on two-dimensional radiography was 28% and 58% for iCAT CBCT. The reported intra-examiner agreement for complete fractures was 38% for two-dimensional imaging and 78% for iCAT CBCT (127).

Intra-examiner agreement in the present study was comparable to these previously reported values in Goldman and Brady. The comparison to Brady is the more important comparison because it specifically refers to fracture identification on periapical and CBCT imaging. Overall, the range of intra-examiner agreement kappa values ranged between 63% and 81% with an aggregated intra-examiner kappa value of 72.9%. These

values correspond well with the previous reports by Goldman and Brady. It further reinforces that interpretation of fractures, as is true with all radiographic interpretation is a subjective process. Unlike with Goldman and Pearson, the repeats in the present study were not temporally distanced by months. These repeats were presented in the same interpretation session, and yet among the repeats examiners effectively contradicted their initial assessment in fracture identification almost 27% of the time.

When the evaluators in the present study were compared for agreement, there was not a significant difference based on modality. Inter-evaluator kappa was the lowest among tomosynthesis images at 54% and greatest among CBCT volumes at 68%, with an overall inter-examiner kappa value of 64%. As previously indicated, it seems quite likely that the relatively depressed agreement for tomosynthesis imaging could be improved with further evaluator training and familiarity with the imaging technology. These inter-rater values are similar to those presented in Goldman and Brady, which affirms in some senses the findings of the present study but also more importantly reiterates the subjective nature of radiographic interpretation. It is certainly conceivable that with more training and familiarity the kappa score for tomosynthesis imaging would improve because it is yet a relatively unfamiliar and unique imaging modality for the evaluators. In any case, the subjectivity of radiographic interpretation is reaffirmed by these data.

FUTURE DIRECTIONS

There are many future directions based on this initial project. The most natural future direction would be to repeat the protocol here with the use of multiple angles of tomosynthesis imaging. As discussed previously, tomosynthesis imaging is angle dependent and Figure #28 clearly demonstrates how multiple angles may be requisite to

adequately evaluate a tooth for a root fracture. Fortunately, these existing samples have already been imaged with four different angles (centered, left, right, vertical). All of the existing imaging could be reevaluated and the odds ratio based on number of angles could be calculated to determine which combination of angles would most predictably detect root fractures. Although it would significantly increase the time required of the evaluate the additional imaging, this would be relatively simple to repeat. The benefit of this comparison is that, in the current study, the comparison is made between a single tomosynthesis image to a pair of periapical images. This may not be a fair comparison. Tomosynthesis may be an imaging modality that requires multiple angles when applied specifically to crack detection.

Another future direction would be to change the method of fracture induction or to use clinical fractures. These fractures may have been overstated, which may limit the applicability of conclusions drawn to in vivo fractures. As other studies have done, the use of an Instron machine might create more subtle fractures. The great clinical challenge is in the detection of early fractures, so identifying a preferred imaging modality for these elusive fractures would be most useful.

Samples would be most representative to use clinically confirmed vertical root fractures. This might mean teeth that are surgically exposed with fractures confirmed. Another method would be using teeth extracted due to vertical root fracture. However, extracted teeth may have had fractures induced or exaggerated in the extraction process.

While the purpose of this study was to evaluate the applications of tomosynthesis in fracture detection. However, it seems that this radiographic technology has many potential applications elsewhere in dentistry.

There are instances in endodontics where a tomosynthesis image may provide more information than a periapical alone. For example, one could investigate how tomosynthesis imaging, or multiple angles of tomosynthesis imaging, compares to PA and CBCT imaging in canal detection. A similar experimental protocol could be used asking evaluators to interpret the Vertucci type canal configuration. If this technology is useful in that regard, it would decrease the time and radiation exposure to patient by reducing the number of shift images or CBCT volumes necessary to determine root canal anatomy. In fact, this study could easily be executed because all of the imaging is already prepared. There are twenty maxillary premolar and twenty mandibular molar extracted tooth samples that are mounted in simulated alveoli and imaged by PA, CBCT and tomosynthesis imaging in a manner identical to the present study.

Intraoperatively, tomosynthesis could be extremely useful in working length determination. An intraoperative working length periapical image in teeth with multiple canals can obscure and confound interpretation due to overlap and flattening of a three-dimensional object onto a two-dimensional image. Often, multiple images and application of the buccal object rule are necessary to adequately interpret working length images with multiple canals. CBCT cannot be used for working images because the tooth must be closed and typically the rubber dam and clamp are removed. A tomosynthesis image using an intraoral sensor would provide three-dimensional imaging for a tooth with files in place. Tomosynthesis could allow the operator to determine in a single image a working length for each file, potentially with greater appreciation of where each file exist the tooth, with fewer requisite images. Utilizing this technology thusly would likely be attractive to most endodontists.

Tomosynthesis imaging could be applied to perforation detection, which can be difficult on periapical imaging. Figure #30 demonstrates two endodontically treated teeth in the same individual who has some severe apical dilacerations. Periapical imaging reveals the severity of these dilacerations, but it is impossible to tell if the obturation in #20 or in the mesiolingual canal of #31 are simply ledged or if they are apically perforated. It is possible a tomosynthesis image, with the same exposure to the patient as a periapical radiograph, could demonstrate that the obturation material is confined to the tooth or if apical perforations are present here.

Figure #30: Endodontic treatment of #20 and #31 in the same individual who has a series of severe apical curvatures. On periapical imaging alone, it is difficult to determine if these teeth have apical perforation. Perhaps s-IOT would identify such perforations.

A similar application could be in the diagnosis of strip perforations, particularly in mesial roots of mandibular molars and mesiobuccal roots of maxillary molars. Strip perforations can be extremely difficult to diagnose on a periapical radiograph alone, but might be easily revealed in a tomosynthesis stack. Furthermore, they could be identified not just the pre-operative or post-operative setting, as is the case with CBCT. Since s-IOT can be utilized with an intraoral sensor as a working imaging modality, it could be a

radiographic technology that is helpful in the recognition of these types of perforations pre-operatively as well as intraoperatively in the course of treatment.

Figure #31: Although the obturation material appears to be confined to the root, it is unclear based on periapical imaging alone if the large cervical preparations in #30 have resulted in strip perforations

And furthermore, the applications of this nascent technology will necessarily continue to present themselves as it is applied in new and different ways.

CONCLUSIONS

Within the limitations of this study, it can be concluded that:

- Stationary intraoral tomosynthesis improves the sensitivity of detection of induced root fractures compared to a single radiograph.
- Limited-FOV CBCT is the most sensitive imaging modality for detection of fractures among obturated and unobturated root samples.
- There is no significant difference in specificity or overall accuracy in fracture detection among periapical, CBCT, and tomosynthesis imaging.
- The presence of obturation material has a statistically significant reduction in sensitivity of fracture detection and accuracy for periapical radiographs. Obturation status did not have a significant impact on sensitivity for

tomosynthesis imaging. So, removal of obturation material may improve fracture detection. Furthermore, tomosynthesis imaging is superior to periapical imaging in root fracture detection insofar as the presence of obturation material does not significantly reduce fracture detection.

- Reported evaluator confidence was directly correlated with increased accuracy in all imaging modalities.
- Utilizing a pair of angled periapical radiographs significantly improves sensitivity of fracture detection.

While it might appear that the utilization of tomosynthesis in fracture detection has merely a modest benefit, when considering the clinical implications of its application this imaging modality becomes highly attractive. Comparing tomosynthesis to a single periapical image, the s-IOT stack provides a great deal of additional information obscured by the periapical image. Tomosynthesis images, unlike CBCT imaging, can be performed intraoperatively in the same way as periapical imaging. The radiation exposure to the patient is comparable to that of periapical imaging. But, the resulting image stack provides three-dimensional imaging that may be incredibly revealing to the clinician. Restricting application of this radiographic technology to fracture detection is myopic. If tomosynthesis can also be utilized for caries detection and periapical radiolucency detection, it could become indispensable.

As it has been applied in medicine and now dentistry, tomosynthesis has been referred to as three-dimensional radiographic technology. I submit that this categorization is misleading. Certainly, it is true that stationary intraoral tomosynthesis imaging provides three-dimensional information. However, this study has demonstrated the extent

to which tomosynthesis imaging is angle dependent, unlike true three-dimensional imaging. Tomosynthesis stacks are also only high resolution towards the center of the stack while the shallowest and deepest planes within the stack demonstrate poor resolution. Instead, this application of tomosynthesis imaging is somewhere between two-dimensional and three-dimensional. When comparing tomosynthesis to two-dimensional imaging instead of CBCT, the benefits of this new technology are clear: more clinical information provided without any drawbacks in terms of ease-of-use, radiation dose, or imaging time.

There are many new avenues of further research may demonstrate how stationary intraoral tomosynthesis can be applied to dentistry and endodontics that will stimulate its application to clinical practice and, perhaps, adoption as an integral part of our clinical armamentarium.

BIBLIOGRAPHY

1 Rivera Eric, Walton E Richard. Cracking The Cracked Tooth Code: Detection and Treatment of Various Longitudinal Tooth Fractures. Endod Colleagues Excell 2008;Summer:2–7.

2 Talwar Sangeeta, Utneja Shivani, Nawal Ruchika Roongta, Kaushik Aishwarya, Srivastava Dhirendra, Oberoy Sukhvinder Singh. Role of Cone-beam Computed Tomography in Diagnosis of Vertical Root Fractures: A Systematic Review and Meta-analysis. J Endod 2016;42(1):12–24. Doi: 10.1016/j.joen.2015.09.012.

3 Chang Edwin, Lam Ernest, Shah Prakesh, Azarpazhooh Amir. Cone-beam Computed Tomography for Detecting Vertical Root Fractures in Endodontically Treated Teeth: A Systematic Review. J Endod 2016:177–85. Doi: 10.1016/j.joen.2015.10.005.

4 Tingberg Anders. X-ray tomosynthesis: A review of its use for breast and chest imaging. Radiat Prot Dosimetry 2010;139(1–3):100–7. Doi: 10.1093/rpd/ncq099.

5 Dobbins James T, McAdams H Page. Chest tomosynthesis: Technical principles and clinical update. Eur J Radiol 2009;72(2):244–51. Doi: 10.1016/j.ejrad.2009.05.054.

6 Dobbins James T, McAdams H Page, Godfrey Devon J, Li Christina M. Digital Tomosynthesis of the Chest. J Thorac Imaging 2008;23(2):86–92. Doi: 10.1097/RTI.0b013e318173e162.

7 Mermuys Koen, De Geeter Frank, Bacher Klaus, et al. Digital tomosynthesis in the detection of urolithiasis: Diagnostic performance and dosimetry compared with digital radiography with MDCT as the reference standard. Am J Roentgenol 2010;195(1):161–7. Doi: 10.2214/AJR.09.3075.

8 Gomi Tsutomu, Hirano Hiroshi. Clinical potential of digital linear tomosynthesis imaging of total joint arthroplasty. J Digit Imaging 2008;21(3):312–22. Doi: 10.1007/s10278-007-9040-9.

9 Geijer Mats, Börjesson Annika M, Göthlin Jan H. Clinical utility of tomosynthesis in suspected scaphoid fracture. A pilot study. Skeletal Radiol 2011;40(7):863–7. Doi: 10.1007/s00256-010-1049-3.

10 Haas Brian M, Kalra Vivek, Geisel Jaime, Raghu Madhavi, Durand Melissa, Philpotts Liane E. Comparison of Tomosynthesis Plus Digital Mammography and Digital Mammography Alone for Breast Cancer Screening. Radiology 2013;269(3):694–700. Doi: 10.1148/radiol.13130307.

11 Shan J, Tucker AW, Gaalaas LR, et al. Stationary intraoral digital tomosynthesis using a carbon nanotube X-ray source array. Dentomaxillofacial Radiol 2015;44(9):1–9. Doi: 10.1259/dmfr.20150098.

12 Rivera Eric M, Walton Richard E. Longitudinal tooth fractures : findings that contribute to complex endodontic diagnoses. Endod Top 2009;16(1):82–111. Doi: 10.1111/j.1601-1546.2009.00243.x.

13 Tsesis Igor, Rosen Eyal, Tamse Aviad, Taschieri Silvio, Kfir Anda. Diagnosis of vertical root fractures in endodontically treated teeth based on clinical and radiographic indices: A systematic review. J Endod 2010;36(9):1455–8. Doi: 10.1016/j.joen.2010.05.003.

14 Sathorn C, Palamara Joseph EA, Palamara D, Messer Harold H. Effect of Root Canal Size and External Root Surface Morphology on Fracture Susceptibility and Pattern: A Finite Element Analysis. J Endod 2005;31(4):288–92. Doi: 10.1097/01.don.0000140579.17573.f7.

15 Andreasen JO Hjørting-Hansen E. Intraalveolar root fractures: radiographic and histologic study of 50 cases. J Oral Surg 1967;25(5):414–26.

16 Walton Richard E. Walton-JOE-1984_p48-56.pdf. J Endod 1984:48–56.

17 Tamse Aviad. Vertical root fractures in endodontically treated teeth: diagnostic signs and clinical management. Endod Top 2006;13(1):84–94. Doi: 10.1111/j.1601-1546.2006.00200.x.

18 Morfis AS. Vertical Root Fractures. Oral Surg Oral Med Oral Pathol 1990;68:631–5.

19 Fuss Z, Lustig J, Tamse A. Prevalence of vertical root fractures in extracted endodontically treated teeth. Int Endod J 1999;32(4):283–6. Doi: 10.1046/j.1365-2591.1999.00208.x.

20 Coppens, C.R.M., DeMoor RJG. Prevalence of vertical root fractures in extracted

endodontically treated teeth. Int Endod J 2003;36:926.

21 Lustig Joseph P, Tamse Aviad, Fuss Zvi. Pattern of bone resorption in vertically fractured, endodontically treated teeth. Oral Surgery, Oral Med Oral Pathol Oral Radiol Endodontology 2000;90(2):224–7. Doi: 10.1067/moe.2000.107445.

22 Todd Randolph. Cone beam computed tomography updated technology for endodontic diagnosis. Dent Clin North Am 2014;58(3):523–43. Doi: 10.1016/j.cden.2014.03.003.

23 Tamse Aviad, Fuss Zvi, Lustig Joseph P, Kaplavi J. An evaluation of endodontically treated vertically fractured teeth. J Endod 1999;25(7):506–8. Doi: 10.1016/S0099-2399(99)80292-1.

24 Testori Tiziano, Badino Mario, Castagnola Marco. Vertical root fractures in endodontically treated teeth: A clinical survey of 36 cases. J Endod 1993;19(2):87–90. Doi: 10.1016/S0099-2399(06)81202-1.

25 Moule a J, Kahler B. Diagnosis and management of teeth with vertical root fractures. Aust Dent J 1999;44(2):75–87. Doi: 10.1016/S0099-2399(83)80150-2.

26 Pitts David L, Natkin Eugene. Diagnosis and treatment of vertical root fracture. J Endod 1983;9(8):338–46. Doi: 10.1016/S0099-2399(83)80150-2.

27 Siqueira Jose F. Periapical Actinomycosis and infection with Propionibacterium Propionicum. Endod Top 2003;6(1):78–95. Doi: 10.1111/j.1601-1546.2003.00037.x.

28 Arola D, Reprogel RK. Effect of Aging on the Mechanical Behavior of Human Dentin. Biomaterials 2005;26:4051–61.

29 Bajaj Devendra, Sundaram Naryana, Nazari Ahmad, Arola D. Age, Dehydration an Fatigue Crack Growth in Dentin. Biomaterials 2006;27:2507–17.

30 Gher ME, Dunlap RM, Anderson MH, Kuhl L V. Clinical survey of fractured teeth. J Am Dent Assoc 1987;114(2):174–7. Doi: 10.14219/jada.archive.1987.0006.

31 Tamse A. Iatrogenic vertical root fractures in endodontically treated teeth. Endod Dent Traumatol 1988;4(5):190–6. Doi: 10.1111/j.1600-9657.1988.tb00321.x.

32 Meister Jr. F, Lommel TJ, Gerstein H, Meister F, Lommel TJ, Gerstein H.

Diagnosis and possible causes of vertical root fractures. Oral Surg Oral Med Oral Pathol 1980;49(3):243–53. Doi: 10.1016/0030-4220(80)90056-0.

33 Tang Weirong, Wu Younong, Smales Roger J. Identifying and Reducing Risks for Potential Fractures in Endodontically Treated Teeth. J Endod 2010;36(4):609–17. Doi: 10.1016/j.joen.2009.12.002.

34 Holcomb John Q, Pitts David L, Nicholls Jack I, Holcomb Q, Pitts David L. Further investigation of spreader loads required to cause vertical root fracture during lateral condensation. J Endod 1987;13(6):277–84. Doi: 10.1016/S0099-2399(87)80044-4.

35 Lertchirakarn Veera, Palamara Joseph Ea, Messer Harold H. Patterns of vertical root fracture: factors affecting stress distribution in the root canal. J Endod 2003;29(8):523–8. Doi: 10.1097/00004770-200308000-00008.

36 Saw Lip Hean, Messer Harold H. Root strains associated with different obturation techniques. J Endod 1995;21(6):314–20. Doi: 10.1016/S0099-2399(06)81008-3.

37 Lertchirakarn V, Palamara JE, Messer HH. Load and strain during lateral condensation and vertical root fracture. J Endod 1999;25(2):99–104. Doi: 10.1016/S0099-2399(99)80005-3.

38 Schmidt KJ, Walker TL, Johnson JD, Nicoll BK. Comparison of nickel-titanium and stainless-steel spreader penetration and accessory cone fit in curved canals. J Endod 2000;26(1):42–4. Doi: 10.1097/00004770-200001000-00011.

39 Gharai Saman R, Thorpe Jeffrey R, Strother James M, McClanahan Scott B. Comparison of Generated Forces and Apical Microleakage Using Nickel-Titanium and Stainless Steel Finger Spreaders in Curved Canals. J Endod 2005;31(3):198–200. Doi: 10.1097/01.don.0000137648.77797.ea.

40 Gimlin Dennis R, Parr Charles H, Aguirre-Ramirez Gilbert. A comparison of stresses produced during lateral and vertical condensation using engineering models. J Endod 1986;12(6):235–41. Doi: 10.1016/S0099-2399(86)80254-0.

41 White J, Lacefield W, Chavers L, Eleazer Paul D. The Effect of Three Commonly Used Endodontic Materials on the Strength and Hardness of Root Dentin. J Endod 2002;28(12):828–30. Doi: 10.1097/00004770-200212000-00008.

42 Grigoratos D, Knowles J, Ng YL, Gulabivala K. Effect of exposing dentine to sodium hypochlorite and calcium hydroxide on its flexural strength and elastic modulus. Int Endod J 2001;34(2):113–9. Doi: 10.1046/j.1365-2591.2001.00356.x.

43 Goldsmith M, Gulabivala K, Knowles JC. The effect of sodium hypochlorite irrigant concentration on tooth surface strain. J Endod 2002;28(8):575–9. Doi: 10.1097/00004770-200208000-00003.

44 Saleh AA, Ettman WM. Effect of endodontic irrigation solutions on microhardness of root canal dentine. J Dent 1999;27(1):43–6. Doi: 10.1016/S0300-5712(98)00018-9.

45 Niu W, Yoshioka T, Kobayashi C, Suda H. A scanning electron microscopic study of dentinal erosion by final irrigation with EDTA and NaOCl solutions. Int Endod J 2002;35(11):934–9. Doi: 10.1046/j.1365-2591.2002.00594.x.

46 Zarei Mina, Afkhami Farzaneh, Malek Poor Zahra. Fracture resistance of human root dentin exposed to calcium hydroxide intervisit medication at various time periods: An in vitro study. Dent Traumatol 2013;29(2):156–60. Doi: 10.1111/j.1600-9657.2012.01158.x.

47 Doyon Glen E, Dumsha Thom, von Fraunhofer J Anthony. Fracture resistance of human root dentin exposed to intracanal calcium hydroxide. J Endod 2005;31(12):895–7. Doi: 10.1097/01.don.0000194542.02521.af.

48 Marending M, Stark WJ, Brunner TJ, Fischer J, Zehnder M. Comparative assessment of time-related bioactive glass and calcium hydroxide effects on mechanical properties of human root dentin. Dent Traumatol 2009;25(1):126–9. Doi: 10.1111/j.1600-9657.2008.00735.x.

49 Lertchirakarn Veera, Palamara Joseph EA, Messer Harold H. Finite element analysis and strain-gauge studies of vertical root fracture. J Endod 2003;29(8):529–34. Doi: 10.1097/00004770-200308000-00009.

50 Kishen Anil. Mechanisms and risk factors for fracture predilection in endodontically treated teeth. Endod Top 2006;13(1):57–83. Doi: 10.1111/j.1601-1546.2006.00201.x.

51 Cormier Clarence J, Burns David R, Moon Peter. In vitro comparison of the

fracture resistance and failure mode of fiber, ceramic, and conventional post systems at various stages of restoration. J Prosthodont 2001;10(1):26–36. Doi: 10.1053/jpro.2001.23777.

52 Newman Marcela P, Yaman Peter, Dennison Joseph, Rafter Mary, Billy Edward. Fracture resistance of endodontically treated teeth restored with composite posts. J Prosthet Dent 2003;89(4):360–7. Doi: 10.1067/mpr.2003.75.

53 Schwartz R, Robbins J. Post Placement and Restoration of Endodontically Treated Teeth: A Literature Review. J Endod 2004;30(5):289–301. Doi: 10.1097/00004770-200405000-00001.

54 Chan CP, Tseng SC, Lin CP, Huang CC, Tsai TP, Chen CC. Vertical root fracture in nonendodontically treated teeth--a clinical report of 64 cases in Chinese patients. J Endod 1998;24(10):678–81. Doi: 10.1016/S0099-2399(98)80154-4.

55 Liao Wan Chuen, Tsai Yi Ling, Wang Chen Ying, et al. Clinical and Radiographic Characteristics of Vertical Root Fractures in Endodontically and Nonendodontically Treated Teeth. J Endod 2017;43(5):687–93. Doi: 10.1016/j.joen.2016.12.009.

56 Yang Shue Fen, Rivera Eric M, Walton Richard E. Vertical root fracture in nonendodontically treated teeth. J Endod 1995;21(6):337–9. Doi: 10.1016/S0099-2399(06)81013-7.

57 Cohen Stephen, Blanco Lucia, Berman Louis. Vertical root fractures Clinical and radiographic diagnosis. J Am Assoc 2003;134(4):434–41.

58 Tsesis I, Tamse A, Lustig J, Kaffe I. Vertical root fractures in endodontically treated teeth part I: clinical and radiographic diagnosis. Endod Top 2006;23(1):13–7, 68. Doi: 10.1111/j.1601-1546.2006.00200.x.

59 Lommel TJ, Meister F, Gerstein H, Davies EE, Tilk MA. Alveolar bone loss associated with vertical root fractures. Report of six cases. Oral Surg Oral Med Oral Pathol 1978;45(6):909–19.

60 Stewart ML, McClanahan SB. Cemental tear: a case report. Int Endod J 2006;39(1):81–6. Doi: 10.1111/j.1365-2591.2005.01034.x.

61 Tulkki Michael J, Baisden Michael K, McClanahan Scott B. Cemental Tear: A

Case Report of a Rare Root Fracture. J Endod 2006;32(10):1005–7. Doi: 10.1016/j.joen.2006.02.032.

62 Arakawa S, Cobb CM, Rapley JW, Killoy WJ, Spencer P. Treatment of root fracture by CO2 and Nd:YAG lasers: an in vitro study. J Endod 1996;22(12):662–7. Doi: 10.1016/S0099-2399(96)80060-4.

63 Dederich Douglas N. Case Report CO2 Laser Fusion of a Vertical Root Fracture 2001;130(August 1999):1195–9.

64 Sugaya T, Kawanami M, Noguchi H, Kato H, Masaka N. Periodontal healing after bonding treatment of vertical root fracture. Dent Traumatol 2001;17(4):174–9. Doi: 10.1034/j.1600-9657.2001.170407.x.

65 Kawai Keiji, Masaka Nobuo. Vertical root fracture treated by bonding fragments and rotational replantation. Dent Traumatol 2002;18(1):42–5. Doi: edt180106 [pii].

66 Kudou Yoshiyuki, Kubota Minoru. Replantation with intentional rotation of a complete vertically fractured root using adhesive resin cement. Dent Traumatol 2003;19(2):115–7. Doi: 10.1034/j.1600-9657.2003.00101.x.

67 Unver S, Onay EO, Ungor M. Intentional re-plantation of a vertically fractured tooth repaired with an adhesive resin. Int Endod J 2011;44(11):1069–78. Doi: 10.1111/j.1365-2591.2011.01922.x.

68 Nizam N, Kaval ME, Gürlek O, Atila A, Çalişkan MK. Intentional replantation of adhesively reattached vertically fractured maxillary single-rooted teeth. Int Endod J 2016;49(3):227–36. Doi: 10.1111/iej.12444.

69 Sugaya Tsutomu, Tomita Mahito, Motoki Youji, Miyaji Hirofumi, Kawamami Masamitsu. Influence of enamel matrix derivative on healing of root surfaces after bonding treatment and intentional replantation of vertically fractured roots. Dent Traumatol 2016;32(5):397–401. Doi: 10.1111/edt.12270.

70 Wilcox LR, Roskelley C, Sutton T. The relationship of root canal enlargement to finger-spreader induced vertical root fracture. J Endod 1997;23(8):533–4. Doi: 10.1016/S0099-2399(97)80316-0.

71 Special Committee to Revise the Joint AAE/AAOMR Position Statement on use of

CBCT in Endodontics. AAE and AAOMR Joint Position Statement: Use of Cone Beam Computed Tomography in Endodontics 2015 Update. Oral Surg Oral Med Oral Pathol Oral Radiol 2015;120(4):508–12. Doi: 10.1016/j.oooo.2015.07.033.

72 van der Stelt Paul. Principles of Digital Imaging. OOO&E 2000;44:237–48.

73 Sanderink Gerard, Miles Dale A. Intraoral Detectors. Dent Clin North Am 2000;(44):249–55.

74 Bhakdinaronk A, Manson-Hing LR. Effect of radiographic technique upon prediction of tooth length in intraoral radiography. OOO&E 1981;51(1):100–7.

75 Forsberg Jarl. Radiographic reproduction of endodontic "working length" comparing the paralleling and bisecting-angle techniques. OOO&E 1987;64:353–60.

76 Forsberg Jarl, Halse A. Periapical radiolucencies as evaluated by bisecting-angle and paralleling radiographic techniques. Int Endod J 1997;30:115–23.

77 Brynolf. Roentgenologic periapical diagnosis IV. When is one roentgenogram not sufficient? Swed Dent 1970:415–23.

78 Tamse Aviad. Zygomatic arch interference with correct radiographic diagnosis in maxillary molar endodontics. Oral Surgery, Oral Med Oral Pathol Oral Radiol Endodontology 1980:563–5.

79 Huumonen Sisko, Ørstavik D. Radiological aspects of apical periodontitis. Endod Top 2002:3–25. Doi: 10.1034/j.1601-1546.2002.10102.x.

80 Phillips John L, Weller R Norman, Kulild James C. The Mental Foramen: Part I. Size, Orientation, and Positional Relationship to the Mandibular Second Premolar. J Endod 1990;16:221–3.

81 Phillips John L, Weller R Norman, Kulild James C. The Mental Foramen: Part II. Radiographic Position in Relationto the Mandibular Second Premolar. J Endod 1992;18:271–4.

82 Barthel Claudia R, Zimmer Stefan, Trope Martin. Relationship of radiologic and histologic signs of inflammation in human root-filled teeth. J Endod 2004;30(2):75–9. Doi: 10.1097/00004770-200402000-00003.

83 Bender IB, Seltzer S. Roentgenographic and direct observation of experimental

lesions in bone: I. JADA 1961;62:152–60.

84 Bender IB, Seltzer Samuel. Roentgenographic and direct observation of experimental lesions in bone: II. JADA 1961:708–16.

85 Bohay Richard N. The sensitivity, specificity, and reliability of radiographic periapical diagnosis of posterior teeth. Oral Surgery, Oral Med Oral Pathol Oral Radiol Endodontology 2000;89(5):639–42. Doi: 10.1067/moe.2000.105908.

86 Richards Albert G. The Buccal Object Rule. DRP 1980;53:37–56.

87 Goerig Albert, Neaverth Elmer. A Simplified Look at the Buccal Object Rule in Endodontics. J Endod 1987;13(12):570–2.

88 Walton Richard E. Endodontic Radiographic Tecnhniques. DRP 1973;46:51–9.

89 Slowey Ronald R. Radiographic aids in the detectino of extra root canals. OOO&E 1974;37:762–70.

90 Slowey Ronald R. Root Canal Anatomy: Road Map to Successful Endodontics. Dent Clin North Am 1979;23:55–73.

91 Hoen Michael M, Pink Frank E. Contemporary Endodontic Retreatments : An Analysis based on Clinical Treatment Findings. J Endod 2002;28(12):12–4.

92 Paurazas Susan B, Geist James R, Pink Frank E, Hoen Michael M, Steiman H Robert. Comparison of diagnostic accuracy of digital imaging by using CCD and CMOS-APS sensors with E-speed film in the detection of periapical bony lesions. Oral Surg Oral Med Oral Pathol Oral Radiol Endod 2000;89(3):356–62. Doi: 10.1067/moe.2000.103525.

93 Scarfe William C, Farman Allan G. What is Cone-Beam CT and How Does it Work? Dent Clin North Am 2008;52(4):707–30. Doi: 10.1016/j.cden.2008.05.005.

94 Jeger Franziska B, Janner Simone FM, Bornstein Michael M, Lussi Adrian. Endodontic working length measurement with preexisting cone-beam computed tomography scanning: A prospective, controlled clinical study. J Endod 2012;38(7):884–8. Doi: 10.1016/j.joen.2012.03.024.

95 Patel S. New dimensions in endodontic imaging: Part 2. Cone beam computed tomography. Int Endod J 2009;42(6):463–75. Doi: 10.1111/j.1365-2591.2008.01531.x.

96 McClammy Thomas V. Endodontic applications of cone beam computed tomography. Dent Clin North Am 2014:545–59. Doi: 10.1016/j.cden.2014.03.004.

97 Matherne Ryan P, Angelopoulos Christos, Kulild James C, Tira Daniel. Use of Cone-Beam Computed Tomography to Identify Root Canal Systems In Vitro. J Endod 2008;34(1):87–9. Doi: 10.1016/j.joen.2007.10.016.

98 Domark Jeffrey D, Hatton John F, Benison Roxanne P, Hildebolt Charles F. An ex vivo comparison of digital radiography and cone-beam and micro computed tomography in the detection of the number of canals in the mesiobuccal roots of maxillary molars. J Endod 2013;39(7):901–5. Doi: 10.1016/j.joen.2013.01.010.

99 Angelopoulos Christos. Cone Beam Tomographic Imaging Anatomy of the Maxillofacial Region. Dent Clin North Am 2008;52(4):731–52. Doi: 10.1016/j.cden.2008.07.002.

100 Angelopoulos Christos. Anatomy of the Maxillofacial Region in the Three Planes of Section. Dent Clin North Am 2014;58(3):497–521. Doi: 10.1016/j.cden.2014.03.001.

101 Kim Thomas S, Caruso Joseph M, Christensen Heidi, Torabinejad Mahmoud. A comparison of cone-beam computed tomography and direct measurement in the examination of the mandibular canal and adjacent structures. J Endod 2010;36(7):1191–4. Doi: 10.1016/j.joen.2010.03.028.

102 Patel S, Dawood A, Pitt Ford T, Whaites E. The potential applications of cone beam computed tomography in the management of endodontic problems. Int Endod J 2007;40(10):818–30. Doi: 10.1111/j.1365-2591.2007.01299.x.

103 Carruth Paul, He Jianing, Benson Byron W, Schneiderman Emet D. Analysis of the Size and Position of the Mental Foramen Using the CS 9000 Cone-beam Computed Tomographic Unit. J Endod 2015;41(7):1032–6. Doi: 10.1016/j.joen.2015.02.025.

104 Brüllmann Dan Dominik, Schmidtmann Irene, Hornstein Silke, Schulze Ralf K. Correlation of cone beam computed tomography (CBCT) findings in the maxillary sinus with dental diagnoses : a retrospective cross-sectional study 2012:1023–9. Doi: 10.1007/s00784-011-0620-1.

105 Estrela Carlos, Bueno Mike Reis, Leles Cláudio Rodrigues, Azevedo Bruno, Azevedo José Ribamar. Accuracy of Cone Beam Computed Tomography and Panoramic and Periapical Radiography for Detection of Apical Periodontitis. J Endod 2008;34(3):273–9. Doi: 10.1016/j.joen.2007.11.023.

106 Patel S, Wilson R, Dawood A, Mannocci F. The detection of periapical pathosis using periapical radiography and cone beam computed tomography - Part 1: Pre-operative status. Int Endod J 2012;45(8):702–10. Doi: 10.1111/j.1365-2591.2011.01989.x.

107 Patel S, Wilson R, Dawood A, Foschi F, Mannocci F. The detection of periapical pathosis using digital periapical radiography and cone beam computed tomography - Part 2: A 1-year post-treatment follow-up. Int Endod J 2012;45(8):711–23. Doi: 10.1111/j.1365-2591.2012.02076.x.

108 Cotton Taylor P, Geisler Todd M, Holden David T, Schwartz Scott A, Schindler William G. Endodontic Applications of Cone-Beam Volumetric Tomography. J Endod 2007;33(9):1121–32. Doi: 10.1016/j.joen.2007.06.011.

109 Makins Scott R. Artifacts interfering with interpretation of cone beam computed tomography images. Dent Clin North Am 2014;58(3):485–95. Doi: 10.1016/j.cden.2014.04.007.

110 Sarid Dror. Fowler–Nordheim Tunneling. *Explor. Scanning Probe Microsc. with Math.* Weinheim, Germany: Wiley-VCH Verlag GmbH & Co. KGaA; n.d. p. 160–9.

111 J. Zhang, Yang G, Cheng Y, et al. Stationary scanning X-ray source based on carbon nanotube field emitters. Appl Phys Lett 2005;86(184104).

112 X. Qian, Rajaram R, Calderon-Colon X, et al. Design and characterization of a spatially distributed multibeam field emission x-ray source for stationary digital breast tomosynthesis. Med Phys 2009;36:10.

113 Inscoe Christina R, Wu Gongting, Soulioti Danai E, et al. Stationary intraoral tomosynthesis for dental imaging 2017;10132:1013203. Doi: 10.1117/12.2254632.

114 American Association of Endodontists. Colleagues for Excellence: Cone Beam-Computed Tomography in Endodontics n.d. Doi: 10.1038/sj.bdj.2011.1037.

115 Preece John W. Isn't it about time we changed our perception of diagnostic radiation risks? Oral Surgery, Oral Med Oral Pathol Oral Radiol Endodontology 1997;84(4):329. Doi: 10.1016/S1079-2104(97)90022-6.

116 Ball Randy L, Barbizam Joao V., Cohenca Nestor. Intraoperative endodontic applications of cone-beam computed tomography. J Endod 2013;39(4):548–57. Doi: 10.1016/j.joen.2012.11.038.

117 Inscoe Christina R, Puett Connor, Platin Enrique, Lu Jianping, Zhou Otto. *Characterization of a clinical prototype stationary intraoral tomosynthesis system*. n.d.

118 da Silveira Priscila Fernanda, Vizzotto Mariana Boessio, Liedke Gabriela Salatino, da Silveira Heloísa Emília Dias Heraldo Luis Dias, Montagner Francisco, da Silveira Heloísa Emília Dias Heraldo Luis Dias. Detection of vertical root fractures by conventional radiographic examination and cone beam computed tomography - an in vitro analysis. Dent Traumatol 2013;29(1):41–6. Doi: 10.1111/j.1600-9657.2012.01126.x.

119 Chavda Rajesh, Mannocci Francesco, Andiappan Manoharan, Patel Shanon. Comparing the in vivo diagnostic accuracy of digital periapical radiography with cone-beam computed tomography for the detection of vertical root fracture. J Endod 2014;40(10):1524–9. Doi: 10.1016/j.joen.2014.05.011.

120 Yiit Özer Senem. Detection of vertical root fractures of different thicknesses in endodontically enlarged teeth by cone beam computed tomography versus digital radiography. J Endod 2010;36(7):1245–9. Doi: 10.1016/j.joen.2010.03.021.

121 Tamse Aviad, Kaffe Israel, Lustig Joseph, Ganor Yehuda, Fuss Zvi. Radiographic features of vertically fractured endodontically treated mesial roots of mandibular molars. Oral Surgery, Oral Med Oral Pathol Oral Radiol Endodontology 2006;101(6):797–802. Doi: 10.1016/j.tripleo.2005.09.014.

122 Patel S, Brady E, Wilson R, Brown J, Mannocci F. The detection of vertical root fractures in root filled teeth with periapical radiographs and CBCT scans. Int Endod J 2013;46(12):1140–52. Doi: 10.1111/iej.12109.

123 Ardakani Fatemeh Ezzodini, Razavi Seyed Hossein, Tabrizizadeh Mehdi.

Diagnostic value of cone-beam computed tomography and periapical radiography in detection of vertical root fracture. Iran Endod J 2015;10(2):122–6.

124 Varshosaz Masoud, Tavakoli Mohammad A, Mostafavi Maryam, Baghban Alireza A. Comparison of conventional radiography with cone beam computed tomography for detection of vertical root fractures: an in vitro study. J Oral Sci 2010;52(4):593–7. Doi: 10.2334/josnusd.52.593.

125 Hassan Bassam, Metska Maria Elissavet, Ozok Ahmet Rifat, van der Stelt Paul, Wesselink Paul Rudolf. Detection of Vertical Root Fractures in Endodontically Treated Teeth by a Cone Beam Computed Tomography Scan. J Endod 2009;35(5):719–22. Doi: 10.1016/j.joen.2009.01.022.

126 Tofangchiha Maryam, Bakhshi Mahin, Fakhar Hoorieh Bashizadeh, Panjnoush Mehrdad. Conventional and digital radiography in vertical root fracture diagnosis: A comparison study. Dent Traumatol 2011;27(2):143–6. Doi: 10.1111/j.1600-9657.2010.00973.x.

127 Brady E, Mannocci F, Brown J, Wilson R, Patel S. A comparison of cone beam computed tomography and periapical radiography for the detection of vertical root fractures in nonendodontically treated teeth. Int Endod J 2014;47(8):735–46. Doi: 10.1111/iej.12209.

128 Takeshita WiltonMitsunari, Iwaki Lilian CristinaVessoni, da Silva MarilianiChicarelli, Sabio Sergio, Ricardo Paulo, Albino Febrairo. Comparison of periapical radiography with cone beam computed tomography in the diagnosis of vertical root fractures in teeth with metallic post. J Conserv Dent 2014;17(3):225. Doi: 10.4103/0972-0707.131781.

129 Rud Jorgen, Omnell Karl-Ake. Root fractures due to corrosion Diagnostic aspects. Eur J Oral Sci 1970;78(1–4):397–403. Doi: 10.1111/j.1600-0722.1970.tb02088.x.

130 Nicopoulou-Karayianni K, Bragger U, Lang NP. Patterns of periodontal destruction associated with incomplete root fractures. Dentomaxillofacial Radiol 1997;26(6):321–6. Doi: 10.1038/sj.dmfr.4600264.

131 Youssefzadeh Soraya, Gahleitner André, Dorffner Roland, Bernhart Thomas, Kainberger Franz M. Head and Neck Imaging Dental Vertical Root Fractures:

Value of CT in Detection 1 n.d.

132 Yiit Özer Senem. Detection of vertical root fractures by using cone beam computed tomography with variable voxel sizes in an in vitro model. J Endod 2011;37(1):75–9. Doi: 10.1016/j.joen.2010.04.021.

133 Fayad Mohamed I, Ashkenaz Paul J, Johnson Bradford R. Different representations of vertical root fractures detected by cone-beam volumetric tomography: A case series report. J Endod 2012;38(10):1435–42. Doi: 10.1016/j.joen.2012.05.015.

134 Wang P, Yan XB, Lui DG, Zhang WL, Zhang Y, Ma XC. Detection of dental root fractures by using cone-beam computed tomography. Dentomaxillofacial Radiol 2011;40(5):290–8. Doi: 10.1259/dmfr/84907460.

135 Edlund Mitchell, Nair Madhu K, Nair Umadevi P. Detection of vertical root fractures by using cone-beam computed tomography: A clinical study. J Endod 2011;37(6):768–72. Doi: 10.1016/j.joen.2011.02.034.

136 Melo Saulo Leonardo Sousa, Bortoluzzi Eduardo Antunes, Abreu Jr. Murillo, Corr?a Let?cia Ruhland, Corr?a Marcio. Diagnostic Ability of a Cone-Beam Computed Tomography Scan to Assess Longitudinal Root Fractures in Prosthetically Treated Teeth. J Endod 2010;36(11):1879–82. Doi: 10.1016/j.joen.2010.08.025.

137 Coolidge Edgar D. The thickness of the human periodontal memberane. J Am Dent Assoc Dent Cosm 1937;24(8):1260–70. Doi: 10.14219/jada.archive.1937.0229.

138 Lee, Nettey-Marbell. Using extracted teeth for research: the effect of storage medium and sterilization on dentin bond strengths. JADA 2007;138(12):1599–603.

139 Tate W H White RR. Disinfection of human teeth for educational purposes. J Dent Educ 1991;55(9):583–5.

140 Sandhu Simarpreet V, Tiwari Rajiv, Bhullar Raman Preet K, et al. Sterilization of extracted human teeth: A comparative analysis. J Oral Biol Craniofacial Res 2012;2(3):170–5. Doi: 10.1016/j.jobcr.2012.09.002.

141 Goodis HE, Marshall GW, White JM, Gee L, Hornberger B, Marshall SJ. Storage

effects on dentin permeability and shear bond strengths. Dent Mater 1993;9(2):79–84. Doi: 10.1016/0109-5641(93)90079-6.

142 DeWald Janice P. The use of extracted teeth for in vitro bonding studies: A review of infection control considerations. Dent Mater 1997;13(2):74–81. Doi: 10.1016/S0109-5641(97)80015-2.

143 Mora Maria A, Mol André, Tyndall Donald A, Rivera Eric M. In vitro assessment of local computed tomography for the detection of longitudinal tooth fractures. Oral Surgery, Oral Med Oral Pathol Oral Radiol Endodontology 2007;103(6):825–9. Doi: 10.1016/j.tripleo.2006.09.009.

144 Carestream Dental. Digital Intraoral Sensors | RVG 6200. Available at: http://www.carestreamdental.com/us/en/rvgimaging/6200#Resource_Library:TechnicalSpecifications. Accessed July 17, 2017, 2017.

145 Samei Ehsan, Badano Aldo, Chakraborty Dev, et al. Assessment of display performance for medical imaging systems: Executive summary of AAPM TG18 report. Med Phys 2005;32(4):1205–25. Doi: 10.1118/1.1861159.

146 Haahr Mads, Haahr Svend. Random Sequence Generator. Random.org. Available at: https://www.random.org/sequences/. Accessed April 10, 2017, 2017.

147 Hassan Bassam, Metska Maria Elissavet, Ozok Ahmet Rifat, van der Stelt Paul, Wesselink Paul Rudolf. Comparison of Five Cone Beam Computed Tomography Systems for the Detection of Vertical Root Fractures. J Endod 2010;36(1):126–9. Doi: 10.1016/j.joen.2009.09.013.

148 Kajan Z Dalili, Taromsari M. Value of cone beam CT in detection of dental root fractures. Dentomaxillofacial Radiol 2012;41(1):3–10. Doi: 10.1259/dmfr/25194588.

149 Tang Lu, Zhou Xue-dong, Wang Yao, Zhang Lan, Zheng Qing-hua, Huang Ding-ming. Detection of vertical root fracture using cone beam computed tomography: report of two cases. Dent Traumatol 2011;27(6):484–8. Doi: 10.1111/j.1600-9657.2011.01030.x.

150 Melo Saulo Leonardo Sousa, Haiter-Neto F, Correa LR, Scarfe WC, Farman AG. Comparative diagnostic yield of cone beam CT reconstruction using various

software programs on the detection of vertical root fractures. Dentomaxillofacial Radiol 2013;42(9). Doi: 10.1259/dmfr.20120459.

151 Liang KY, Zeger S. Longitudinal data analysis using generalized linear models. Biometrika 1986;73(1):13–22.

152 Baisden Michael K, Kulild James C, Weller R Norman. Root canal configuration of the mandibular first premolar. J Endod 1992;18(10):505–8. Doi: 10.1016/S0099-2399(06)81352-X.

153 Trope Martin, Elfenbein Leslie, Tronstad Leif. Mandibular premolars with more than one root canal in different race groups. J Endod 1986;12(8):343–5. Doi: 10.1016/S0099-2399(86)80035-8.

154 Fan Bing, Yang Jun, Gutmann James L, Fan Mingwen. Root Canal Systems in Mandibular First Premolars with C-shaped Root Configurations. Part I: Microcomputed Tomography Mapping of the Radicular Groove and Associated Root Canal Cross-sections. J Endod 2008;34(11):1337–41. Doi: 10.1016/j.joen.2008.08.006.

155 Vizzotto MB, Silveira PF, Arús NA, Montagner F, Gomes BPFA, da Silveira HED. CBCT for the assessment of second mesiobuccal (MB2) canals in maxillary molar teeth: Effect of voxel size and presence of root filling. Int Endod J 2013;46(9):870–6. Doi: 10.1111/iej.12075.

156 DiAngelis Anthony J, Andreasen Jens O, Ebeleseder Kurt A, et al. International Association of Dental Traumatology guidelines for the management of traumatic dental injuries: 1. Fractures and luxations of permanent teeth. Dent Traumatol 2012;28(1):2–12. Doi: 10.1111/j.1600-9657.2011.01103.x.

157 Goldman Melvin, Pearson Arthur H, Darzenta Nicholas. Endodontic success - Who's reading the radiograph? OOO&E 1972;33(3):432–7.

158 Goldman Melvin, Pearson Arthur H, Darzenta Nicholas. Reliability of radiographic interpretations. OOO&E 1974;38(2):287–93.

Appendix I: Study Imaging

The following section includes all the imaging evaluated in the study. Each figure includes two periapical images (straight and shifted), a screenshot of a tomosynthesis image, and a screenshot of a limited-FOV cone-beam CT. It should be clear though that tomosynthesis images and CBCT volumes are three-dimensional and can be navigated. The screenshots of tomosynthesis imaging and CBCT's depicted below in unfractured teeth are oriented in the midroot area, and among fractured teeth a screenshot is included to best demonstrate the presence of the fracture in the subjective assessment of the principal investigator for the purposes of illustration. These images contain the tooth samples and have been further cropped. The layout is as follows:

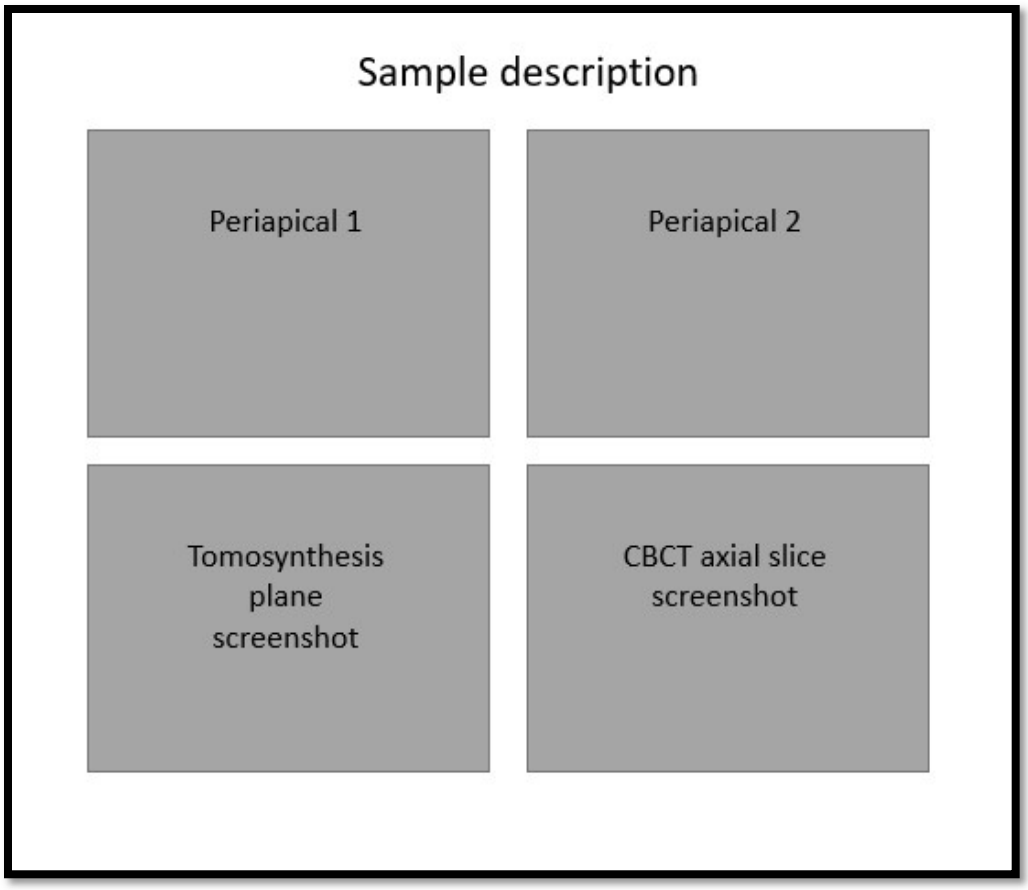

Unobturated and fracture absent

Unobturated and fracture absent #1

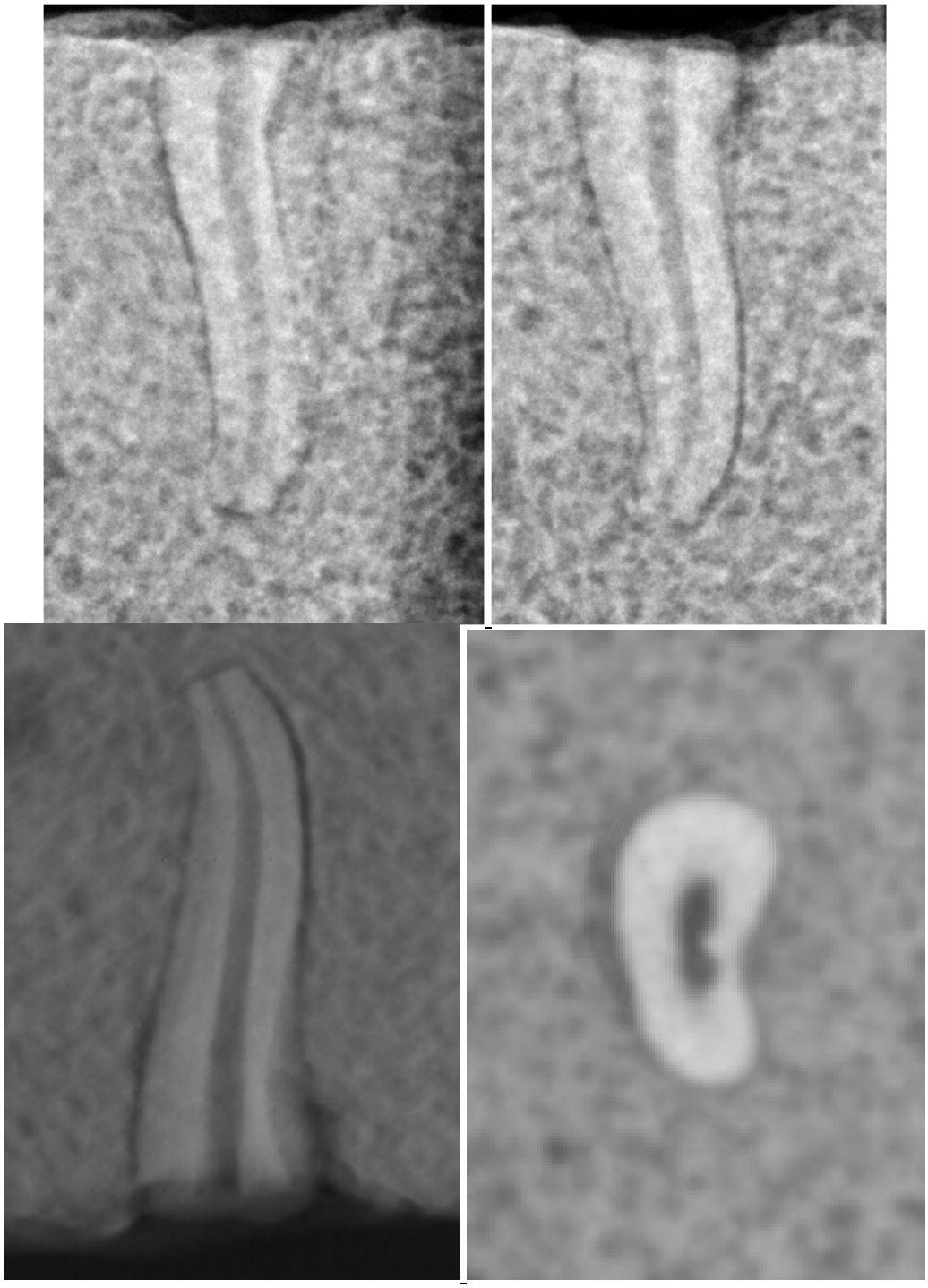

Unobturated and fracture absent #2

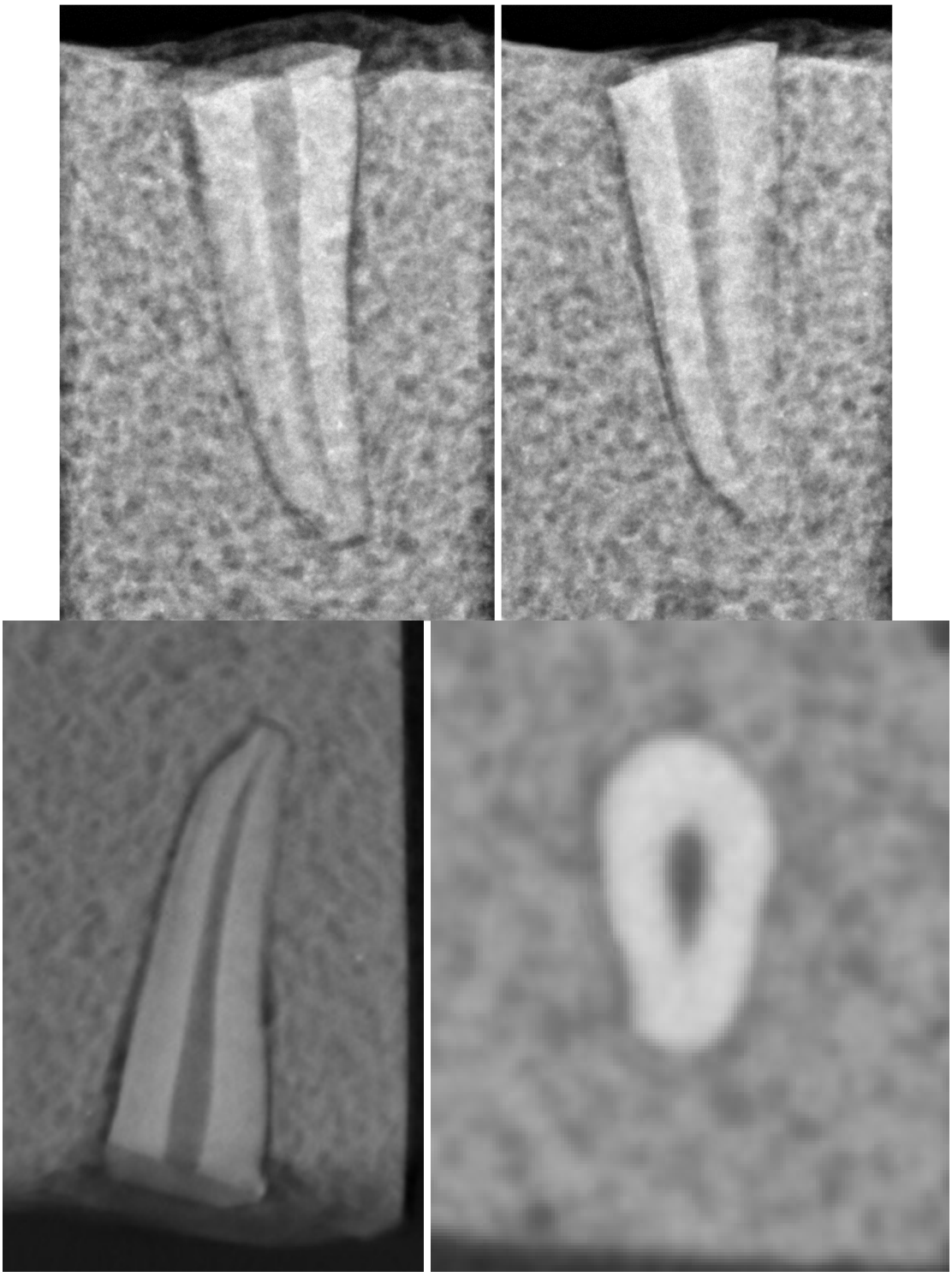

Unobturated and fracture absent #3

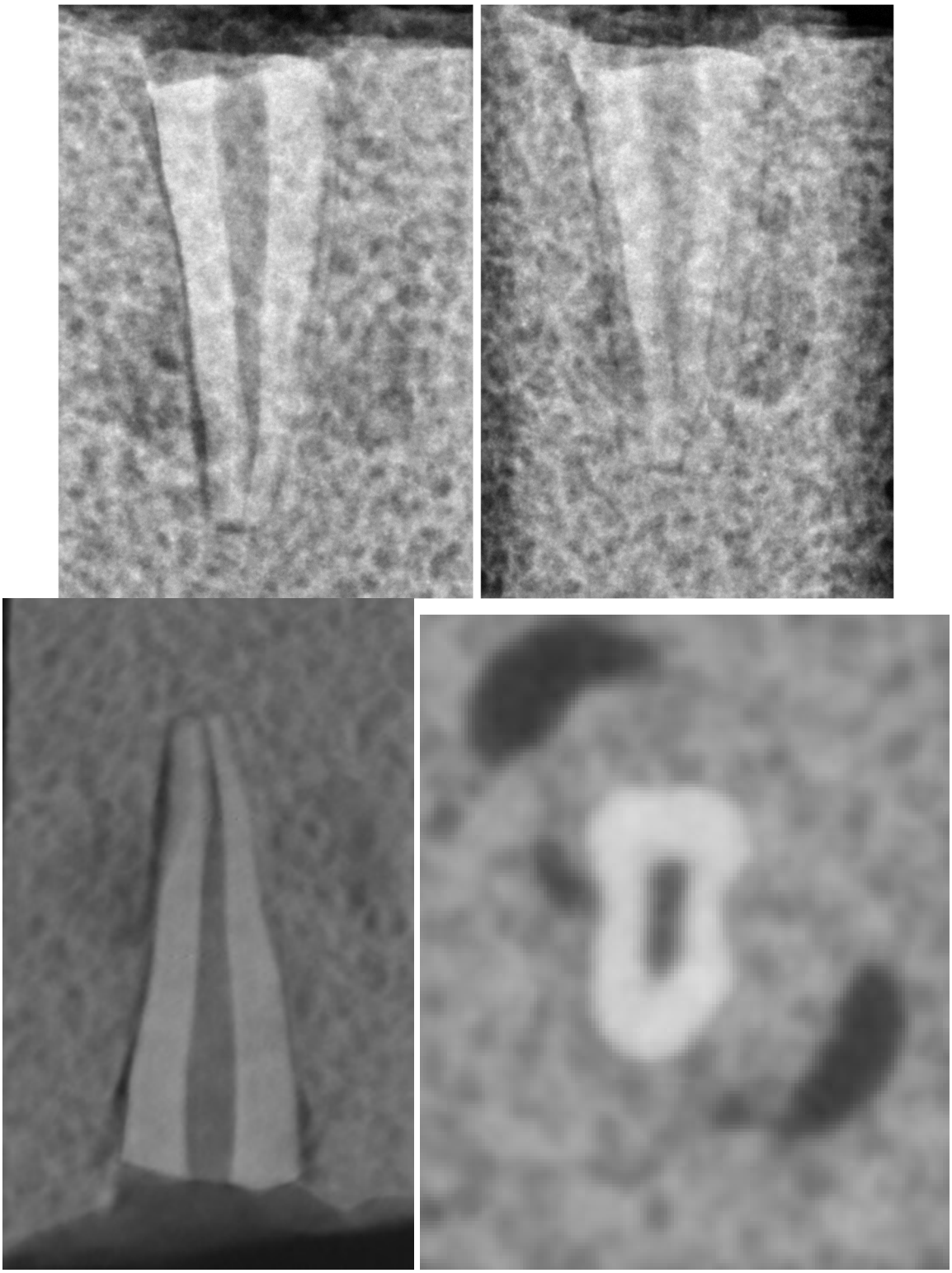

Unobturated and fracture absent #4

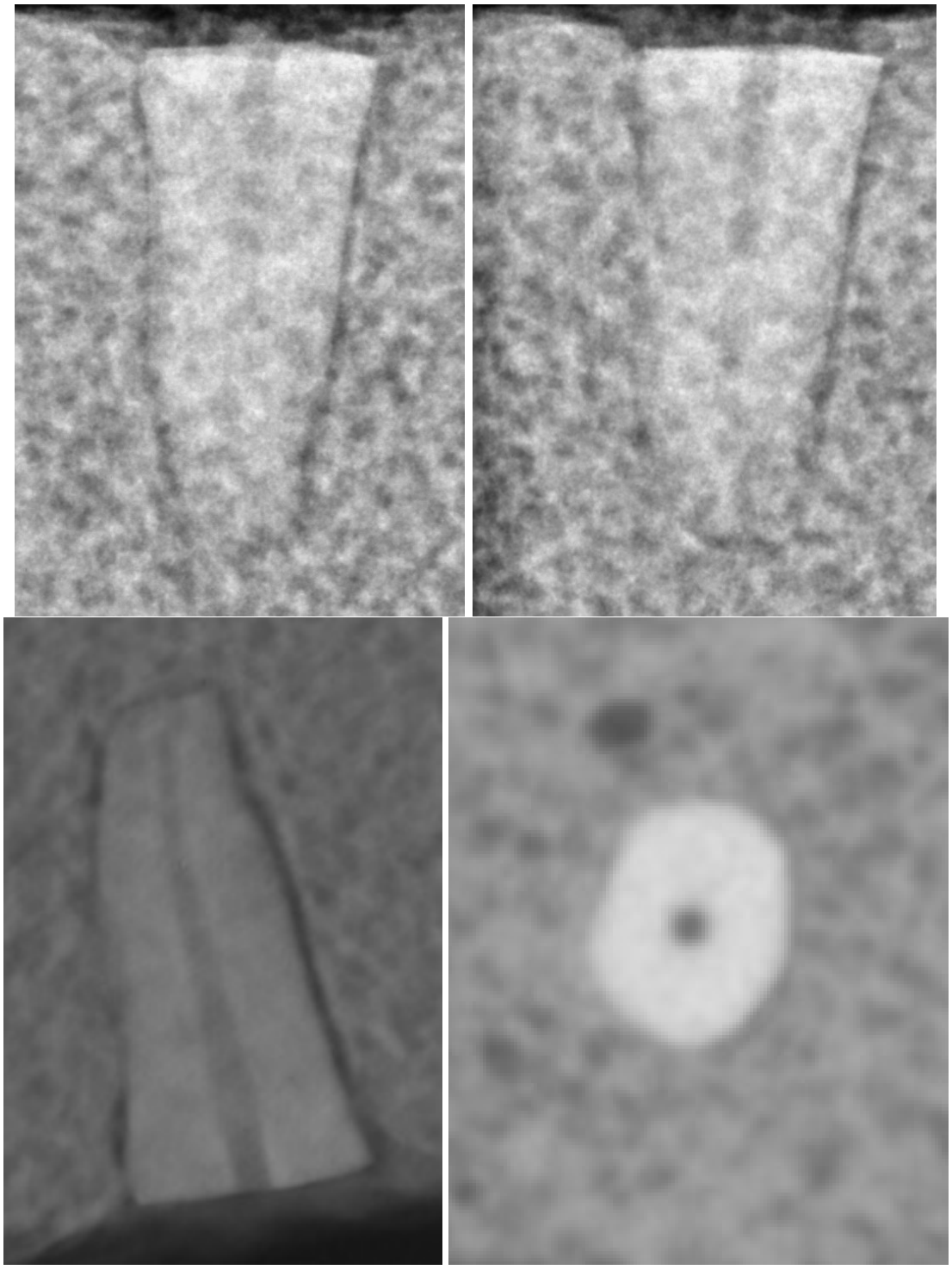

Unobturated and fracture absent #5

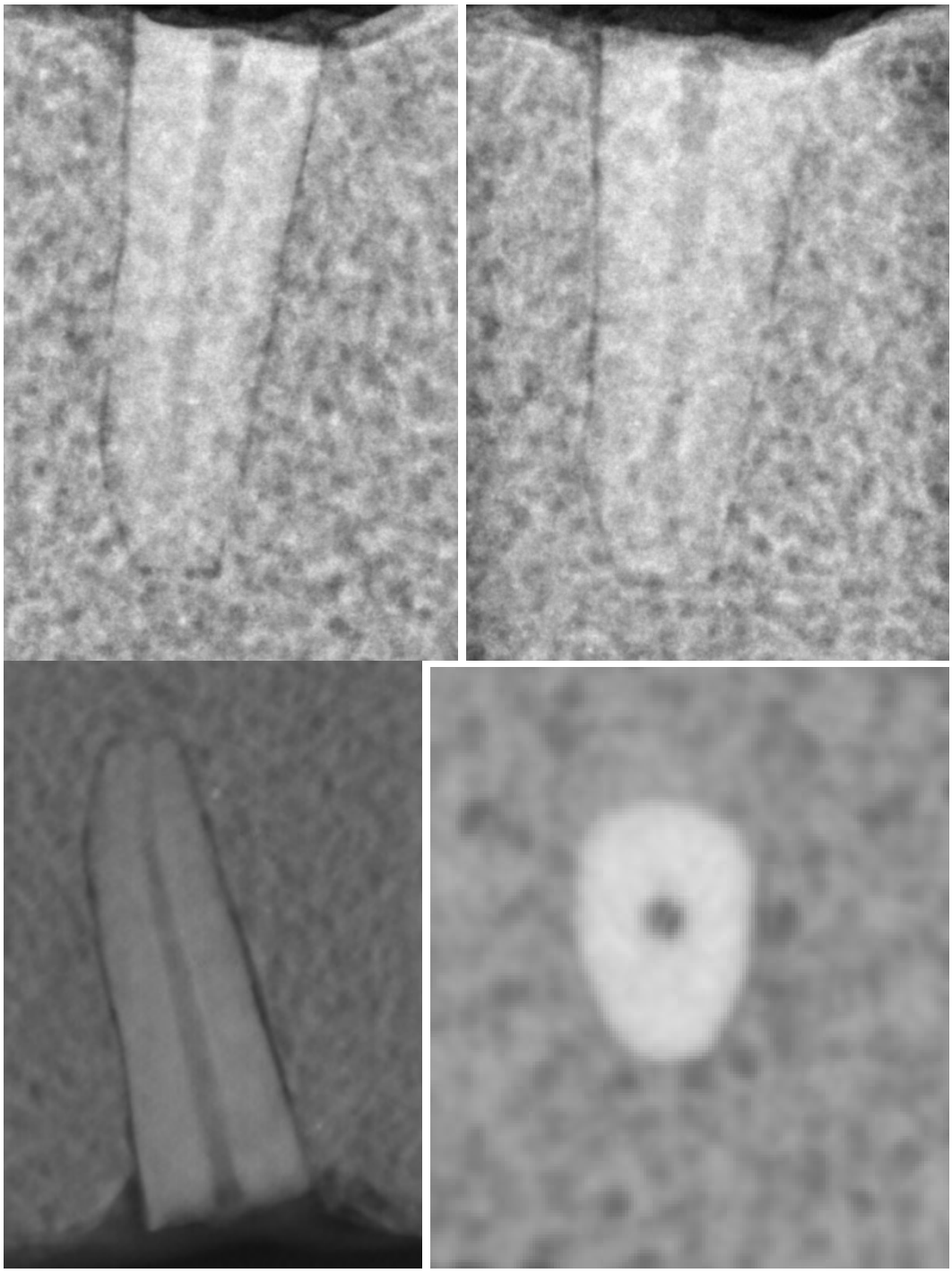

Unobturated and fracture absent #6

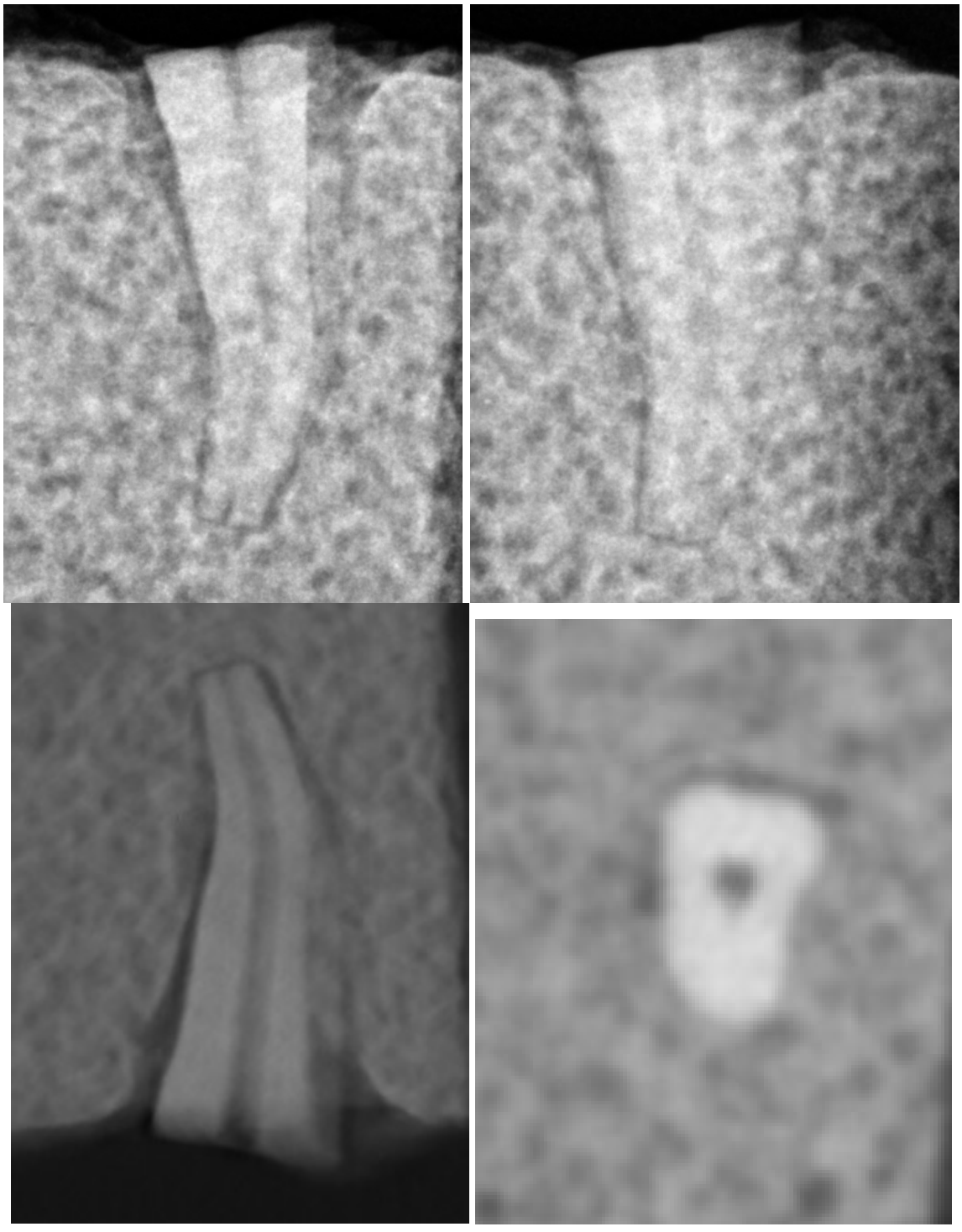

Unobturated and fracture absent #7

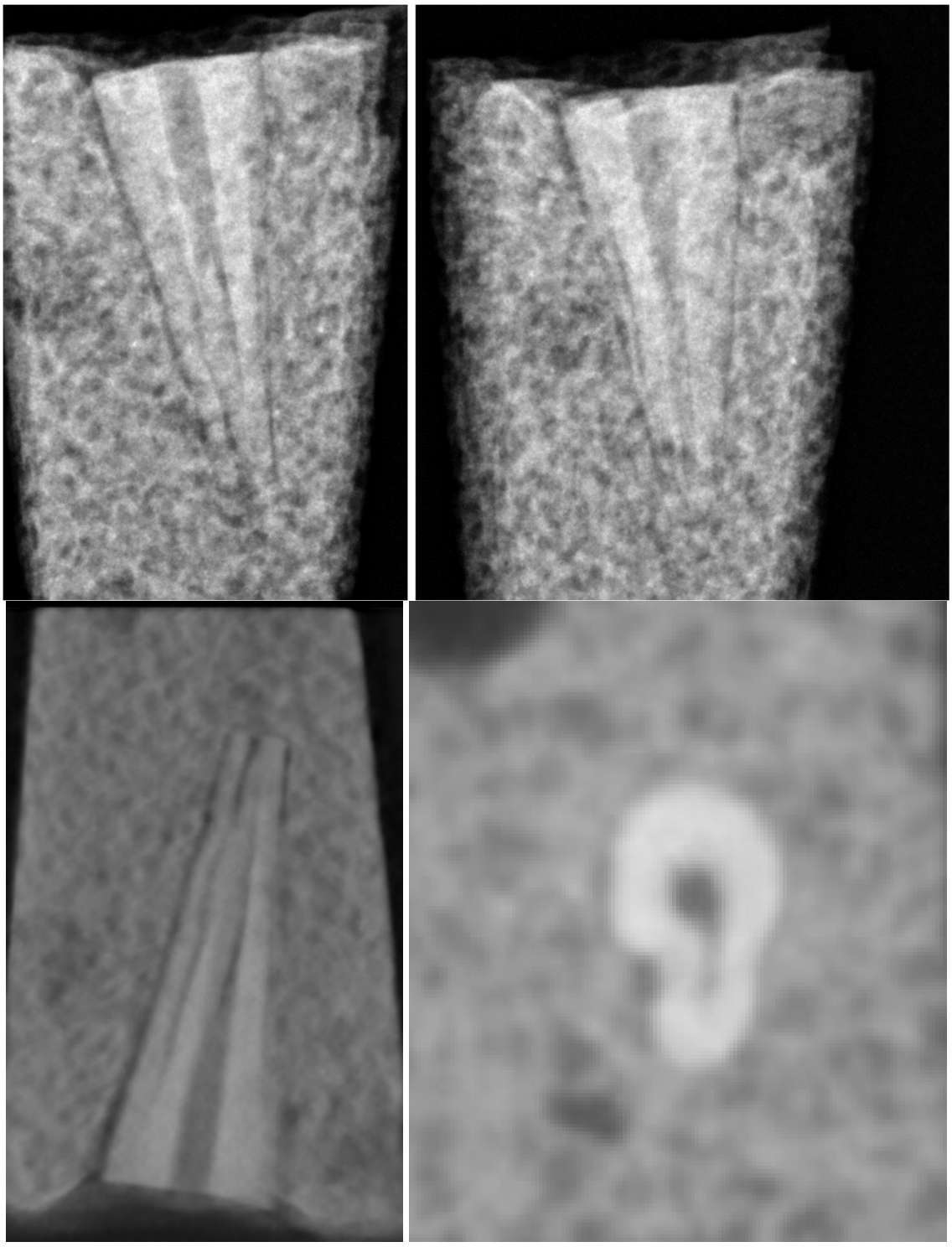

Unobturated and fracture absent #8

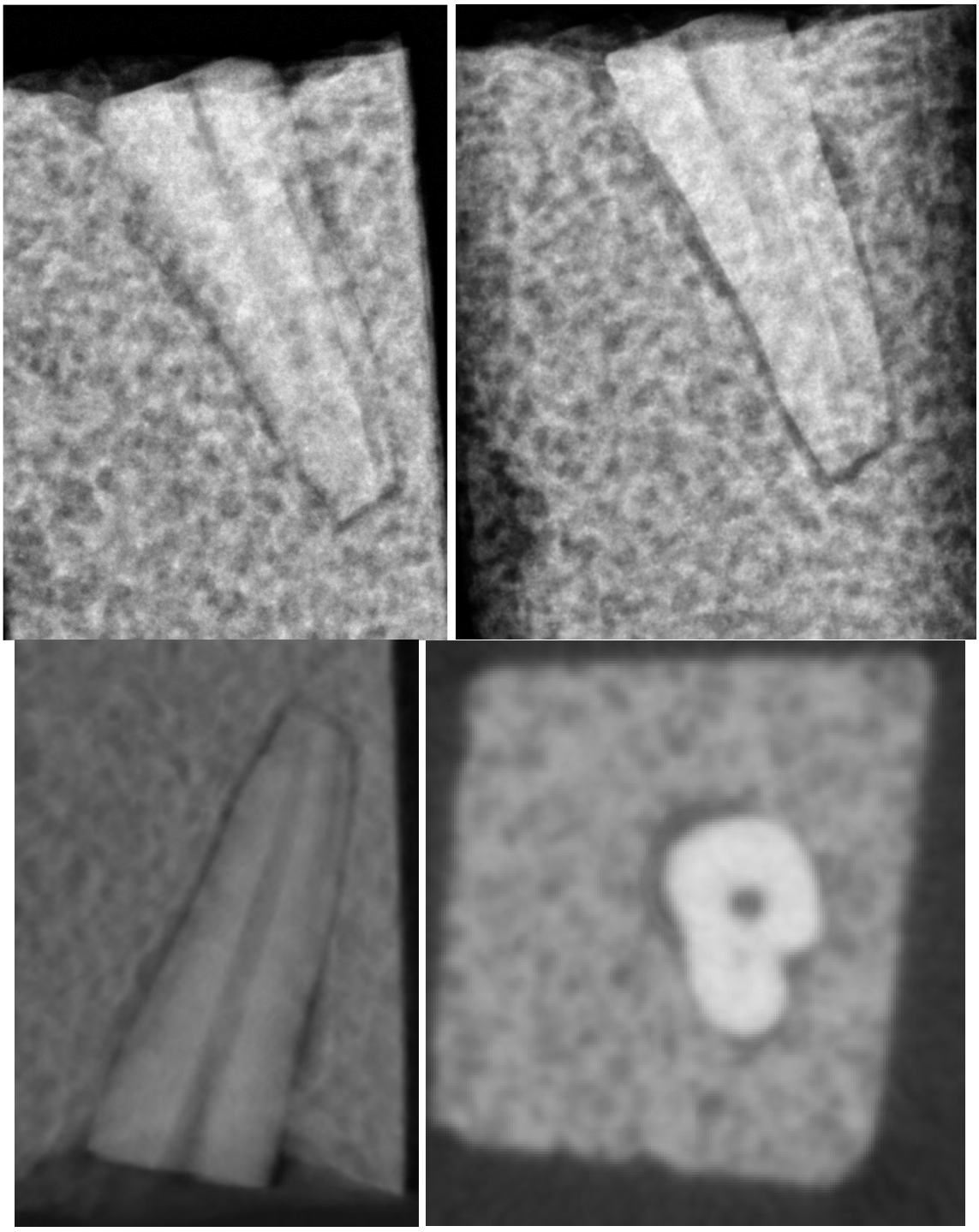

Unobturated and fracture absent #9

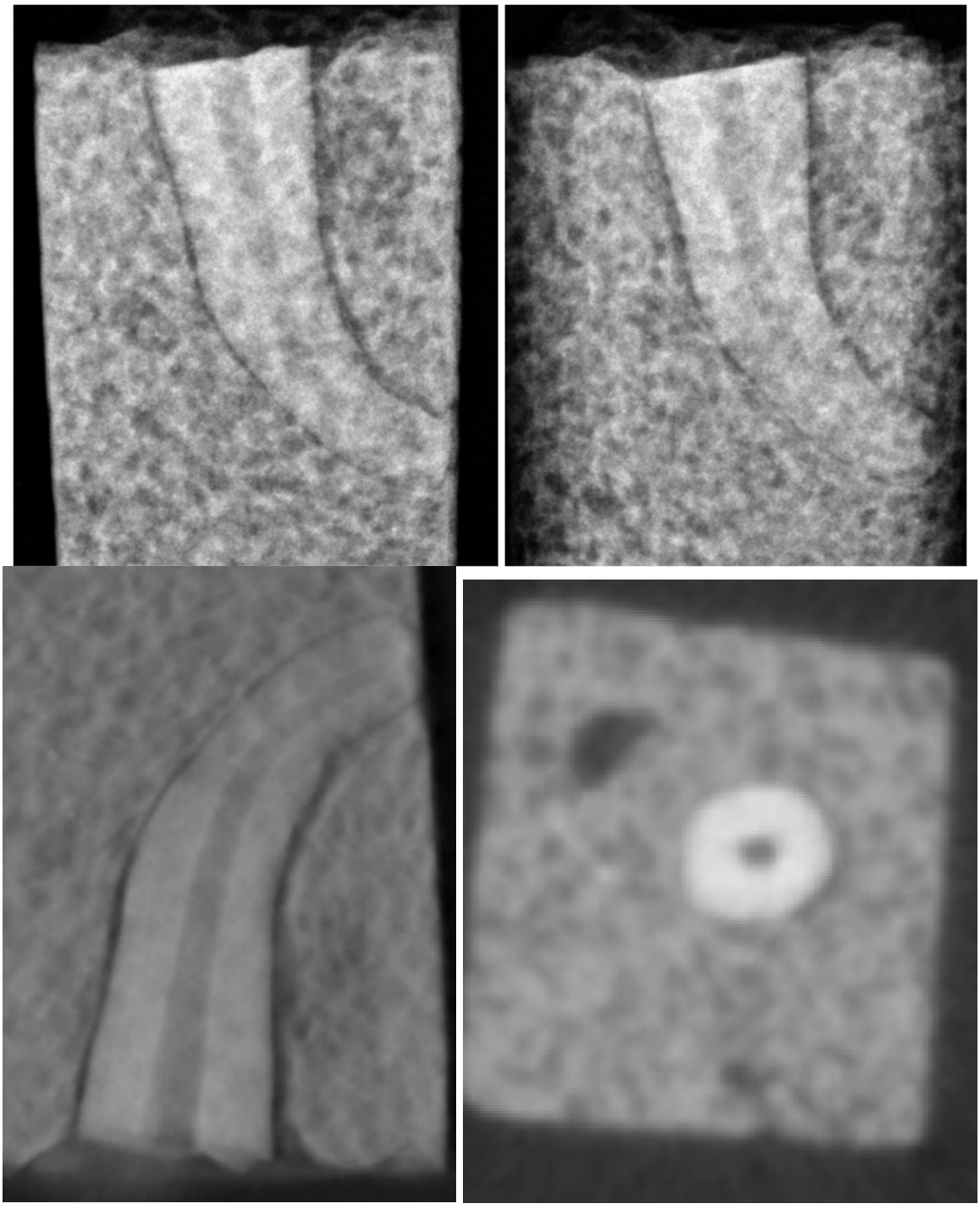

Unobturated and fracture absent #10

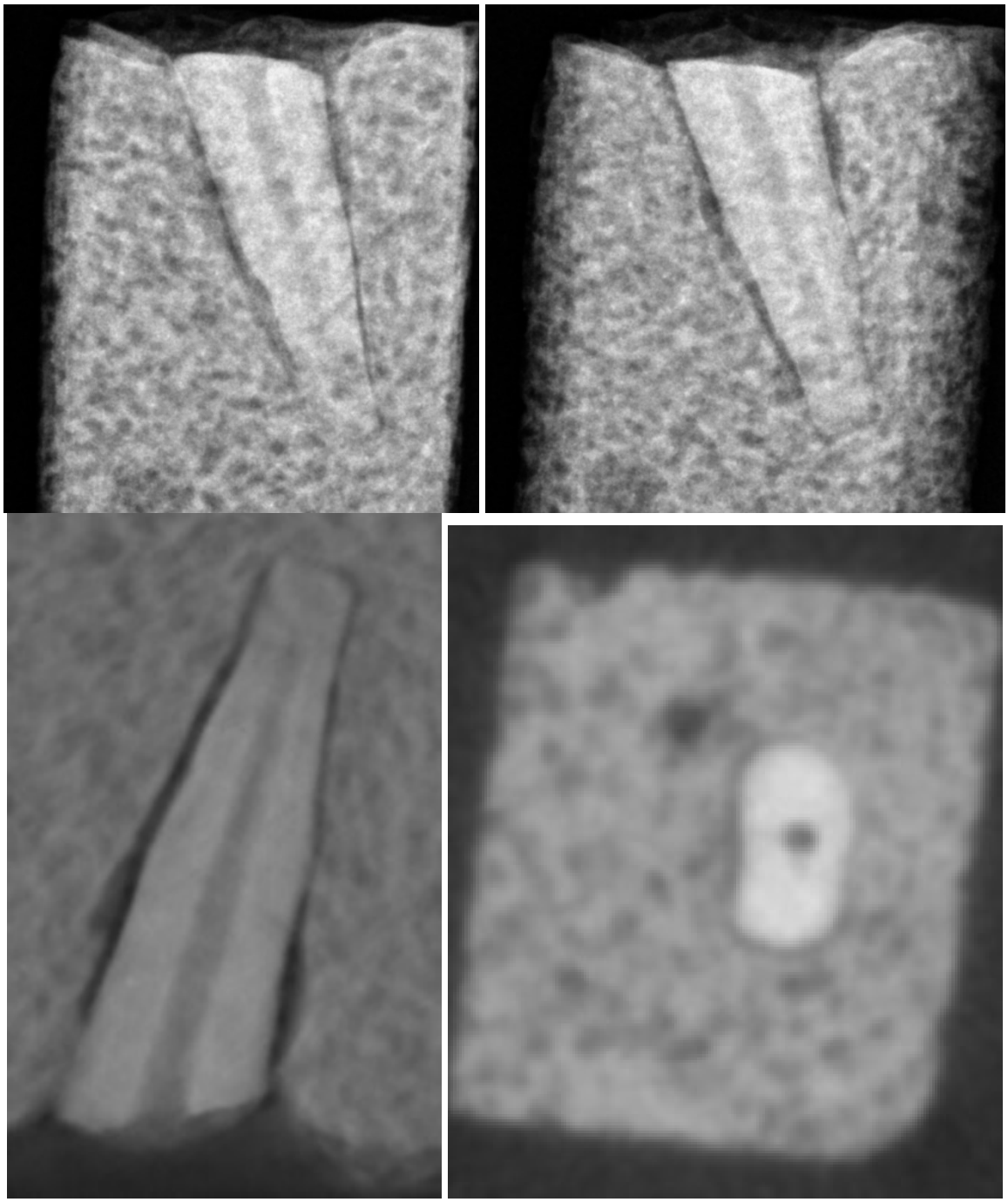

Unobturated and fracture absent #11

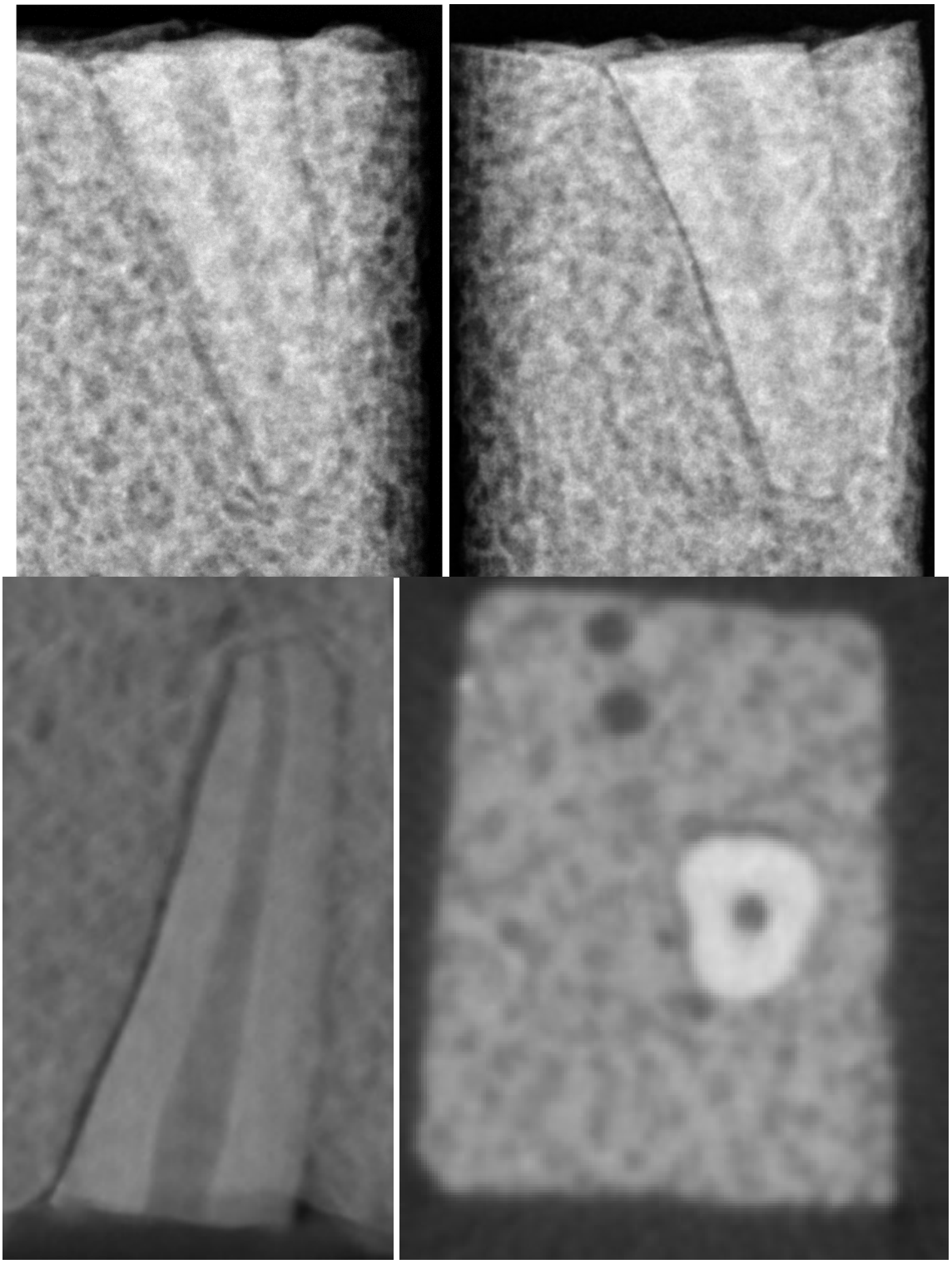

Unobturated and fracture absent #12

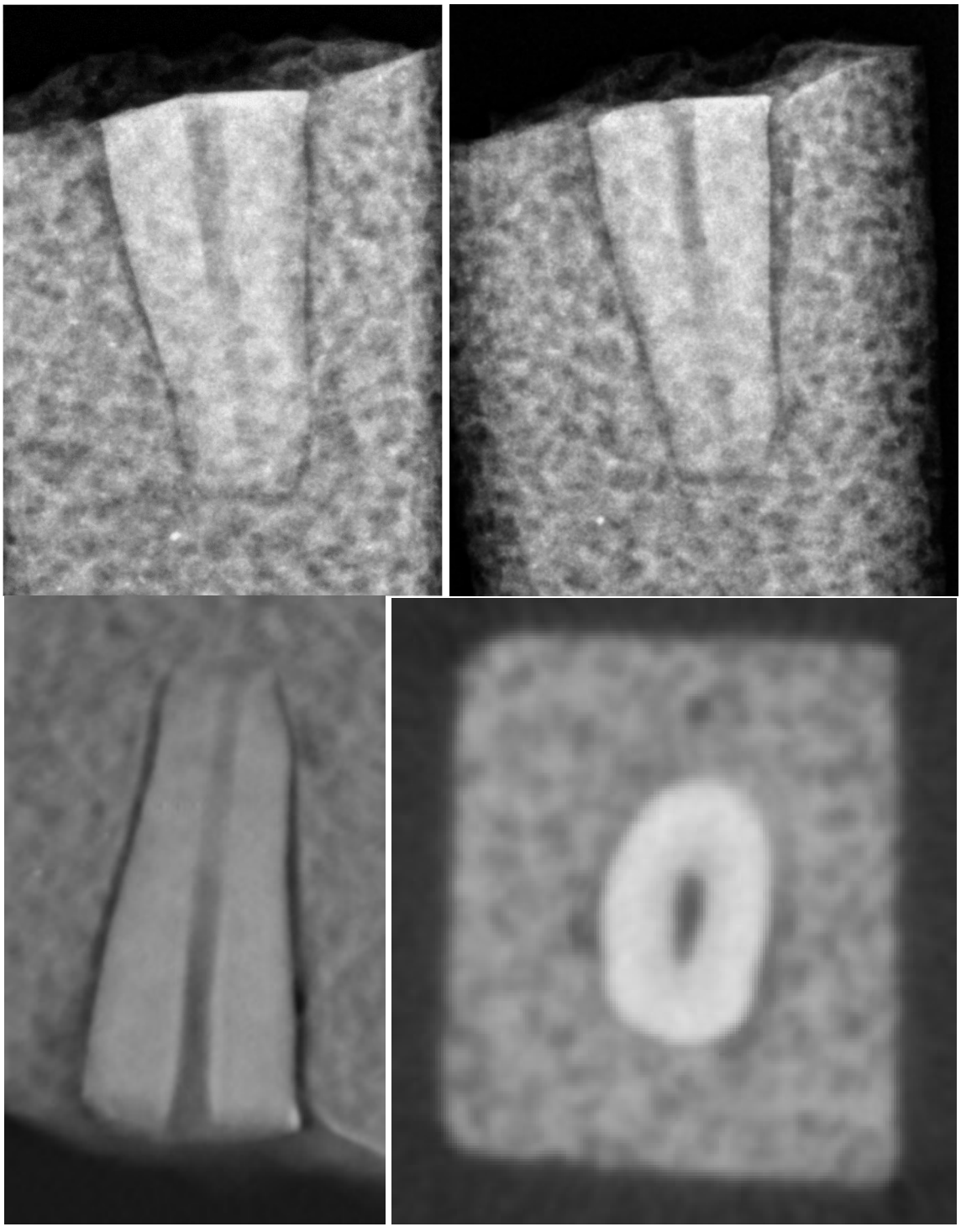

Unobturated and fracture absent #13

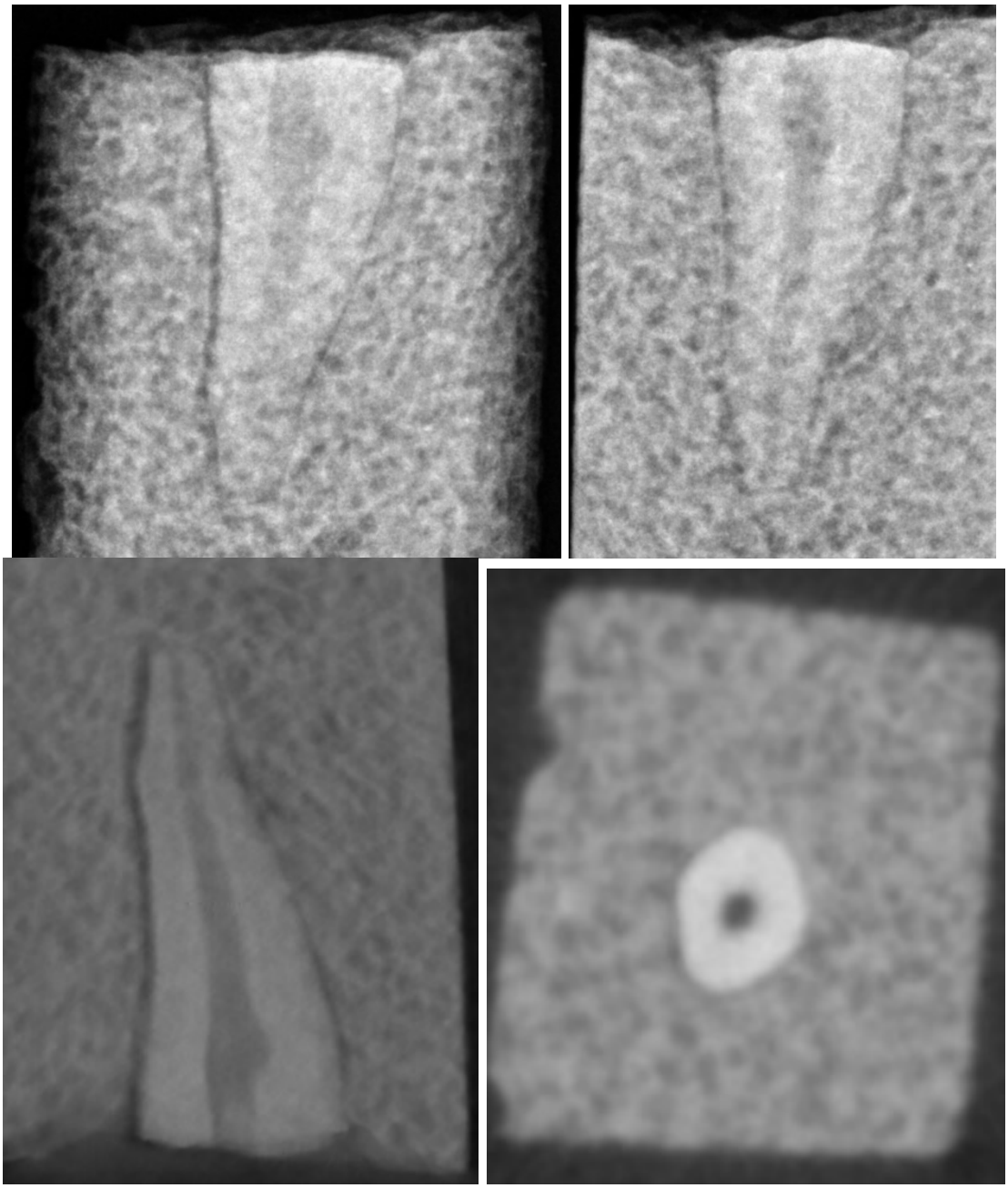

Unobturated and fracture absent #14

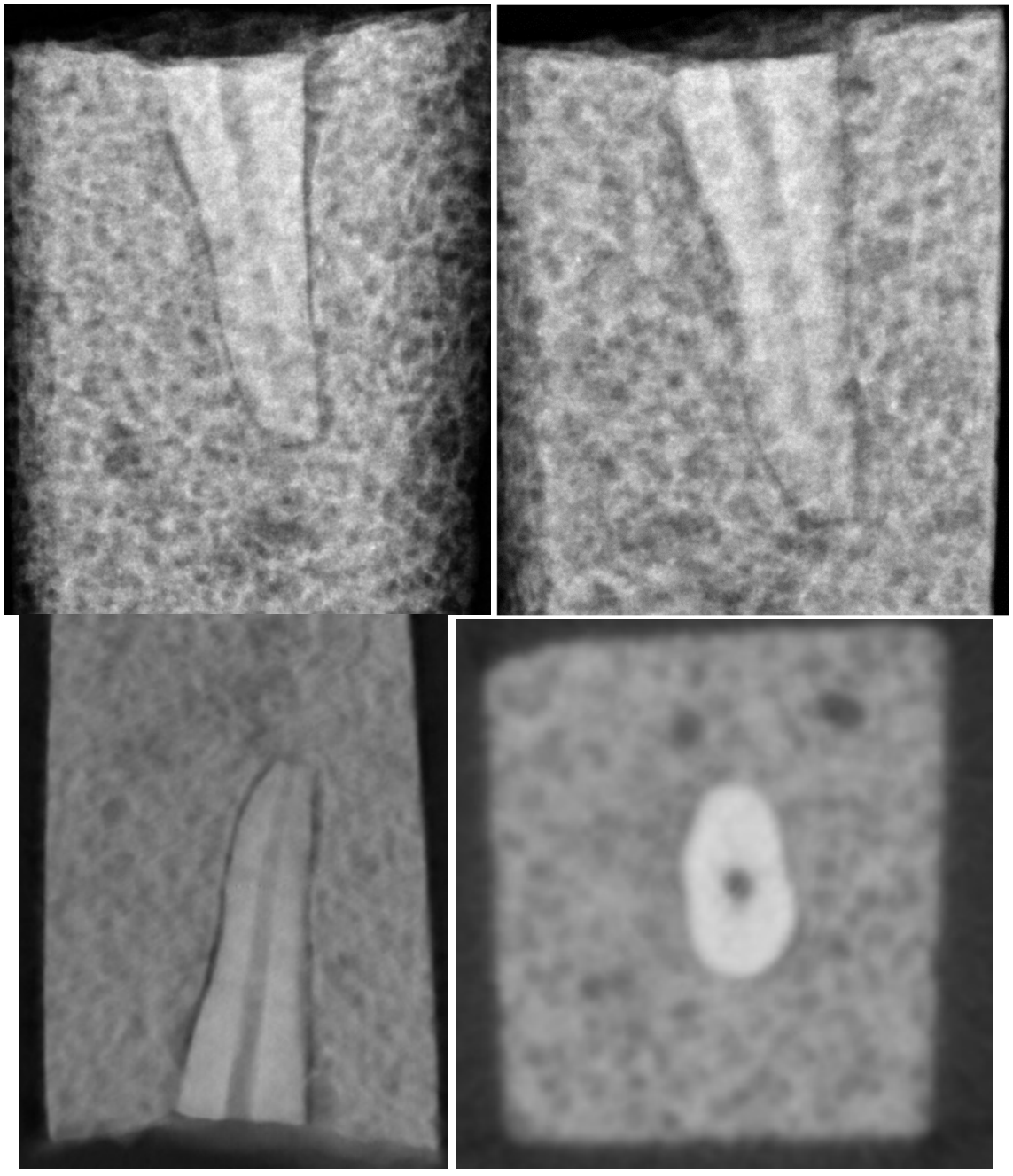

Unobturated and fracture absent #15

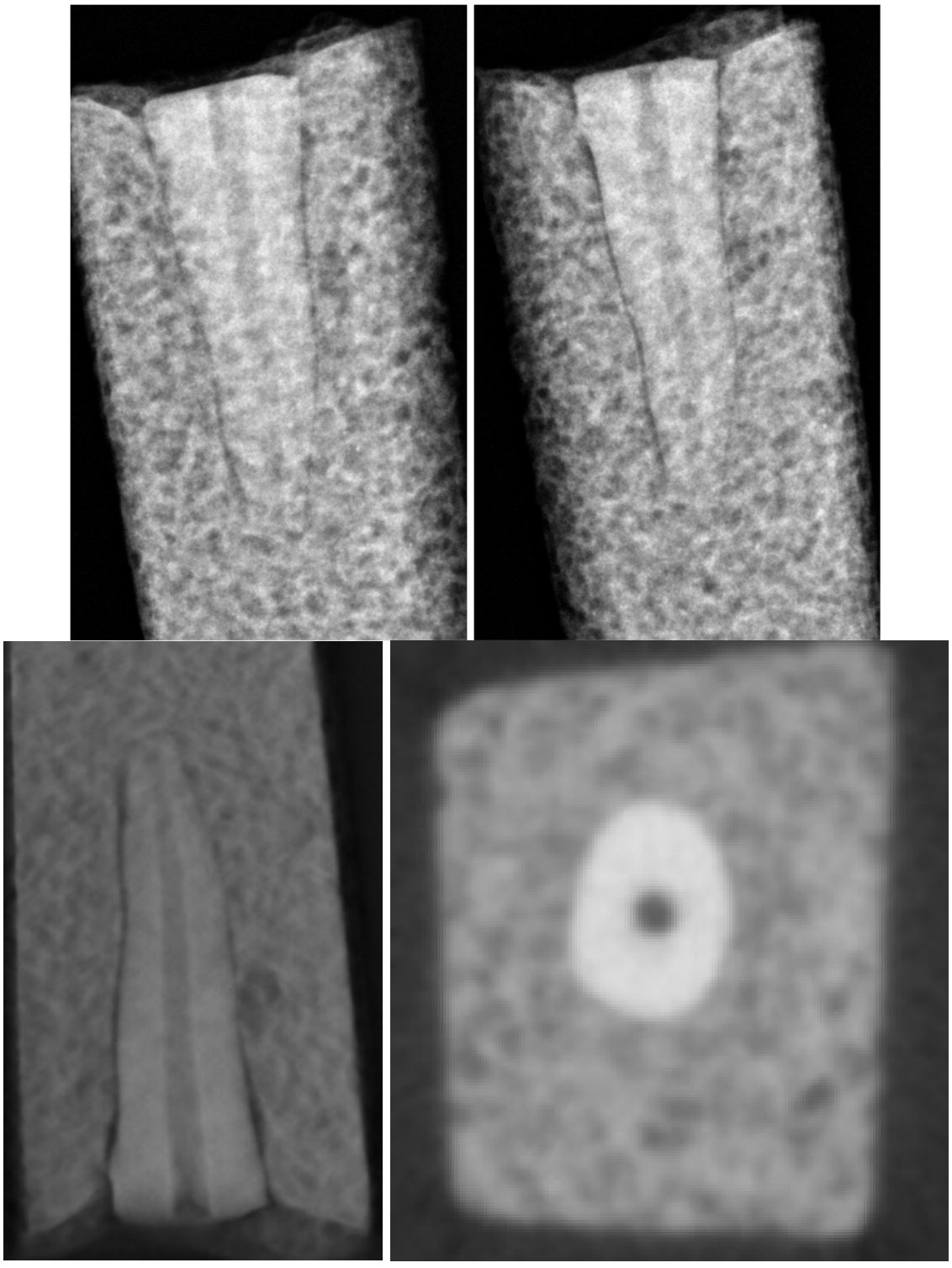

Unobturated and fracture present

Unobturated and fracture present #1

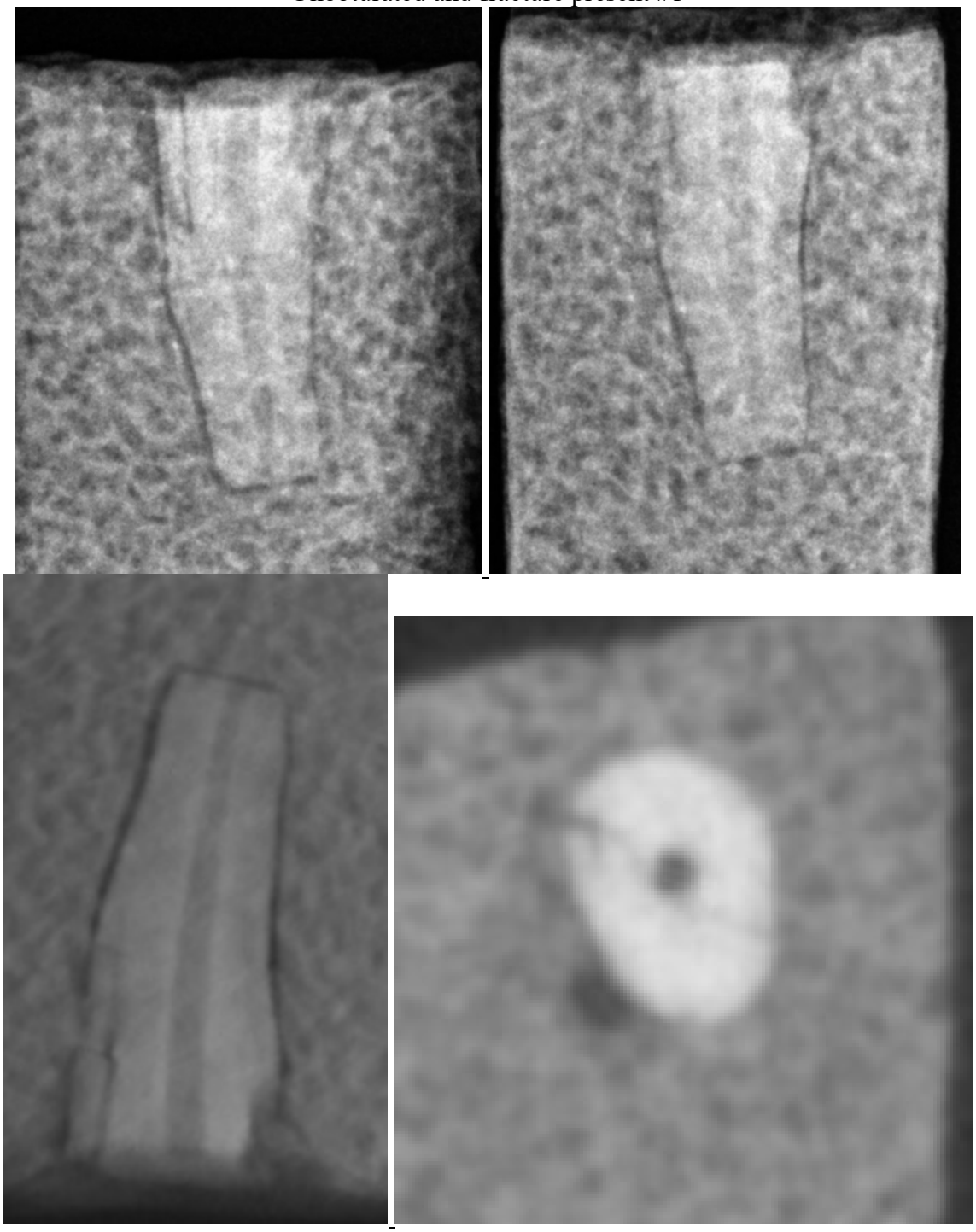

Unobturated and fracture present #2

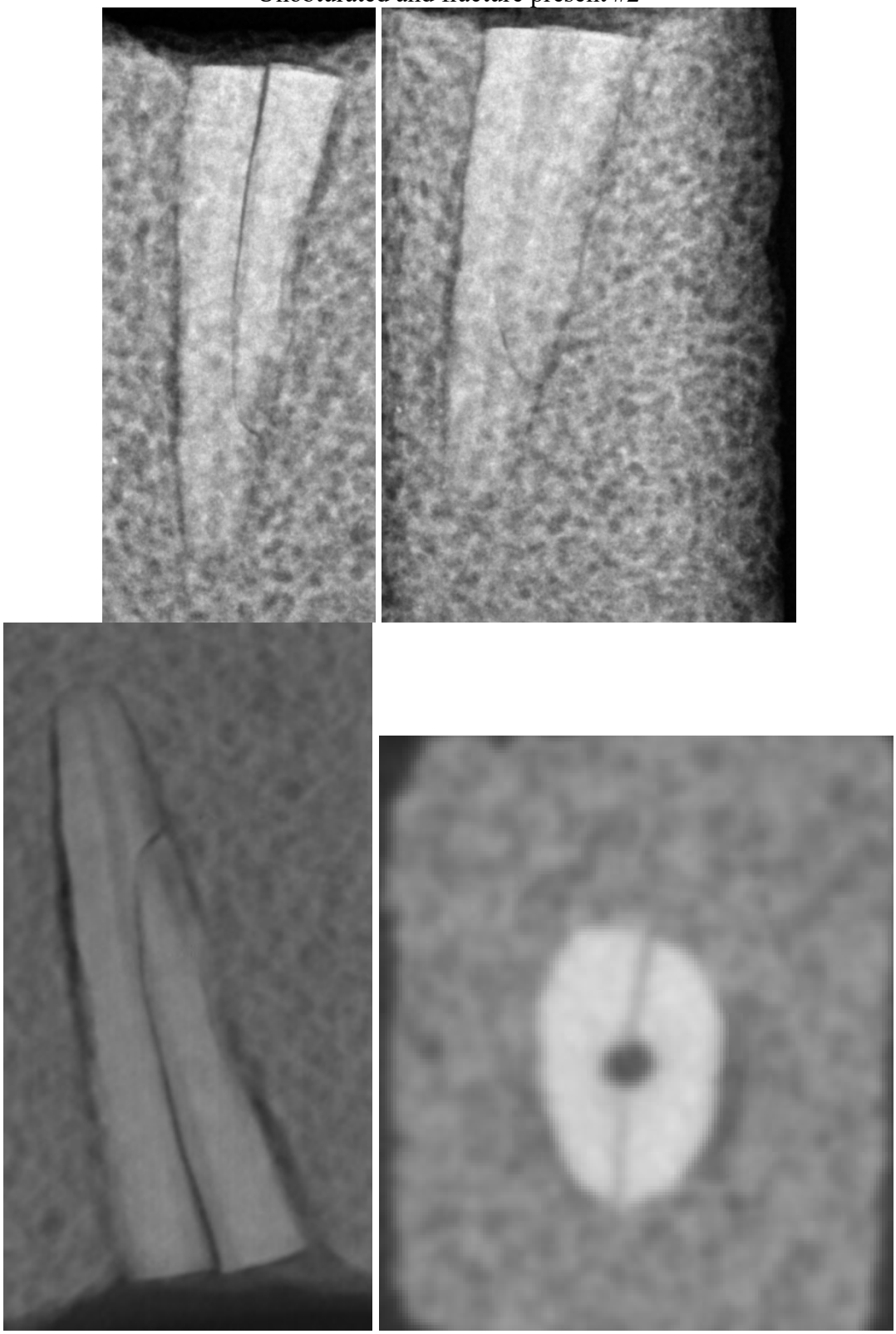

Unobturated and fracture present #3

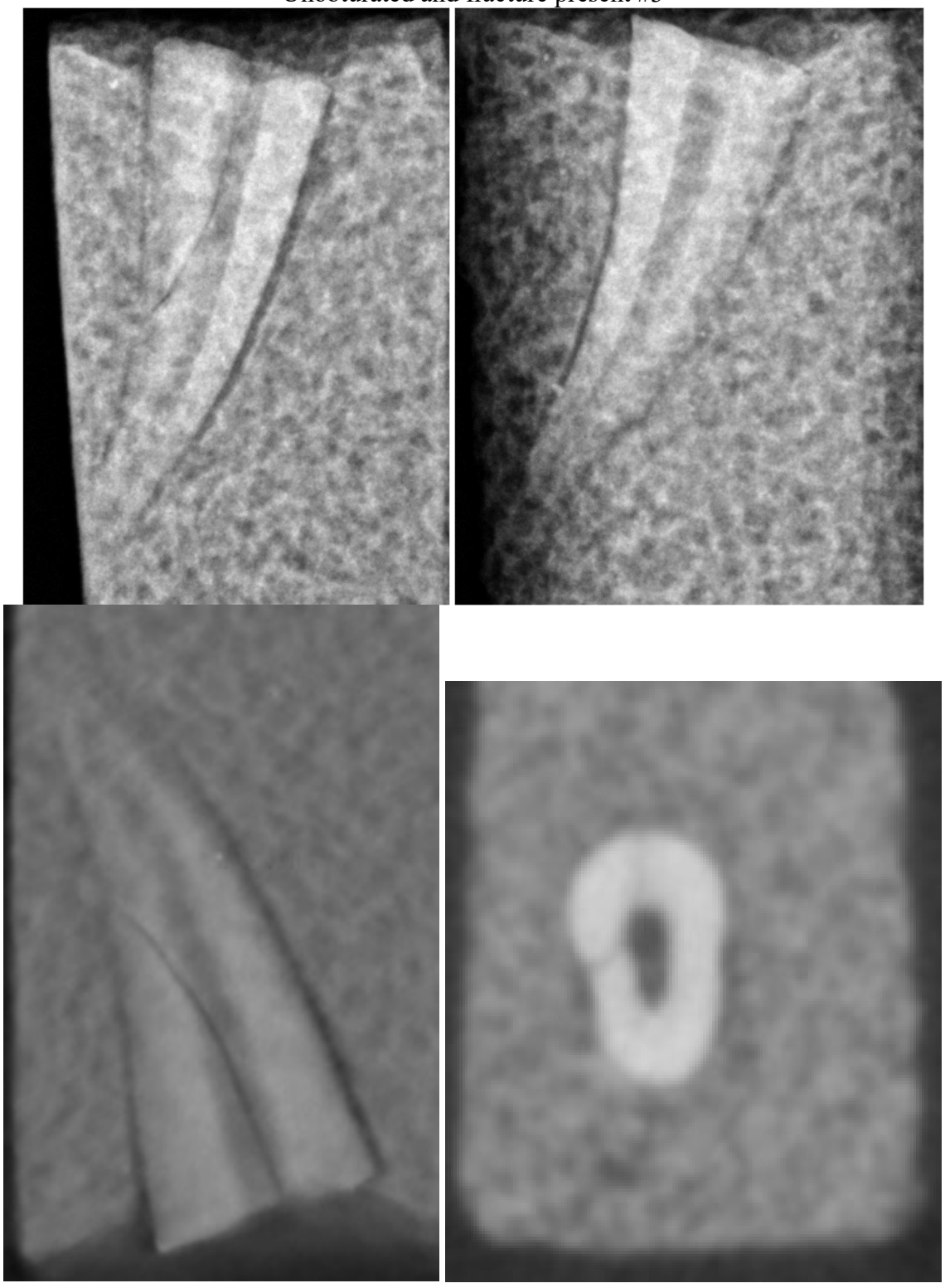

Unobturated and fracture present #4

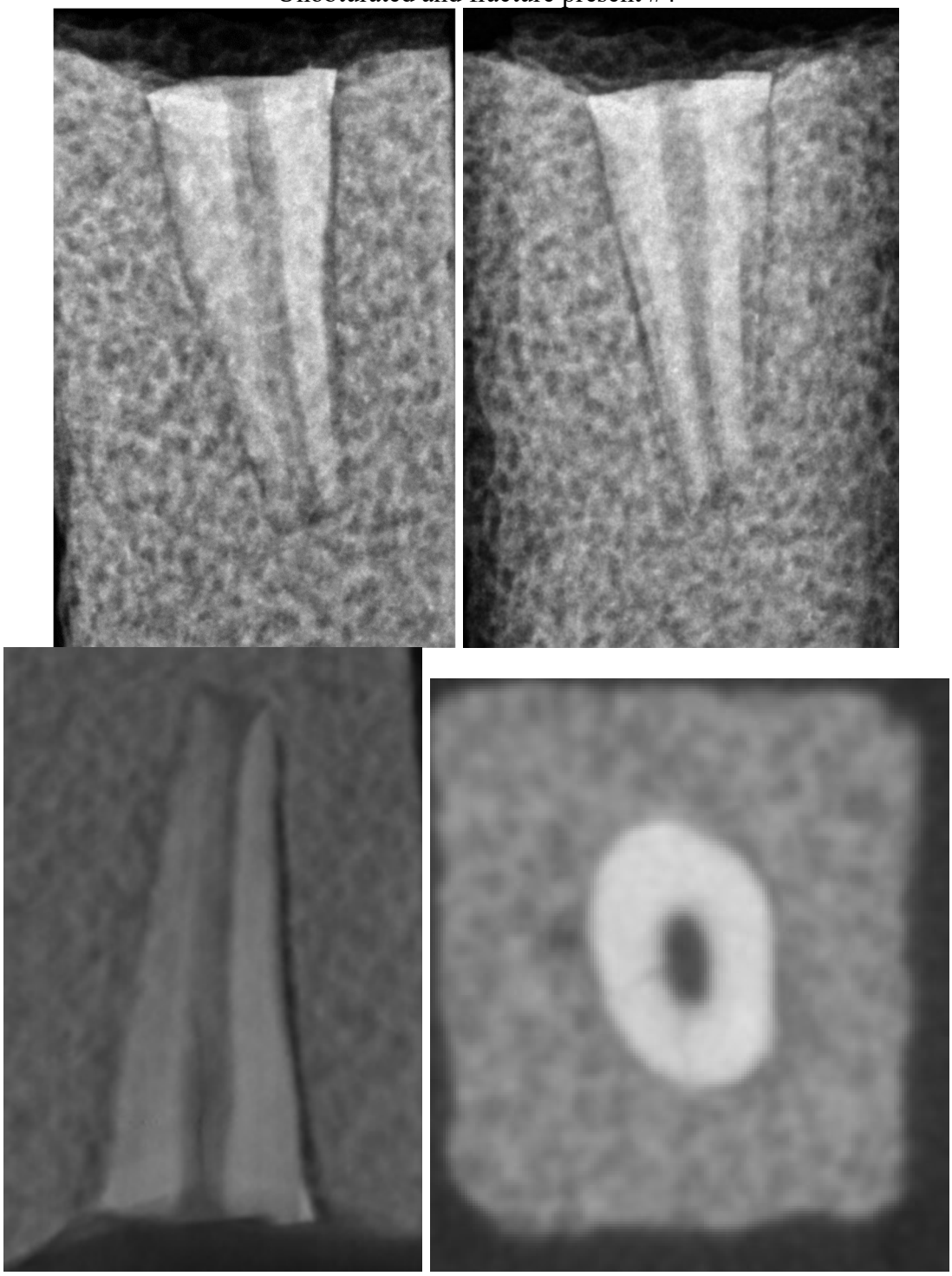

Unobturated and fracture present #5

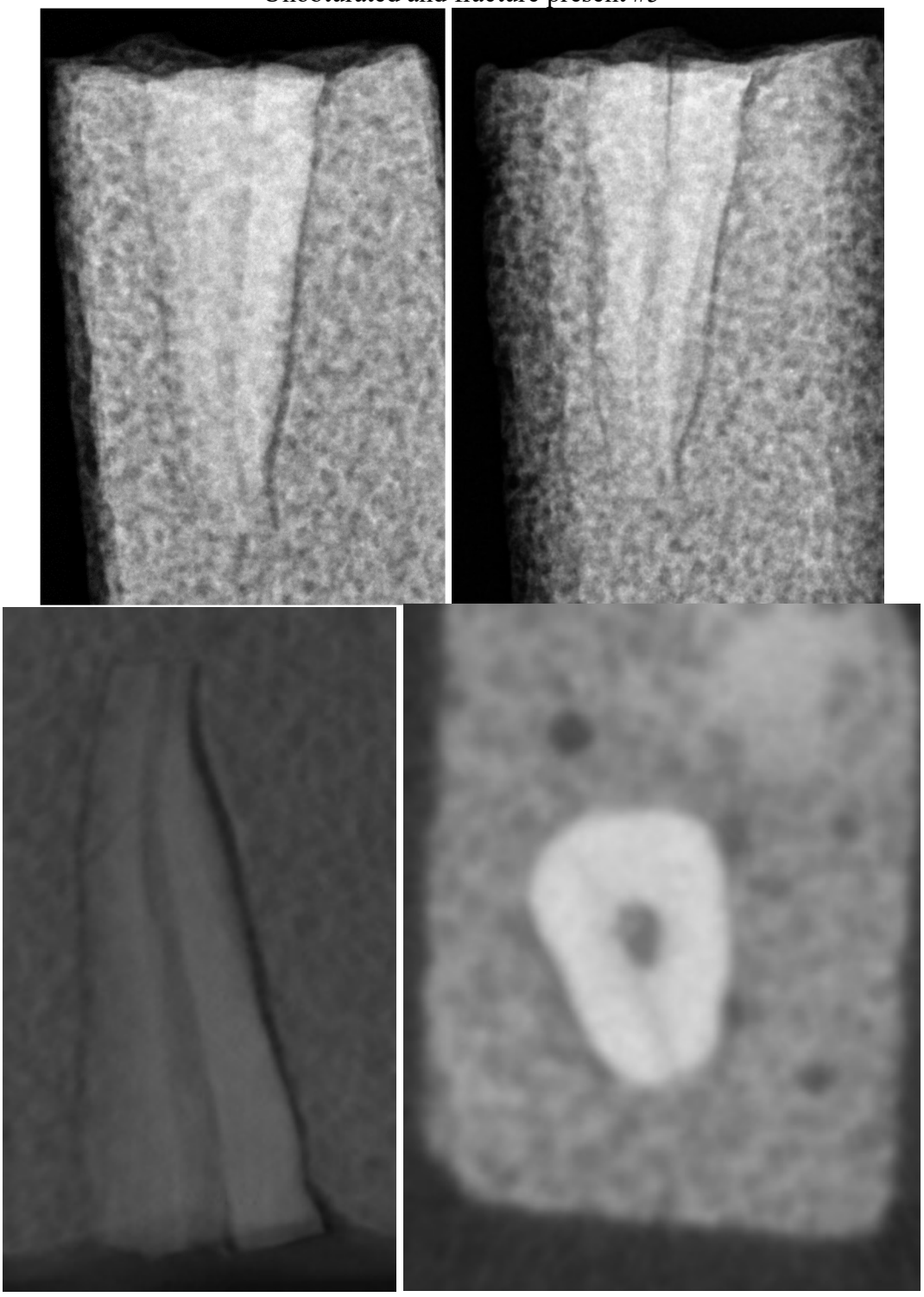

Unobturated and fracture present #6

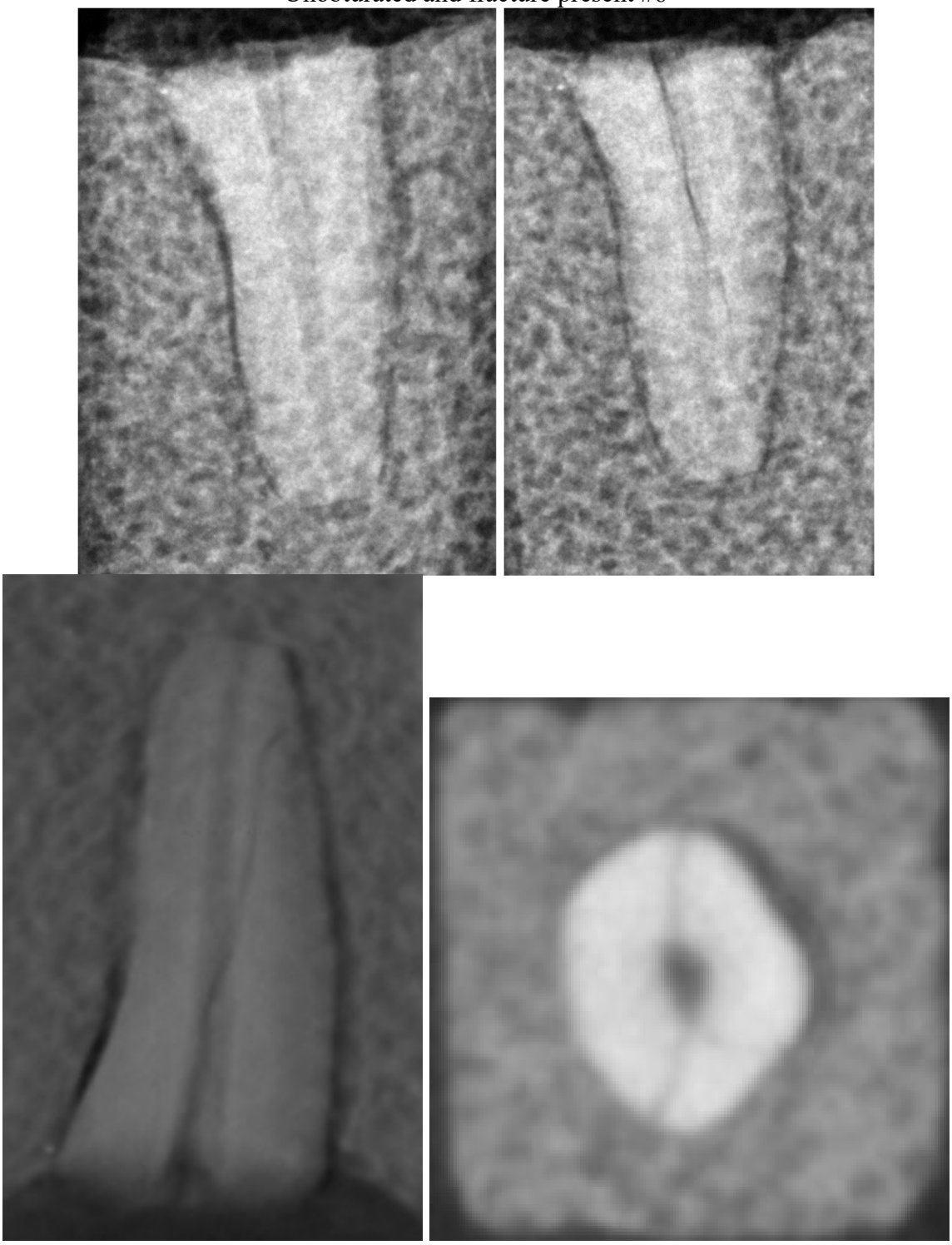

Unobturated and fracture present #7

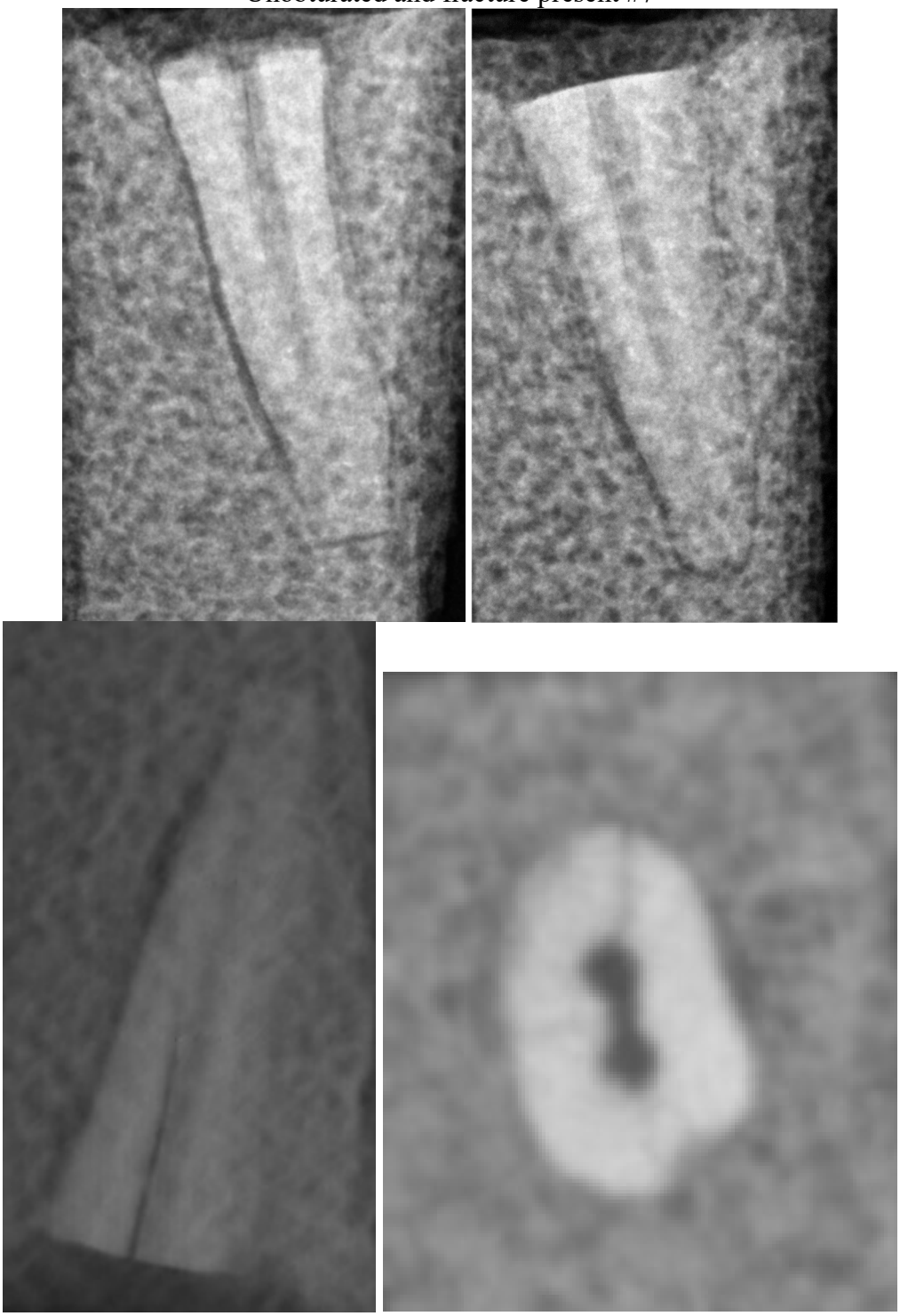

Unobturated and fracture present #8

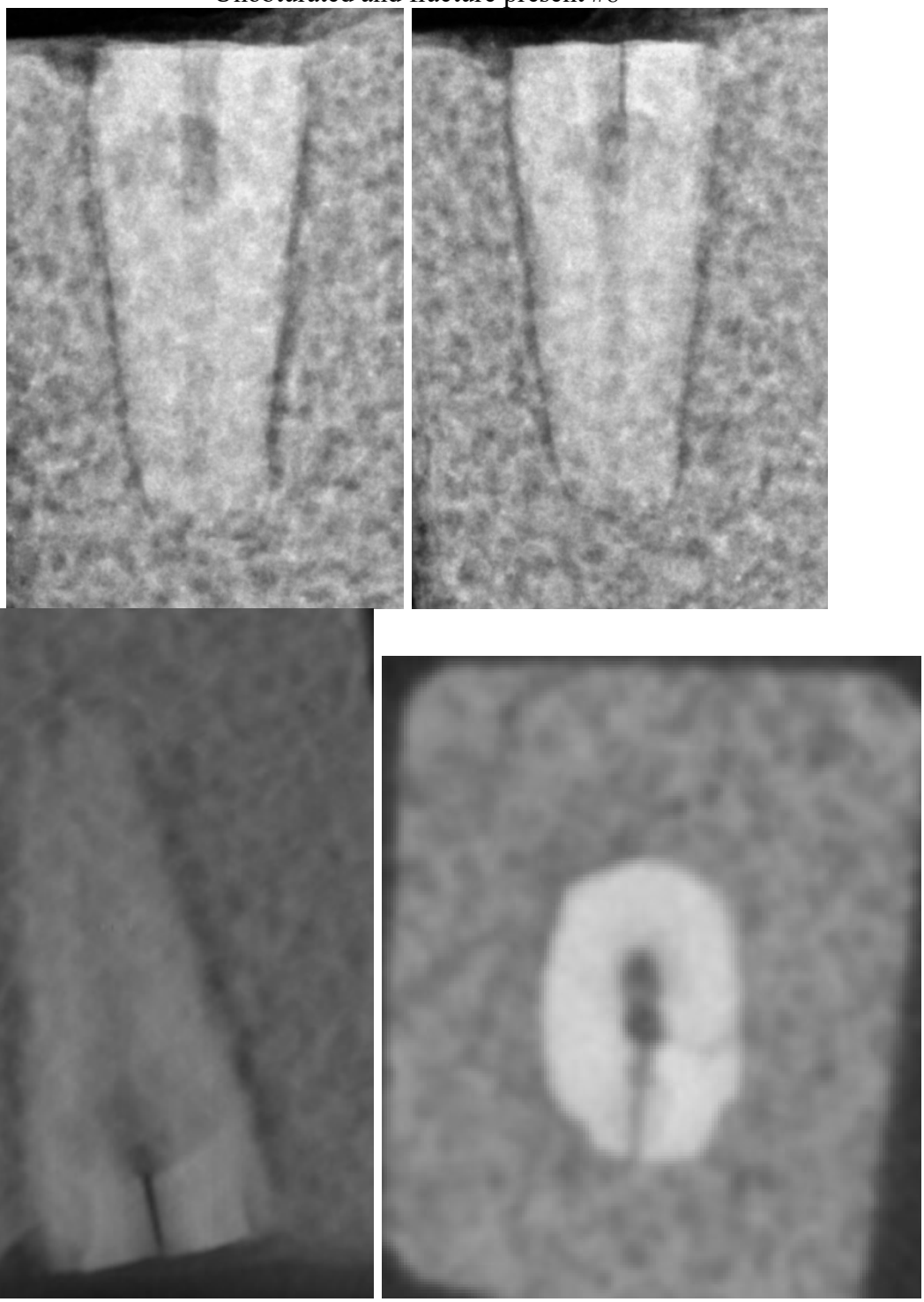

Unobturated and fracture present #9

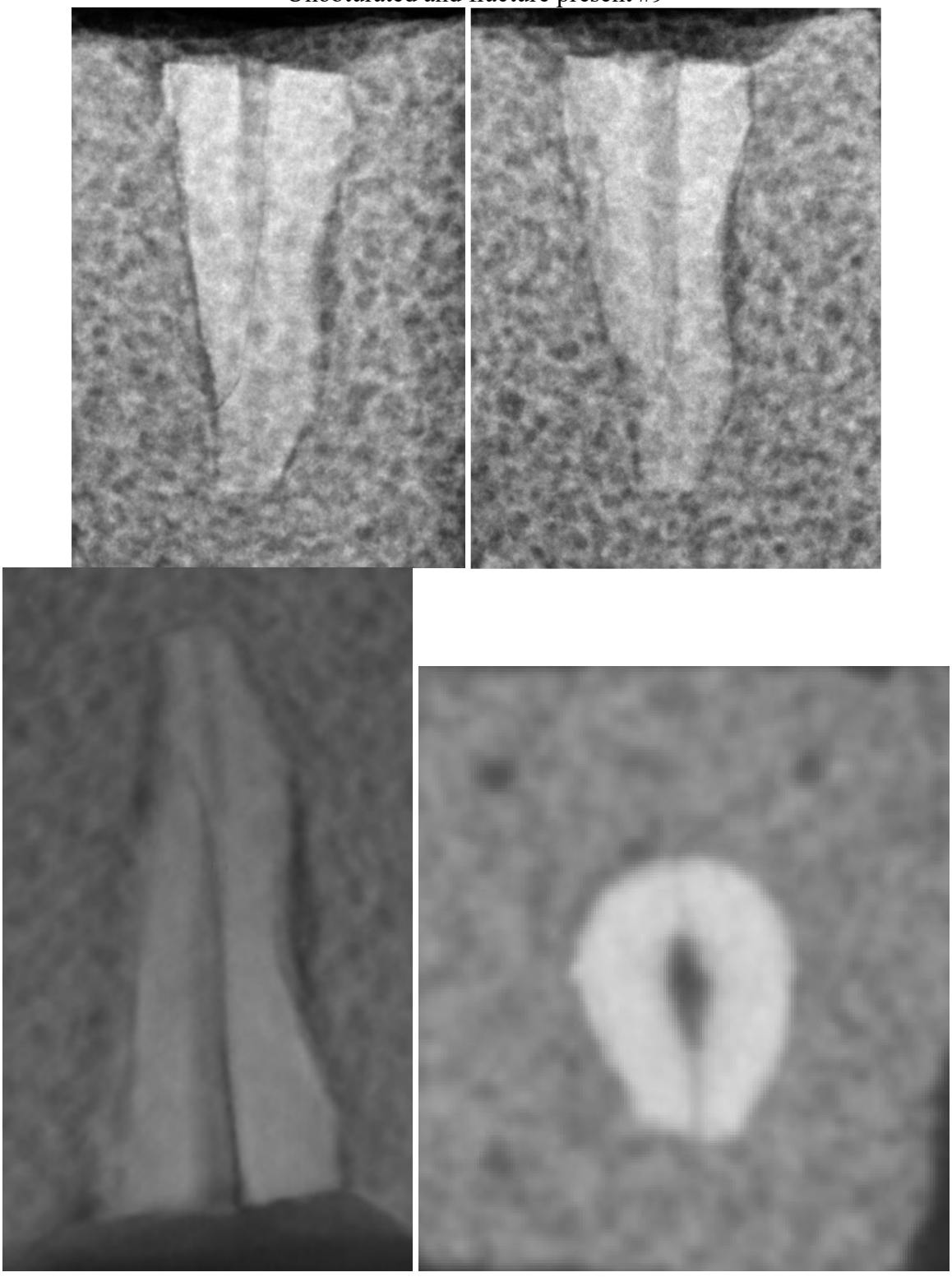

Unobturated and fracture present #10

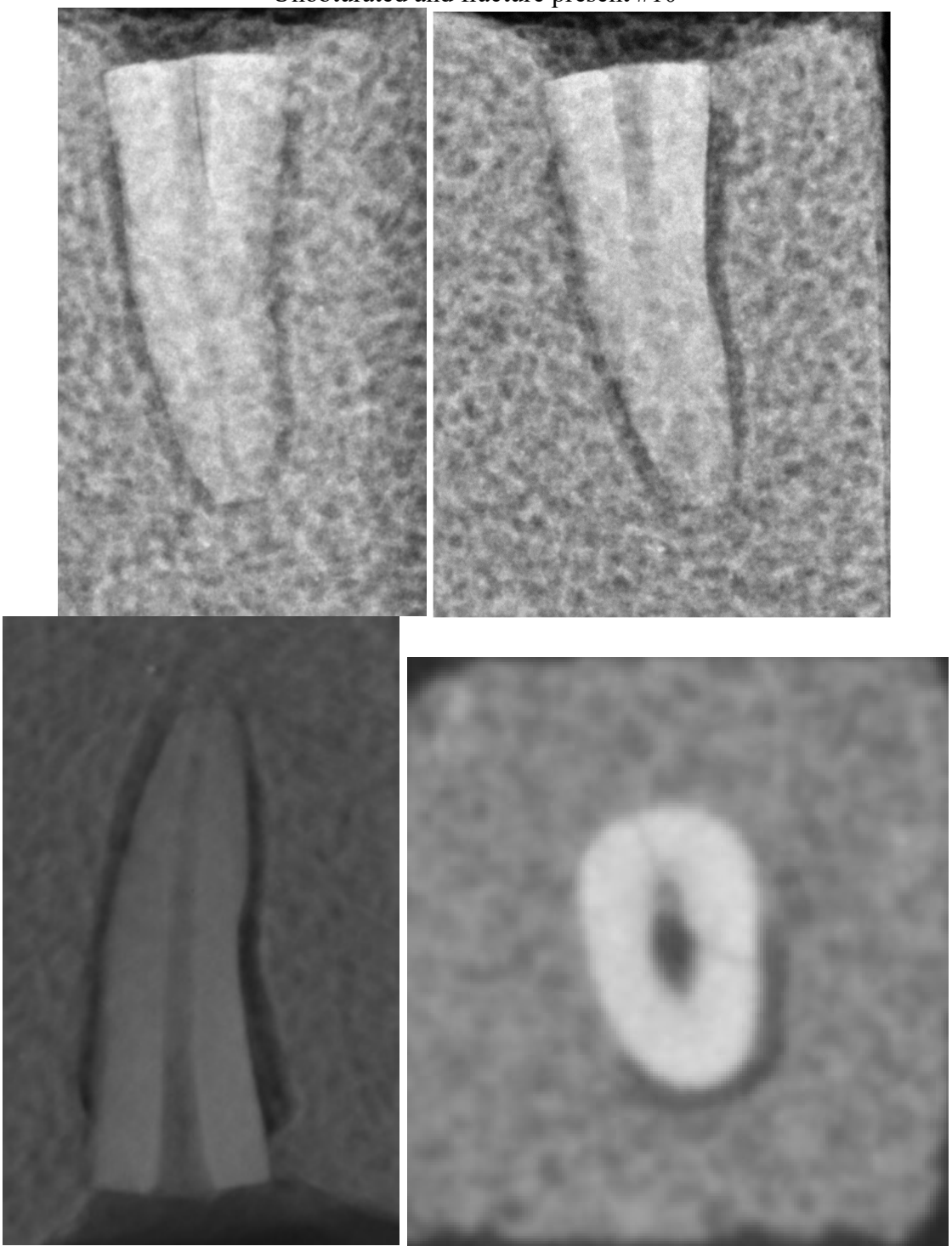

Unobturated and fracture present #11

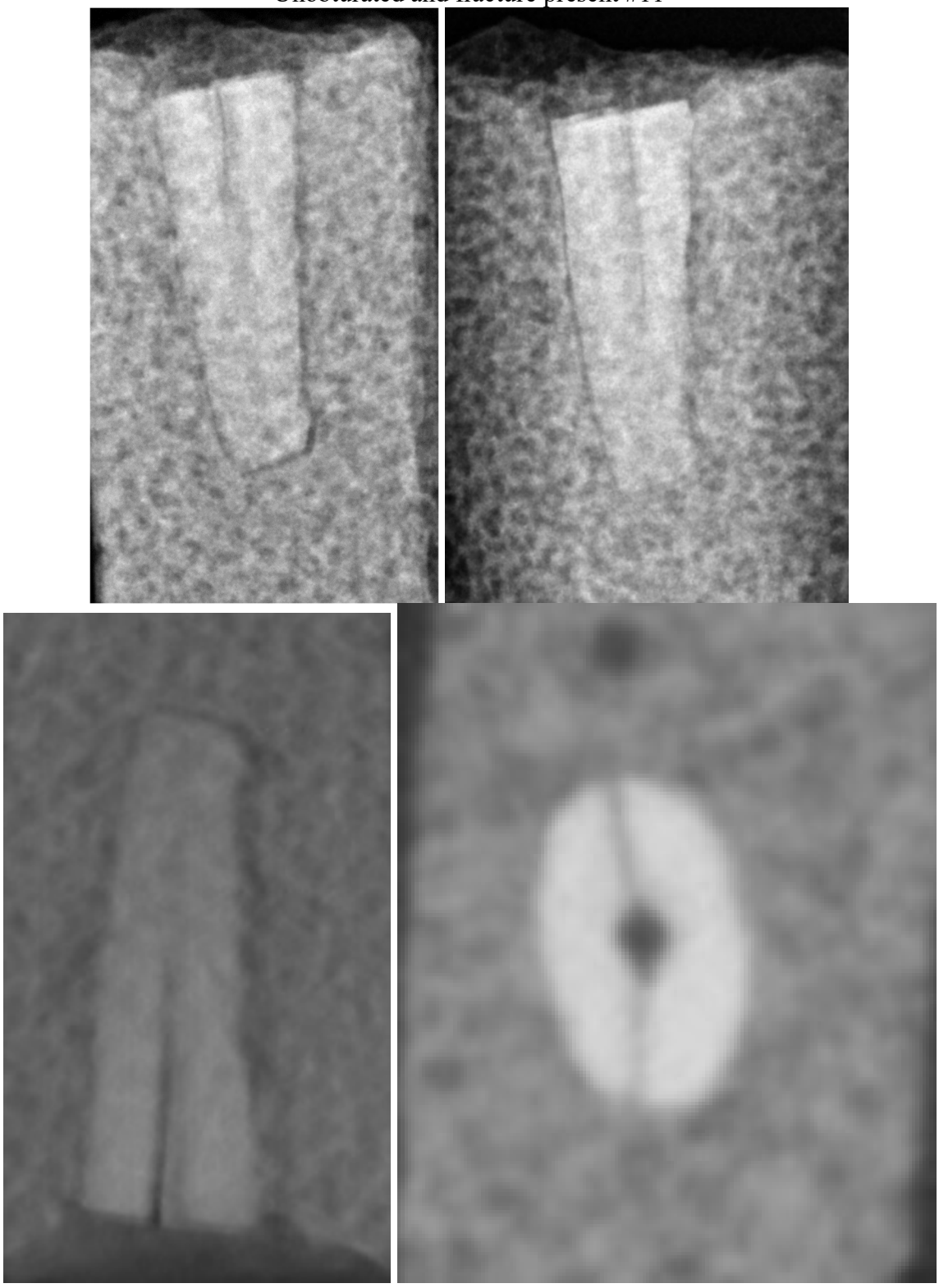

Unobturated and fracture present #12

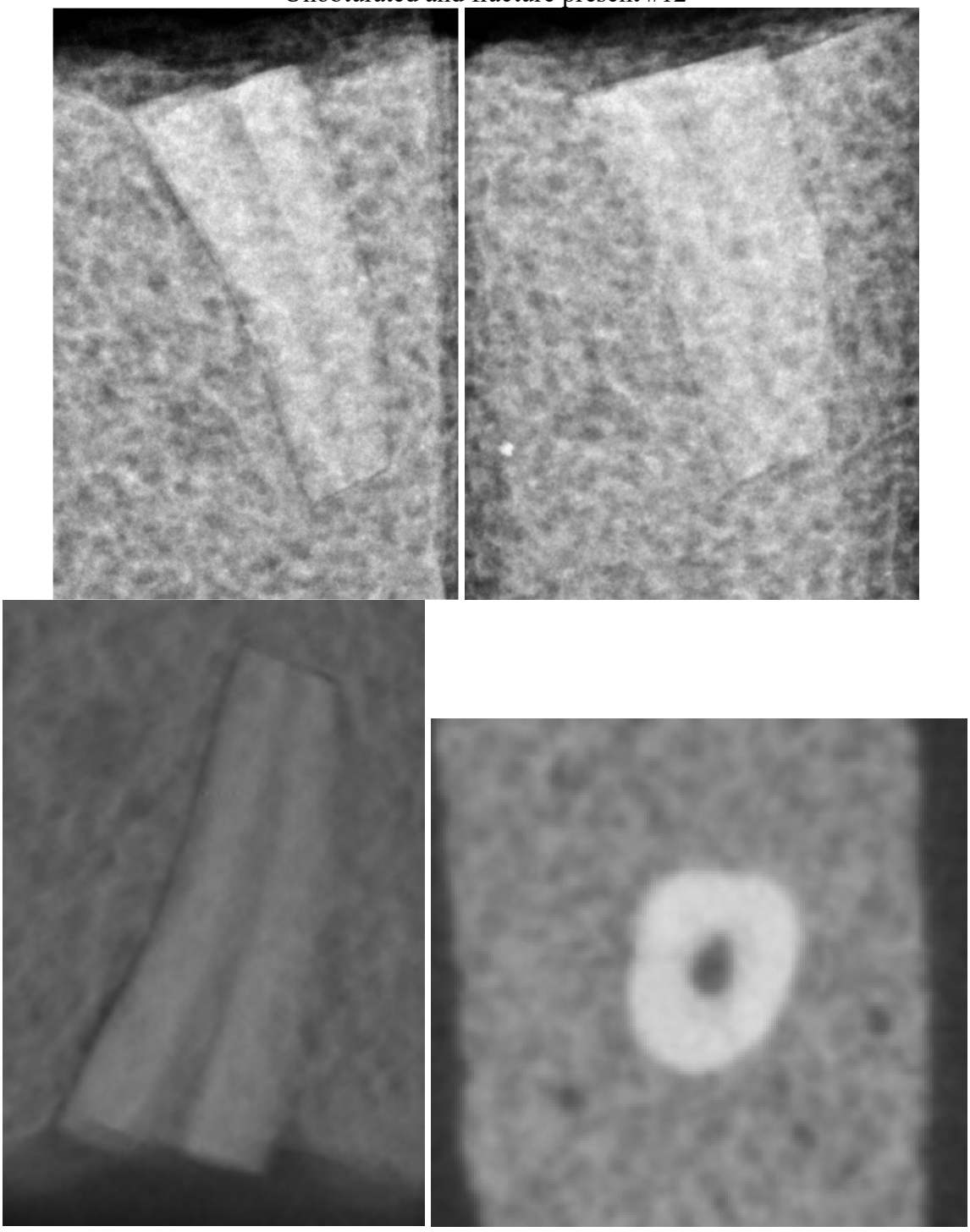

Unobturated and fracture present #13

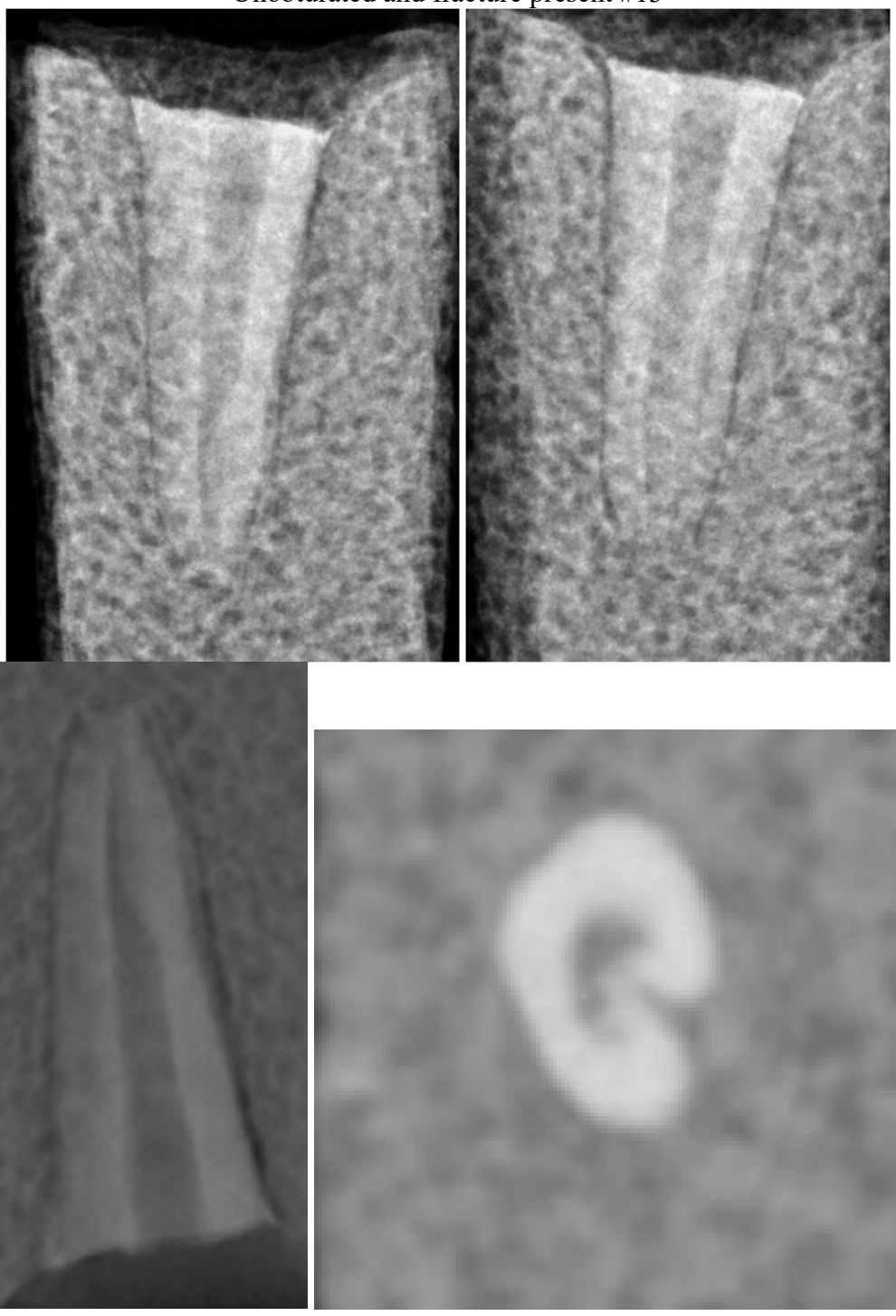

Unobturated and fracture present #14

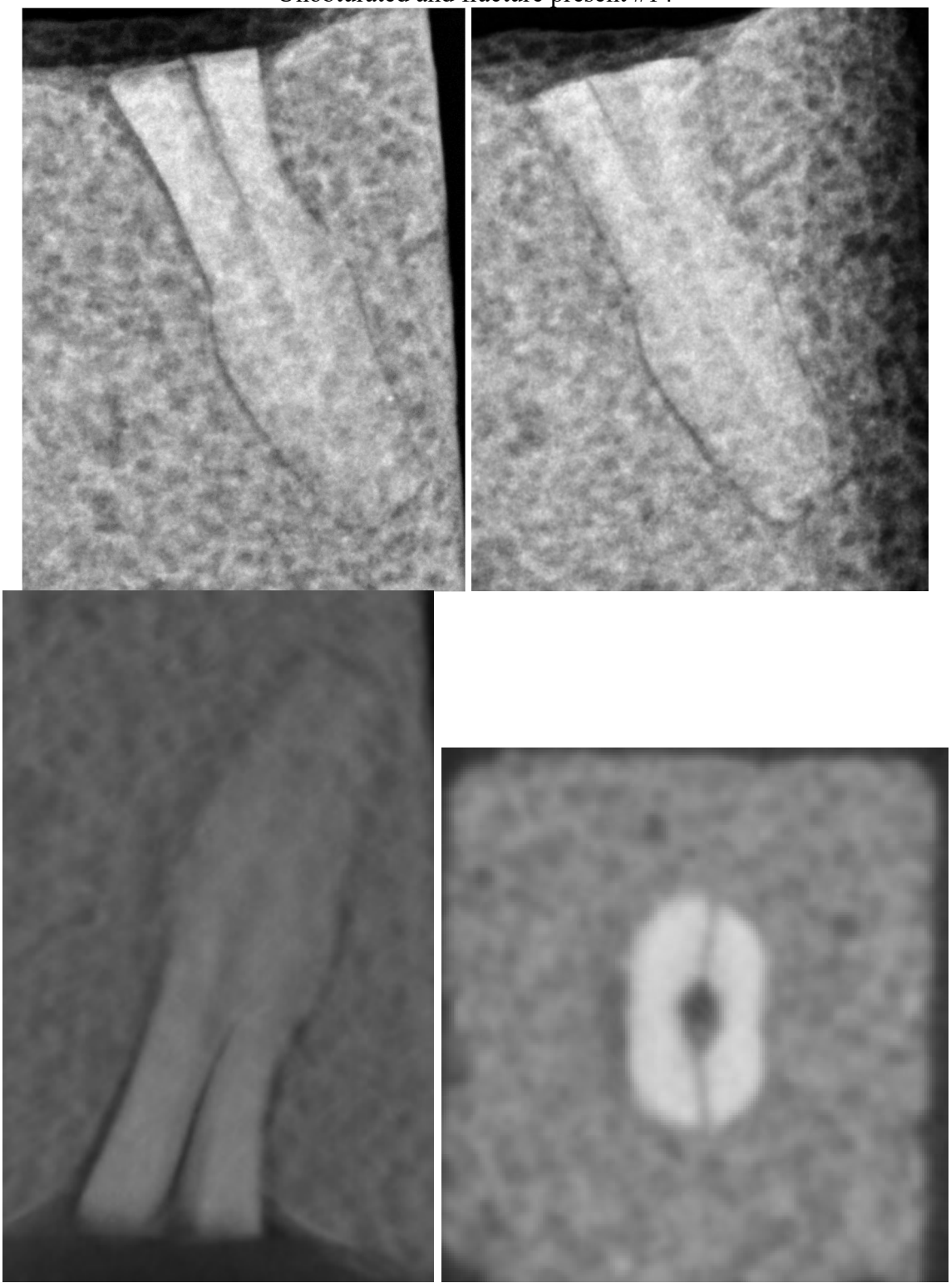

Unobturated and fracture present #15

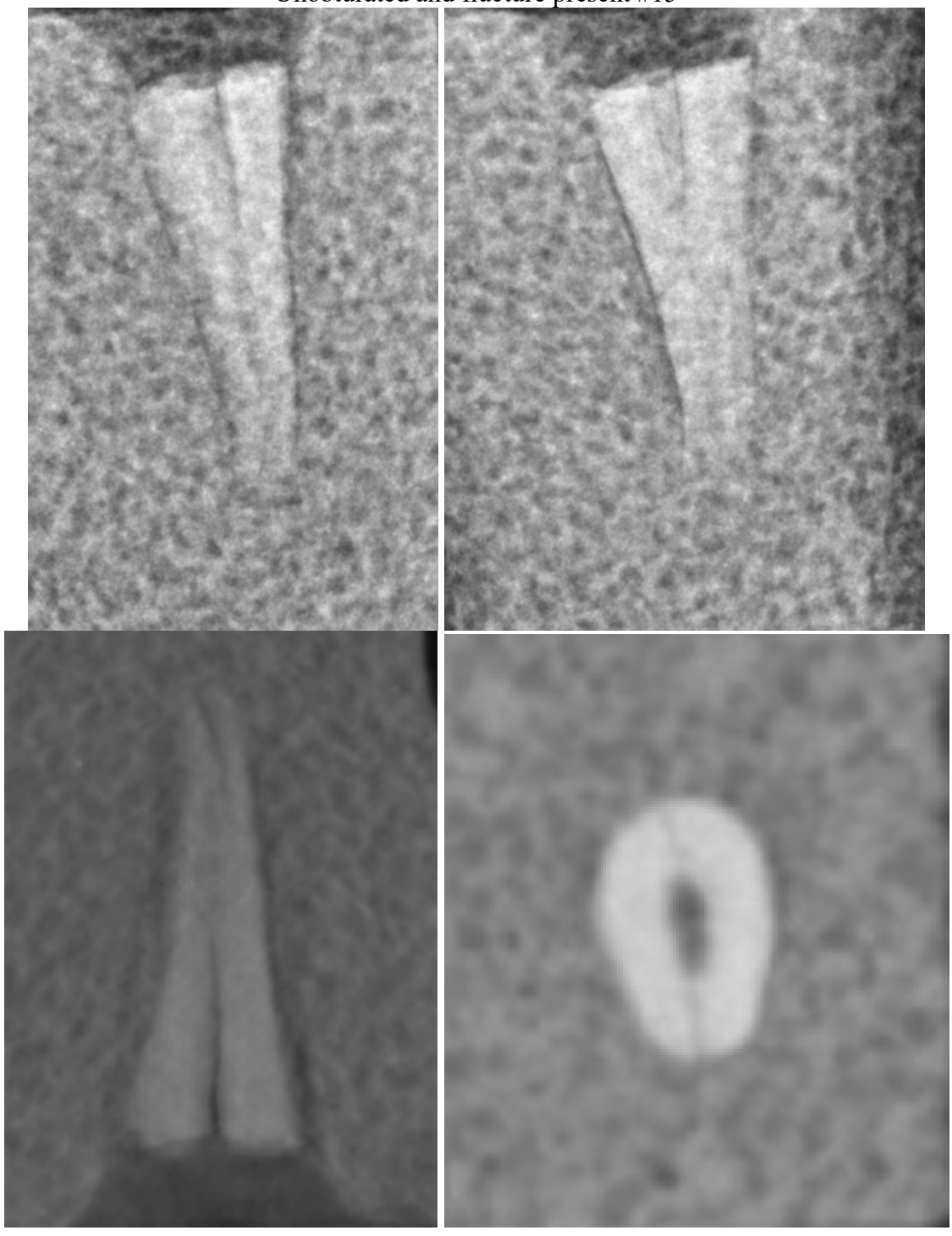

Obturated and fracture absent

Obturated and fracture absent #1

Obturated and fracture absent #2

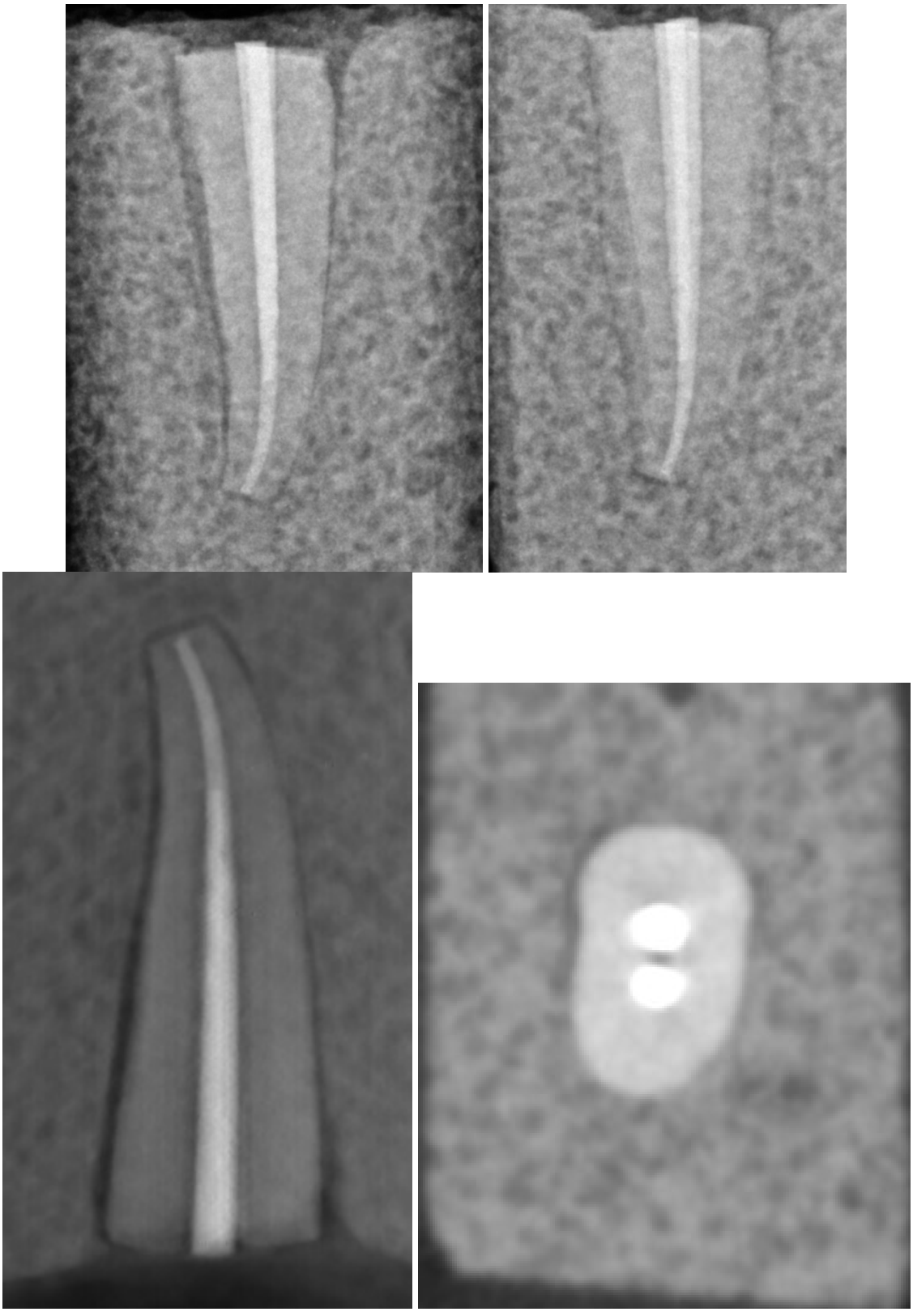

Obturated and fracture absent #3

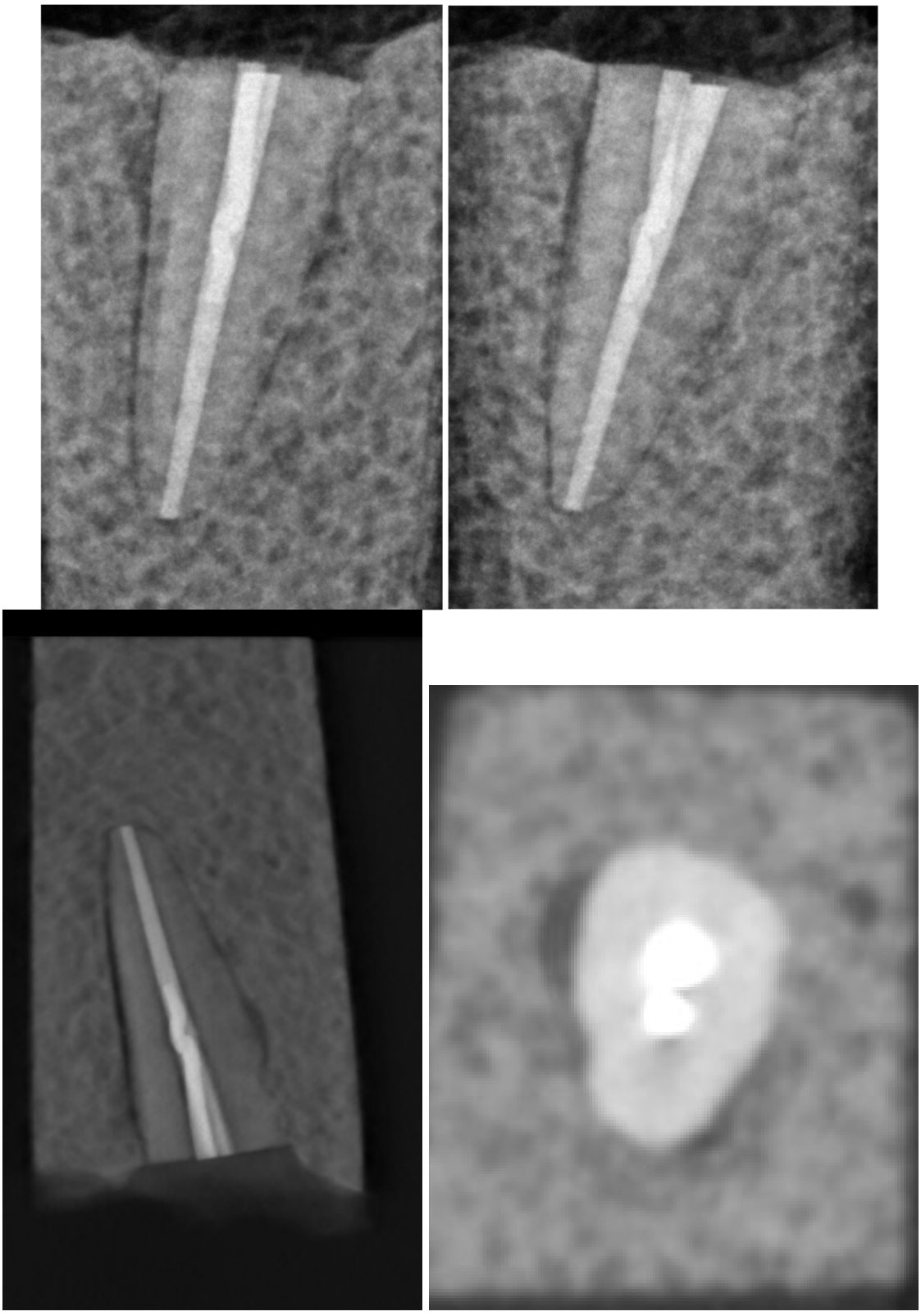

Obturated and fracture absent #4

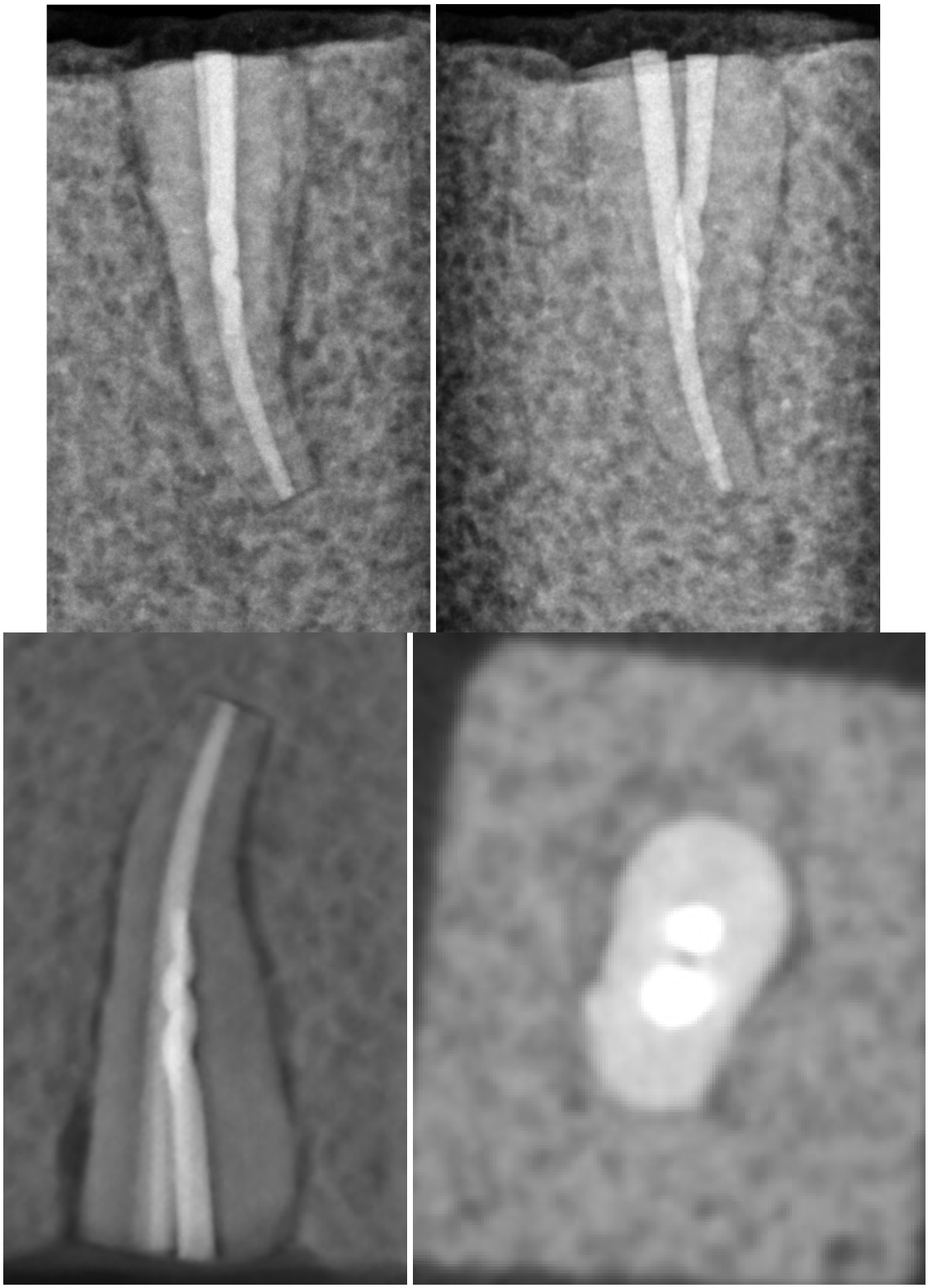

Obturated and fracture absent #5

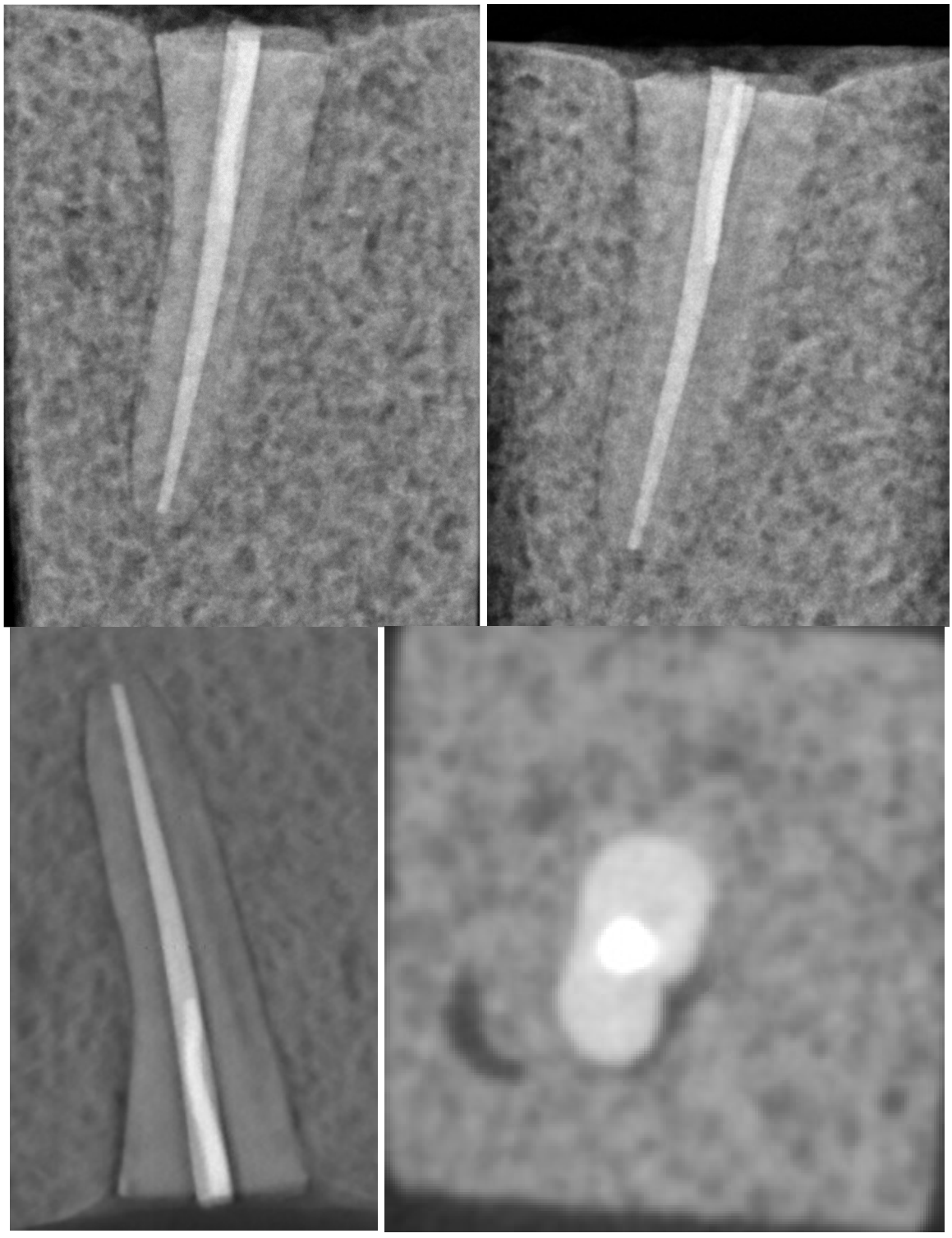

Obturated and fracture absent #6

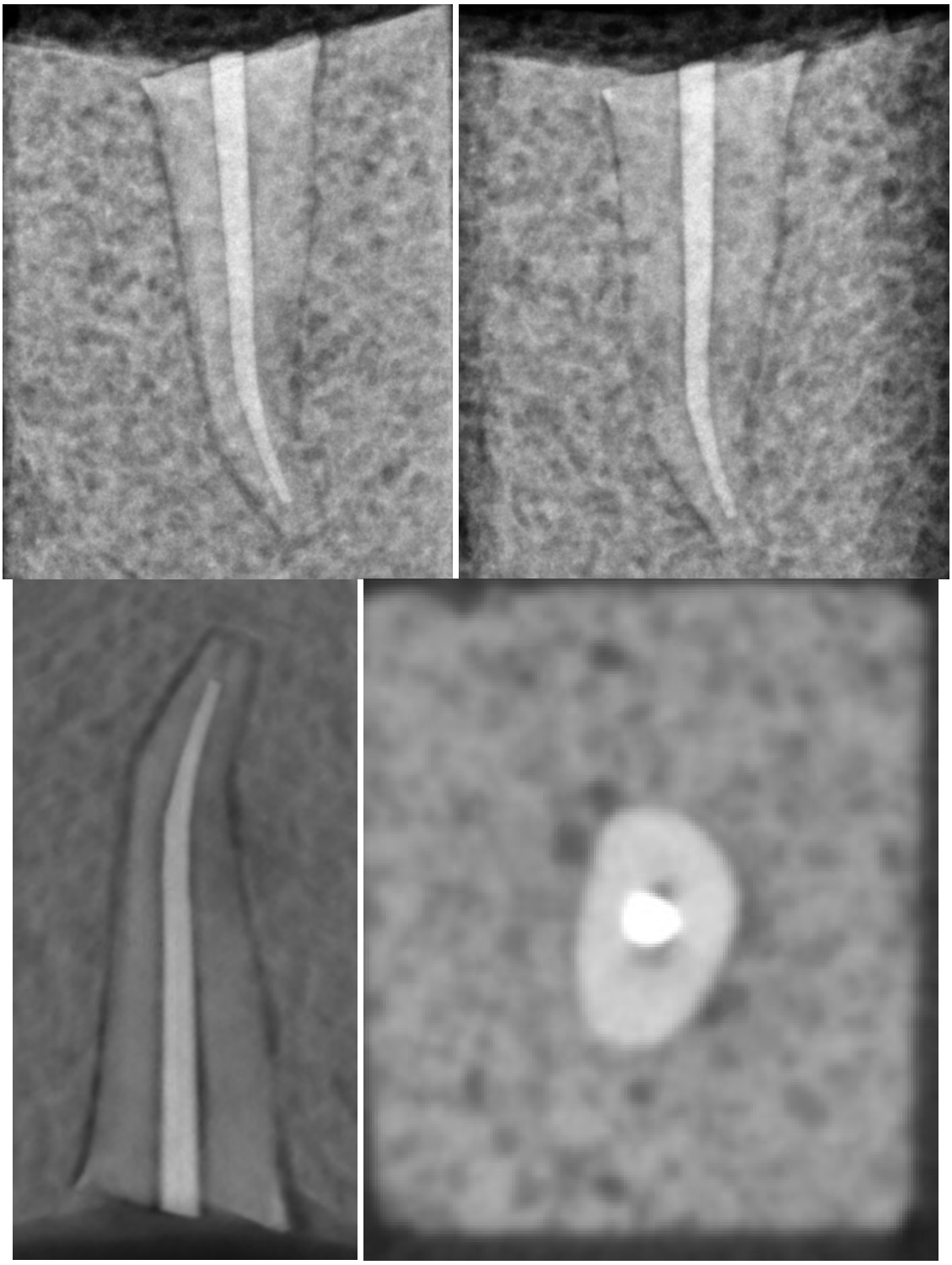

Obturated and fracture absent #7

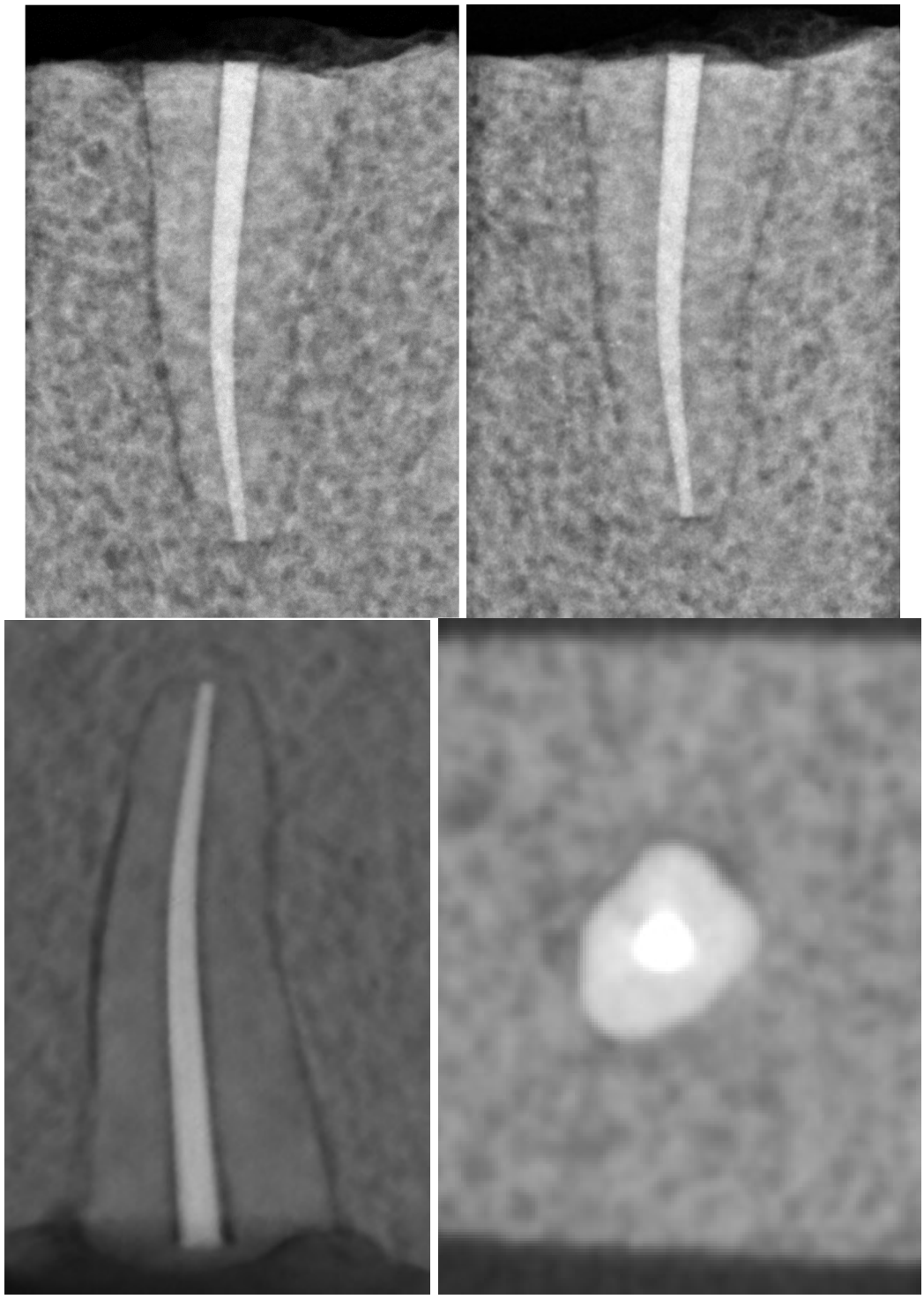

Obturated and fracture absent #8

Obturated and fracture absent #9

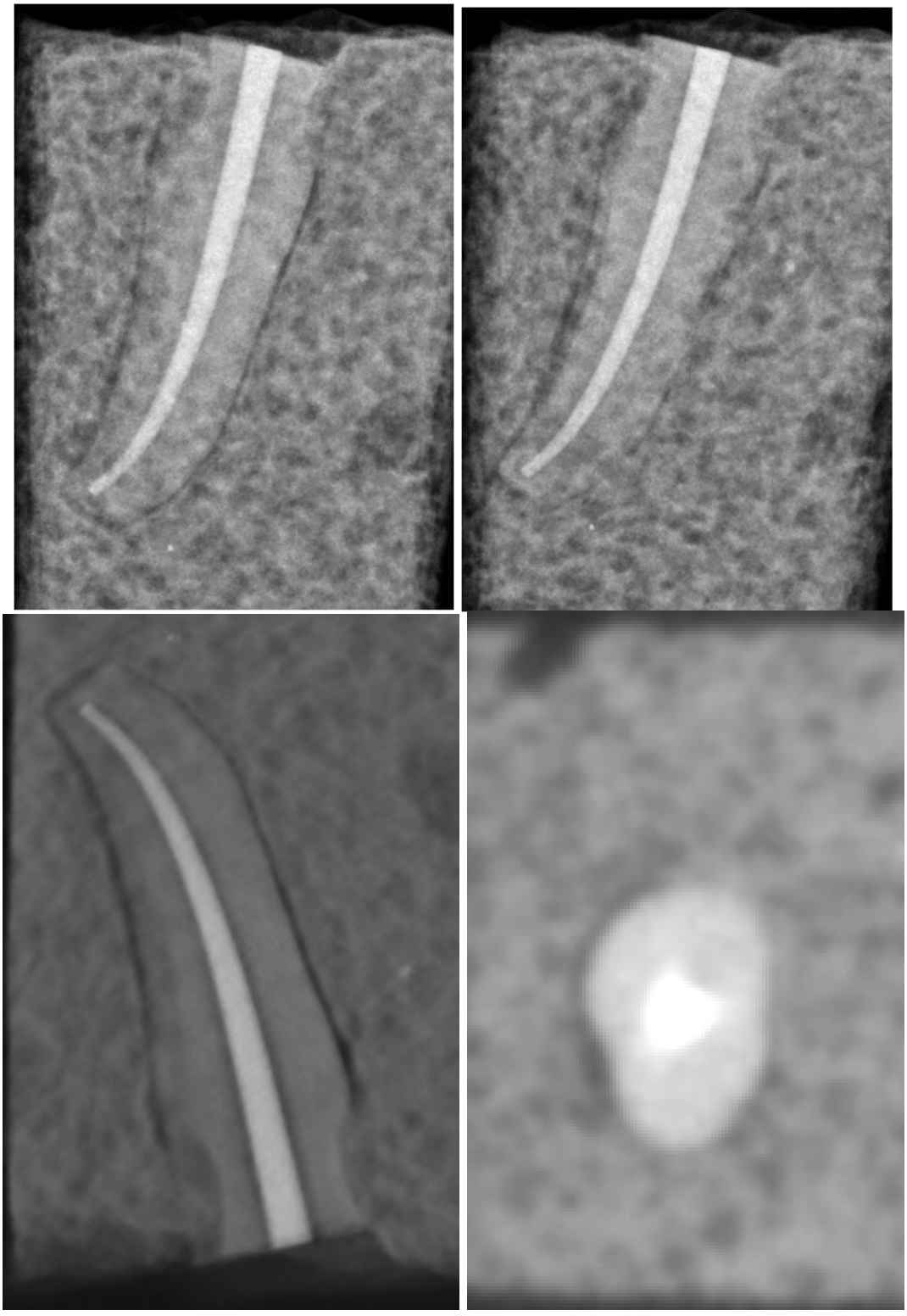

Obturated and fracture absent #10

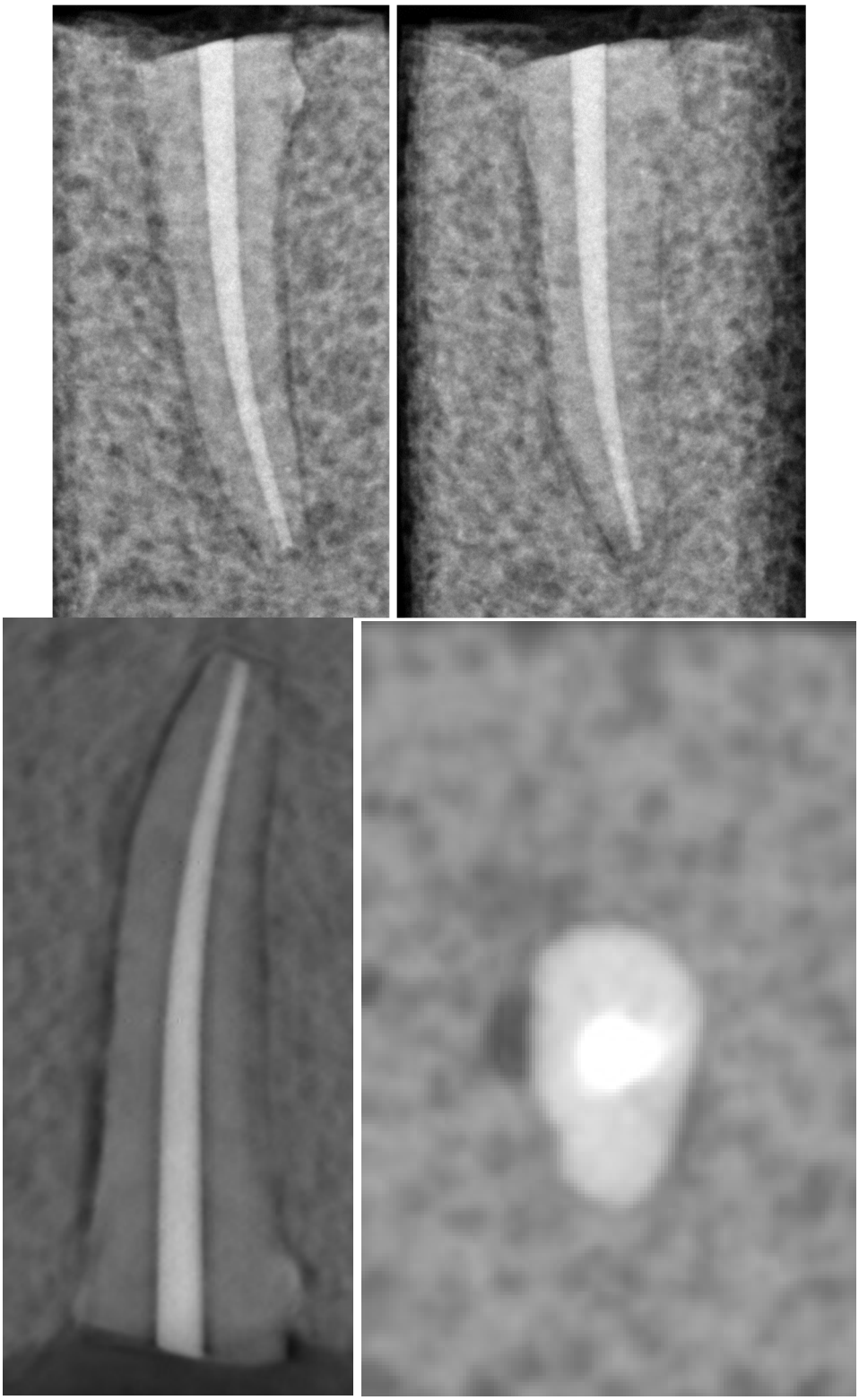

Obturated and fracture absent #11

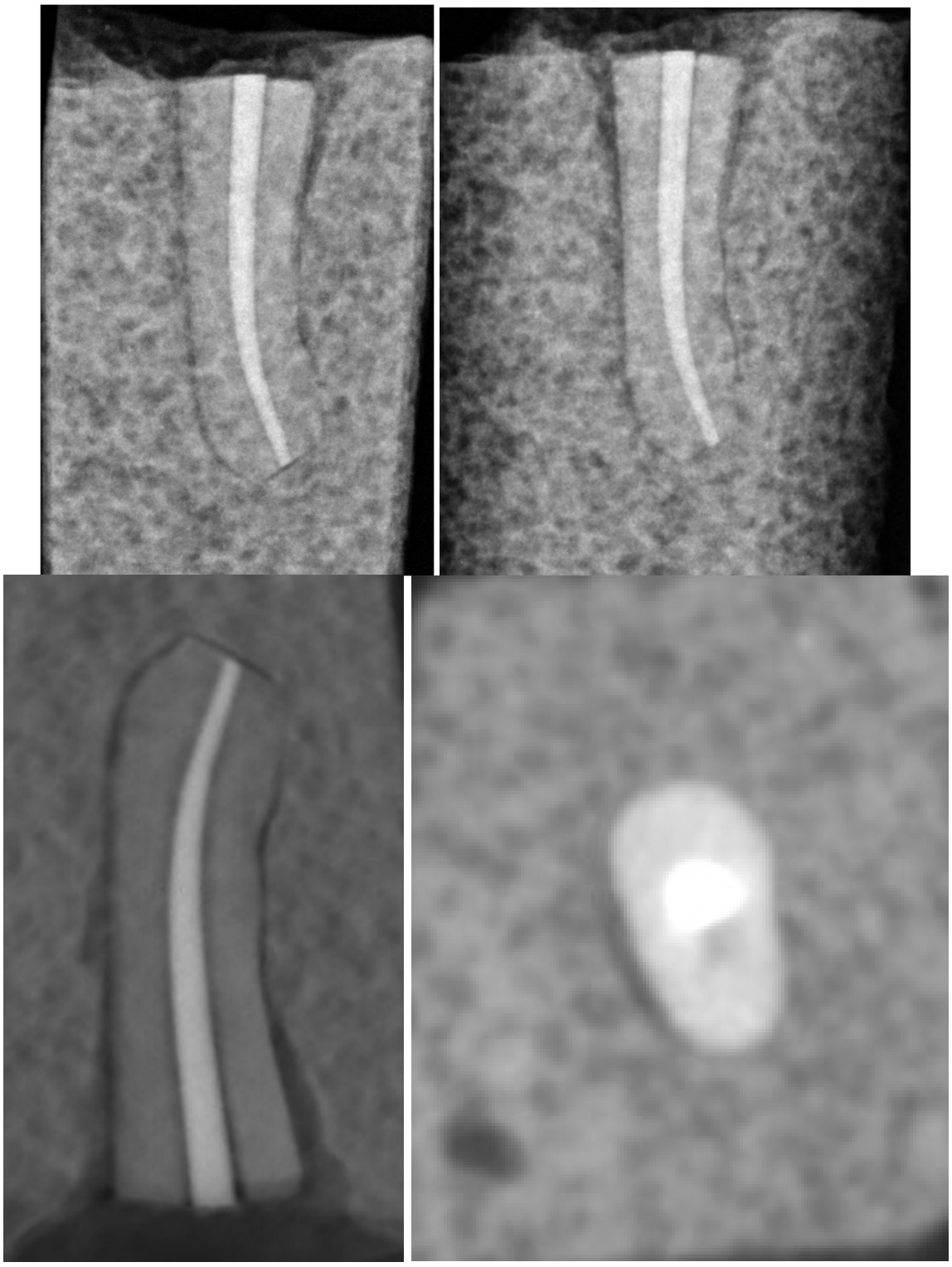

Obturated and fracture absent #12

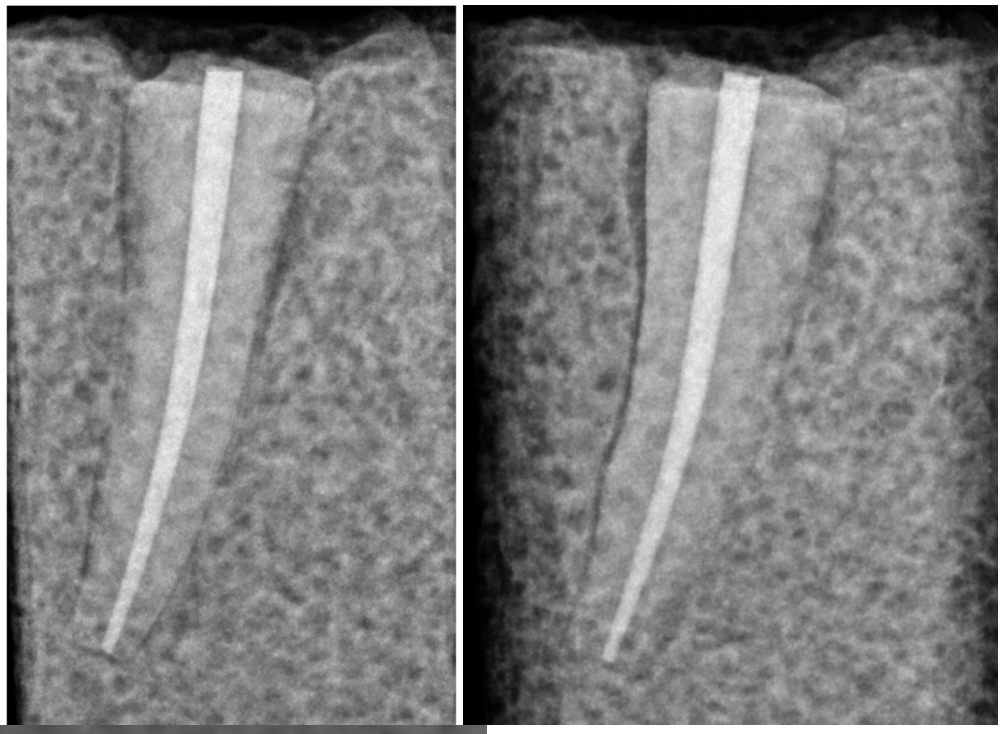

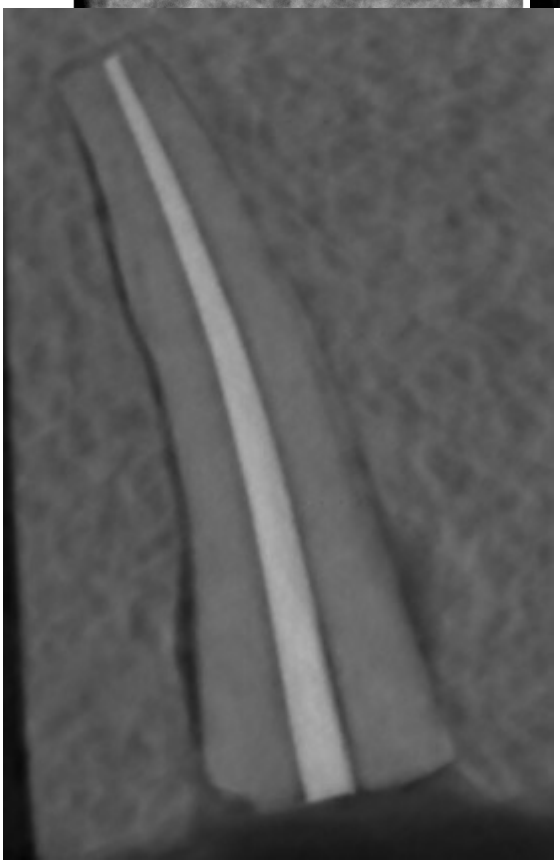

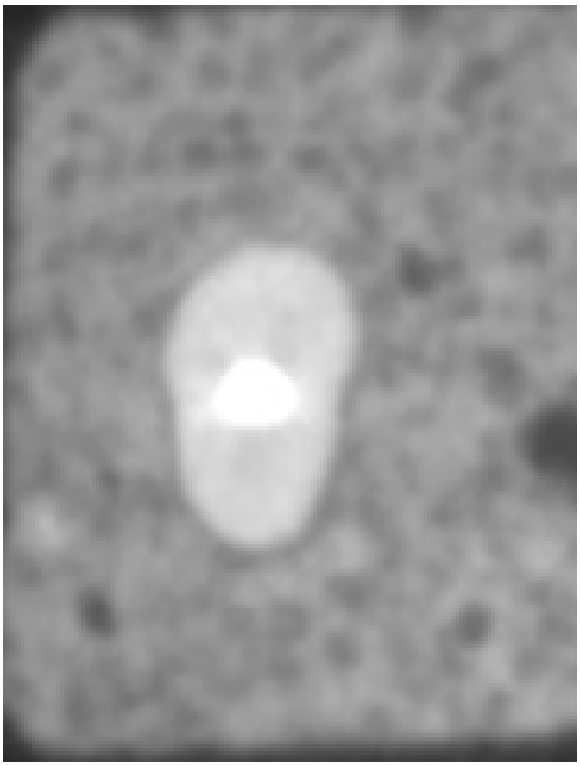

Obturated and fracture absent #13

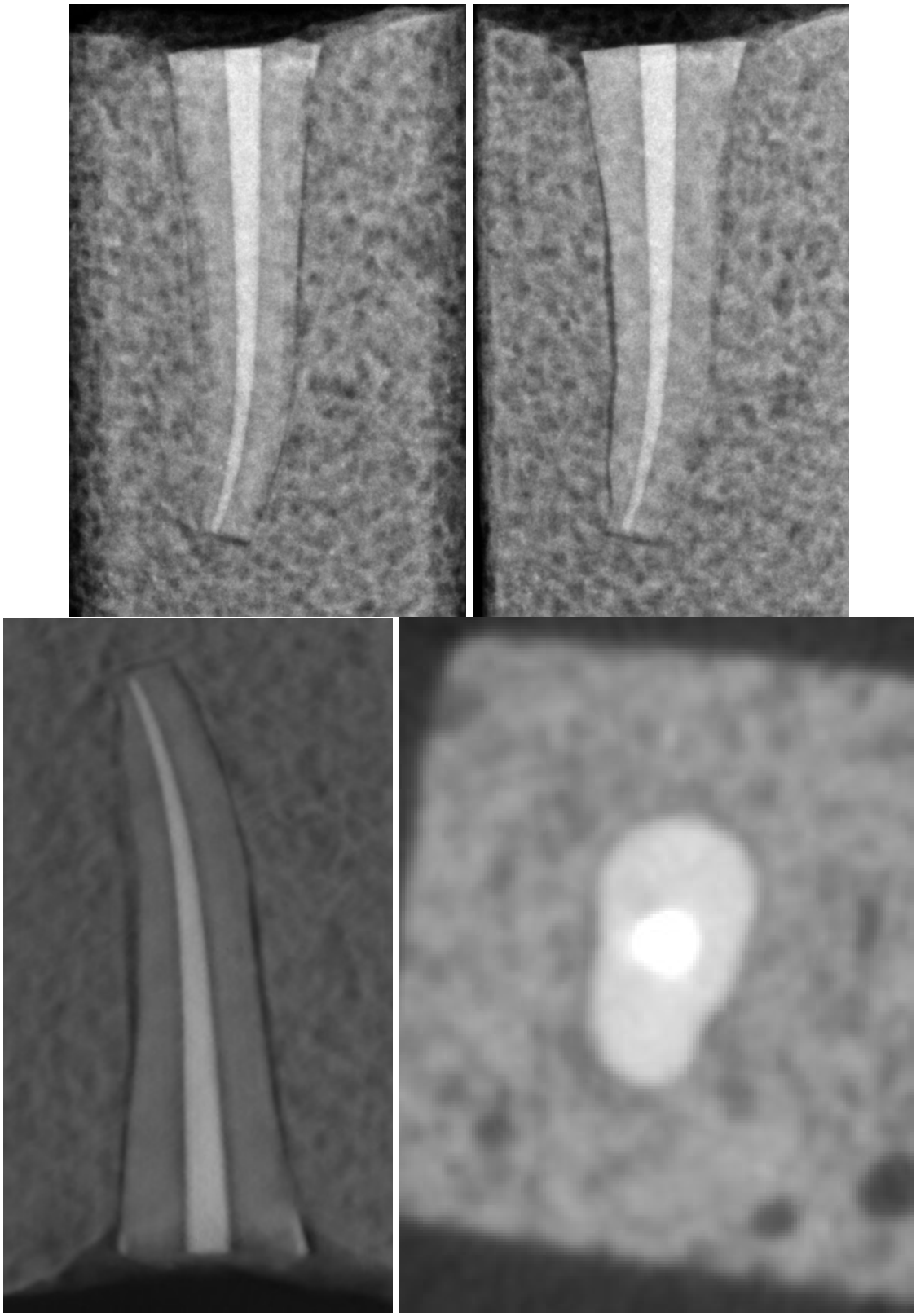

Obturated and fracture absent #14

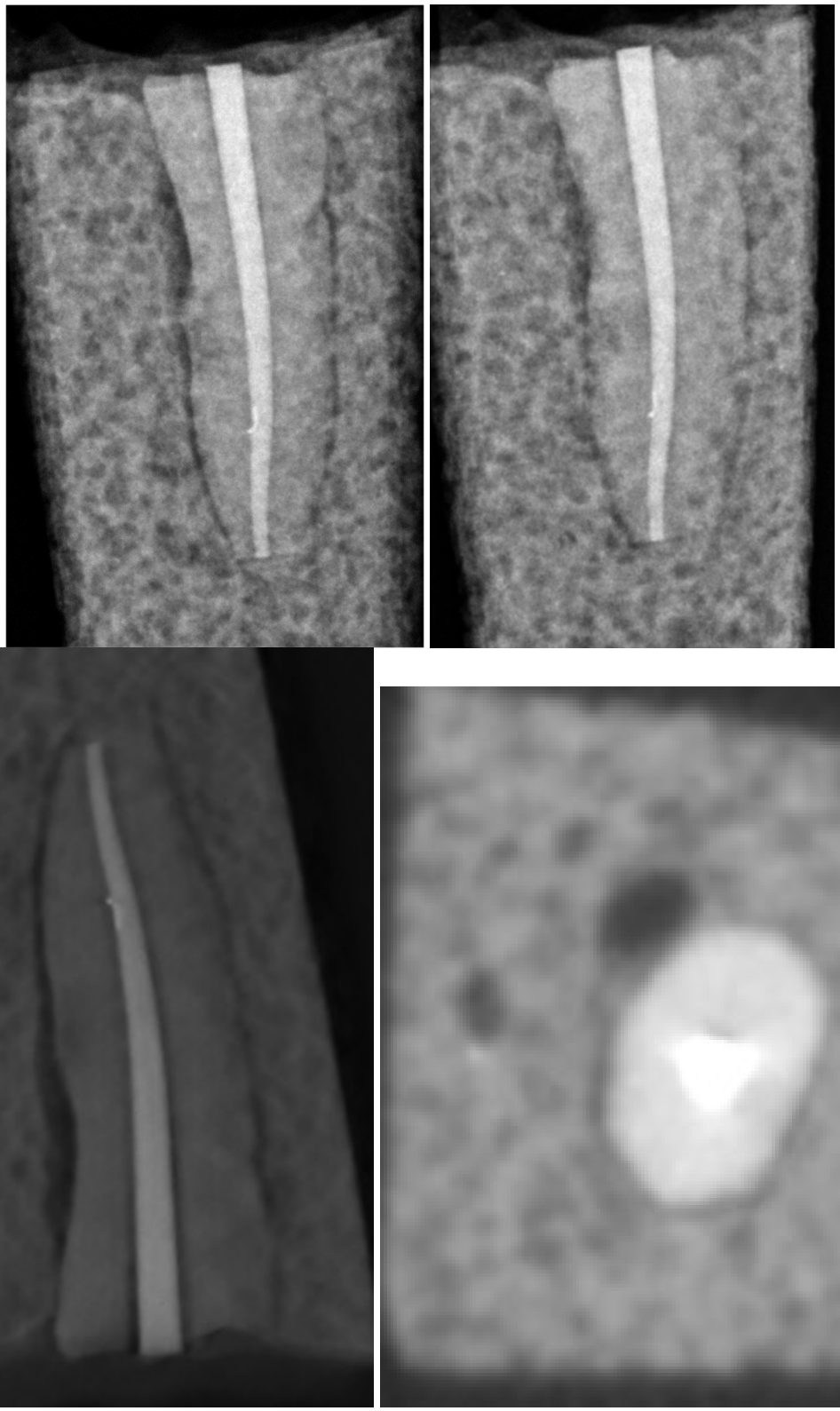

Obturated and fracture absent #15

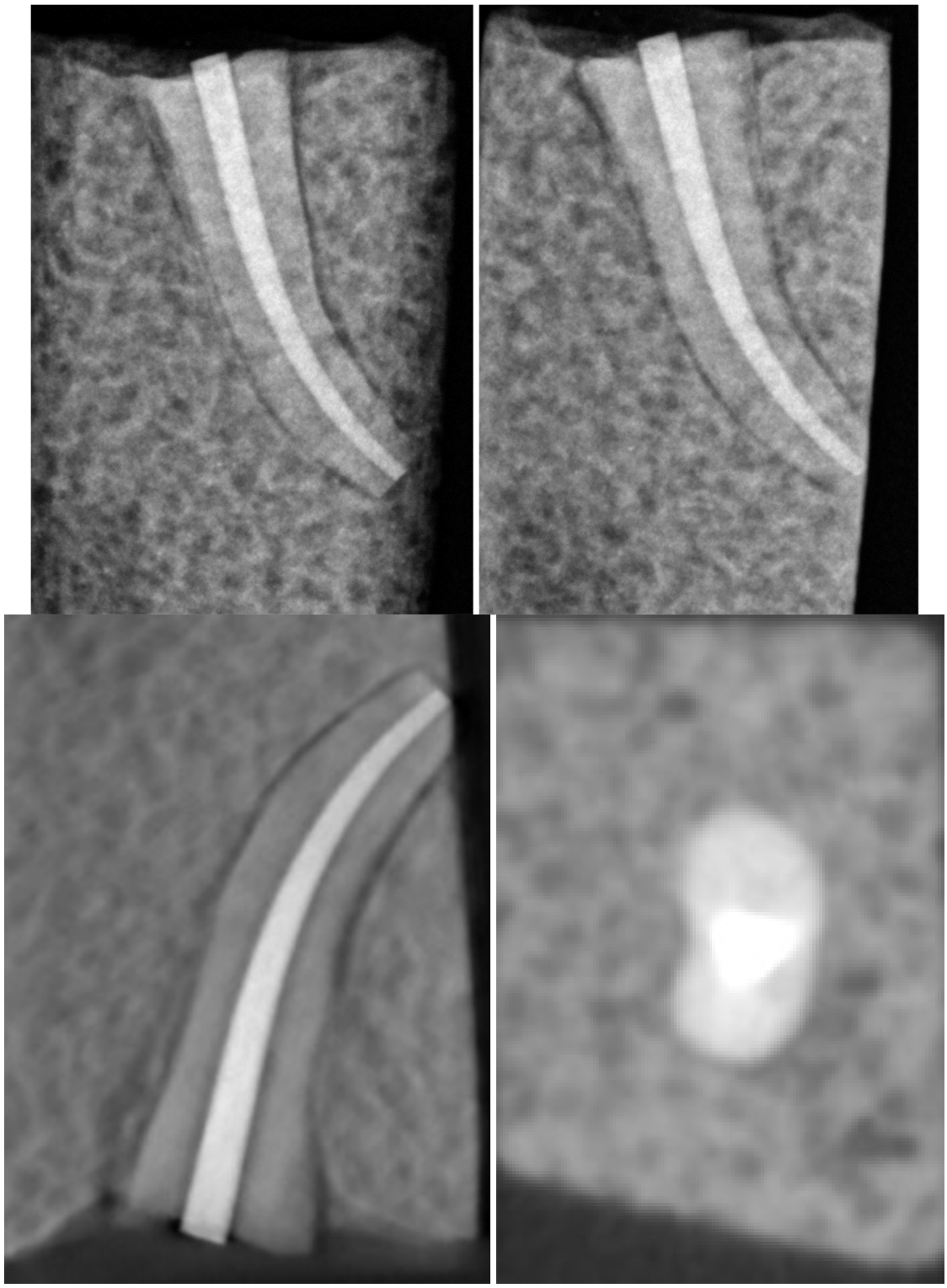

Obturated and fracture present

Obturated and fracture present #1

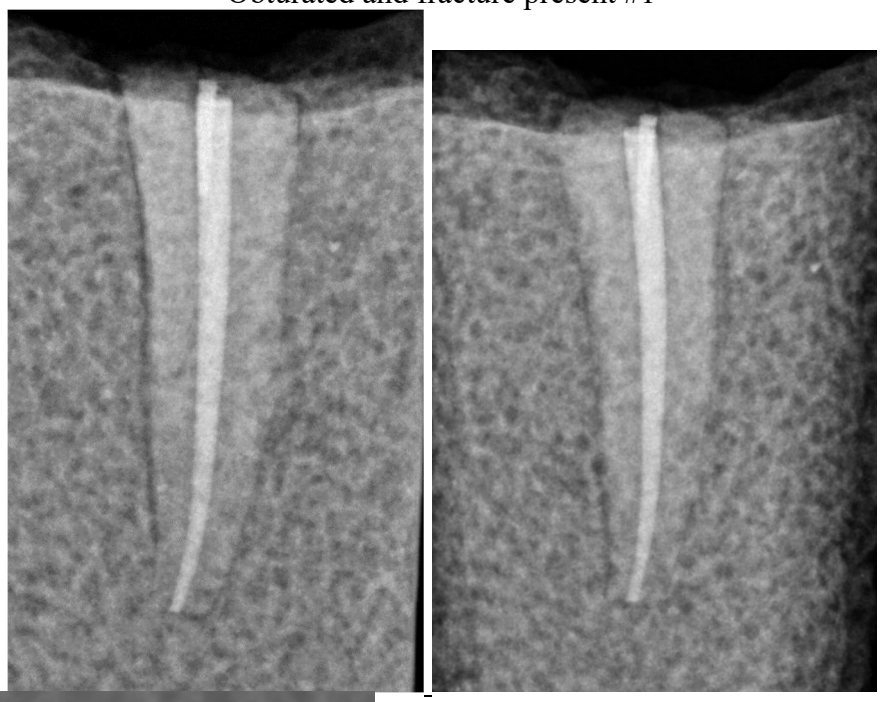

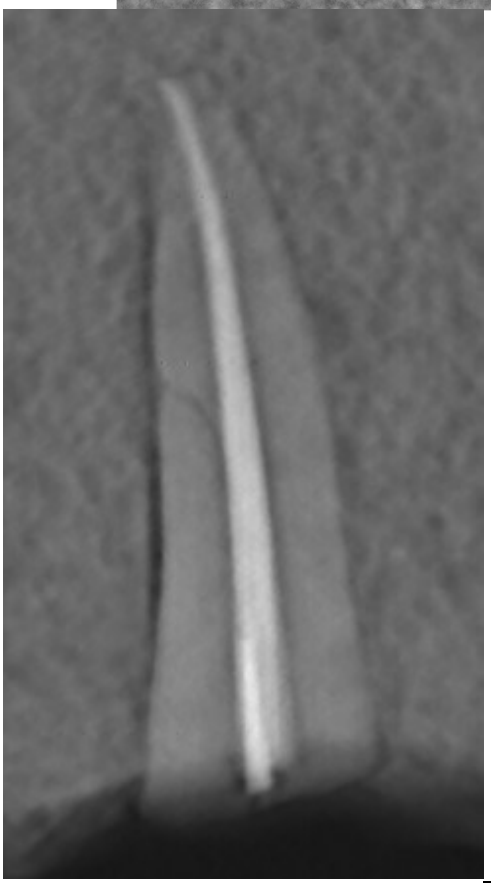

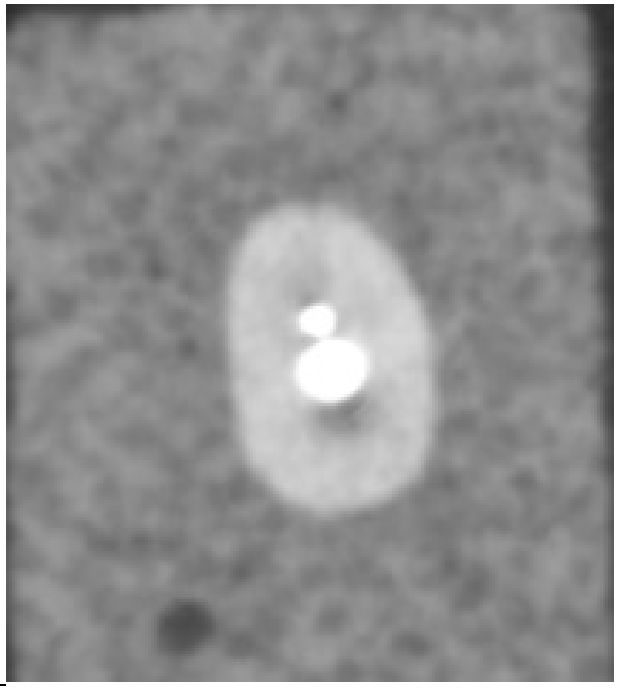

Obturated and fracture present #2

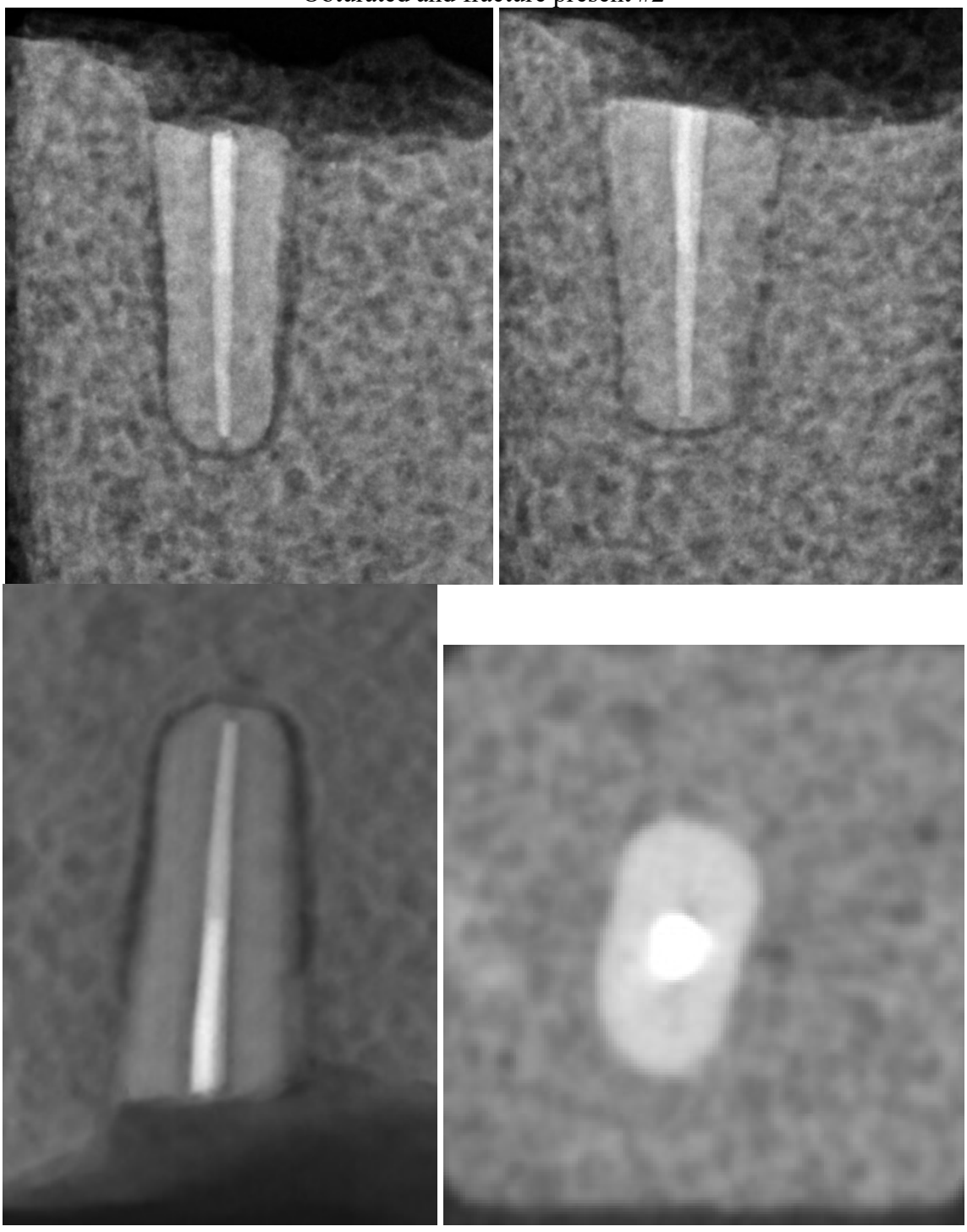

Obturated and fracture present #3

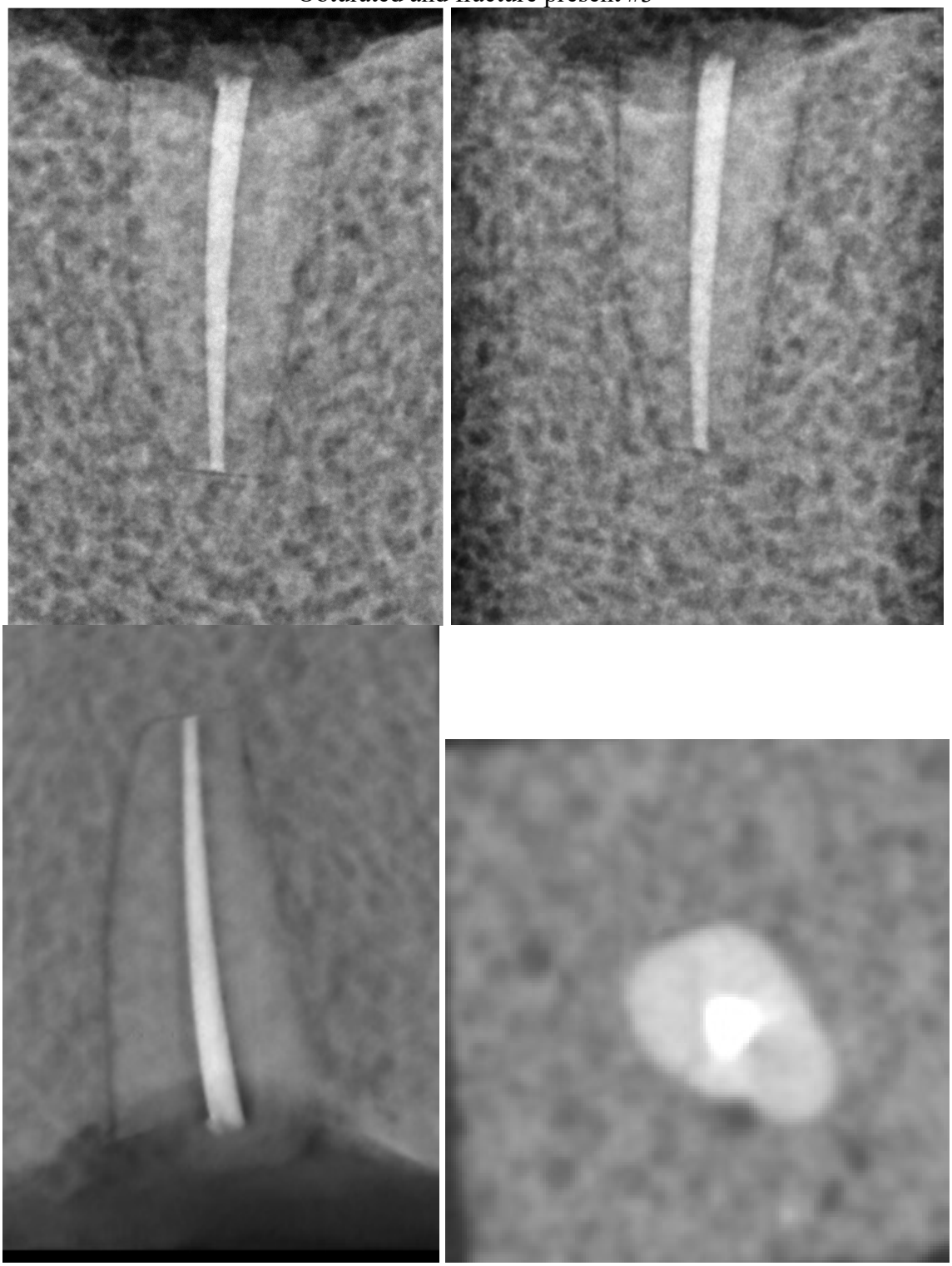

Obturated and fracture present #4

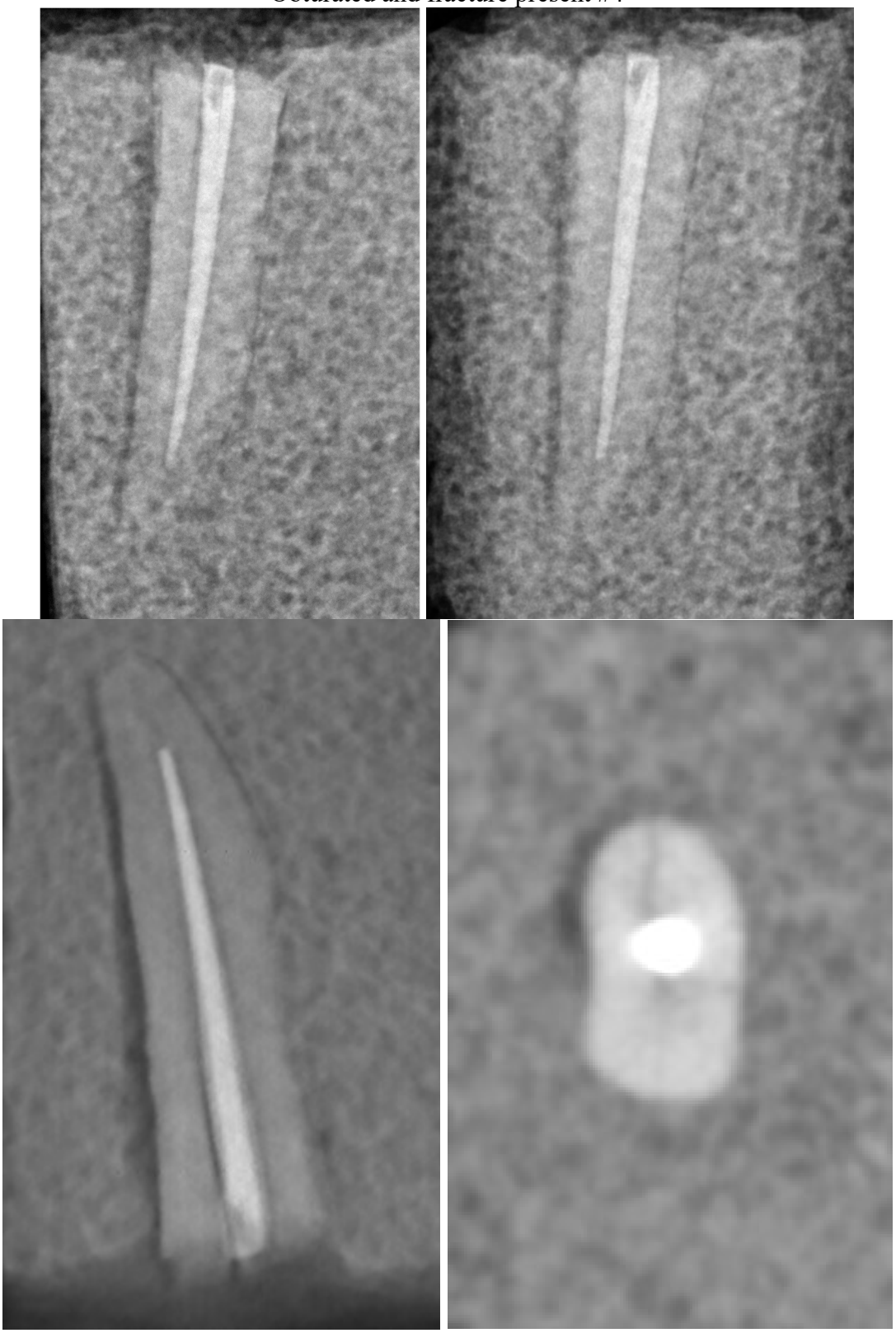

Obturated and fracture present #5

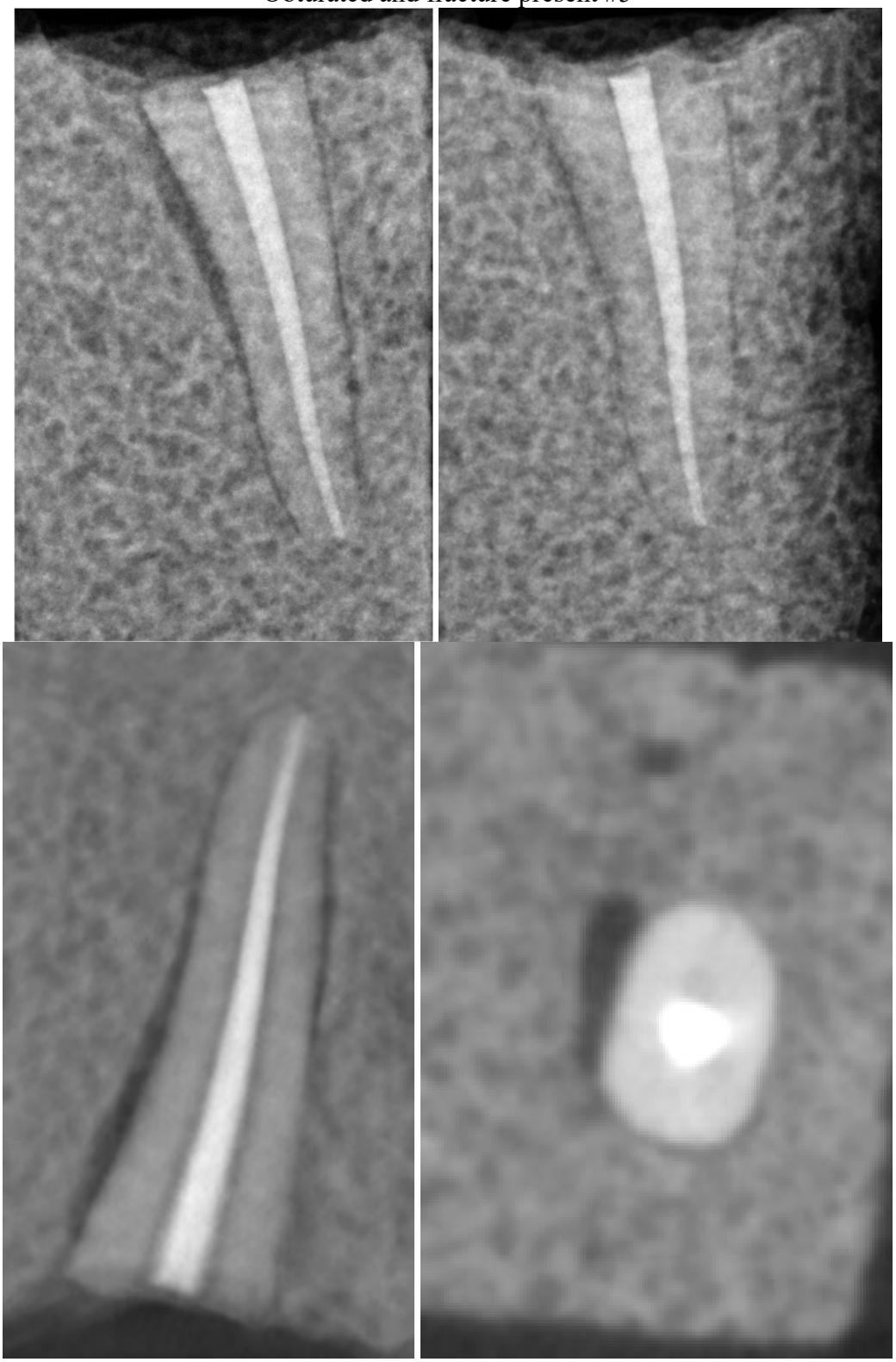

Obturated and fracture present #6

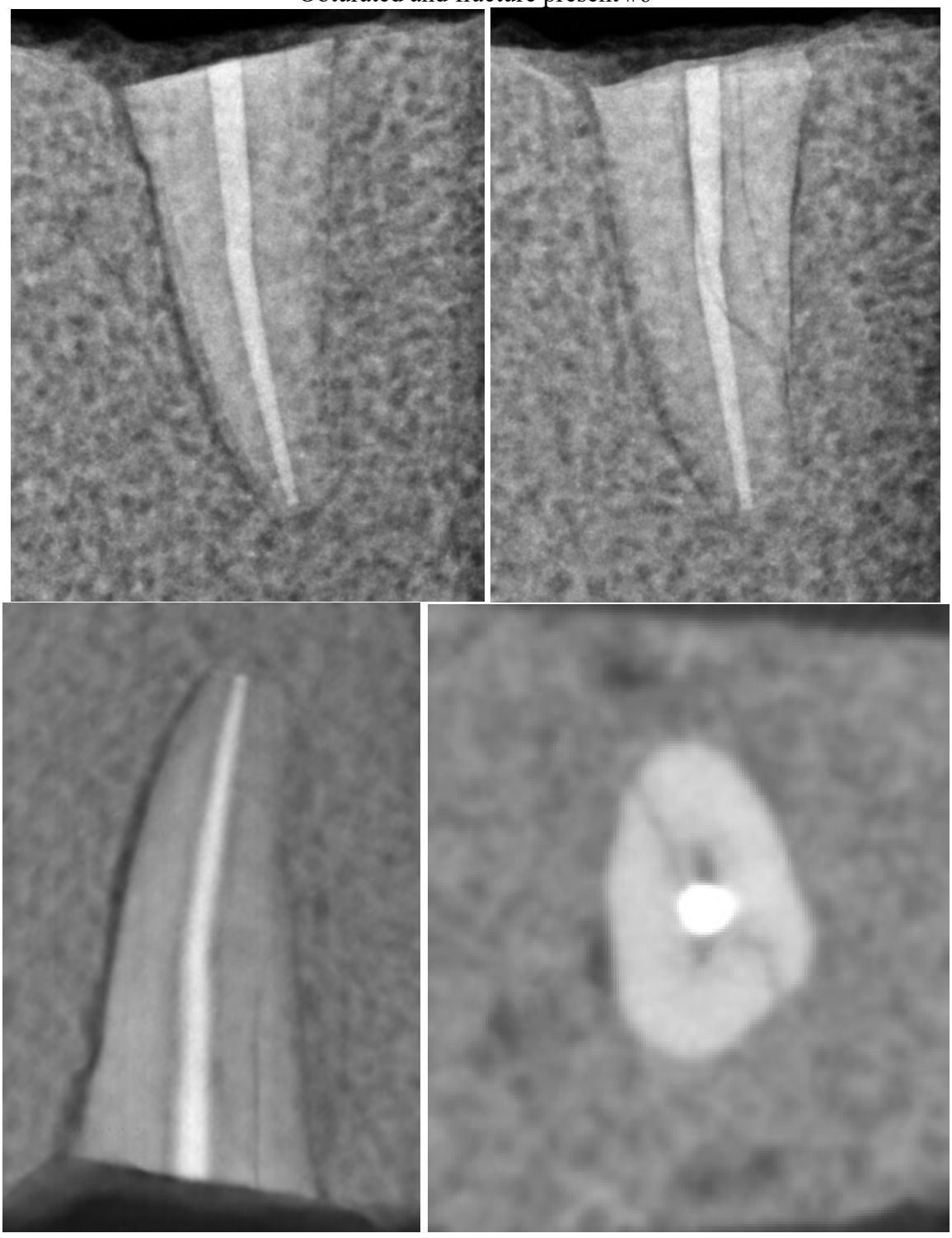

Obturated and fracture present #7

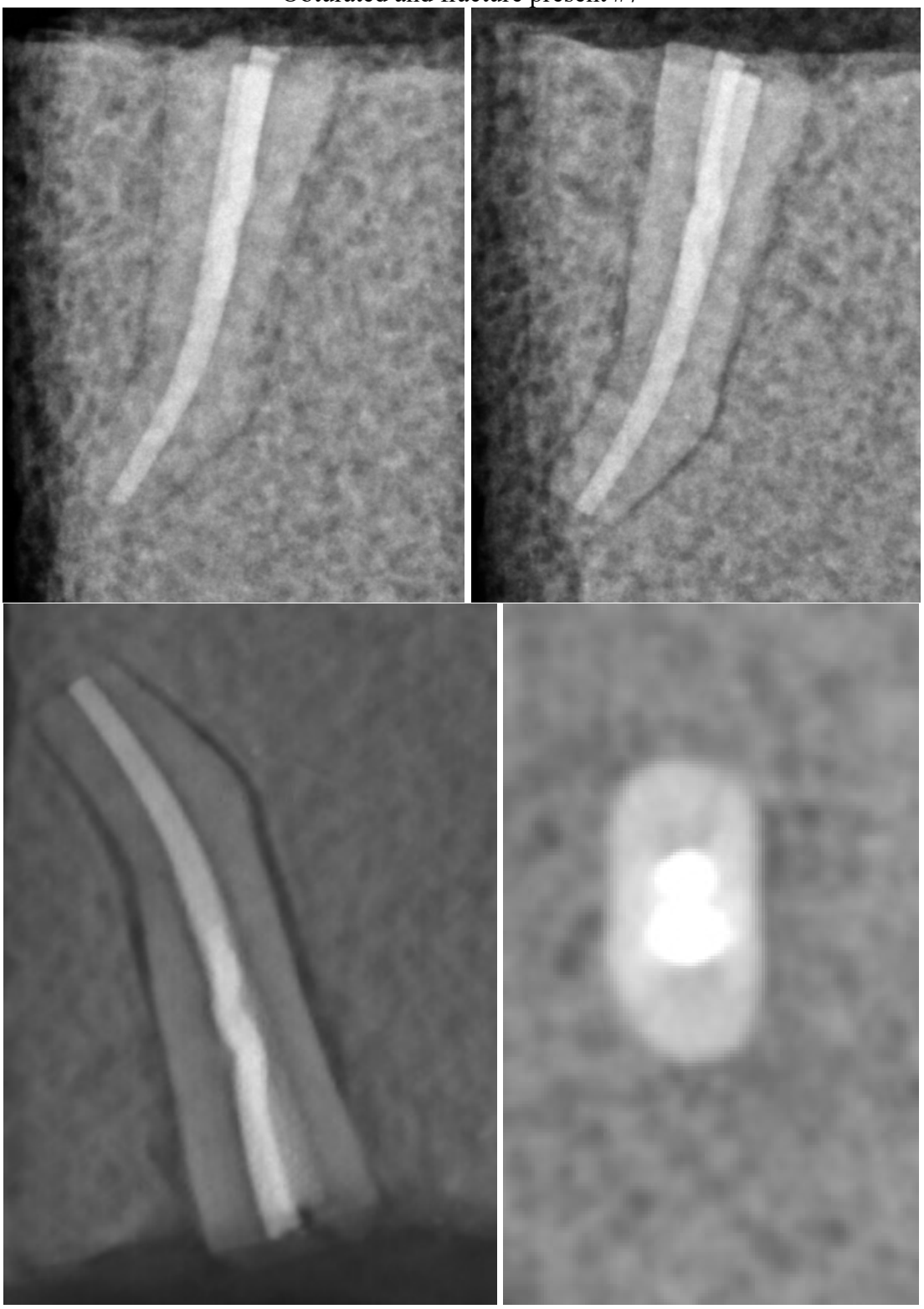

Obturated and fracture present #8

Obturated and fracture present #9

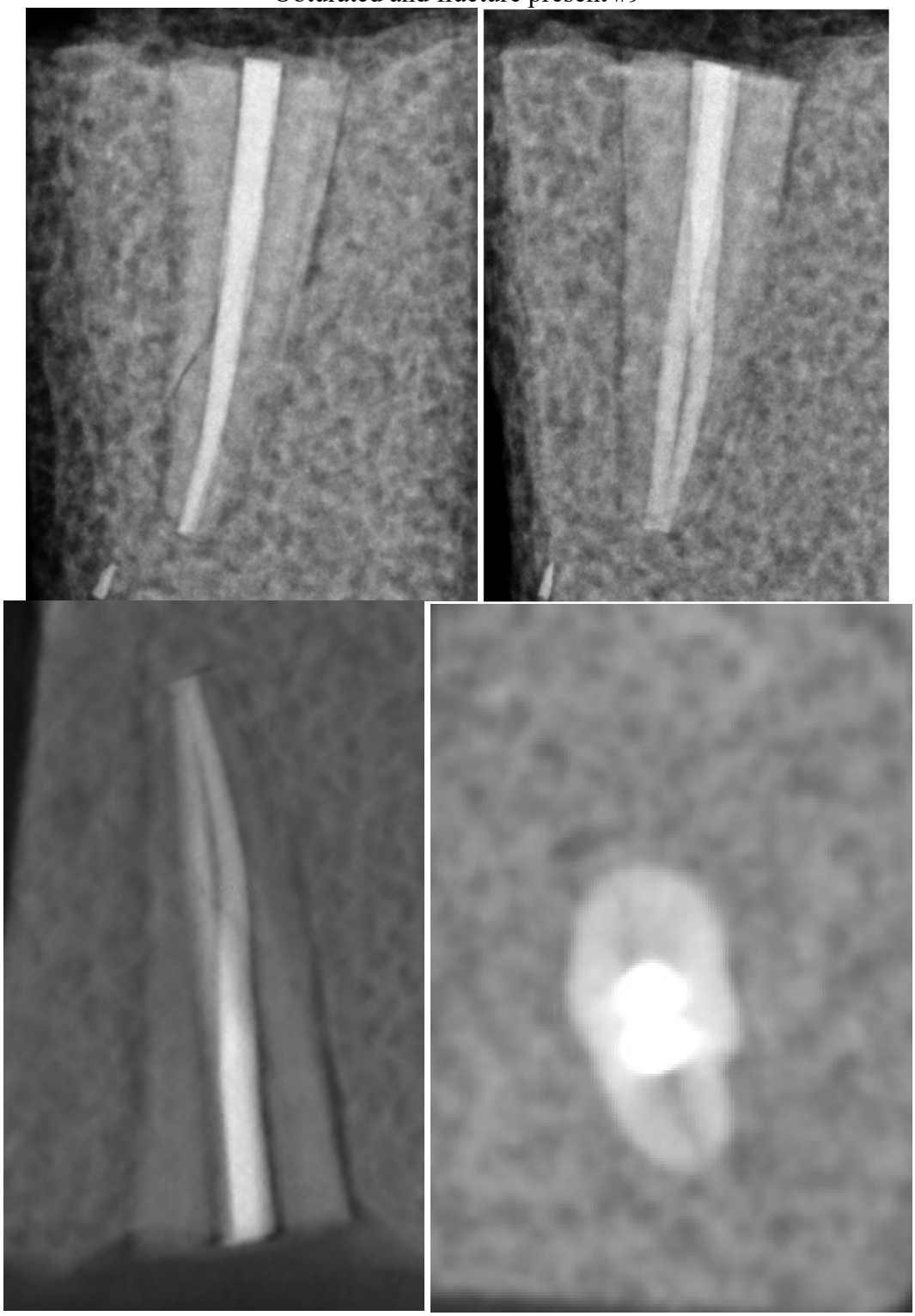

Obturated and fracture present #10

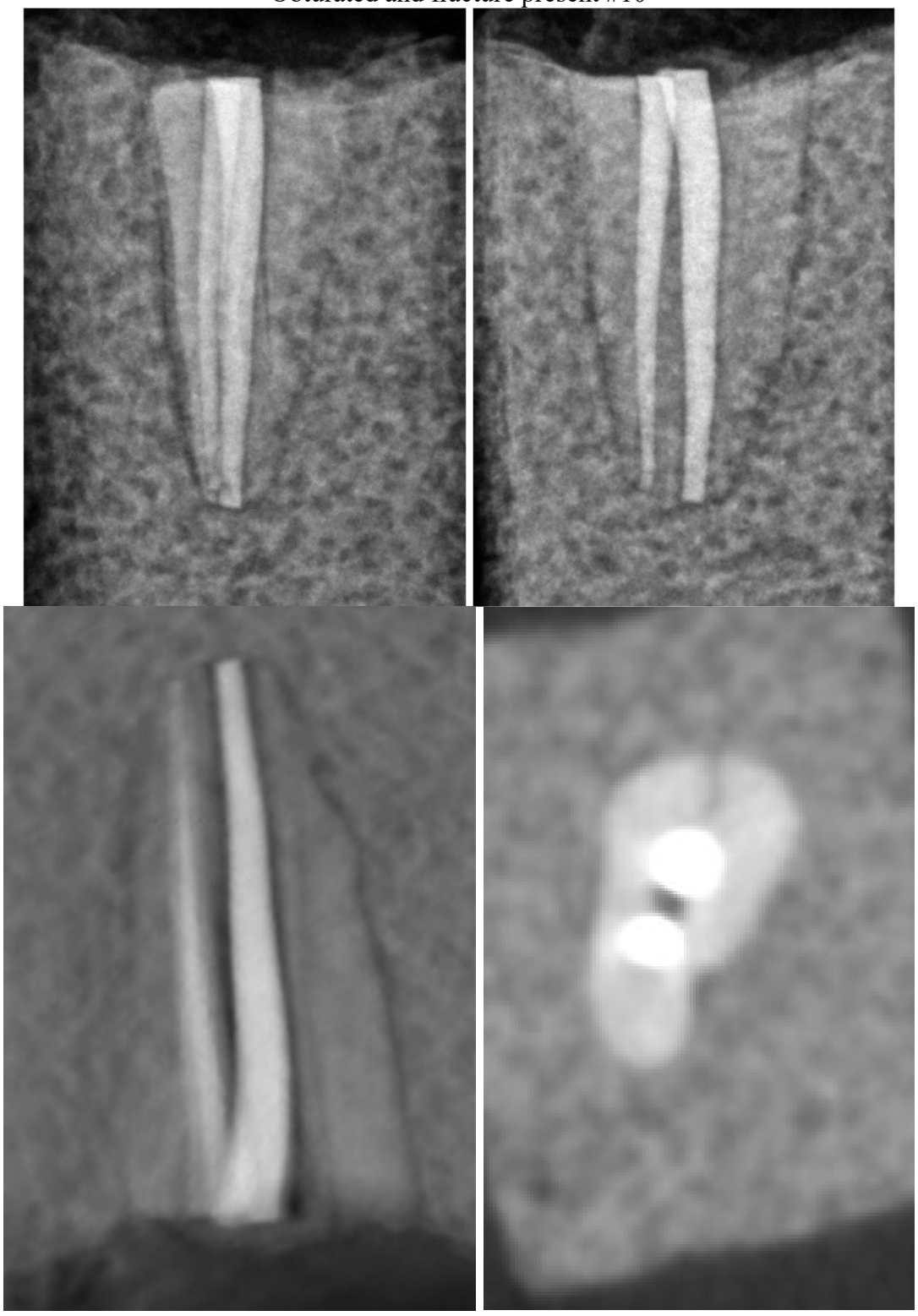

Obturated and fracture present #11

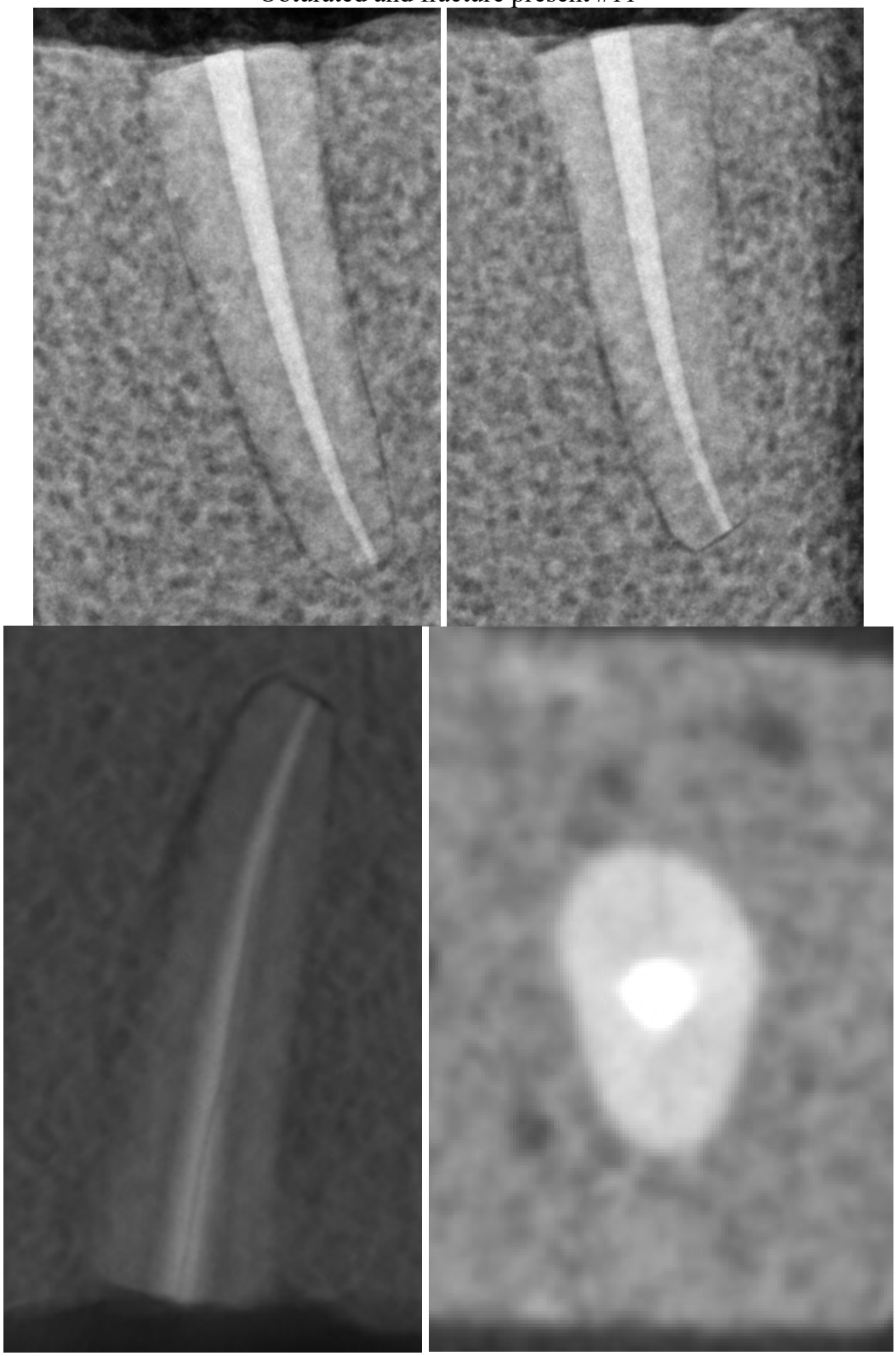

Obturated and fracture present #12

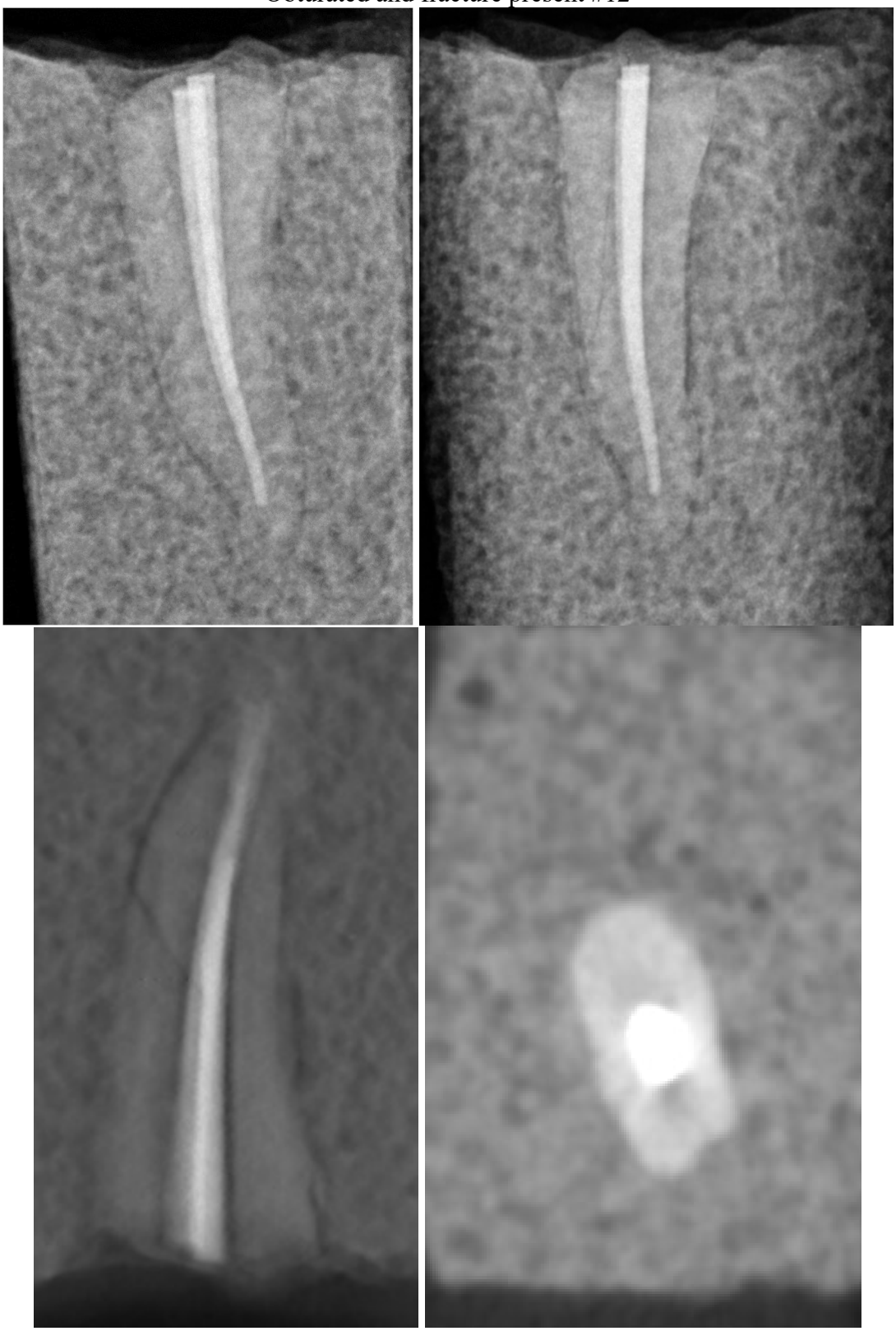

Obturated and fracture present #13

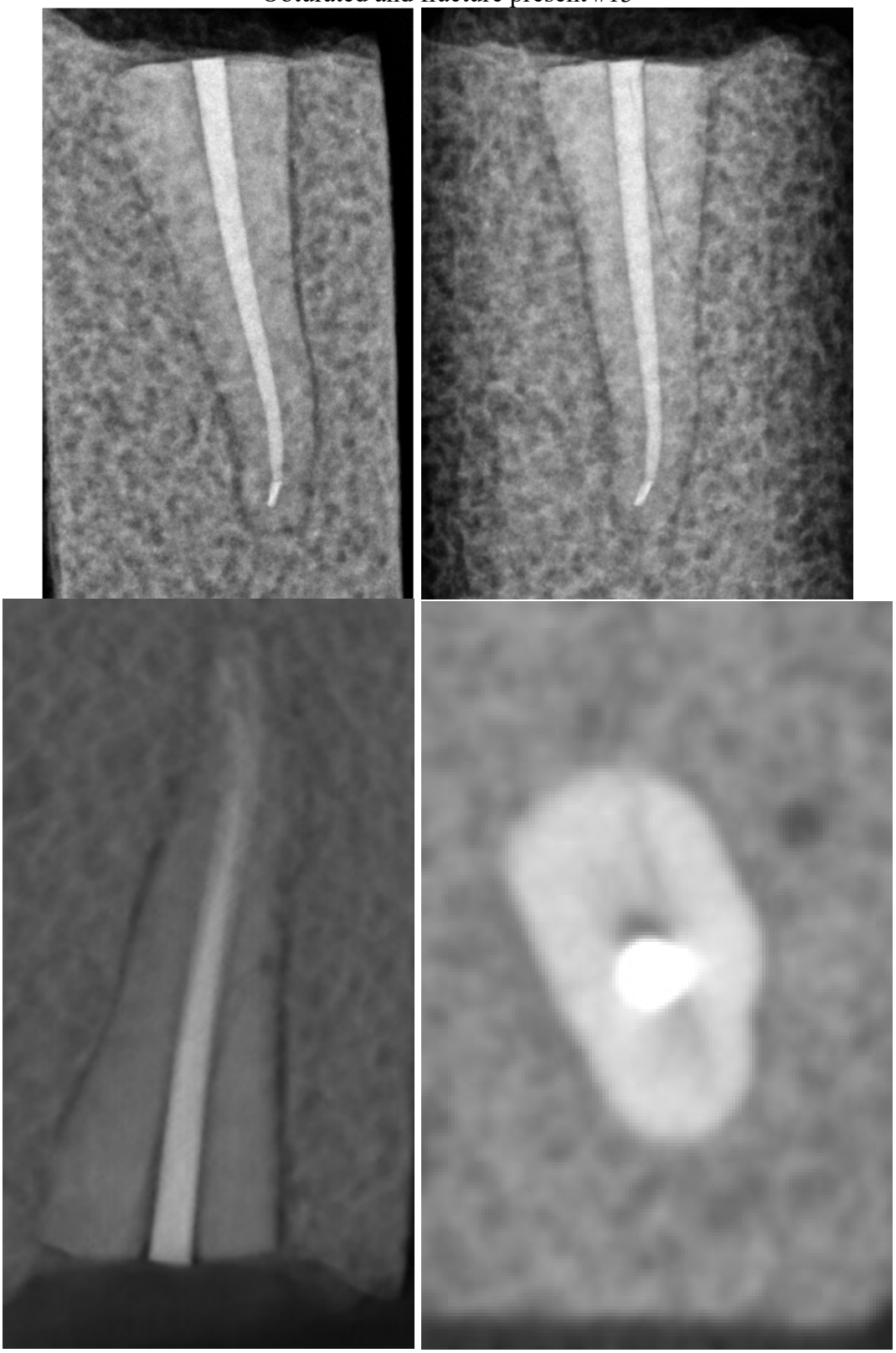

Obturated and fracture present #14

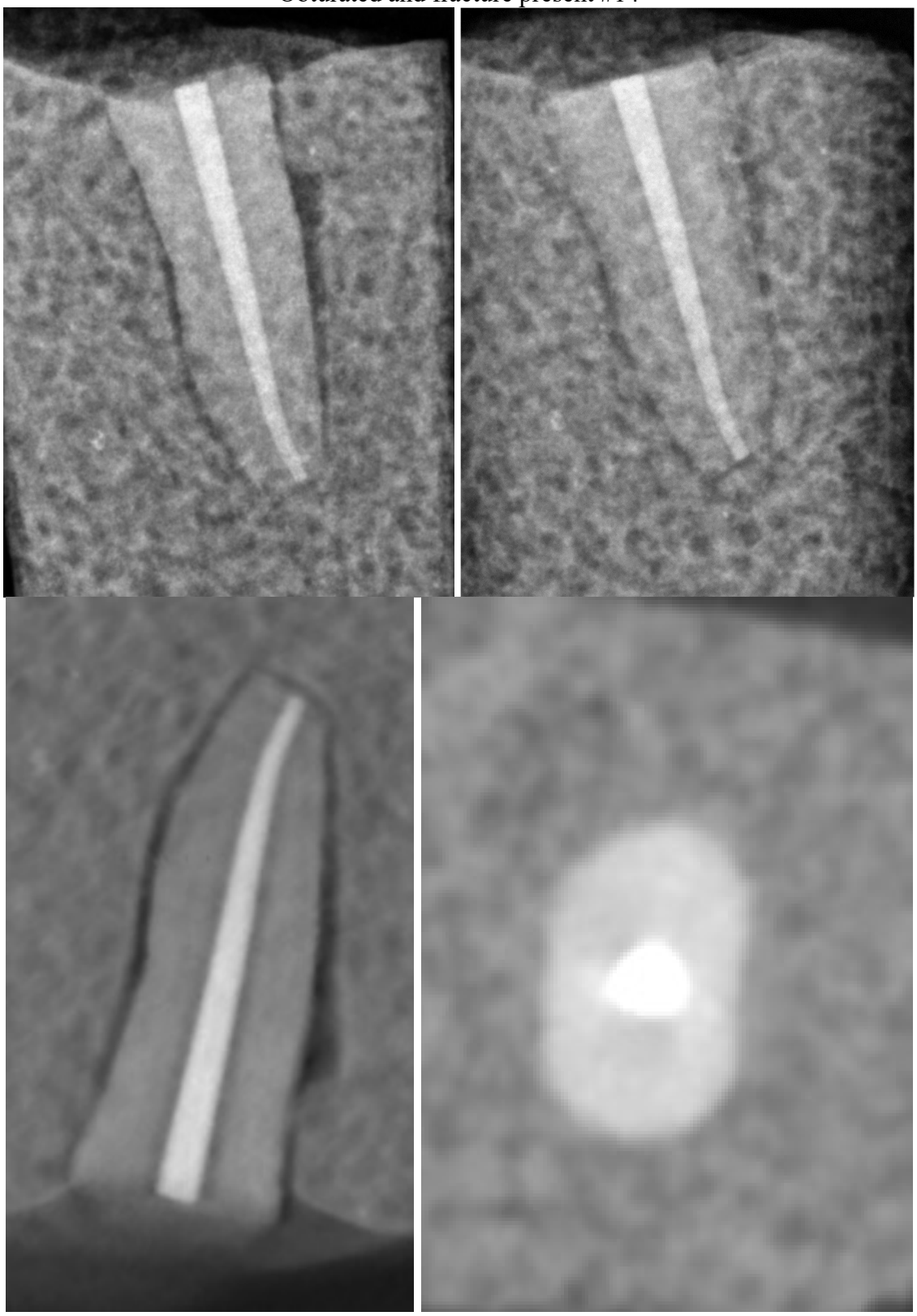

Obturated and fracture present #15

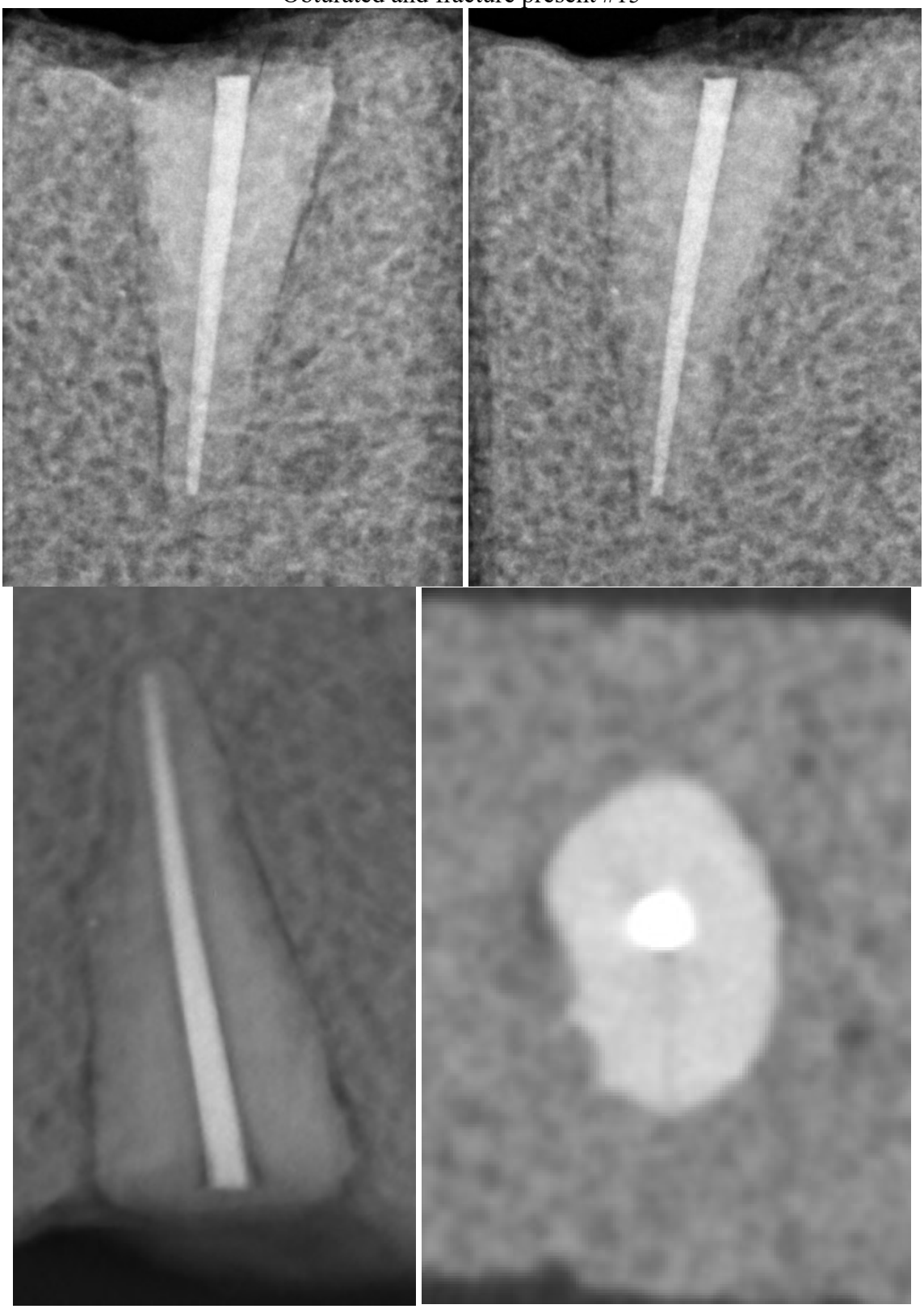

Appendix II: Evaluator instructions

Study Instructions

1. Your task as the evaluator is to assess for the presence of cracks / fractures in tooth samples in three different imaging modalities: periapical radiograph, tomosynthesis, and cone-beam CT.

2. These images are randomized and included in the imaging folder provided in folders listed numerically. These samples correspond to the sample numbers in the Excel document for reporting your interpretation of these images.

	A	B	C	D	E	F
1	Evaluator:					
2		Crack/fracture				
3		presence?				
4	Sample #	(No=0, Yes=1)	Level of certainty 1-5	1=Completely uncertain		
5	1			2=25% certainty		
6	2			3=50% certainty		
7	3			4=75% certainty		
8	4a			5=100% certainty		
9	4b					
10	5a					
11	5b					
12	6a					
13	6b					
14	7					
15	8					
16	9					
17	10a					
18	10b					
19	STOP	STOP -->	**Verify Next DICOM Image # Matches Data Collection Sheet #			
20	11					
21	12					

3. In each folder, there will be either a pair of periapical radiographs, a single tomosynthesis file, or a series of files for a CBCT volume. These are viewed differently. Please review the separate isntructions for how to load and view imaging.

4. On the spreadsheet, each evaluator will make two assessments: a) presence/absence of a crack, and (b) degree of certainty. Presence/absence is recorded as either 1 or 0 in column 2. Degree of certainty is recorded as a number from 1-5.

5. It is important that these images and volumes are interpreted **in order**. Do **not** go back and look at an image twice (except if there is a recording error and it is necessary to correct it). This is also true of periapical imaging. First, view image 1, record your interpretation and certainty. Then, open image 2, and record your interpretation after having viewed both images. Again, do not allow your interpretation of the second image impact your first assessment.

6. These are tooth samples prepared with simulated alveolar bone and PDL. There are no intentionally created lesions, radiolucencies, or PDL widening. Appearance of surrounding simulated bone should not be used as an indication of fracture.

7. *Fatigue:* Observers will self-determine their level of fatigue throughout the study. If you feel fatigued, please take a break at any time. Do not continue when fatigued.
    i. *When possible, image review periods should not exceed 60 continuous minutes without a break.*
    ii. A suggested break would be 1hr time lapse between image review sessions
    iii. Take as much time as needed, there are no time limits.
8. ***Questions:*** Assistance or clarification can be requested at any time.

Instructions for Opening and Viewing Study Images

1. Locate and open the "Blinded imaging" folder provided. Contained are a series of numbered folders 1 through 216.

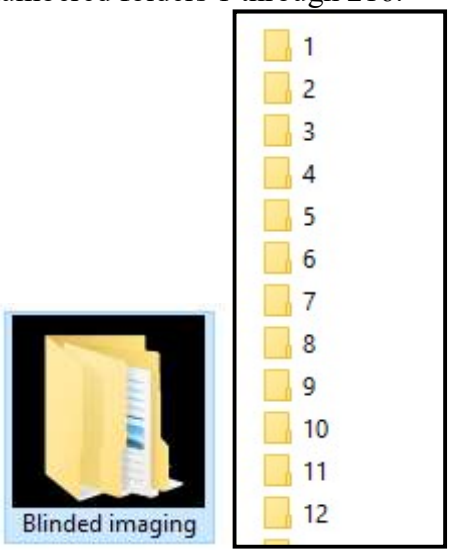

2. Locate and open the RadiAnt DICOM Viewer 64-bit program

3. RadiAnt DICOM Viewer (64-bit) Tutorial

- **OVERVIEW: Basic RadiAnt User Controls Review**
  http://www.radiantviewer.com/dicom-viewer-manual/

- **Deidentify imaging:** Click the drop-down next to the "A" button to turn OFF annotations, and select "Hide patient data". If the program is ever closed, it is critical that this step be repeated BEFORE any imaging is loaded.

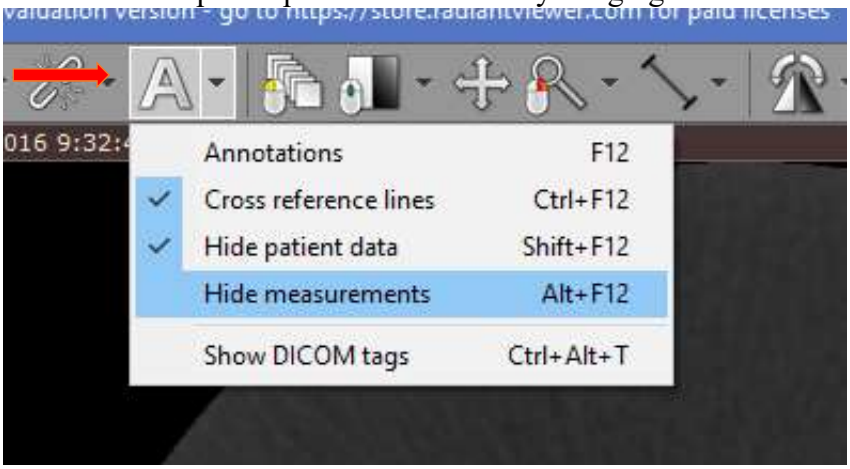

- **Changing Brightness and Contrast:**

Click the **Adjust image window** button on the toolbar (or press the **W** key).

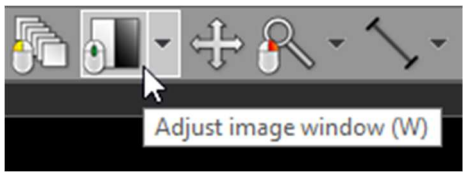

Next, press the left mouse button over the image and drag the mouse to change brightness (window level - WL), or contrast (window width - WW):
•Up to decrease brightness (window level goes up)
•Down to increase brightness (window level goes down)
•Left to increase contrast (window width shrinks)
•Right to decrease contrast (window width expands)

- **Changing perspective in CBCT's**
  By default, CBCT's will load in the axial perspective. This is most likely the preferred perspective for crack identification. If desired, the observer may also evaluate the sample from the coronal or sagittal perspective by clicking the "Multiplanar Reconstruction" button

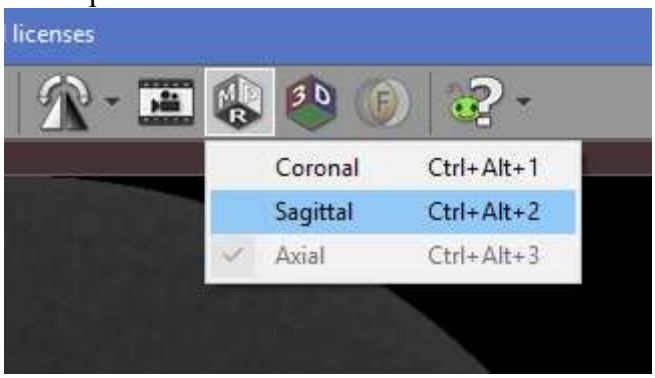

4. **Loading images:** On your desktop, view the folders in a list with the opened RadiAnt program.
   - **Again, ensure that you have selected "Hide patient data"**
   - To load a CBCT or Tomo image (starting with #1), simply drag the folder and drop anywhere into the RadiAnt program window. The selected image should

now be open and ready for manipulation and interpretation.

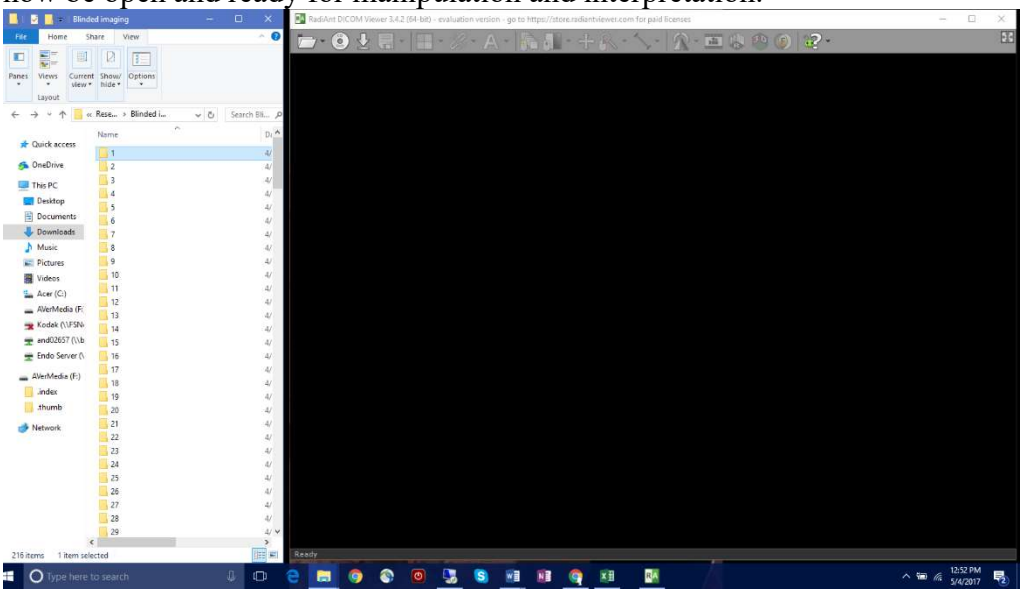

- Each successive CBCT or Tomo can simply be dragged and dropped into the RadiAnt program window. It will automatically overlay over your past image, therefore you do not need to close a previous image file to view a new one. Do **not** close the RadiAnt viewer.
- Periapical images cannot be viewed in RadiAnt. These should be opened directly. Ensure that your window settings are such that the files are listed without thumbnails. They should be a simple list.

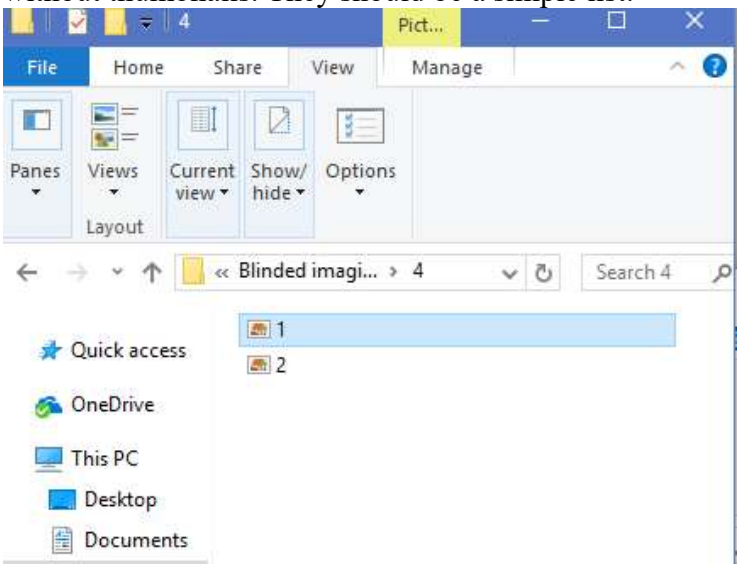

5. For instructions on how to interpret these images, please refer to the attached Study Instructions. You can tell the difference between periapicals versus CBCT or Tomo based on the Excel spreadsheet. Periapical images will have two entries (e.g. 4a and 4b), while CBCT or Tomo's will have a single entry (e.g. 1).

Assessing the Accuracy and Reliability of Crack/Fracture

1. A separation of the adjacent root segments on multiple contiguous image slices without the continuation of the hypo-attenuated line into the adjacent tissue (or simulated bone as was present in this ex-vivo study design). This hypo-attenuated line must be observed within the confines of tooth structure, delineated by:
    a. *External tooth surface:* bounded by enamel, the external surface of dentin, or cemental tissue depending on the level of axial slice.

    And\or

    b. *Internal tooth surface:* external extent of the pulpal cavity

For purposes of this study, the physical discontinuity must have the following criteria to be given a designation of a crack/fracture.

1. Radiolucent line(s) must extend from the external boundary of the tooth and/or the pulpal cavity (or vice versa)* on multiple contiguous image slices.^
2. The overall contour of the external tooth surface and pulpal cavity must be maintained.**

Explanation of stated criteria:

*A. *These cracks are thought to be clinically significant.*

B. ^The criteria of multiple image slices allows for detection of an angled crack.

*C. **To prevent gross root discontinuities from mistakenly being classified as a crack.*

Furthermore, it is important to differentiate cracks/fractures from other commonly encountered pathologic changes in tooth morphology that may be observed in CBCT, and to rule out artifact and possible false positive identification. The following entities should be differentiated from cracks/fractures:

- Cases with metallic restorations or root fillings that usually exhibit multiple streak artifacts that traversed the root and adjacent tissue.
- Aberrations in dental anatomy or morphology which may include
    - Accessory, lateral or secondary pulp canal(s)
    - Canal ramifications
- Physiologic or pathologic processes which may include
    - Root Resorption (Inflammatory, Replacement, Surface, Cervical, External, Internal)
    - Caries

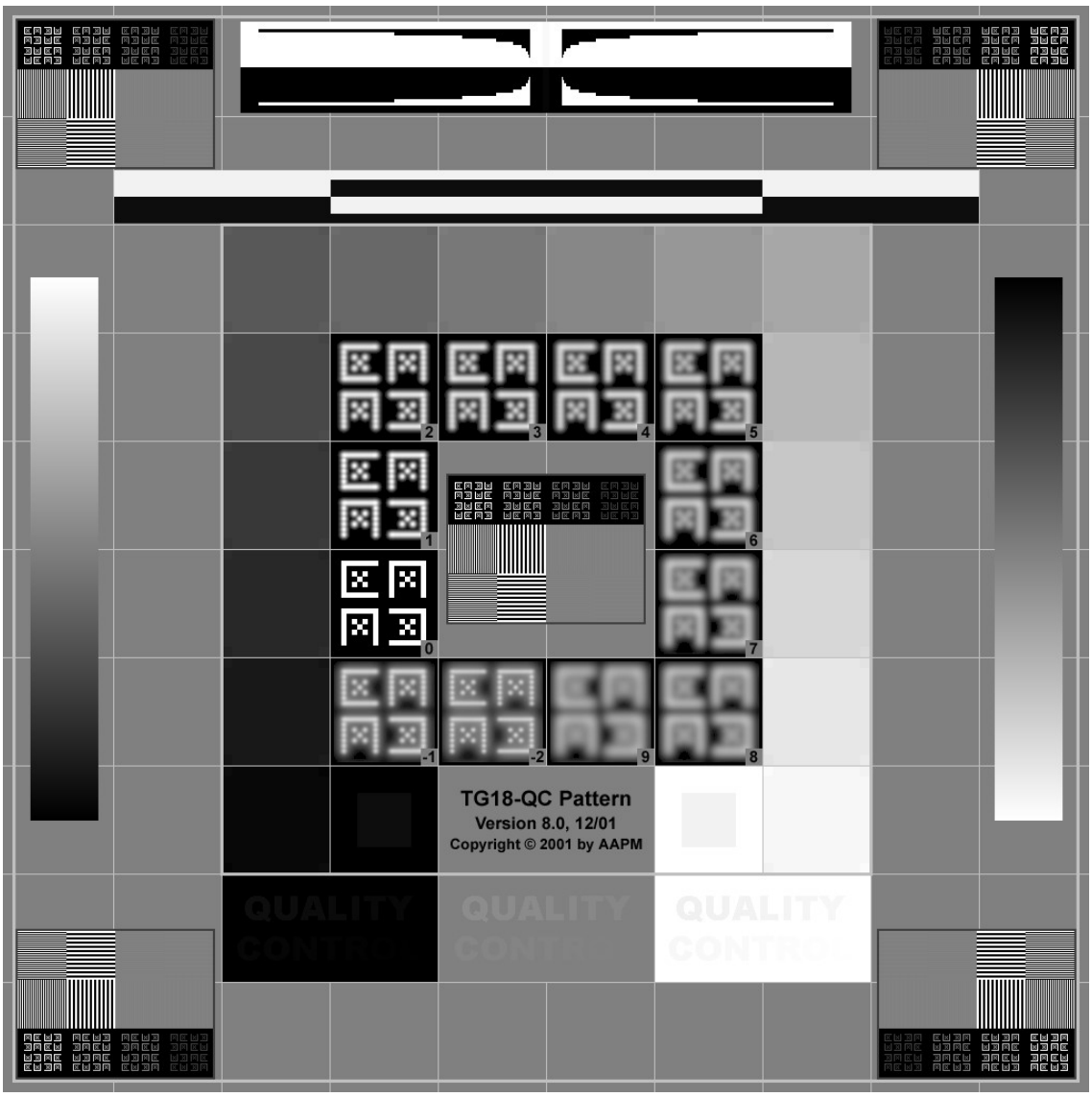
TG18-QC Pattern
Version 8.0, 12/01
Copyright © 2001 by AAPM
QUALITY CONTROL

TG18 (145)

Appendix III: Sample Identification & Evaluator Output

			Evaluator 1		Evaluator 2		Evaluator 3		Evaluator 4		Evaluator 5	
	Modality	Sample	Crack	Cert	Crack	Cert	Crack	Cert	Crack	Cert	Crack	Cert
58	CBCT	CF1	1	5	1	5	1	4	1	5	1	4
203	CBCT	CF1	1	5	1	5	1	5	1	5	1	5
15a	PA	CF1	0	4	0	2	0	4	0	5	0	4
15b	PA	CF1	1	3	1	3	1	3	1	3	0	4
145	TOMO	CF1	1	5	1	5	1	5	1	5	1	5
149	CBCT	CF10	1	5	1	5	1	5	1	5	1	5
104a	PA	CF10	0	3	1	2	1	3	1	3	0	4
104b	PA	CF10	1	4	1	4	1	4	1	5	1	5
205a	PA	CF10	0	4	0	2	1	2	0	3	1	3
205b	PA	CF10	1	5	1	4	1	5	1	4	1	4
40	TOMO	CF10	0	4	1	4	1	5	1	5	1	3
87	CBCT	CF11	1	5	1	5	1	4	1	5	1	3
36a	PA	CF11	0	4	0	4	0	4	0	3	0	5
36b	PA	CF11	0	4	0	4	0	4	0	3	0	5
120	TOMO	CF11	1	5	1	5	0	4	1	5	1	5
83	CBCT	CF12	1	5	1	5	1	5	1	5	1	4
180a	PA	CF12	1	5	1	5	1	5	1	5	1	5
180b	PA	CF12	1	5	1	5	1	4	1	5	1	2
105	TOMO	CF12	1	5	1	5	1	4	1	5	1	5
38	CBCT	CF13	1	5	1	4	1	5	1	5	1	5
47a	PA	CF13	1	5	1	5	1	5	1	5	1	5
47b	PA	CF13	1	5	1	5	1	4	1	5	1	3
100	TOMO	CF13	1	5	1	5	1	4	1	5	1	4
73	CBCT	CF14	0	4	0	3	0	4	0	5	0	5
117a	PA	CF14	0	4	1	1	0	4	0	4	1	2
117b	PA	CF14	0	4	0	3	0	4	0	4	0	4
215a	PA	CF14	0	4	0	3	0	4	0	3	0	4
215b	PA	CF14	0	4	0	4	0	3	0	4	0	4
157	TOMO	CF14	0	4	0	2	0	4	0	3	0	5
195	TOMO	CF14	0	4	0	4	0	4	0	4	1	3
167	CBCT	CF15	1	5	1	3	1	4	1	3	1	4
79a	PA	CF15	1	3	1	5	1	4	1	3	1	5
79b	PA	CF15	1	3	1	5	1	4	1	0	1	3
63	TOMO	CF15	0	4	0	3	0	4	0	3	0	4
202	TOMO	CF15	0	4	0	4	1	4	0	3	1	3
111	CBCT	CF2	0	3	0	2	1	3	0	4	0	5
41a	PA	CF2	0	4	0	3	0	3	0	3	0	4
41b	PA	CF2	0	4	0	4	0	4	0	4	0	5
33	TOMO	CF2	0	4	1	4	0	5	0	2	0	4
112	CBCT	CF3	1	5	1	4	1	5	1	3	1	3
44a	PA	CF3	0	4	1	4	0	4	0	3	0	4
44b	PA	CF3	0	4	1	2	0	4	0	4	0	4
85	TOMO	CF3	0	5	0	4	0	4	1	3	1	3
20	CBCT	CF4	1	5	1	4	1	5	1	5	1	5
169a	PA	CF4	0	4	1	2	0	4	0	3	1	3
169b	PA	CF4	0	4	1	5	0	4	1	2	1	4
37	TOMO	CF4	0	3	1	5	0	4	1	2	1	4
50	CBCT	CF5	1	5	1	5	0	4	0	3	1	3
129a	PA	CF5	0	4	0	3	0	4	0	4	0	4
129b	PA	CF5	0	4	0	4	0	4	0	4	0	5
199a	PA	CF5	0	4	0	3	1	1	0	3	0	4
199b	PA	CF5	0	4	0	4	0	1	0	4	0	5
35	TOMO	CF5	0	5	0	2	0	4	0	4	1	4
127	CBCT	CF6	1	5	1	5	1	5	1	5	1	5
78a	PA	CF6	1	5	1	5	1	5	1	5	1	5
78b	PA	CF6	1	5	1	5	1	5	1	5	1	3
186a	PA	CF6	1	5	1	5	1	5	1	5	1	5

186b	PA	CF6	1	5	1	5	1	5	1	5	1	3
155	TOMO	CF6	1	5	1	5	1	4	1	4	1	5
62	CBCT	CF7	1	5	1	5	1	4	1	5	1	3
48a	PA	CF7	0	3	1	4	0	3	0	2	0	4
48b	PA	CF7	0	3	1	4	0	3	0	2	0	4
200a	PA	CF7	0	4	1	3	1	3	0	3	0	4
200b	PA	CF7	1	3	1	2	0	2	0	4	0	4
164	TOMO	CF7	0	5	0	3	0	4	0	2	1	4
190	TOMO	CF7	0	4	0	4	1	5	0	4	1	4
151	CBCT	CF8	1	5	1	5	1	5	1	5	1	5
4a	PA	CF8	0	3	0	5	0	4	1	1	0	2
4b	PA	CF8	1	5	1	5	1	5	1	5	1	5
136	TOMO	CF8	1	5	1	5	1	5	1	5	1	5
25	CBCT	CF9	1	5	1	5	1	5	1	5	1	5
52a	PA	CF9	1	5	1	5	1	5	1	5	1	5
52b	PA	CF9	1	5	1	5	1	3	1	5	1	3
194a	PA	CF9	1	5	1	5	1	5	1	5	1	5
194b	PA	CF9	1	5	1	5	1	5	1	5	1	3
82	TOMO	CF9	1	5	1	5	1	3	1	4	0	4
16	CBCT	F1	0	4	1	3	1	2	0	3	1	3
91a	PA	F1	0	4	0	4	0	4	0	4	0	4
91b	PA	F1	0	4	0	4	0	3	0	5	0	5
107	TOMO	F1	0	4	0	4	0	4	0	4	0	4
102	CBCT	F10	0	4	0	2	0	4	0	4	0	5
137a	PA	F10	0	4	0	2	0	4	0	4	0	4
137b	PA	F10	0	4	0	3	0	4	0	5	0	4
9	TOMO	F10	0	4	0	3	0	4	1	4	0	4
206	TOMO	F10	0	4	0	4	1	3	0	4	0	4
76	CBCT	F11	0	4	0	3	0	4	0	5	0	5
75a	PA	F11	0	4	1	2	0	5	0	3	1	2
75b	PA	F11	0	4	1	2	0	5	0	3	0	4
23	TOMO	F11	0	5	0	2	0	3	0	4	0	4
192	TOMO	F11	0	5	0	4	0	4	0	4	0	4
144	CBCT	F12	1	4	0	4	0	4	0	4	1	3
109a	PA	F12	0	4	0	3	0	4	0	3	0	5
109b	PA	F12	0	4	0	4	0	4	0	4	0	5
70	TOMO	F12	0	4	0	4	0	4	0	4	1	4
211	TOMO	F12	0	4	0	4	0	4	1	4	1	3
31	CBCT	F13	0	4	1	4	0	4	0	5	0	4
183	CBCT	F13	0	4	0	4	0	3	0	4	0	4
51a	PA	F13	0	4	0	4	0	4	0	4	0	5
51b	PA	F13	0	4	0	4	0	4	0	4	0	5
8	TOMO	F13	0	4	0	4	0	3	0	4	1	4
13	CBCT	F14	0	5	1	4	0	3	0	5	0	4
160a	PA	F14	0	4	0	3	0	4	0	3	0	3
160b	PA	F14	1	3	0	3	0	4	0	2	0	4
201a	PA	F14	0	4	0	3	0	4	0	3	0	4
201b	PA	F14	0	3	0	3	0	4	0	4	0	5
134	TOMO	F14	1	4	0	4	0	4	0	4	0	4
132	CBCT	F15	1	5	1	5	0	4	1	5	0	4
154a	PA	F15	0	4	0	4	0	4	0	2	0	4
154b	PA	F15	0	4	1	2	1	3	1	3	0	5
140	TOMO	F15	0	5	0	4	1	2	0	4	0	4
159	CBCT	F2	0	5	0	4	0	4	0	5	0	5
77a	PA	F2	0	4	0	4	0	4	0	4	0	5
77b	PA	F2	0	4	0	4	0	5	0	4	0	4
90	TOMO	F2	0	5	0	5	0	4	0	3	0	4
185	TOMO	F2	0	4	0	3	1	4	0	3	1	2
108	CBCT	F3	0	4	0	2	1	4	0	5	0	5
130a	PA	F3	0	4	0	3	0	4	0	4	0	5
130b	PA	F3	0	4	0	3	1	3	0	4	0	4
158	TOMO	F3	0	4	0	4	0	4	0	2	1	2

14	CBCT	F4	0	4	0	3	1	3	0	4	1	3
65a	PA	F4	0	3	0	2	0	4	0	4	0	4
65b	PA	F4	0	4	0	2	0	4	0	4	0	5
133	TOMO	F4	0	4	0	2	0	3	0	4	1	3
122	CBCT	F5	0	4	0	3	0	4	0	4	0	5
10a	PA	F5	0	4	1	4	0	4	0	3	0	4
10b	PA	F5	0	4	1	3	1	3	0	4	0	3
128	TOMO	F5	0	4	1	3	1	4	0	4	1	3
173	CBCT	F6	0	4	0	4	1	3	0	5	0	4
101a	PA	F6	0	4	1	4	0	4	0	2	0	4
101b	PA	F6	0	4	1	3	0	4	0	2	0	5
21	TOMO	F6	0	5	0	3	1	5	0	4	0	3
148	CBCT	F7	0	4	0	4	0	2	0	5	0	5
42a	PA	F7	0	4	0	3	0	4	0	2	0	5
42b	PA	F7	0	4	0	4	0	4	0	2	0	5
216a	PA	F7	0	4	0	4	0	4	0	3	0	4
216b	PA	F7	0	4	0	4	0	4	0	4	0	4
84	TOMO	F7	0	4	1	3	0	4	0	4	0	4
116	CBCT	F8	1	3	1	3	1	3	0	4	0	4
193	CBCT	F8	1	4	0	2	1	4	0	4	0	5
171a	PA	F8	0	4	0	3	0	3	0	3	0	3
171b	PA	F8	0	4	0	3	0	4	0	4	0	3
49	TOMO	F8	0	4	0	3	0	4	0	4	0	3
59	CBCT	F9	0	2	0	4	0	3	0	5	0	5
98a	PA	F9	0	4	0	2	0	3	0	4	0	5
98b	PA	F9	0	4	0	2	0	4	0	4	0	5
196a	PA	F9	0	4	0	4	1	4	0	3	0	4
196b	PA	F9	0	4	0	4	1	4	0	4	0	5
53	TOMO	F9	0	4	0	3	0	5	0	5	0	5
150	CBCT	X1	0	4	0	5	0	3	0	5	0	5
188	CBCT	X1	1	3	0	5	0	3	0	5	0	5
143a	PA	X1	0	4	0	3	1	2	0	3	0	3
143b	PA	X1	0	4	1	1	1	3	0	4	0	4
11	TOMO	X1	0	5	0	4	0	5	0	4	1	2
19	CBCT	X10	0	4	0	3	0	3	0	4	0	4
115a	PA	X10	0	4	0	2	0	4	0	3	0	4
115b	PA	X10	0	4	0	2	0	4	0	4	0	5
55	TOMO	X10	1	4	1	5	1	3	1	5	0	4
97	CBCT	X11	0	3	1	2	0	4	0	5	0	5
197	CBCT	X11	0	4	0	5	1	3	0	5	0	5
5a	PA	X11	0	4	0	3	0	4	0	3	0	4
5b	PA	X11	0	4	0	3	0	4	0	4	0	5
207a	PA	X11	0	4	0	4	0	4	0	1	0	4
207b	PA	X11	0	3	0	4	0	4	0	3	0	5
177	TOMO	X11	0	4	0	4	0	4	0	4	0	4
174	CBCT	X12	0	4	0	1	0	4	0	5	0	5
89a	PA	X12	0	4	0	3	0	3	0	3	0	5
89b	PA	X12	0	4	0	3	0	4	0	4	0	5
72	TOMO	X12	0	5	0	4	0	4	0	4	0	5
168	CBCT	X13	0	4	0	3	0	4	0	4	0	5
46a	PA	X13	0	4	0	2	0	4	0	2	0	4
46b	PA	X13	0	4	0	2	0	4	0	3	0	5
178	TOMO	X13	0	4	0	4	0	5	0	4	0	4
34	CBCT	X14	0	5	0	2	0	3	0	4	0	5
66a	PA	X14	0	4	0	2	0	4	0	4	0	4
66b	PA	X14	0	4	0	2	0	4	0	4	0	5
17	TOMO	X14	0	4	0	3	0	4	0	4	0	4
43	CBCT	X15	0	4	1	4	1	3	0	5	1	5
6a	PA	X15	0	4	0	3	0	4	1	3	1	2
6b	PA	X15	0	4	0	4	0	4	0	3	0	5
118	TOMO	X15	0	4	0	4	0	4	0	2	0	5
184	TOMO	X15	0	5	0	3	0	2	0	5	0	4

69	CBCT	X2	0	4	0	4	0	4	0	5	0	5
170a	PA	X2	0	4	0	2	0	4	0	3	0	4
170b	PA	X2	0	3	0	4	0	4	0	3	0	3
93	TOMO	X2	0	4	0	5	1	4	1	5	1	4
163	CBCT	X3	0	4	0	5	0	4	0	5	0	5
189	CBCT	X3	0	4	0	5	0	3	0	5	0	5
114a	PA	X3	0	3	0	1	1	4	0	4	0	4
114b	PA	X3	0	4	1	3	1	4	0	4	0	5
210a	PA	X3	0	3	0	3	1	3	0	3	0	4
210b	PA	X3	0	3	1	2	1	4	0	4	0	4
110	TOMO	X3	0	5	0	4	0	4	0	4	1	2
172	CBCT	X4	1	3	0	5	0	3	0	5	0	5
156a	PA	X4	0	4	0	1	0	3	1	2	0	4
156b	PA	X4	0	4	0	2	0	3	1	1	0	4
212a	PA	X4	0	4	1	2	0	4	0	3	0	4
212b	PA	X4	0	4	1	2	1	2	0	2	0	4
57	TOMO	X4	0	3	0	4	1	3	0	5	0	5
121	CBCT	X5	0	5	1	4	0	3	0	4	0	5
56a	PA	X5	1	2	1	2	0	4	0	3	0	4
56b	PA	X5	1	1	1	2	0	4	0	3	0	5
1	TOMO	X5	0	3	0	4	0	5	1	4	0	4
45	CBCT	X6	0	4	1	3	0	3	0	5	0	4
147a	PA	X6	0	3	0	2	0	3	0	3	0	4
147b	PA	X6	0	3	1	4	0	3	0	4	1	3
187a	PA	X6	0	3	0	2	0	3	0	2	0	4
187b	PA	X6	0	3	1	2	0	4	0	3	1	3
175	TOMO	X6	0	4	0	4	0	4	0	4	0	4
139	CBCT	X7	0	3	1	3	0	4	0	4	1	4
81a	PA	X7	0	3	1	2	0	2	0	2	0	4
81b	PA	X7	0	4	1	5	0	2	0	4	1	3
179	TOMO	X7	0	3	1	5	1	5	0	1	1	4
24	CBCT	X8	0	5	1	4	0	4	0	2	1	3
166a	PA	X8	0	3	0	1	1	4	0	3	1	3
166b	PA	X8	0	3	0	2	1	5	0	3	1	3
204a	PA	X8	0	3	1	4	1	4	0	2	1	3
204b	PA	X8	0	4	1	2	1	5	0	2	1	4
113	TOMO	X8	0	4	1	3	1	5	0	2	1	3
26	CBCT	X9	0	5	0	3	0	4	0	4	0	5
191	CBCT	X9	0	5	0	4	0	4	0	5	0	5
131a	PA	X9	0	4	0	3	0	4	0	4	0	5
131b	PA	X9	0	4	0	4	0	4	0	4	0	5
141	TOMO	X9	0	3	0	4	0	4	0	4	1	2
60	CBCT	XC1	1	5	1	5	1	4	1	5	1	5
165a	PA	XC1	1	4	1	5	1	5	1	5	1	5
165b	PA	XC1	1	3	1	5	1	5	1	2	1	4
54	TOMO	XC1	1	5	1	5	1	5	1	5	1	5
182	TOMO	XC1	1	5	1	5	1	4	1	5	1	5
88	CBCT	XC10	1	5	1	5	1	5	1	5	1	5
124a	PA	XC10	1	5	1	5	1	5	1	5	1	5
124b	PA	XC10	1	5	1	5	1	5	1	5	1	2
181a	PA	XC10	1	5	1	5	1	5	1	5	1	5
181b	PA	XC10	1	5	1	5	1	4	1	5	1	3
22	TOMO	XC10	1	3	0	1	0	4	0	3	0	5
2	CBCT	XC11	1	5	1	5	1	5	1	5	1	5
103a	PA	XC11	1	3	1	4	1	4	1	5	1	4
103b	PA	XC11	1	4	1	5	1	4	1	5	1	5
125	TOMO	XC11	1	3	1	5	1	5	1	5	1	5
176	CBCT	XC12	1	5	1	5	1	4	1	3	1	4
198	CBCT	XC12	1	5	1	5	1	5	1	4	1	4
153a	PA	XC12	1	3	1	4	1	2	1	5	1	4
153b	PA	XC12	1	3	1	4	1	2	1	5	1	4
138	TOMO	XC12	0	5	1	3	1	2	0	4	1	3

12	CBCT	XC13	0	5	1	2	0	3	0	5	0	5
146a	PA	XC13	1	3	1	2	1	2	0	3	1	3
146b	PA	XC13	1	2	1	1	1	3	0	4	0	4
32	TOMO	XC13	0	5	0	1	0	4	0	4	0	4
161	CBCT	XC14	1	5	1	5	1	5	1	5	1	5
68a	PA	XC14	0	4	1	5	1	5	1	5	1	5
68b	PA	XC14	0	4	1	5	1	5	1	5	1	5
209a	PA	XC14	1	5	1	5	1	4	1	5	1	4
209b	PA	XC14	1	4	1	5	1	5	1	5	1	5
152	TOMO	XC14	1	5	1	5	1	5	1	5	1	5
18	CBCT	XC15	1	5	1	5	1	5	1	5	1	5
64a	PA	XC15	1	2	1	5	1	5	1	5	1	3
64b	PA	XC15	0	3	1	5	1	5	1	5	1	5
213a	PA	XC15	1	5	1	5	1	4	1	5	1	3
213b	PA	XC15	1	5	1	5	1	5	1	5	1	4
7	TOMO	XC15	1	5	1	4	1	5	1	5	1	5
67	CBCT	XC2	1	5	1	5	1	5	1	5	1	5
126a	PA	XC2	1	5	1	5	1	4	1	5	1	4
126b	PA	XC2	1	5	1	5	1	5	1	5	1	5
27	TOMO	XC2	1	5	1	5	1	5	1	5	1	5
30	CBCT	XC3	1	5	1	5	1	5	1	5	1	5
123a	PA	XC3	0	4	1	5	1	2	0	4	1	4
123b	PA	XC3	1	5	1	5	1	5	1	5	1	5
28	TOMO	XC3	1	5	1	5	1	5	1	5	1	5
74	CBCT	XC4	1	5	1	4	1	5	1	5	1	4
39a	PA	XC4	0	4	0	2	0	3	0	3	0	4
39b	PA	XC4	1	4	1	5	1	4	1	4	1	5
94	TOMO	XC4	1	5	1	5	0	4	1	5	1	5
96	CBCT	XC5	1	5	1	5	1	5	1	5	1	5
214	CBCT	XC5	1	5	1	5	1	5	1	5	1	5
162a	PA	XC5	1	5	1	5	1	5	1	5	1	5
162b	PA	XC5	1	5	1	5	1	2	1	5	1	3
29	TOMO	XC5	1	5	1	5	1	3	1	3	1	4
142	CBCT	XC6	1	5	1	5	1	5	1	5	1	5
208	CBCT	XC6	1	5	1	5	1	5	1	5	1	5
86a	PA	XC6	1	2	1	5	1	5	1	3	1	4
86b	PA	XC6	1	5	1	5	1	5	1	5	1	5
3	TOMO	XC6	1	5	1	5	1	5	1	5	1	5
135	CBCT	XC7	1	5	1	5	1	5	1	5	1	5
95a	PA	XC7	1	4	1	5	1	4	1	4	1	5
95b	PA	XC7	1	4	1	5	1	5	1	5	1	5
71	TOMO	XC7	1	4	1	5	1	5	1	5	1	5
92	CBCT	XC8	1	5	1	5	1	5	1	5	1	5
99a	PA	XC8	0	4	0	1	1	3	1	3	0	3
99b	PA	XC8	1	4	1	5	1	5	1	5	1	5
61	TOMO	XC8	0	3	1	5	1	5	1	5	1	5
119	CBCT	XC9	1	5	1	5	1	5	1	5	1	5
80a	PA	XC9	1	5	1	5	1	5	1	5	1	5
80b	PA	XC9	1	5	1	5	1	3	1	5	1	3
106	TOMO	XC9	1	5	1	5	1	5	1	5	1	5

Appendix IV: Statistical Analysis

Table 1 of Crack_Eval 1 by cracked			
Controlling for filled=0 Modality=CBCT			
Crack_Eval 1(Crack_Eval 1)	**cracked**		
Frequency Percent Row Pct Col Pct	**0**	**1**	**Total**
0	14 46.67 93.33 93.33	1 3.33 6.67 6.67	15 50.00
1	1 3.33 6.67 6.67	14 46.67 93.33 93.33	15 50.00
Total	15 50.00	15 50.00	30 100.00

Table 2 of Crack_Eval 1 by cracked			
Controlling for filled=0 Modality=PAa			
Crack_Eval 1(Crack_Eval 1)	**cracked**		
Frequency Percent Row Pct Col Pct	**0**	**1**	**Total**
0	14 46.67 77.78 93.33	4 13.33 22.22 26.67	18 60.00
1	1 3.33 8.33 6.67	11 36.67 91.67 73.33	12 40.00
Total	15 50.00	15 50.00	30 100.00

Table 3 of Crack_Eval 1 by cracked			
Controlling for filled=0 Modality=PAb			
Crack_Eval 1(Crack_Eval 1)	cracked		
Frequency Percent Row Pct Col Pct	0	1	Total
0	14 46.67 87.50 93.33	2 6.67 12.50 13.33	16 53.33
1	1 3.33 7.14 6.67	13 43.33 92.86 86.67	14 46.67
Total	15 50.00	15 50.00	30 100.00

Table 4 of Crack_Eval 1 by cracked			
Controlling for filled=0 Modality=TOMO			
Crack_Eval 1(Crack_Eval 1)	cracked		
Frequency Percent Row Pct Col Pct	0	1	Total
0	14 46.67 82.35 93.33	3 10.00 17.65 20.00	17 56.67
1	1 3.33 7.69 6.67	12 40.00 92.31 80.00	13 43.33
Total	15 50.00	15 50.00	30 100.00

Table 5 of Crack_Eval 1 by cracked			
Controlling for filled=1 Modality=CBCT			
Crack_Eval 1(Crack_Eval 1)	**cracked**		
Frequency Percent Row Pct Col Pct	**0**	**1**	**Total**
0	12 40.00 85.71 80.00	2 6.67 14.29 13.33	14 46.67
1	3 10.00 18.75 20.00	13 43.33 81.25 86.67	16 53.33
Total	15 50.00	15 50.00	30 100.00

Table 6 of Crack_Eval 1 by cracked			
Controlling for filled=1 Modality=PAa			
Crack_Eval 1(Crack_Eval 1)	**cracked**		
Frequency Percent Row Pct Col Pct	**0**	**1**	**Total**
0	15 50.00 60.00 100.00	10 33.33 40.00 66.67	25 83.33
1	0 0.00 0.00 0.00	5 16.67 100.00 33.33	5 16.67
Total	15 50.00	15 50.00	30 100.00

Table 7 of Crack_Eval 1 by cracked			
Controlling for filled=1 Modality=PAb			
Crack_Eval 1(Crack_Eval 1)	cracked		
Frequency Percent Row Pct Col Pct	0	1	Total
0	14 46.67 66.67 93.33	7 23.33 33.33 46.67	21 70.00
1	1 3.33 11.11 6.67	8 26.67 88.89 53.33	9 30.00
Total	15 50.00	15 50.00	30 100.00

Table 8 of Crack_Eval 1 by cracked			
Controlling for filled=1 Modality=TOMO			
Crack_Eval 1(Crack_Eval 1)	cracked		
Frequency Percent Row Pct Col Pct	0	1	Total
0	14 46.67 63.64 93.33	8 26.67 36.36 53.33	22 73.33
1	1 3.33 12.50 6.67	7 23.33 87.50 46.67	8 26.67
Total	15 50.00	15 50.00	30 100.00

Table 1 of acc_Eval 1 by Modality					
Controlling for filled=0					
acc_Eval 1	Modality(Modality)				
Frequency Percent Row Pct Col Pct	CBCT	PAa	PAb	TOMO	Total
0	2 1.67 14.29 6.67	5 4.17 35.71 16.67	3 2.50 21.43 10.00	4 3.33 28.57 13.33	14 11.67
1	28 23.33 26.42 93.33	25 20.83 23.58 83.33	27 22.50 25.47 90.00	26 21.67 24.53 86.67	106 88.33
Total	30 25.00	30 25.00	30 25.00	30 25.00	120 100.00

Table 2 of acc_Eval 1 by Modality					
Controlling for filled=1					
acc_Eval 1	Modality(Modality)				
Frequency Percent Row Pct Col Pct	CBCT	PAa	PAb	TOMO	Total
0	5 4.17 15.63 16.67	10 8.33 31.25 33.33	8 6.67 25.00 26.67	9 7.50 28.13 30.00	32 26.67
1	25 20.83 28.41 83.33	20 16.67 22.73 66.67	22 18.33 25.00 73.33	21 17.50 23.86 70.00	88 73.33
Total	30 25.00	30 25.00	30 25.00	30 25.00	120 100.00

Table 1 of Certainty_Eval 1 by Modality					
Controlling for filled=0					
Certainty_Eval 1(Certainty_Eval 1)	**Modality(Modality)**				
Frequency Percent Row Pct Col Pct	**CBCT**	**PAa**	**PAb**	**TOMO**	**Total**
1	0 0.00 0.00 0.00	0 0.00 0.00 0.00	1 0.83 100.00 3.33	0 0.00 0.00 0.00	1 0.83
2	0 0.00 0.00 0.00	3 2.50 75.00 10.00	1 0.83 25.00 3.33	0 0.00 0.00 0.00	4 3.33
3	3 2.50 13.04 10.00	7 5.83 30.43 23.33	6 5.00 26.09 20.00	7 5.83 30.43 23.33	23 19.17
4	8 6.67 16.33 26.67	16 13.33 32.65 53.33	16 13.33 32.65 53.33	9 7.50 18.37 30.00	49 40.83
5	19 15.83 44.19 63.33	4 3.33 9.30 13.33	6 5.00 13.95 20.00	14 11.67 32.56 46.67	43 35.83
Total	30 25.00	30 25.00	30 25.00	30 25.00	120 100.00

Table 2 of Certainty_Eval 1 by Modality					
Controlling for filled=1					
Certainty_Eval 1(Certainty_Eval 1)	**Modality(Modality)**				
Frequency Percent Row Pct Col Pct	**CBCT**	**PAa**	**PAb**	**TOMO**	**Total**
1	0 0.00 . 0.00	0 0.00 . 0.00	0 0.00 . 0.00	0 0.00 . 0.00	0 0.00
2	1 0.83 100.00 3.33	0 0.00 0.00 0.00	0 0.00 0.00 0.00	0 0.00 0.00 0.00	1 0.83
3	2 1.67 16.67 6.67	5 4.17 41.67 16.67	4 3.33 33.33 13.33	1 0.83 8.33 3.33	12 10.00
4	11 9.17 16.18 36.67	21 17.50 30.88 70.00	21 17.50 30.88 70.00	15 12.50 22.06 50.00	68 56.67
5	16 13.33 41.03 53.33	4 3.33 10.26 13.33	5 4.17 12.82 16.67	14 11.67 35.90 46.67	39 32.50
Total	30 25.00	30 25.00	30 25.00	30 25.00	120 100.00

Table 1 of Crack_Eval 2 by cracked			
Controlling for filled=0 Modality=CBCT			
Crack_Eval 2(Crack_Eval 2)	**cracked**		
Frequency Percent Row Pct Col Pct	**0**	**1**	**Total**
0	9 30.00 100.00 60.00	0 0.00 0.00 0.00	9 30.00
1	6 20.00 28.57 40.00	15 50.00 71.43 100.00	21 70.00
Total	15 50.00	15 50.00	30 100.00

Table 2 of Crack_Eval 2 by cracked			
Controlling for filled=0 Modality=PAa			
Crack_Eval 2(Crack_Eval 2)	cracked		
Frequency Percent Row Pct Col Pct	0	1	Total
0	13 43.33 86.67 86.67	2 6.67 13.33 13.33	15 50.00
1	2 6.67 13.33 13.33	13 43.33 86.67 86.67	15 50.00
Total	15 50.00	15 50.00	30 100.00

Table 3 of Crack_Eval 2 by cracked			
Controlling for filled=0 Modality=PAb			
Crack_Eval 2(Crack_Eval 2)	cracked		
Frequency Percent Row Pct Col Pct	0	1	Total
0	10 33.33 100.00 66.67	0 0.00 0.00 0.00	10 33.33
1	5 16.67 25.00 33.33	15 50.00 75.00 100.00	20 66.67
Total	15 50.00	15 50.00	30 100.00

Table 4 of Crack_Eval 2 by cracked			
Controlling for filled=0 Modality=TOMO			
Crack_Eval 2(Crack_Eval 2)	cracked		
Frequency Percent Row Pct Col Pct	0	1	Total
0	12 40.00 85.71 80.00	2 6.67 14.29 13.33	14 46.67
1	3 10.00 18.75 20.00	13 43.33 81.25 86.67	16 53.33
Total	15 50.00	15 50.00	30 100.00

Table 5 of Crack_Eval 2 by cracked			
Controlling for filled=1 Modality=CBCT			
Crack_Eval 2(Crack_Eval 2)	cracked		
Frequency Percent Row Pct Col Pct	0	1	Total
0	10 33.33 83.33 66.67	2 6.67 16.67 13.33	12 40.00
1	5 16.67 27.78 33.33	13 43.33 72.22 86.67	18 60.00
Total	15 50.00	15 50.00	30 100.00

Table 6 of Crack_Eval 2 by cracked			
Controlling for filled=1 Modality=PAa			
Crack_Eval 2(Crack_Eval 2)	cracked		
Frequency Percent Row Pct Col Pct	0	1	Total
0	12 40.00 70.59 80.00	5 16.67 29.41 33.33	17 56.67
1	3 10.00 23.08 20.00	10 33.33 76.92 66.67	13 43.33
Total	15 50.00	15 50.00	30 100.00

Table 7 of Crack_Eval 2 by cracked			
Controlling for filled=1 Modality=PAb			
Crack_Eval 2(Crack_Eval 2)	cracked		
Frequency Percent Row Pct Col Pct	0	1	Total
0	11 36.67 73.33 73.33	4 13.33 26.67 26.67	15 50.00
1	4 13.33 26.67 26.67	11 36.67 73.33 73.33	15 50.00
Total	15 50.00	15 50.00	30 100.00

Table 8 of Crack_Eval 2 by cracked			
Controlling for filled=1 Modality=TOMO			
Crack_Eval 2(Crack_Eval 2)	cracked		
Frequency Percent Row Pct Col Pct	0	1	Total
0	13 43.33 72.22 86.67	5 16.67 27.78 33.33	18 60.00
1	2 6.67 16.67 13.33	10 33.33 83.33 66.67	12 40.00
Total	15 50.00	15 50.00	30 100.00

Table 1 of acc_Eval 2 by Modality					
Controlling for filled=0					
acc_Eval 2	Modality(Modality)				
Frequency Percent Row Pct Col Pct	CBCT	PAa	PAb	TOMO	Total
0	6 5.00 30.00 20.00	4 3.33 20.00 13.33	5 4.17 25.00 16.67	5 4.17 25.00 16.67	20 16.67
1	24 20.00 24.00 80.00	26 21.67 26.00 86.67	25 20.83 25.00 83.33	25 20.83 25.00 83.33	100 83.33
Total	30 25.00	30 25.00	30 25.00	30 25.00	120 100.00

Table 2 of acc_Eval 2 by Modality					
Controlling for filled=1					
acc_Eval 2	Modality(Modality)				
Frequency Percent Row Pct Col Pct	CBCT	PAa	PAb	TOMO	Total
0	7 5.83 23.33 23.33	8 6.67 26.67 26.67	8 6.67 26.67 26.67	7 5.83 23.33 23.33	30 25.00
1	23 19.17 25.56 76.67	22 18.33 24.44 73.33	22 18.33 24.44 73.33	23 19.17 25.56 76.67	90 75.00
Total	30 25.00	30 25.00	30 25.00	30 25.00	120 100.00

Table 1 of Certainty_Eval 2 by Modality					
Controlling for filled=0					
Certainty_Eval 2(Certainty_Eval 2)	**Modality(Modality)**				
Frequency Percent Row Pct Col Pct	**CBCT**	**PAa**	**PAb**	**TOMO**	**Total**
1	1 0.83 11.11 3.33	4 3.33 44.44 13.33	2 1.67 22.22 6.67	2 1.67 22.22 6.67	9 7.50
2	3 2.50 16.67 10.00	9 7.50 50.00 30.00	6 5.00 33.33 20.00	0 0.00 0.00 0.00	18 15.00
3	5 4.17 31.25 16.67	5 4.17 31.25 16.67	3 2.50 18.75 10.00	3 2.50 18.75 10.00	16 13.33
4	5 4.17 21.74 16.67	2 1.67 8.70 6.67	5 4.17 21.74 16.67	11 9.17 47.83 36.67	23 19.17
5	16 13.33 29.63 53.33	10 8.33 18.52 33.33	14 11.67 25.93 46.67	14 11.67 25.93 46.67	54 45.00
Total	30 25.00	30 25.00	30 25.00	30 25.00	120 100.00

Table 2 of Certainty_Eval 2 by Modality					
Controlling for filled=1					
Certainty_Eval 2(Certainty_Eval 2)	**Modality(Modality)**				
Frequency Percent Row Pct Col Pct	**CBCT**	**PAa**	**PAb**	**TOMO**	**Total**
1	0 0.00 0.00 0.00	1 0.83 100.00 3.33	0 0.00 0.00 0.00	0 0.00 0.00 0.00	1 0.83
2	3 2.50 15.79 10.00	7 5.83 36.84 23.33	5 4.17 26.32 16.67	4 3.33 21.05 13.33	19 15.83
3	7 5.83 23.33 23.33	7 5.83 23.33 23.33	8 6.67 26.67 26.67	8 6.67 26.67 26.67	30 25.00
4	10 8.33 26.32 33.33	9 7.50 23.68 30.00	10 8.33 26.32 33.33	9 7.50 23.68 30.00	38 31.67
5	10 8.33 31.25 33.33	6 5.00 18.75 20.00	7 5.83 21.88 23.33	9 7.50 28.13 30.00	32 26.67
Total	30 25.00	30 25.00	30 25.00	30 25.00	120 100.00

Table 1 of Crack_Eval 3 by cracked			
Controlling for filled=0 Modality=CBCT			
Crack_Eval 3(Crack_Eval 3)	cracked		
Frequency Percent Row Pct Col Pct	0	1	Total
0	14 46.67 93.33 93.33	1 3.33 6.67 6.67	15 50.00
1	1 3.33 6.67 6.67	14 46.67 93.33 93.33	15 50.00
Total	15 50.00	15 50.00	30 100.00

Table 2 of Crack_Eval 3 by cracked			
Controlling for filled=0 Modality=PAa			
Crack_Eval 3(Crack_Eval 3)	cracked		
Frequency Percent Row Pct Col Pct	0	1	Total
0	12 40.00 92.31 80.00	1 3.33 7.69 6.67	13 43.33
1	3 10.00 17.65 20.00	14 46.67 82.35 93.33	17 56.67
Total	15 50.00	15 50.00	30 100.00

Table 3 of Crack_Eval 3 by cracked			
Controlling for filled=0 Modality=PAb			
Crack_Eval 3(Crack_Eval 3)	cracked		
Frequency Percent Row Pct Col Pct	0	1	Total
0	12 40.00 100.00 80.00	0 0.00 0.00 0.00	12 40.00
1	3 10.00 16.67 20.00	15 50.00 83.33 100.00	18 60.00
Total	15 50.00	15 50.00	30 100.00

Table 4 of Crack_Eval 3 by cracked			
Controlling for filled=0 Modality=TOMO			
Crack_Eval 3(Crack_Eval 3)	**cracked**		
Frequency Percent Row Pct Col Pct	**0**	**1**	**Total**
0	10 33.33 76.92 66.67	3 10.00 23.08 20.00	13 43.33
1	5 16.67 29.41 33.33	12 40.00 70.59 80.00	17 56.67
Total	15 50.00	15 50.00	30 100.00

Table 5 of Crack_Eval 3 by cracked			
Controlling for filled=1 Modality=CBCT			
Crack_Eval 3(Crack_Eval 3)	**cracked**		
Frequency Percent Row Pct Col Pct	**0**	**1**	**Total**
0	10 33.33 83.33 66.67	2 6.67 16.67 13.33	12 40.00
1	5 16.67 27.78 33.33	13 43.33 72.22 86.67	18 60.00
Total	15 50.00	15 50.00	30 100.00

Table 6 of Crack_Eval 3 by cracked			
Controlling for filled=1 Modality=PAa			
Crack_Eval 3(Crack_Eval 3)	**cracked**		
Frequency Percent Row Pct Col Pct	**0**	**1**	**Total**
0	15 50.00 62.50 100.00	9 30.00 37.50 60.00	24 80.00
1	0 0.00 0.00 0.00	6 20.00 100.00 40.00	6 20.00
Total	15 50.00	15 50.00	30 100.00

Table 7 of Crack_Eval 3 by cracked			
Controlling for filled=1 Modality=PAb			
Crack_Eval 3(Crack_Eval 3)	cracked		
Frequency Percent Row Pct Col Pct	0	1	Total
0	12 40.00 63.16 80.00	7 23.33 36.84 46.67	19 63.33
1	3 10.00 27.27 20.00	8 26.67 72.73 53.33	11 36.67
Total	15 50.00	15 50.00	30 100.00

Table 8 of Crack_Eval 3 by cracked			
Controlling for filled=1 Modality=TOMO			
Crack_Eval 3(Crack_Eval 3)	cracked		
Frequency Percent Row Pct Col Pct	0	1	Total
0	12 40.00 60.00 80.00	8 26.67 40.00 53.33	20 66.67
1	3 10.00 30.00 20.00	7 23.33 70.00 46.67	10 33.33
Total	15 50.00	15 50.00	30 100.00

Table 1 of acc_Eval 3 by Modality					
Controlling for filled=0					
acc_Eval 3	Modality(Modality)				
Frequency Percent Row Pct Col Pct	CBCT	PAa	PAb	TOMO	Total
0	2 1.67 11.76 6.67	4 3.33 23.53 13.33	3 2.50 17.65 10.00	8 6.67 47.06 26.67	17 14.17
1	28 23.33 27.18 93.33	26 21.67 25.24 86.67	27 22.50 26.21 90.00	22 18.33 21.36 73.33	103 85.83
Total	30 25.00	30 25.00	30 25.00	30 25.00	120 100.00

Table 2 of acc_Eval 3 by Modality					
Controlling for filled=1					
acc_Eval 3	Modality(Modality)				
Frequency Percent Row Pct Col Pct	CBCT	PAa	PAb	TOMO	Total
0	7 5.83 18.92 23.33	9 7.50 24.32 30.00	10 8.33 27.03 33.33	11 9.17 29.73 36.67	37 30.83
1	23 19.17 27.71 76.67	21 17.50 25.30 70.00	20 16.67 24.10 66.67	19 15.83 22.89 63.33	83 69.17
Total	30 25.00	30 25.00	30 25.00	30 25.00	120 100.00

Table 1 of Certainty_Eval 3 by Modality					
Controlling for filled=0					
Certainty_Eval 3(Certainty_Eval 3)	Modality(Modality)				
Frequency Percent Row Pct Col Pct	CBCT	PAa	PAb	TOMO	Total
2	0 0.00 0.00 0.00	5 4.17 55.56 16.67	3 2.50 33.33 10.00	1 0.83 11.11 3.33	9 7.50
3	8 6.67 38.10 26.67	5 4.17 23.81 16.67	5 4.17 23.81 16.67	3 2.50 14.29 10.00	21 17.50
4	10 8.33 21.74 33.33	13 10.83 28.26 43.33	12 10.00 26.09 40.00	11 9.17 23.91 36.67	46 38.33
5	12 10.00 27.27 40.00	7 5.83 15.91 23.33	10 8.33 22.73 33.33	15 12.50 34.09 50.00	44 36.67
Total	30 25.00	30 25.00	30 25.00	30 25.00	120 100.00

Table 2 of Certainty_Eval 3 by Modality					
Controlling for filled=1					
Certainty_Eval 3(Certainty_Eval 3)	Modality(Modality)				
Frequency Percent Row Pct Col Pct	CBCT	PAa	PAb	TOMO	Total
2	2 1.67 66.67 6.67	0 0.00 0.00 0.00	0 0.00 0.00 0.00	1 0.83 33.33 3.33	3 2.50
3	6 5.00 27.27 20.00	5 4.17 22.73 16.67	7 5.83 31.82 23.33	4 3.33 18.18 13.33	22 18.33
4	14 11.67 19.44 46.67	20 16.67 27.78 66.67	19 15.83 26.39 63.33	19 15.83 26.39 63.33	72 60.00
5	8 6.67 34.78 26.67	5 4.17 21.74 16.67	4 3.33 17.39 13.33	6 5.00 26.09 20.00	23 19.17
Total	30 25.00	30 25.00	30 25.00	30 25.00	120 100.00

Table 1 of Crack_Eval 4 by cracked			
Controlling for filled=0 Modality=CBCT			
Crack_Eval 4(Crack_Eval 4)	cracked		
Frequency Percent Row Pct Col Pct	0	1	Total
0	15 50.00 93.75 100.00	1 3.33 6.25 6.67	16 53.33
1	0 0.00 0.00 0.00	14 46.67 100.00 93.33	14 46.67
Total	15 50.00	15 50.00	30 100.00

Table 2 of Crack_Eval 4 by cracked			
Controlling for filled=0 Modality=PAa			
Crack_Eval 4(Crack_Eval 4)	cracked		
Frequency Percent Row Pct Col Pct	0	1	Total
0	13 43.33 81.25 86.67	3 10.00 18.75 20.00	16 53.33
1	2 6.67 14.29 13.33	12 40.00 85.71 80.00	14 46.67
Total	15 50.00	15 50.00	30 100.00

Table 3 of Crack_Eval 4 by cracked			
Controlling for filled=0 Modality=PAb			
Crack_Eval 4(Crack_Eval 4)	cracked		
Frequency Percent Row Pct Col Pct	0	1	Total
0	14 46.67 93.33 93.33	1 3.33 6.67 6.67	15 50.00
1	1 3.33 6.67 6.67	14 46.67 93.33 93.33	15 50.00
Total	15 50.00	15 50.00	30 100.00

Table 4 of Crack_Eval 4 by cracked			
Controlling for filled=0 Modality=TOMO			
Crack_Eval 4(Crack_Eval 4)	cracked		
Frequency Percent Row Pct Col Pct	0	1	Total
0	12 40.00 80.00 80.00	3 10.00 20.00 20.00	15 50.00
1	3 10.00 20.00 20.00	12 40.00 80.00 80.00	15 50.00
Total	15 50.00	15 50.00	30 100.00

Table 5 of Crack_Eval 4 by cracked			
Controlling for filled=1 Modality=CBCT			
Crack_Eval 4(Crack_Eval 4)	cracked		
Frequency Percent Row Pct Col Pct	0	1	Total
0	14 46.67 82.35 93.33	3 10.00 17.65 20.00	17 56.67
1	1 3.33 7.69 6.67	12 40.00 92.31 80.00	13 43.33
Total	15 50.00	15 50.00	30 100.00

Table 6 of Crack_Eval 4 by cracked			
Controlling for filled=1 Modality=PAa			
Crack_Eval 4(Crack_Eval 4)	cracked		
Frequency Percent Row Pct Col Pct	0	1	Total
0	15 50.00 65.22 100.00	8 26.67 34.78 53.33	23 76.67
1	0 0.00 0.00 0.00	7 23.33 100.00 46.67	7 23.33
Total	15 50.00	15 50.00	30 100.00

Table 7 of Crack_Eval 4 by cracked			
Controlling for filled=1 Modality=PAb			
Crack_Eval 4(Crack_Eval 4)	cracked		
Frequency Percent Row Pct Col Pct	0	1	Total
0	14 46.67 70.00 93.33	6 20.00 30.00 40.00	20 66.67
1	1 3.33 10.00 6.67	9 30.00 90.00 60.00	10 33.33
Total	15 50.00	15 50.00	30 100.00

Table 8 of Crack_Eval 4 by cracked			
Controlling for filled=1 Modality=TOMO			
Crack_Eval 4(Crack_Eval 4)	cracked		
Frequency Percent Row Pct Col Pct	0	1	Total
0	14 46.67 73.68 93.33	5 16.67 26.32 33.33	19 63.33
1	1 3.33 9.09 6.67	10 33.33 90.91 66.67	11 36.67
Total	15 50.00	15 50.00	30 100.00

Table 1 of acc_Eval 4 by Modality					
Controlling for filled=0					
acc_Eval 4	Modality(Modality)				
Frequency Percent Row Pct Col Pct	CBCT	PAa	PAb	TOMO	Total
0	1 0.83 7.14 3.33	5 4.17 35.71 16.67	2 1.67 14.29 6.67	6 5.00 42.86 20.00	14 11.67
1	29 24.17 27.36 96.67	25 20.83 23.58 83.33	28 23.33 26.42 93.33	24 20.00 22.64 80.00	106 88.33
Total	30 25.00	30 25.00	30 25.00	30 25.00	120 100.00

Table 2 of acc_Eval 4 by Modality					
Controlling for filled=1					
acc_Eval 4	Modality(Modality)				
Frequency Percent Row Pct Col Pct	CBCT	PAa	PAb	TOMO	Total
0	4 3.33 16.00 13.33	8 6.67 32.00 26.67	7 5.83 28.00 23.33	6 5.00 24.00 20.00	25 20.83
1	26 21.67 27.37 86.67	22 18.33 23.16 73.33	23 19.17 24.21 76.67	24 20.00 25.26 80.00	95 79.17
Total	30 25.00	30 25.00	30 25.00	30 25.00	120 100.00

Table 1 of Certainty_Eval 4 by Modality					
Controlling for filled=0					
Certainty_Eval 4(Certainty_Eval 4)	Modality(Modality)				
Frequency Percent Row Pct Col Pct	CBCT	PAa	PAb	TOMO	Total
0	0 0.00 . 0.00	0 0.00 . 0.00	0 0.00 . 0.00	0 0.00 . 0.00	0 0.00
1	0 0.00 0.00 0.00	0 0.00 0.00 0.00	1 0.83 50.00 3.33	1 0.83 50.00 3.33	2 1.67
2	1 0.83 14.29 3.33	3 2.50 42.86 10.00	1 0.83 14.29 3.33	2 1.67 28.57 6.67	7 5.83
3	1 0.83 4.76 3.33	13 10.83 61.90 43.33	5 4.17 23.81 16.67	2 1.67 9.52 6.67	21 17.50
4	6 5.00 18.18 20.00	5 4.17 15.15 16.67	11 9.17 33.33 36.67	11 9.17 33.33 36.67	33 27.50
5	22 18.33 38.60 73.33	9 7.50 15.79 30.00	12 10.00 21.05 40.00	14 11.67 24.56 46.67	57 47.50
Total	30 25.00	30 25.00	30 25.00	30 25.00	120 100.00

Table 2 of Certainty_Eval 4 by Modality					
Controlling for filled=1					
Certainty_Eval 4(Certainty_Eval 4)	Modality(Modality)				
Frequency Percent Row Pct Col Pct	CBCT	PAa	PAb	TOMO	Total
0	0 0.00 0.00 0.00	0 0.00 0.00 0.00	1 0.83 100.00 3.33	0 0.00 0.00 0.00	1 0.83
1	0 0.00 0.00 0.00	1 0.83 100.00 3.33	0 0.00 0.00 0.00	0 0.00 0.00 0.00	1 0.83
2	0 0.00 0.00 0.00	4 3.33 30.77 13.33	5 4.17 38.46 16.67	4 3.33 30.77 13.33	13 10.83
3	4 3.33 17.39 13.33	11 9.17 47.83 36.67	4 3.33 17.39 13.33	4 3.33 17.39 13.33	23 19.17
4	6 5.00 14.29 20.00	9 7.50 21.43 30.00	12 10.00 28.57 40.00	15 12.50 35.71 50.00	42 35.00
5	20 16.67 50.00 66.67	5 4.17 12.50 16.67	8 6.67 20.00 26.67	7 5.83 17.50 23.33	40 33.33
Total	30 25.00	30 25.00	30 25.00	30 25.00	120 100.00

Table 1 of Crack_Eval 5 by cracked			
Controlling for filled=0 Modality=CBCT			
Crack_Eval 5(Crack_Eval 5)	**cracked**		
Frequency **Percent** **Row Pct** **Col Pct**	**0**	**1**	**Total**
0	12 40.00 92.31 80.00	1 3.33 7.69 6.67	13 43.33
1	3 10.00 17.65 20.00	14 46.67 82.35 93.33	17 56.67
Total	15 50.00	15 50.00	30 100.00

Table 2 of Crack_Eval 5 by cracked			
Controlling for filled=0 Modality=PAa			
Crack_Eval 5(Crack_Eval 5)	**cracked**		
Frequency **Percent** **Row Pct** **Col Pct**	**0**	**1**	**Total**
0	13 43.33 86.67 86.67	2 6.67 13.33 13.33	15 50.00
1	2 6.67 13.33 13.33	13 43.33 86.67 86.67	15 50.00
Total	15 50.00	15 50.00	30 100.00

Table 3 of Crack_Eval 5 by cracked			
Controlling for filled=0 Modality=PAb			
Crack_Eval 5(Crack_Eval 5)	**cracked**		
Frequency Percent Row Pct Col Pct	**0**	**1**	**Total**
0	12 40.00 92.31 80.00	1 3.33 7.69 6.67	13 43.33
1	3 10.00 17.65 20.00	14 46.67 82.35 93.33	17 56.67
Total	15 50.00	15 50.00	30 100.00

Table 4 of Crack_Eval 5 by cracked			
Controlling for filled=0 Modality=TOMO			
Crack_Eval 5(Crack_Eval 5)	**cracked**		
Frequency Percent Row Pct Col Pct	**0**	**1**	**Total**
0	9 30.00 81.82 60.00	2 6.67 18.18 13.33	11 36.67
1	6 20.00 31.58 40.00	13 43.33 68.42 86.67	19 63.33
Total	15 50.00	15 50.00	30 100.00

Table 5 of Crack_Eval 5 by cracked			
Controlling for filled=1 Modality=CBCT			
Crack_Eval 5(Crack_Eval 5)	**cracked**		
Frequency **Percent** **Row Pct** **Col Pct**	**0**	**1**	**Total**
0	12 40.00 85.71 80.00	2 6.67 14.29 13.33	14 46.67
1	3 10.00 18.75 20.00	13 43.33 81.25 86.67	16 53.33
Total	15 50.00	15 50.00	30 100.00

Table 6 of Crack_Eval 5 by cracked			
Controlling for filled=1 Modality=PAa			
Crack_Eval 5(Crack_Eval 5)	**cracked**		
Frequency **Percent** **Row Pct** **Col Pct**	**0**	**1**	**Total**
0	14 46.67 63.64 93.33	8 26.67 36.36 53.33	22 73.33
1	1 3.33 12.50 6.67	7 23.33 87.50 46.67	8 26.67
Total	15 50.00	15 50.00	30 100.00

Table 7 of Crack_Eval 5 by cracked			
Controlling for filled=1 Modality=PAb			
Crack_Eval 5(Crack_Eval 5)	**cracked**		
Frequency Percent Row Pct Col Pct	**0**	**1**	**Total**
0	15 50.00 68.18 100.00	7 23.33 31.82 46.67	22 73.33
1	0 0.00 0.00 0.00	8 26.67 100.00 53.33	8 26.67
Total	15 50.00	15 50.00	30 100.00

Table 8 of Crack_Eval 5 by cracked			
Controlling for filled=1 Modality=TOMO			
Crack_Eval 5(Crack_Eval 5)	**cracked**		
Frequency Percent Row Pct Col Pct	**0**	**1**	**Total**
0	10 33.33 71.43 66.67	4 13.33 28.57 26.67	14 46.67
1	5 16.67 31.25 33.33	11 36.67 68.75 73.33	16 53.33
Total	15 50.00	15 50.00	30 100.00

Table 1 of acc_Eval 5 by Modality					
Controlling for filled=0					
acc_Eval 5	Modality(Modality)				
Frequency Percent Row Pct Col Pct	CBCT	PAa	PAb	TOMO	Total
0	4 3.33 20.00 13.33	4 3.33 20.00 13.33	4 3.33 20.00 13.33	8 6.67 40.00 26.67	20 16.67
1	26 21.67 26.00 86.67	26 21.67 26.00 86.67	26 21.67 26.00 86.67	22 18.33 22.00 73.33	100 83.33
Total	30 25.00	30 25.00	30 25.00	30 25.00	120 100.00

Table 2 of acc_Eval 5 by Modality					
Controlling for filled=1					
acc_Eval 5	Modality(Modality)				
Frequency Percent Row Pct Col Pct	CBCT	PAa	PAb	TOMO	Total
0	5 4.17 16.67 16.67	9 7.50 30.00 30.00	7 5.83 23.33 23.33	9 7.50 30.00 30.00	30 25.00
1	25 20.83 27.78 83.33	21 17.50 23.33 70.00	23 19.17 25.56 76.67	21 17.50 23.33 70.00	90 75.00
Total	30 25.00	30 25.00	30 25.00	30 25.00	120 100.00

Table 1 of Certainty_Eval 5 by Modality					
Controlling for filled=0					
Certainty_Eval 5(Certainty_Eval 5)	**Modality(Modality)**				
Frequency Percent Row Pct Col Pct	**CBCT**	**PAa**	**PAb**	**TOMO**	**Total**
2	0 0.00 0.00 0.00	1 0.83 20.00 3.33	1 0.83 20.00 3.33	3 2.50 60.00 10.00	5 4.17
3	1 0.83 7.14 3.33	5 4.17 35.71 16.67	6 5.00 42.86 20.00	2 1.67 14.29 6.67	14 11.67
4	5 4.17 13.89 16.67	16 13.33 44.44 53.33	5 4.17 13.89 16.67	10 8.33 27.78 33.33	36 30.00
5	24 20.00 36.92 80.00	8 6.67 12.31 26.67	18 15.00 27.69 60.00	15 12.50 23.08 50.00	65 54.17
Total	30 25.00	30 25.00	30 25.00	30 25.00	120 100.00

Table 2 of Certainty_Eval 5 by Modality					
Controlling for filled=1					
Certainty_Eval 5(Certainty_Eval 5)	**Modality(Modality)**				
Frequency Percent Row Pct Col Pct	**CBCT**	**PAa**	**PAb**	**TOMO**	**Total**
2	0 0.00 0.00 0.00	3 2.50 60.00 10.00	1 0.83 20.00 3.33	1 0.83 20.00 3.33	5 4.17
3	7 5.83 31.82 23.33	3 2.50 13.64 10.00	6 5.00 27.27 20.00	6 5.00 27.27 20.00	22 18.33
4	8 6.67 17.39 26.67	12 10.00 26.09 40.00	10 8.33 21.74 33.33	16 13.33 34.78 53.33	46 38.33
5	15 12.50 31.91 50.00	12 10.00 25.53 40.00	13 10.83 27.66 43.33	7 5.83 14.89 23.33	47 39.17
Total	30 25.00	30 25.00	30 25.00	30 25.00	120 100.00